Synthesis, Characterization, Photochemistry and Anticancer Activity of Novel Photoactivatable Platinum(IV) Diazidodihydroxido Complexes

A thesis submitted in partial fulfilment of the requirements for the degree of Doctor of Philosophy

By

Yao Zhao, *B.Sc, M.S*.

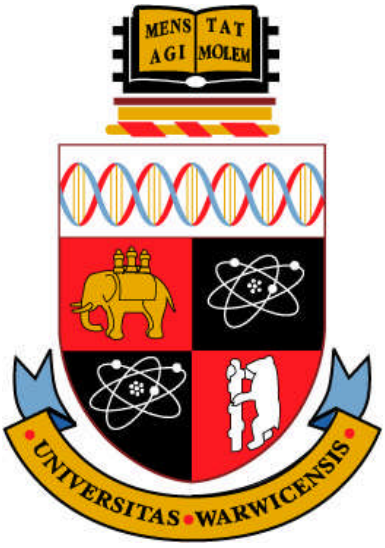

Department of Chemistry

University of Warwick

June 2012

Contents

Table of Contents

List of Tables, Figures and Schemes

Chapter 1

Chapter 2

Chapter 3

Chapter 4

Chapter 6

Acknowledgement

First and foremost, I would like to thank **Prof Peter J. Sadler** for offering me this great opportunity to engage in the pioneering research in a multicultural team and also for his encouragement and excellent supervision through the course of my study. I am particularly grateful for his kindness to me and rigorous attitude toward science and education. I truly couldn't have done this work without his generous support and inspiring guidance.

I would like to express my appreciation to the entire PJS group for their support and friendship all through my study in University of Warwick. A very special thank you must go to **Dr Nicola J. Farrer** for all her help in general discussion about my research project, encouragement and suggestions when I face difficulties, advices in revising my paperwork, and, particularly, support with NMR and MS experiments. I also need to thank **Dr Ana Pizarro** for her kind guidance in HPLC and cytotoxicity study, **Dr Luca Salassa** for his cooperation in the DFT and TD-DFT calculations, **Miss Jennifer S. Butler** for EPR study, **Dr. Abraha Habtemariam**, **Dr Hazel Phillips**, **Dr Sarah Farly, Dr Julie Ann Lough, Dr Zhe Liu, Dr Ying Fu, Miss Ruth McQuitty, Miss Isolda Romero, Miss Bushra Qamar,** and **Miss Evyenia Shaili** for all their support and friendship all the way.

My sincere thanks also go to **Dr Julie A. Woods** and **Miss Kim S. Robinson** from University of Dundee for their hard work in the photocytoxicity study, **Miss Huichung Tai** and **Prof. Robert Deeth** for collaboration in DFT and TD-DFT calculations, **Dr Guy Clarkson** for his work in crystal structure determination, **Dr Ivan Prokes** and **Dr Adam Clarke** for their guidance in NMR spectroscopy, **Miss Huilin Li** for useful discussion in MS spectroscopy, **Dr Lijiang Song, Mr Philip**

Aston for support in using MS, ICP and HPLC facilities, **Prof. Viktor Brabec** and his team from Czech Republic in the Pt-DNA interaction studies, **Dr Gareth M. Roberts, Mr S. E. Greenough, Prof Vasillios G. Stavros** for two photon excitation study, **Dr. Hendrik Schaefer** for GC facilities, and **Prof. Martin Wills** for helpful discussion and support.

I would like to thank the **WPRS**, **ORSAS** and the **University of Warwick** for financial support during my research project.

I would like to dedicate this thesis to my parents **Mr Heping Zhao** and **Mrs Daomei Tai**, and my dear fiancée **Miss Jia Zhou**. Thank them very much for all their love and understanding.

This work is also dedicated to the memory of my grandmother **Mrs Qingyi Wang** and **Mrs Xianying Meng**. They always encouraged me to carry on this study and have been my real source of motivation throughout my work.

Last but not least, thanks to all my family, friends and house/flatmates over the years in Warwick for their constant support. I am so grateful to have them in my life.

Declaration

I hereby declare that the work contained in this thesis is the original work of the author, except where specific reference is made to other sources, with the nature and extent of the author's contribution indicated (as appropriate) where work was based on collaborative research. The work was undertaken at the Department of Chemistry, University of Warwick between September 2008 and June 2012 and has not been submitted, in whole or in part, for any other degree, diploma or other qualification. A list of research papers published or in preparation from this work is given below.

Yao Zhao

June 2012

Abstract

Pt^{IV}-diazidodihydroxido complexes are inert in the dark, but can be selectively activated by irradiation with light and become potently cytotoxic towards cancer cells. By site-specific irradiation to tumour tissue, the side-effects to healthy tissue associated with conventional chemotherapeutics, such as cisplatin, can be circumvented. This thesis aims to develop design photoactivatable platinum(IV) diazidodihydroxido complexes to achieve higher photocytotoxicity, lower cross-resistance and longer wavelength of activation.

A series of Pt^{IV} diazidodihydroxido complexes with *trans* azido, *trans* hydryxido groups and mixed *trans* aliphatic/aromatic amines, was designed, synthesized and characterized. *Trans, trans, trans*-[$Pt(N_3)_2(OH)_2$(MA)(Py)] (**5**) and *trans, trans, trans*-[$Pt(N_3)_2(OH)_2$(MA)(Tz)] (**8**) are potently cytotoxic towards A2780, OE19 and HaCaT cell lines upon irradiation with UVA**.** Remarkably, they also showed potent cytotoxic effects towards A2780cis (cisplatin-resistant ovarian cancer cell subline). Also, the photocytotoxicity towards the A2780, A2780cis, OE19 and HaCaT cell lines upon irradiation with blue light (λ_{max} = 420 nm) is still potent compared to that upon irradiation with UVA. These complexes are highly inert in the absence of light and have almost no dark toxicity.

Upon irradiation with UVA/blue light, the complex **5** was observed to release free azide anions N_3^-, azidyl radicals N_3•, nitrogen gas N_2 and form nitrene intermediates. It was of importance to discover that singlet oxygen ($^1O_2$) is generated from photoreactions in the absence of an exogenous source of oxygen, whereas hydrogen peroxide (H_2O_2) and hydroxyl radical intermediates did not appear to be formed.

Mono-functional and bi-functional Pt adducts were captured from the photoinduced binding of complexes **5** and **8** to 5'-GMP and a DNA oligonucleotide. It was discovered for the first time that the oxidation of 5'-GMP can occur during the photoreaction of complex **5** upon irradiation with UVA. Singlet oxygen and nitrene intermediate generated from this photoreaction are likely to be the cause of the oxidative damage to guanine.

4-Nitropyridine, 2,2'-bipyridine, and terpyridines were used as ligands in novel photoactivable Pt^{IV} (di)azido complexes and two were activated by green light. A new two-photon-activatable Pt^{II} complex, *cis*-[$PtCl_2$(MOPEP)$_2$](**42**), was also designed, synthesized and characterized. It was observed that this complex was sensitive to one-photon excitation below 500 nm and the ligand MOPEP underwent rapid solvent (acetonitrile) substitution upon irradiation. The same photoreaction was also triggered by two-photon excitation with fs-pulses laser light between 600 – 700 nm.

Abbreviations

2D	two-dimensional
4-py-NO_2	4-nitropyridine
5'-GMP	guanosine 5'-monophosphate
8-oxo-G	8-oxo-guanine or 8-hydroxyguanine
Bpy	2,2'-bipyridine
CCDC	Cambridge Crystallographic Data Centre
CID	collision-induced disassociation
COD	1, 5-cyclooctadiene
COSY	correlation spectroscopy
CRT1	copper transport protein 1
CSA	chemical shift anisotropy
DEPT	distorsionless enhancement by polarization transfer
DFT	density functional theory
DMA	dimethylamine
DMF	dimethylformamide
DMPO	5, 5-dimethyl-pyrroline-N-oxide
DMSO	dimethyl sulfoxide
DNA	deoxyribonucleic acid
EPR	electron paramagnetic resonance or electron spin resonance (ESR)
ESI-MS	electrospray ionisation mass spectrometry
FDA	US Food and Drug Administration
fs	femto second
G	guanine
GSH	reduced glutathione
h	hour
HMBC	heteronuclear multiple-bond correlation spectroscopy
HMQC	heteronuclear multiple-quantum coherence
HOMO	highest occupied molecular orbital
HPLC	high-performance liquid chromatography
HSQC	heteronuclear single-quantum coherence
ICP-OES	inductively coupled plasma – optical emission spectroscopy
IPA	isopropylamine
IR	infrared
ISC	intersystem crossing
JMOD	J modulation
LED	light emitting diode
LHRH	luteinizing hormone-releasing hormone
LMCT	ligand-to-metal charge transfer
LUMO	lowest unoccupied molecular orbital
MA	methylamine
MeCN	acetonitrile

MLCT	metal-to-ligand charge transfer
mol equiv	molar equivalents
MOPEP	4-[2-(4-methoxyphenyl)ethynyl]pyridine
MS	mass spectrometry
NMR	nuclear magnetic resonance
NOE	nuclear Overhauser effect
NOESY	nuclear Overhauser effect spectroscopy
OPA	one-photon absorption
PDT	photodynamic therapy
PENDENT	polarization enhancement during attached nucleus testing
ppm	parts per million
PS	photosensitizer
PWHH	peak width at half height
Py	pyridine
r.t.	room temperature
RedSp	N-formylamidoiminohydantoin (hydrolysed 8-oxo-G)
ROS	reactive oxygen species
RT	retention time
s	second
SOSG	Singlet Oxygen Sensor Green®
TOCSY	total correlation spectroscopy
TPA	two-photon-absorption
Tpy	2,2':6',2''-terpyridine
TTpy	4'-(4-Methylphenyl)-2,2':6',2''-terpyridine
Tz	thiazole
UVA	ultra violet a light
UV-Vis	ultraviolet-visible
VC	L-ascorbic acid

Publications

1. Farrer, N. J.; Woods, J. A.; Salassa, L.; Zhao, Y.; Robinson, K. S.; Clarkson, G.; Mackay, F. S.; Sadler, P. J., **A potent trans-diimine platinum anticancer complex photoactivated by visible light**. *Angew. Chem. Int. Ed.* **2010,** *49* (47), 8905-8908.

2. Tai, H.-C.; Zhao, Y.; Farrer, N. J.; Anastasi, A. E.; Clarkson, G.; Sadler, P. J.; Deeth, R. J., **A computational approach to tuning the photochemistry of platinum(IV) anticancer agents**, *Chem. Eur. J.*, **2012**, accepted.

3. Zhao, Y.; Farrer, N. J.; Woods, J. A.; Salassa, L.; Butler, J. S.; Robinson, K. S.; Mackay, F. S.; Clarkson, G.; Song, L.; Sadler, P. J., **Novel visible-light-activitable platinum(IV) diazido anticancer prodrugs** (in preparation). **2012**.

4. Zhao, Y.; Butler, J. S.; Farrer, N. J.; Li, H.; McQuitty, R. J.; Habtemariam, A.; Sadler, P. J., **Unprecedented singlet oxygen generation and the oxidation of guanine in the UVA-activation of platinum(IV)-diazidodihydroxyl complex** (in preparation). **2012**.

5. Zhao, Y.; Farrer, N. J.; Roberts, G. M.; S. E. Greenough; Stavros, V. G.; Sadler, P. J., **Two-photon labilization of Pt-Py bond in a new platinum(II) complex** (in preparation). **2012**.

Conferences attended

16/06/2010	Warwick Chemistry Post Graduate Symposium	University of Warwick, UK	Poster
22-26/06/2010	10th European Biological Inorganic Chemistry Conference (Eurobic10)	Thessaloniki, Greece	Poster
06/01/11	The first meeting of RSC Cancer Chemistry Group	School of Pharmacy, London, UK	Poster
13-14/05/11	COST D39 work group meeting	Brno, Czech Republic	Oral presentation
01/06/2011	Warwick Chemistry Post Graduate Symposium	University of Warwick, UK	Oral presentation
7-12/08/2011	XXV International Conference on Photochemistry (ICP2011)	Beijing, China	Poster
3-5/04/2012	RSC Dalton 2012 Conference	University of Warwick, UK	Poster

Courses and trainings attended

2008 - 2009	Postgraduate Courses	Elemental Analysis Biophysical Advanced Medicinal Chemistry Nuclear Magnetic Resonance Spectroscopy Data Acquisition II
2008 - 2011	Research Student Skills Programme	Effective PowerPoint Presentations Writing Literature Review Academic Writing Time Management
2008 - 2012	Weekly postgraduate Chemical Biology Cluster Seminars	Two oral presentations given
2008 - 2011	Transferable skills courses	Team Development and Networking Decision-Making and Leadership Research Project Management
2008 - 2010	Demonstrator for Undergraduate Chemistry Labs	
7-8/12/2010	WAGS NMR workshop	
9-10/09/2010	Advanced Topics in Mass Spectrometry	

Chapter 1

Introduction

This thesis is concerned with photoactivatable platinum(IV) diazidodihydroxido complexes as potential anticancer agents. An introduction to the coordination chemistry of platinum, platinum based anticancer drugs and the photochemistry of metal complexes are given in this Chapter.

1.1 Platinum

1.1.1 General properties

Platinum is a Group 10 element with an atomic number of 78, which is a very rare metal, occurring as only 5 ppb in the Earth's crust. Its atomic and physical properties are listed in **Table 1.1**.

Table 1.1 Atomic and physical properties of platinum.[1-4]

Atomic Number	78
Atomic Weight (relative to $^{12}C = 12$)	195.084
Density (g/cm^3, at 293 K)	21.45
Melting Point (K)	2045
Boiling Point (K)	4098
Electronic Configuration	[Xe] $4f^{14}$ $5d^9$ $6s^1$ Pt^0 [Xe] $4f^{14}$ $5d^8$ Pt^{II} [Xe] $4f^{14}$ $5d^6$ Pt^{IV}
Pauling Electronegativity	2.28
Electron Affinity (kJ/mol)	205.3
Ionization Energies (kJ/mol)	1st: 870 2nd: 1791
Atomic (crystal) radii (Å)	1.375 (0) (in metal) 0.74 (II) (square-planar) 0.765 (IV) (octahedral)

Platinum has six naturally occurring isotopes: ^{190}Pt, ^{192}Pt, ^{194}Pt, ^{195}Pt, ^{196}Pt, and ^{198}Pt. The most abundant is ^{195}Pt, comprising 33.83% of all platinum. Moreover, ^{195}Pt has a nuclear spin quantum number I = ½, which is the only isotope with NMR activity (**Table 1.2**). As all the other isotopes have zero nuclear spin, ^{195}Pt NMR spectroscopy has found great use both by direct observation of the ^{195}Pt resonance and by observation of ^{195}Pt "satellites". The term "Pt satellites" is used to describe the NMR resonance of a nucleus coupled to ^{195}Pt (*ca*. 1/3 natural abundance of all Pt) which will split into a doublet symmetrically placed beside the central resonance arising from those species containing all the other Pt isotopes. The relative intensity of the three resonances is close to 1:4:1 (**Figure 1.1**).[2, 5] Further discussions on the shape of Pt satellites and Pt NMR can be found in **Chapters 2** and **3**.

Table 1.2 Platinum isotopes and nuclear spin quantum numbers.

Isotopes	Natural Abundance	Nuclear Spin Quantum Number (I)
^{190}Pt	0.01%	I = 0
^{192}Pt	0.078 %	I = 0
^{194}Pt	32.9 %	I = 0
^{195}Pt	33.8 %	I = ½
^{196}Pt	25.3 %	I = 0
^{198}Pt	7.21 %	I = 0

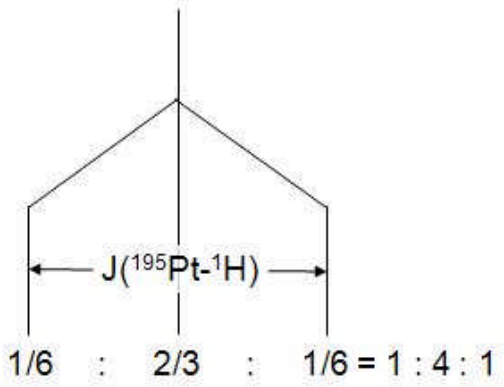

Figure 1.1 Platinum satellites, e.g., for a ^{1}H NMR resonance.

1.1.2 Oxidation states and coordination chemistry

Although platinum can exist in the 0, +1, +2, +3, +4, +5 and +6 oxidation states,[2, 6] the most common oxidation states are +2 and +4. The +1 and +3 states exist generally in molecules that have M–M bonds. Pt^{II} has a strong preference for square-planar geometry and a coordination number of four, and most Pt^{IV} species have octahedral structure and coordination number of six. The splitting of the d-orbitals and electronic configurations with strong field ligands are depicted in **Figure 1.2** The relatively slow substitution rates of Pt^{II} complexes (e.g., the hydrolysis of *cis*-$[Pt(NH_3)_2Cl_2]$ has a first order rate constant of 2.5×10^{-5} s^{-1})[7] facilitates mechanistic studies and has found wide applications in research of geometrical isomerism and reaction mechanisms.[1]

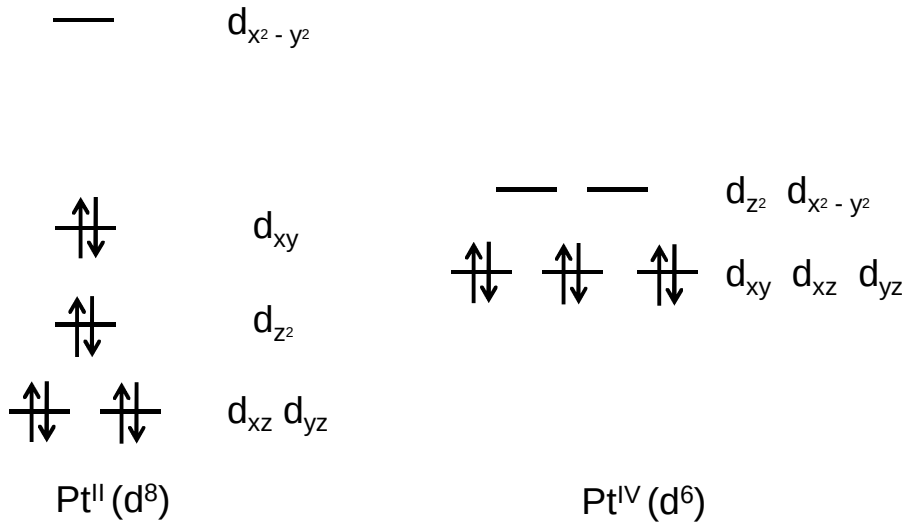

Figure 1.2 Splitting of the d-orbitals in crystal fields of square-planar (Pt^{II}, d^8) and octahedral (Pt^{IV}, d^6) symmetries. The electrons are configured in a strong ligand field.

In Pearson's "soft/hard" acid/base theory, Pt^{II} is classified in the group of "soft" acids, which means that Pt^{II} is easy to polarize and prefers to form complexes with "soft" bases.[8, 9] Many stable Pt^{II} complexes are formed with "soft" ligands such as S

or P donors and ligands that can π-bond, such as CN^-, NO_2^-, alkenes and alkynes. In aqueous solution, the stability of halide complexes with Pt^{II} increases in the order F^- << Cl^- < Br^- < I^-. Although Pt^{II} generally shows low affinity for "hard" (F and O) ligands, in the latter case there are some notable exceptions, such as μ-OH, acetates, diketonates, carboxylates and phenoxides.[3, 10]

Platinum in the +4 oxidation state has a d^6 electronic configuration and the coordination number is invariably 6 with octahedral geometry.[10] Pt^{IV} complexes are almost always low spin due to the large splitting of the d-orbitals and therefore have a large crystal field stabilisation energy. In "hard/soft" acid/base theory, Pt^{IV} is also classified as a "soft" acid, but much harder than Pt^{II}. Pt^{IV} complexes are generally more thermally stable and kinetically inert than Pt^{II} complexes.[2] The substitution reactions of Pt^{IV} complexes can be greatly accelerated by the presence of Pt^{II} species.[10]

1.1.3 *Trans effect*

The *trans effect* is an important kinetic effect first systematized by Chernyaev in the 1920s in the coordination chemistry of metals, particularly platinum(II) and (IV). In short, the *trans effect* is defined as the effect of a given ligand upon the rate of substitution of a leaving group opposite to it in a metal complex.[3] This influence to the opposite, or *trans* groups, is greater than the influence of adjacent, or *cis* groups. The *trans effect* is exclusively a kinetic effect in the substitution reaction, related presumably to the transition state, as well as the ground state. In square-planar substitution reactions, the thermodynamically preferred isomer is not always produced. After comparing the kinetics of a range of ligand substitution reactions, the following empirical series of decreasing *trans effect* was produced: [3, 11, 12]

CO, CN^-, C_2H_4 > PR_3, H^- > CH_3^- > R_2S > $C_6H_5^-$, NO_2^- , I^- > SCN^- > Br^- > Cl^- > pyridine > NH_3 > OH^- > H_2O

Theoretical explanation of the *trans effect* is based on the combination of σ-bonding and π-bonding.[12] Strong σ-donors, such as PR_3 and H^-, contribute high electron density to metal ion, weakening the bond *trans* to it. Some ligands, e.g., CO and CN^-, possess empty orbitals that can act as π-acceptors to remove electron density from the metal ion, making the region *trans* to the ligand electron-deficient and vulnerable to the nucleophile in the transition state. The application of the *trans effect* will be further discussed when describing the synthesis of cisplatin and various analogues in **Chapter 3**.

The *trans-influence* is a concept related to *trans effect* but is a ground-state effect. The *trans-influence* of a ligand is a measure of its effect on the strength of the bond opposite to it in a complex, which can be the lengthening of bonds determined by X-ray diffraction, vibrational strength by IR spectroscopy and coupling constants by NMR spectroscopy. [3, 12]

1.2 Platinum based anticancer drugs

1.2.1 Cisplatin

The anticancer activity of cisplatin (*cis*-$[PtCl_2(NH_3)_2]$, also known as CDDP) was discovered accidently by Dr B. Rosenberg in *ca*. 1968 [13, 14]. The promptly followed clinical trials demonstrated its efficacy towards a variety of solid tumors. Cisplatin was approved by the FDA in 1978 for clinic use in metastatic testicular cancer and ovarian cancer,[15] and later for transitional bladder cancer, lung cancer, lymphomas,

myelomas and melanoma. Today it is routinely used in 32 of 78 clinic treatment regimes listed in Martindale in combination with a wide range of other drugs.[16, 17]

1.2.1.1 Mechanism of action

It is generally accepted that platinum complexes exert their cytotoxicity by entering the cell and binding to DNA.[18, 19] Cisplatin is administered via intravenous injection to the bloodstream of patient, where the relatively high Cl^- concentration in the blood plasma (*ca*. 100 mM) supresses the hydrolysis of chlorido ligands on cisplatin. The complex maintains neutral charge to facilitate the penetration through cell membranes. Much evidence suggests that cisplatin can be attacked by cytoplasmic thiol-containing species such as the tripeptide glutathione and metallothioneins, and this leads to deactivation because platinum is highly affinitive to sulphur.[20, 21] This process is believed as one of the causes of side effects of and resistance to cisplatin (*vide infra*).

The mechanism of cellular uptake of the high polar molecule, cisplatin, is generally believed to be passive diffusion;[22] however, recent research has suggested that the copper transporter (CRT1) is also involved in its cellular influx.[23] Once the complex has entered the cell, the relatively lower concentration of cellular chloride (4 – 20 mM) allows for aquation of cisplatin. **Figure 1.3** describes the hydrolysis reaction, including half reaction times of hydrolysis and pK_a values of the aqua adducts. The highly activated species *cis*-$[PtCl(NH_3)_2(OH_2)]^+$ and *cis*-$[Pt(NH_3)_2(OH_2)_2]^{2+}$ are formed[24] and the former is believed to be responsible for the majority of DNA binding (> 98%).[25, 26]

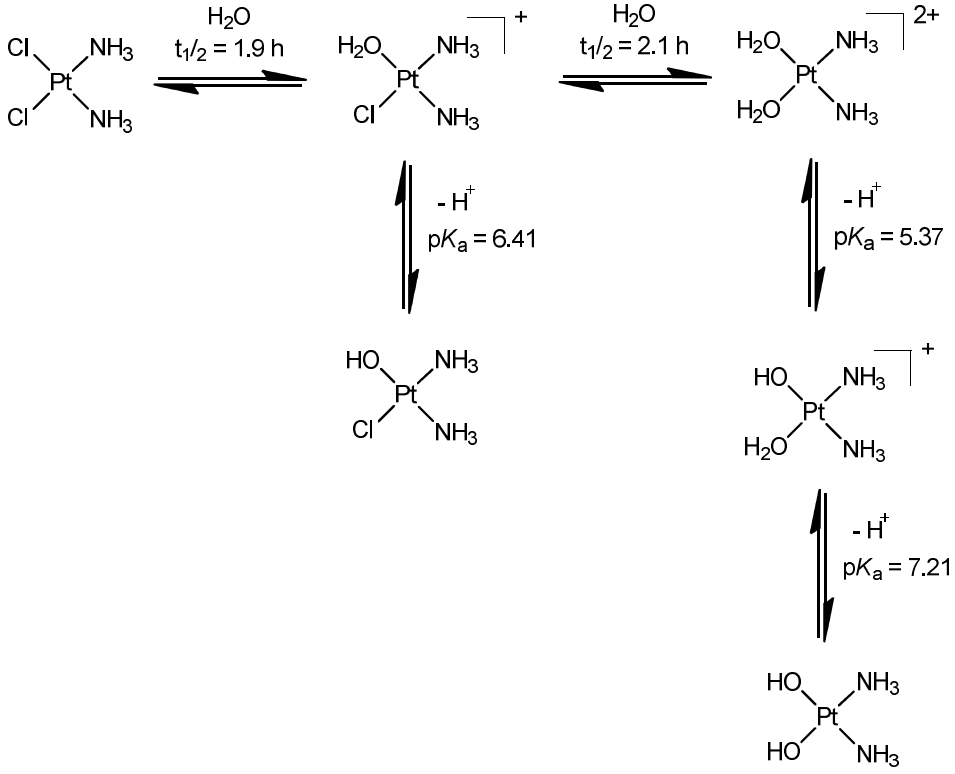

Figure 1.3 Hydrolysis reaction pathways of cisplatin, and the hydrolysis half-reaction times[26] (310 K) and pK_a values[27] (300 K) of aqua species are given.

DNA binding of the mono-aqua species *cis*-$[PtCl(NH_3)_2(OH_2)]^+$ is kinetically controlled, as aquation of cisplatin is the rate-determining step.[28] The preferential binding sites for platinum on DNA are guanine-N7 (**Figure 1.4**), as this is the most nucleophilic site.[19, 29] Other N-donors, such as adenine-N7, can also bind to Pt.

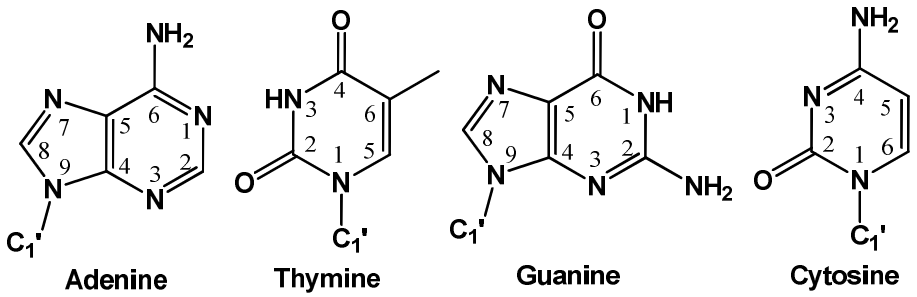

Figure 1.4 DNA bases: adenine, thymine, guanine and cytosine.

Once the mono-aqua species *cis*-$[PtCl(NH_3)_2(OH_2)]^+$ binds to DNA, bifunctional adducts or crosslinks are rapidly formed by ring closure, accompanied by the loss of

the other chloride. Most crosslinks are GpG 1,2 intrastrand (60 – 65% of all adducts) and ApG 1,2 intrastrand (20 – 25%). Other less frequent products include GpXpG 1,3 intrastrand crosslinks (*ca.* 2%) and G-G interstrand crosslinks (*ca.* 2%), and *ca.* 2% adducts on guanines remains monofunctional.[15, 30] In all cases, the two ammine groups (also called "carrier ligands") remain bound to platinum. In 1995, the first crystal structure by X-ray crystallography of GpG intrastrand adduct in a DNA duplex[31] and the solution structure by NMR of a G–G interstrand crosslink[32] were reported.

The binding of Pt^{II} to DNA bases is strong and appears to be essentially irreversible.[10] The formation of the bifunctional adduct causes significant distortion of the DNA, which can be recognized by certain cellular housekeeping proteins.[33] These proteins can either trigger DNA repair or release signal for apoptotic cell death.[19, 34, 35] Nevertheless, it is noted that a number of alternative cellular targets and protein recognition processes have also been discovered.[36]

1.2.1.2 Resistance and side-effects

Cisplatin is indeed very effective and has had a major clinical impact, particularly for testicular or ovarian cancers. However, severe side effects such as nausea and vomiting, nephrotoxicity, ototoxicity, neuropathy and myelo-suppression accompany the treatment, which limits the dose of administration.[37] Cisplatin modifies DNA non-selectively in all actively dividing cells, regardless of whether they are cancerous or not. In addition, cisplatin attacks proteins or peptides in cells and in blood plasma, particularly those with histidine, cysteine and methionine,[15] namely, human serum albumin,[38] metallothioneins[39] and tripeptide glutathione.[40] Very recently, the interaction of cisplatin with a wide range of proteins was studied,

including calmodulin,[41, 42] ubiquitin,[43] copper chaperone proteins,[44] and copper transport proteins.[45] In fact, studies have shown that 24 h after cisplatin administration, 65 – 98% of the platinum in blood plasma is bound to proteins.[46, 47] This protein binding has been blamed for deactivation of the drug and some of the severe side effects of cisplatin treatment.[20, 48-51]

Another important factor that limits the efficacy of cisplatin against a number of malignancies is cellular resistance. The resistance to cisplatin is largely attributed to reduced accumulation, increased cytoplasmic detoxification by cellular thiols and increased DNA repair/tolerance of platinum-DNA adducts.[15, 52] After administration of the platinum complex by intravenous injection, a large proportion of Pt^{II} drugs are lost in the bloodstream before arriving at their ultimate target (*vide supra*). Also, Pt drugs enter cells by passive diffusion or using either transporters, a significant one being the copper transporter CTR1. Loss of CTR1 results in less platinum entering cells and, consequently, drug resistance.[23, 53] In addition, the large volume of damaged cells further causes altered cellular transport, enhanced overexpression of DNA-damage recognition proteins and repair of distorted DNA, and decreased apoptosis contributing to tumour resistance to Pt drugs.[33]

There are several strategies to overcome the resistance to cisplatin,[15]

- Increase the levels of platinum that reach tumours with e.g., liposomal enclosed platinum drugs;
- Combine existing platinum drugs with molecularly targeting moieties;
- Develop new platinum drugs such as oxaliplatin with novel mechanisms that are capable of circumventing cisplatin-mediated resistance;

- Use other drugs either alone or in combination to exploit particular cisplatin-mediated resistance mechanisms.

1.2.2 Development of new platinum anticancer drugs

The discovery of cisplatin stimulated the synthesis and screening of over 2000 different types of Pt complexes with different amines and anionic ligands. Much effort has been devoted to the design of novel Pt anticancer drugs to make chemotherapy safer for patients, in particular, lessening severe side effects, [54, 55] increasing oral bioavailability, [52, 56] and overcoming drug resistance. [22, 23, 40, 57-59] An additional approach involves the use of a photosensitizing agent in combination with light which provides a promising avenue to achieve accurate targeting.[60] Until 2010, 23 new platinum-based drugs have entered clinical trials, and five of them (excluding cisplatin) are approved worldwide or regionally (**Figure 1.5**).[17, 19]

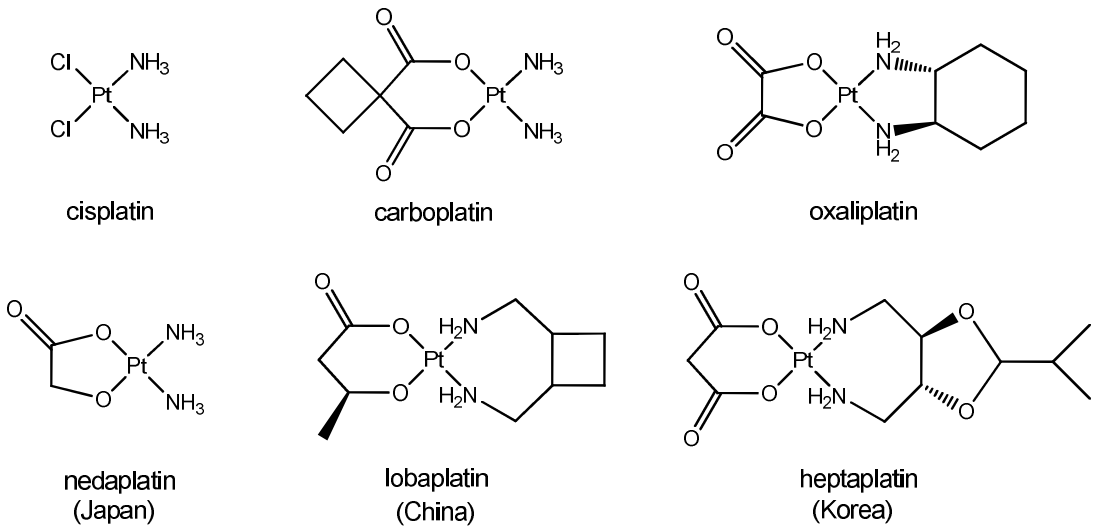

Figure 1.5 Approved platinum anticancer drugs worldwide (cisplatin, carboplatin and oxaliplatin) or regionally (nedaplatin, lobaplatin and heptaplatin).

1.2.2.1 Cisplatin derivatives

The initial structure-activity relationships for further platinum-drug development obey the following rules:[61, 62]

- The active complexes must be *cis* geometry and must be uncharged.
- Leaving groups should be adequately strongly but not tightly bound.
- Amine ligands with more alkyl substituents reduce the activity.

This resulted in the development of carboplatin (*cis*-diammine-[1,1-cyclobutanedicarboxylato]platinum(II), see **Figure 1.5**) in the mid-1980s,[54] which is, broadly speaking, equally effective to cisplatin, but with a more acceptable side-effect profile. Carboplatin was based on the hypothesis that a more stable leaving group than chloride might lower toxicity without affecting antitumour efficacy. This hypothesis turned out to be correct.[15]

After *ca.* 30 years searching for improved anticancer agents in the many analogues of cisplatin, little improvement in spectrum of activity had been observed. Recent devotion to the analogues of cisplatin was concentrated on improving the cytotoxicity and lowering the system toxicity and side effects of the platinum complexes. For example, a water-soluble heptaplatin analogue can improve antitumor activity and reduce toxicity,[63] coupling cisplatin with a androgenic steroid delivery vector can improve the delivery to estrogen-dependent tissues,[64-66] and incorporating other active anticancer agents such as CDK inhibitor bohemine[67] or dichloroacetate[68] in *cis*-platinum complexes can acquire multiple cytotoxic effect.

Recent evidence suggests that the cisplatin analogues usually form a similar range of DNA adducts as cisplatin.[69] Consequently, attention turned to the synthesis of non-triditional platinum anticancer drugs for improved accumulation, oral bioavailability,

and tumour targeting.[70] The classic structure-activity relationships were soon broken and a large number of novel platinum complexes was developed forming a different range of DNA adducts and displaying a different spectrum of anticancer activity compared to cisplatin, as discussed below.

1.2.2.2 *Trans*-platinum complexes

In the early days, it was shown that transplatin exhibits little antitumor activity because of the limited ability to form intrastrand adducts with DNA.[71, 72] On the one hand, steric constraints preclude transplatin from formation of 1,2-intrastrand cross-links in DNA. On the other hand, in the hydrolysis kinetics for transplatin shown in **Figure 1.6**, both k_1 and k_{-1} are faster as compared to cisplatin, but both k_2 and k_{-2} are smaller for the *trans* over the *cis* isomer.[62] This is due to the *trans effect* (Cl > N > O).

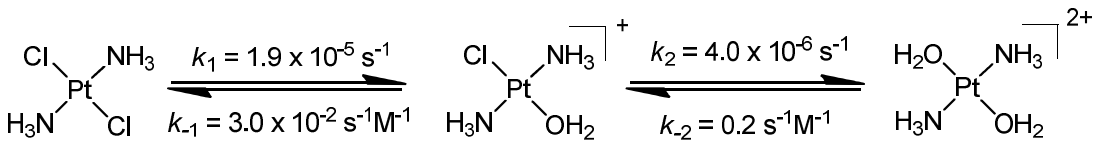

Figure 1.6 Hydrolysis kinetics of transplatin. Data from ref. [62]

However, in recent years, it is recognized that substitution of NH_3 in transplatin to aromatic heterocycle N-donors, sulphoxide, sterically hindered aliphatic amine or imino iminoethers ligands leads to cytotoxic effects on a par with cisplatin.[62, 73, 74] For example, Navarro-Ranninger and co-workers reported that *trans*-$[PtCl_2(DMA)(MA)]$ (MA = methylamine, DMA = dimethylamine, **Figure 1.7**) is more toxic towards MCF-7 cell lines than cisplatin.[75] The aquation chemistry of this compound was examined and compared with its analogues. It was suggested that properly designed bulky carrier ligands may reduce the rate of hydrolysis of chlorido

ligands so as to lower the acute detoxification of *trans* platinum complexes before arriving at the target cells and thus increase their antitumor activity.[76, 77]

More importantly, *trans* platinum complexes often act with mechanisms different from that for cisplatin, so as to circumvent cisplatin resistance. It was also suggested that the Pt-DNA adducts formed by the *trans* isomer are not recognized by HMGB1 protein (modulating the repair of DNA damage in mammalian cells[78]) and the level of DNA repair is lowered. For example, Gibson and coworkers reported novel cationic *trans* Pt^{II} complexes with piperazine ligands that are active against cisplatin-resistant ovarian cancer cell lines.[79] *Trans*-[$PtCl_2$(isopropylamine)(1-methylimidazole)] (**Figure 1.7**) tends to form higher level of DNA interstrand crosslinks between complementary guanine and cytosine residues over its *cis* isomer.[80] Jakupec and coworkers recently reported that the *trans*-configured Pt^{II} oxime complexes lead to higher cytotoxicity, extraordinary cellular accumulation, higher levels of platination with DNA and higher degree of DNA damage in cancer cells over the corresponding *cis* isomers.[81] In general *trans* platinum complexes exhibit a different spectrum of cytostatic activity from cisplatin.[82]

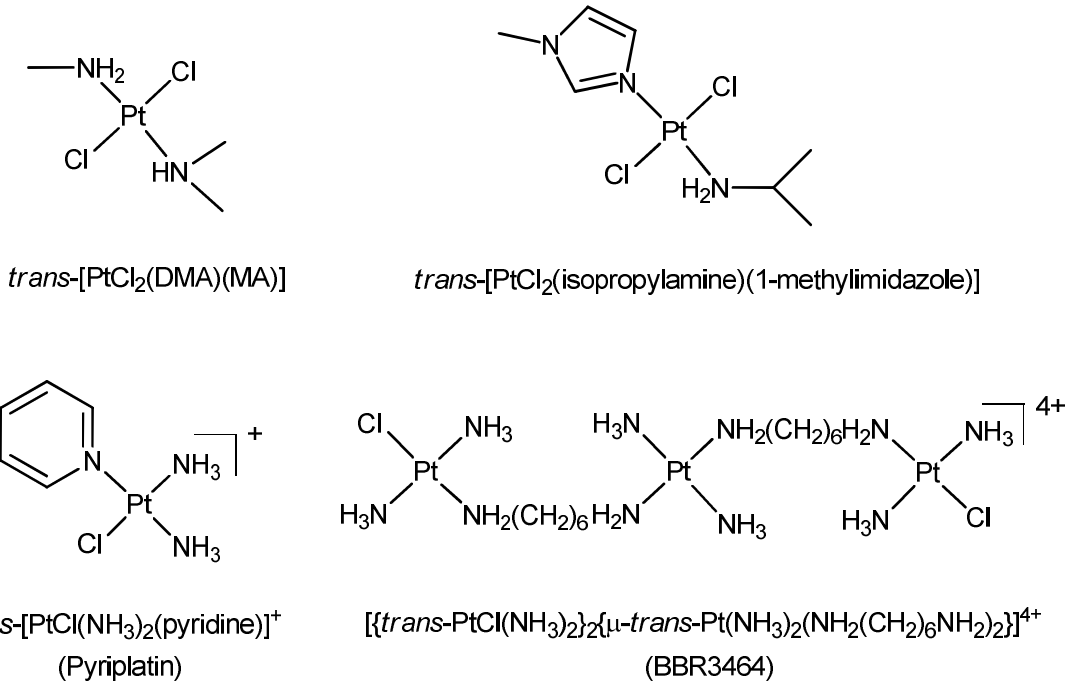

Figure 1.7 Recent developed platinum antitumor complexes with novel mechanism of activity.

1.2.2.3 Monofunctional platinum complexes

It is generally accepted that cisplatin exerts the antitumor activity by forming bifunctional intrastrand crosslinks (CLs) with DNA (*vide supra*). But in recent years, rule-breaking monofunctional Pt^{II} anticancer complexes have been rationally designed and display promising antitumor activities.[83-85] Notably, pyriplatin (*cis*-$[PtCl(NH_3)_2(pyridine)]^+$, **Figure 1.7**)[86] has a distinct cytotoxicity profile from that of cisplatin in cell cultures and inhibits RNA polymerase II *in vitro*.[87] Despite the different nature of its DNA adducts, this monofunctional platinum complex exhibits their antitumor activity in a way very similar to that of cisplatin.[88] In various mammalian cells, pyriplatin reacts with DNA as efficiently as cisplatin, inhibits transcription as strongly as cisplatin, and even its DNA repair mechanism is also nucleotide-excision repair, similar to cisplatin.

1.2.2.4 Multinuclear platinum complexes

Multi-nuclear platinum complexes contain two or more platinum centres connected by designed linkers. One or more Pt centers can covalently bind to DNA, and hence are capable of forming a completely different array of DNA adducts compared to cisplatin.[89, 90] These multi-nuclear complexes represent a completely new paradigm for platinum based anti-cancer complexes, and appear to offer great potential as new anticancer agents.[91-96]

Of all the multinuclear platinum anticancer complexes, a very successful one that first entered the clinical trial *in vitro* and *in vivo* is BBR3464 ([{*trans*-$PtCl(NH_3)_2\}_2\{\mu$-*trans*-$Pt(NH_3)_2(NH_2(CH_2)_6NH_2)_2\}]^{4+}$, **Figure 1.7**).[97, 98] BBR3464 is much more active than cisplatin in all cancer cell lines tested, showing comparable activity at up to 500-fold lower doses *in vitro*.[99, 100] BBR3464 induces a cellular response different from cisplatin [101, 102] and shows activity even in several cancer cell lines that are naturally resistant to cisplatin.[99] Unfortunately, phase I and phase II studies of BBR 3464 treatment in patients with ovarian, non-small/small cell lung cancer and gastric and gastro-oesophageal adenocarcinoma showed limited activity but severe systemic toxicity.[17, 103, 104] Therefore, this drug was not moved into Phase III trials.

1.2.2.5 Prodrugs

An active drug (including anticancer drug) may suffer from one or more of the following restrictions: poor aqueous solubility, low lipophilicity or permeability, parenteral administration, chemical instability, lack of site-specificity, incomplete absorption through membranes and too rapid excretion.[105] In order to overcome these disadvantages, prodrugs are used as pharmacologically inactive derivatives of drugs

that are metabolized or activated in the body to release or generate the active drug (ideally at the site of action).[106] In cancer chemotherapy, prodrugs are widely used in two major aspects. The first is cancer targeting, such as via conjugation of drugs with antibodies,[107] or polymeric cancer cell targeting peptide carriers[108-111] for corresponding cellular receptors, resulting in enhanced permeability and accumulation of drugs. The second aspect is controlled release at the tumor site, including acid-promoted liberation, enzymatic cleavage and hypoxia-mediated release/immunotoxins.[106]

Tumours are often hyperpermeable towards macromolecules because of compromised vasculature and lack of effective lymphatic drainage.[112, 113] Therefore, if the therapeutic agent is coupled to a macromolecular carrier, or packed inside a nano-sized particle, increased drug concentration within the tumour tissue can be obtained.[114]

Lippard and coworkers and other groups have developed a series of nanoparticles, nanotubes and nanorods as prodrugs for targeted delivery of platinum anticancer complexes[115-120]. A higher total fraction of drug delivery to tumours and enhanced anticancer cytotoxicity and efficacy were received.

The cell surface proteins, $\alpha_v\beta_3$ and $\alpha_v\beta_5$ integrins and aminopeptidase N (APN or CD13) are overexpressed in tumour endothelial cells and on certain cancer cells during tumour growth and metastasis, but are barely detected in resting endothelial cells.[121, 122] Those proteins show high affinity for the peptide motifs RGD (Arg-Gly-Asp, for $\alpha_v\beta_3$ and $\alpha_v\beta_5$)[123] and NGR (Asn-Gly-Arg, for APN)[124], respectively. Similarly, luteinizing hormone-releasing hormone (LHRH) has also been found as a targeting moiety (ligand) for LHRH receptors that are overexpressed in the plasma

membrane in breast, ovarian and prostate cancer cells and are not expressed detectably in normal visceral organs.[125] Recently, Fukuda and coworkers reported an IFLLWQR peptide conjugated potent anticancer drug SN-38 efficiently suppressing human colon HCT116 tumour growth in nude mice at low dosages without apparent side effects.[111] As a result, RGD, NGR, LHRH and IFLLWQR peptides motifs have been employed as delivery agents for low molecule-weight drugs to the tumour cells.[108-110]

Improving the delivery of platinum drugs with liposomal capsules (Lipoplatin^{TM}) [126-130] or polymer-based vehicles (ProLindac^{TM}) [131-133] is another attractive strategy and has entered clinical trials. They will become the first macromolecule-based platinum drugs if approved.[17]

Pt^{IV} drugs are also regarded as a group of prodrugs and will be discussed in the next section.

1.2.2.6 Platinum(IV) prodrugs

Octahedral Pt^{IV} complexes are substantially more inert kinetically than their square-planar Pt^{II} analogues, as the substitution reactions of the ligands take place very slowly under physiological conditions.[134, 135] The kinetic inertness of Pt^{IV} complexes provides a promising feature to keep the complex intact before arriving at the cellular target. Although Pt^{IV} complexes with the ligand 1,2-diaminocyclohexane were found to react with 9-methylxanthine, 9-methylhypoxanthine, and guanosine-5′-monophosphate directly,[136] it is widely accepted that Pt^{IV} species have to be reduced to more reactive Pt^{II} form to exert their anticancer activity.[69] In other words, Pt^{IV} complexes can be regarded as the prodrugs of the corresponding Pt^{II} complexes.[137, 138] Pt^{IV} complexes could remain in the higher oxidation state which

would keep their lower reactivity in the bloodstream. This would diminish unwanted side reactions and decrease the activity of the drug.

Biological reducing agents, such as ascorbic acid, cysteine (Cys) and glutathione (GSH) can reduce Pt^{IV} to Pt^{II} in cancer cells, for which direct evidence in cells has been obtained.[139-142] In addition, the higher lipophilicity of some Pt^{IV} complexes would potentially improve their cellular uptake.[137, 143] Recently, Lin and coworkers reported a targeted release of an oxaliplatin moiety from Pt^{IV} based polysilsesquioxane nanoparticles for cancer chemotherpy.[120] However, none of the Pt^{IV} drugs has been approved for clinical use to date. Two failed to pass human clinical trials (iproplatin and ormaplatin), one is undergoing clinical trials for human use (satraplatin) and another one is under development (oxoplatin).[17, 144] Although a number of reasons are attributed to the failures, one of them is that they are readily reduced to Pt^{II} in the bloodstream and thus fail to reach their target.

Although a recent report demonstrated that steric hindrance may affect the rate of reduction of oxaliplatin derivatives,[145] it is widely believed that the ease of reduction is closely related to the nature of the ligands, especially the leaving groups. The am(m)ine ligands are quite stable on Pt^{IV}, by contrast, the chloro, acetato and hydroxo ligands are vulnerable to substitution and are thus considered as leaving groups. These leaving ligands play important roles in determining both the reduction potentials and the rate of reduction by small biomolecules such as ascorbate and GSH. It is generally accepted that this effect increases in the following order $OH^- < OAc^- < Cl^- < I^-$.[137, 146-148] For example, the reduction potential values of a series of Pt^{IV} complexes are given in **Table 1.3**. This correlation has guided the design of Pt^{IV} complexes for many years because it was believed to provide a means of predicting the pharmacology of the prodrugs.

Table 1.3 Reduction potential values of Pt^{IV} complexes with variation of axial ligands.[137]

Complex	Ligand X	E_p[a] (mV)
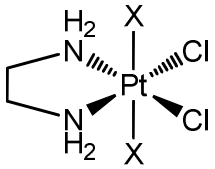	OH	−664
	$OC(O)CH_3$	−326
	$OC(O)CH_2CH_3$	−301
	$OC(O)CH_2CH_2CH_3$	−273
	Cl	−4

[a] The reduction potential values (E_p) are actually half wave potentials from cyclic voltammetry measurement and are adjusted to the standard hydrogen electrode.

1.3 Photoactive anticancer agents

1.3.1 Photochemistry

Photochemistry is concerned with the processes that are activated by interaction between light and matter. Light is a kind of electromagnetic radiation that exhibits both particle-like and wave-like properties. The energy (E) of a photon at a given frequency of the radiation (v) is given by:

$$E = hv = hc / \lambda$$

where h is Planck's constant, λ wavelength of the radiation and c the velocity of light.[149]

There are two fundamental principles for photochemical transformations,[150]

- The first law (Grotthuss-Draper law): light must be absorbed by a matter so that a photochemical reaction can take place.
- The second law (Stark-Einstein law): for each photon of light absorbed by a chemical system, only one molecule can be activated for subsequent reaction(s).

This law is also referred to as "photo-equivalence law" which was derived by Albert Einstein when he developed the quantum theory of light.

When a light beam encounters matter the following phenomena can be observed: reflection, diffusion, transmission, refraction, scattering, absorption, and luminescence. Only absorption is of importance in photochemistry in generation of excited states. In photochemical processes, excitation usually takes place by interaction between one photon and one molecule (multiphoton-excitation will be discussed in **Chapter 6**), so called photoexcitation:

$$R + h\nu \rightarrow R^*$$

where R and R* denote a molecule in its ground and an electronically excited state. The energy of the molecule in an electronically excited state is generally higher than that of the ground state by *ca.* 150 – 1200 kJ/einstein (mole of photons).[149] Photoexcitation can only occur if the difference between the energy of any of the excited states (E_E) and the ground state (E_G) is equal to the energy of the incident photon ($h\nu$):[151]

$$E_E - E_G = h\nu$$

Oscillator strength f is used to describe the possibility of light absorption for a certain transition and is given by: [151]

$$f \equiv \frac{8\pi^2 m_e \nu |\mu|^2}{3he^2} \qquad \mu \equiv \int \Psi_G \hat{H} \Psi_E d\tau$$

where m_e is mass of an electron, μ transition dipole moment, e, charge of an electron, $\hat{H}$, dipole moment operator, $\Psi_{G/E}$, wavefunction of ground/excited state.

The transition dipole moment μ can be zero for certain transitions, in which cases, the oscillator strength f is zero and the transition is hence forbidden. The selection rules states that under the following conditions the transition dipole moment is zero:[149]

- between states of different multiplicity ($\Delta S = 0$, spin-forbidden);
- between states of equal parity (g→g, u→u) ($\Delta l = \pm 1$, orbitally forbidden, also called Laporte Rule);
- the simultaneous excitation of two or more electrons.

Absorption of light in a homogenous medium is often expressed as absorbance (A):

$$A = \log (P_\lambda^0 / P_\lambda) = -\log T$$

where T is the internal transmittance, P_λ^0 the spectral radiant power of incident radiation at wavelength λ, P_λ the radiant power of transmitted radiation. The absorbance of a beam of collimated monochromatic radiation in a homogeneous isotropic solution is proportional to the absorption pathlength l (cm), and to the concentration c (M):

$$A = \varepsilon c l$$

where ε is called the molar absorption coefficient or extinction coefficient ($M^{-1}cm^{-1}$). This law is called the Beer-Lambert Law.

1.3.2 Photochemistry of coordination compounds

1.3.2.1 Electronic transitions

Electronic transitions in general consist in promotion of an electron from one of the highest occupied molecular orbitals (HOMOs) to one of the lowest unoccupied

molecular orbitals (LUMOs) of the molecule. For octahedral transition metal complexes, their molecule orbitals (MOs) can be classified according to their predominant atomic orbital contributions (**Figure 1.8**):[152]

1. Strongly bonding, predominantly ligand centered σ_L orbitals;
2. Bonding, predominantly ligand-centered π_L orbitals;
3. Essentially nonbonding, metal-centered π_M orbitals of t_{2g} symmetry;
4. Antibonding, predominantly metal-centered σ_M^* orbitals of e_g symmetry;
5. Antibonding, predominantly ligand-centered π_L^* orbitals;
6. Strongly antibonding, predominantly metal-centered σ_M^* orbitals.

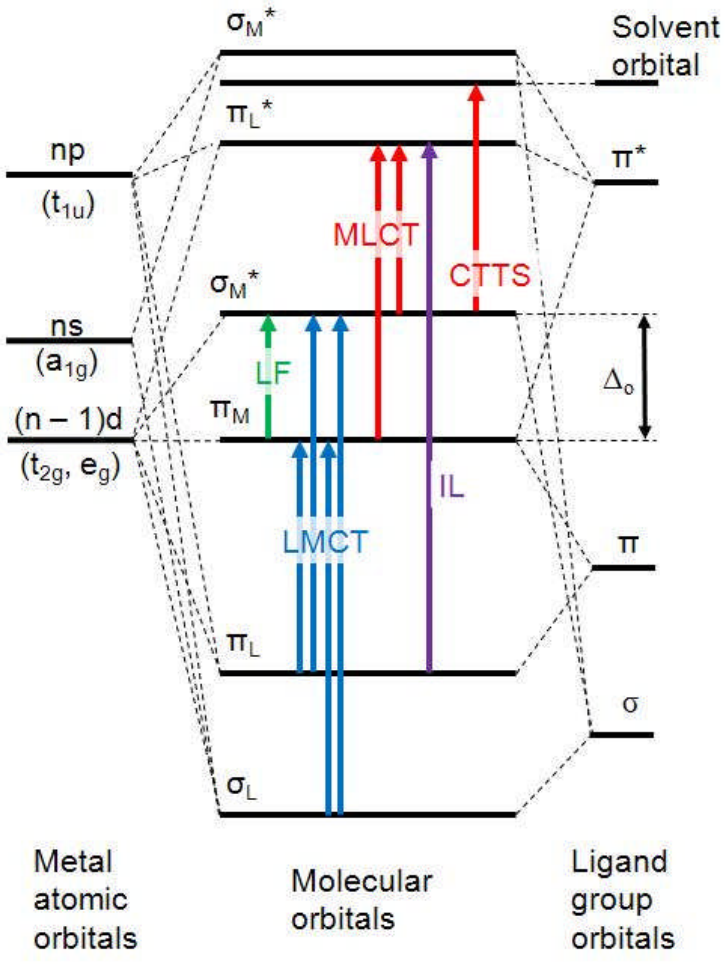

Figure 1.8 Molecule orbitals (MOs) and electronic transitions for an octahedral transition metal complex.[149, 152]

Light can induce a variety of electronic transitions of a transition metal coordination complexes between the MOs shown in **Figure 1.8**,[135, 153] such as ligand-field (LF) transitions or *d-d* transitions, ligand-to-metal-charge-transfer (LMCT) transitions, metal-to-ligand-charge-transfer (MLCT) transitions, charge-transfer-to-solvent (CTTS) transitions and intra-ligand (IL) transitions. For multinuclear complexes, there is a transfer from one central atom to the other: inter-valence-charge-transfer (IVCT) transitions.

The selection rules (*vide supra*) govern the transition in metal complexes. Any transitions with equal parity (i.e. the same symmetry) with respect to the inversion centre, e.g. d→d transitions in a centrosymmetric complex, are Laporte forbidden. However, forbidden transitions still can be observed experimentally, despite their low intensity. For example, if the complex is slightly distorted due to the Jahn-Teller effect, or if the complex undergoes an asymmetrical vibration, the inversion centre is hence destroyed. Also, when π-acceptor and π-donor ligands are mixed with the d-orbitals (d-p mixing), the transitions are no longer purely d-d. In these cases, the Laporte selection rule is relaxed.

The intensities of different transitions are shown in **Table 1.4**, with clear differences in the extinction coefficient depending on whether the transition is allowed or forbidden.

Table 1.4 Intensities of spectroscopic bands in metal complexes.[154]

Band/Transition type	Allowed/forbidden	ε_{max} (L mol^{-1}cm^{-1})
$\Delta S = 0$	Spin-forbidden	< 1
Ligand-field (LF) with centre of symmetry	Laporte-forbidden	~ 10
Ligand-field (LF) without centre of symmetry	Laporte-allowed	~ 10^2
Charge-transfer(CT)	Orbital- and spin-allowed	$10^3 – 10^6$
Intra-ligand (IL)	Orbital- and spin-allowed	$10^3 – 10^5$
Charge-transfer-to-solvent (CTTS)	Orbital- and spin-allowed	$10 – 10^3$

1.3.2.2 Deactivation pathways

The photoexcitation and the variety of deactivation pathways are shown in **Figure 1.9**. Absorption of a photon leads to population of the electronic excited state of the same multiplicity, e.g. from the singlet S_0 ground state to the singlet excited state S_1, S_2, or S_n state, depending on the absorbed photon energy. When excitation leads to higher vibrational states of S_n, the molecular entity relaxes fast into vibrational equilibrium with its environment. The excited state deactivation may also proceed via internal conversion (IC) or intersystem crossing (ISC). The triplet states (differ from the ground state multiplicity) are normally populated via intersystem crossing. The lowest excited states are the relatively long lived, especially those with different multiplicity from the ground state. Therefore, they are the source of luminescence and, moreover, are most often responsible for a photochemical reaction.

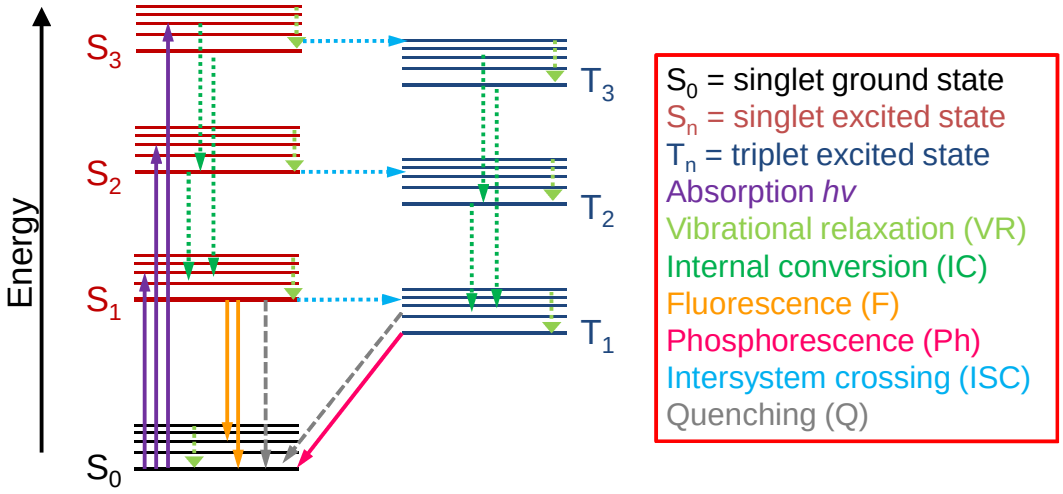

Figure 1.9 Jabłoński diagram. All possible physical processes are represented by solid (radiative) and dashed (radiationless) lines.[149]

Radiationless deactivation processes involve vibrational relaxation (VR), internal conversion (IC), intersystem crossing (ISC), and quenching (Q). Radiative deactivation processes such as fluorescence (F) (singlet–singlet) and phosphorescence (Ph) (triplet–singlet) result in an emission of light with a longer wavelength than that of excitation. Quenching refers to the external environmental influence or even substituent in the excited molecule may also induce the deactivation through a non-radiative inter- or intra-molecular process, respectively. The approximate timescales for these transitions are listed in **Table 1.5**.

Table 1.5 The approximate timescales for the transitions.[150]

Process	Transition	Timescale (s)
Photoexcitation	$S_0 \rightarrow S_n$	*ca.* 10^{-15} (instantaneous)
Internal Conversion	$S_n \rightarrow S_1$	10^{-14} to 10^{-11}
Vibrational Relaxation	$S_n^* \rightarrow S_n$	10^{-12} to 10^{-10}
Intersystem Crossing	$S_1 \rightarrow T_1$	10^{-11} to 10^{-6}
Fluorescence	$S_1 \rightarrow S_0$	10^{-9} to 10^{-6}
Phosphorescence	$T_1 \rightarrow S_0$	10^{-3} to 10^{2}
Non-Radiative Decay	$S_1 \rightarrow S_0$	10^{-7} to 10^{-5}
	$T_1 \rightarrow S_0$	10^{-3} to 10^{2}

1.3.2.3 Photochemical reactions

Photochemical reaction is another deactivation pathway competing with the photophysical decay mechanisms, such as fluorescence and phosphorescence. Photochemical reactions start from excited states, and are hence distinct from thermal reactions that originate from ground electronic states. The energy of a molecular entity in an excited state is usually 150 – 1200 kJ/mol over its ground state, and hence exceeds very much the typical ground state thermal reaction activation energy (E_a = 30 kJ/mol). The activation of an excited reactant needs only negligible activation energy (E_a^* *ca.* 8 – 17 kJ/mol); thereby some new reaction channels can be opened (**Figure 1.10**).

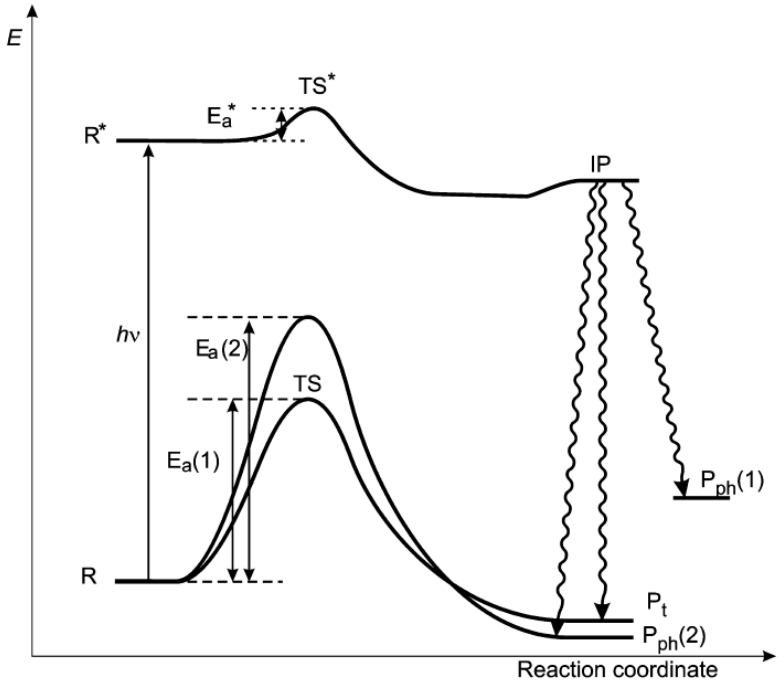

Figure 1.10 Comparison of thermal and photochemical reaction courses; R and R* are the ground state and excited state of the reactant, TS and TS* the corresponding transition states, E_a and E_a^* the corresponding activation energies, respectively; IP means the intermediate photochemical product; P_t and P_{ph} signify products of the thermal and photochemical reactions, respectively. (Adapted from ref.[149])

The transition of electron to an excited state is accompanied by angular or spatial electron shift, leading to the weakening of some bonds within the molecule. The reaction of an excited state may be generally classified as intramolecular or intermolecular. The major types of photoreaction are illustrated in **Figure 1.11**.

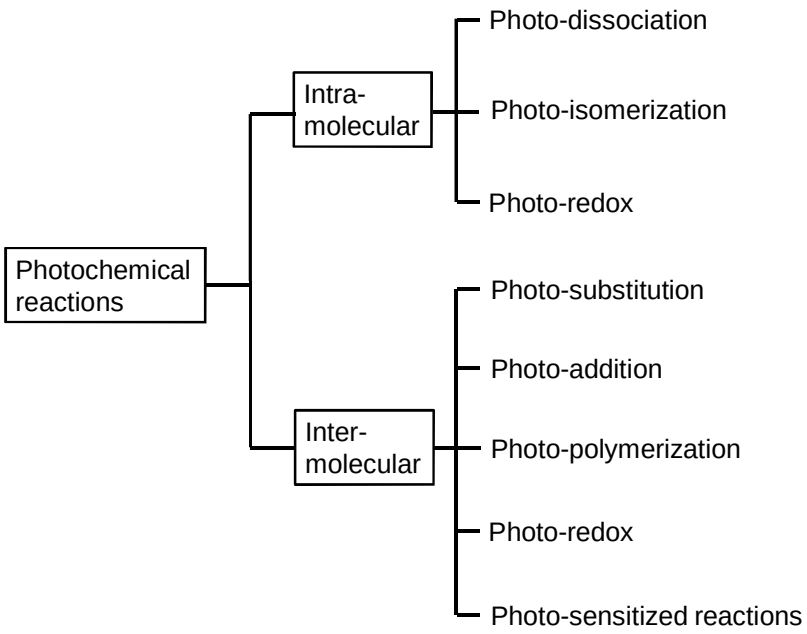

Figure 1.11 Major types of photochemical reactions.[149]

1.3.2.4 Photochemistry of platinum complexes

The photochemical properties of platinum compounds were first recognized in photographic processes during the 1850s.[155] The solutions of Pt^{IV} complexes are long believed to undergo rapid photochemical reaction in light.[10] In 1970s, the photochemistry of $[Pt(CN)_nX_2]$ (n = 2 or 4 for Pt^{II} or Pt^{IV} complexes, respectively) was reported.[135] In aqueous solution, when X = Cl^-, photoaquations, photosubstitutions and photoisomerisations are often observed; whereas when X = N_3^- and NO_2^-, photoreductions, i.e. Pt^{IV} to Pt^{II}, prevail. Interestingly, when the solvent is methanol, irradiation towards the Pt^{IV} complex $[Pt(CN)_4Cl_2]^{2-}$ into its LMCT bands lead to an effective photoreduction, resulting the $[Pt(CN)_4]^{2-}$ complex. When water is the solvent, photoaquation occurs, forming $[Pt(CN)_4OH_2]^{2-}$.[135]

In metal azido complexes, azide is asymmetric with bond lengths which compare well with those of diimide (1.23 Å), and N_2 (1.095 Å).[6] The structure of bound azide is therefore best described as a resonance hybrid (**Figure 1.12**). By contrast, the free

azide anion (N_3^-) in aqueous solution is linear and symmetric, possessing equal N-N distances of ~1.17 Å.

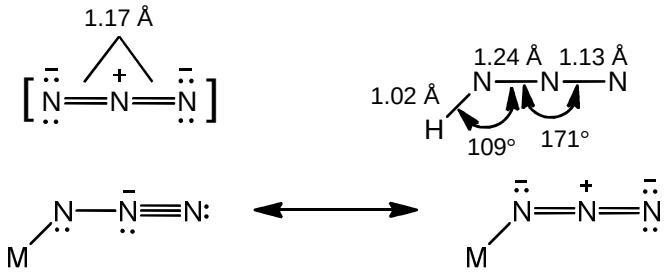

Figure 1.12 Bond lengths and angles of azide in the form of free anion (N_3^-), bound to hydrogen (hydrazoic acid HN_3) and bound to a metal (M-N_3).[6]

Photochemistry of metal azido compounds has been reviewed recently.[156, 157] It has been stated in the literature that almost any transition metal azide complex is light sensitive regardless of its oxidation state.[158-160] The photoreaction of metal azido complexes can involve the following processes.

- Forming nitrene intermediate [161-166]
- Forming nitrido complexes[167-169]
- Forming azidyl radicals (which recombine to give N_2)[170-173]
- Photoeliminations [170, 174, 175]
- Photosubstitutions [176, 177]
- Photoisomerizations [178, 179]
- Photosensitize singlet oxygen [180, 181]

This thesis is focused on the photoredox chemistry of platinum azido complexes. Hence an example of first report in 1978 of photoreductive elimination of azide from a platinum centre is described here. Irradiation into the LMCT bands ($N_3 \rightarrow Pt$, 302 nm, ε = 18300 M^{-1} cm^{-1}) of the Pt^{IV} complex $[Pt(CN)_4(N_3)_2]^{2-}$ leads to $[Pt(CN)_4]^{2-}$

and two $\bullet N_3$ radicals, via a simultaneous two-electron reduction avoiding a platinum(III) intermediate (**Figure 1.13**).[182] The $\bullet N_3$ radicals quickly undergo recombination to give N_2.

$$[Pt(N_3)_2(CN)_4]^{2-} \xrightarrow{h\nu} [Pt(CN)_4]^{2-} + 3N_2$$

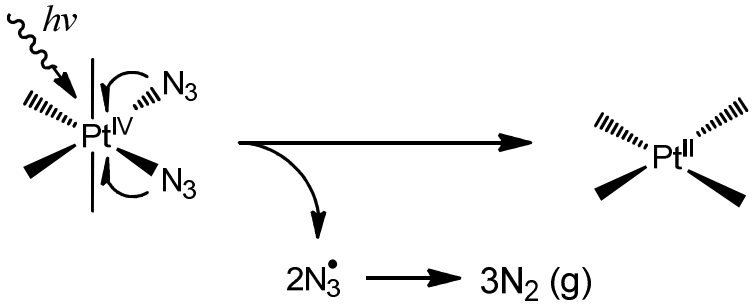

Figure 1.13 Possible mechanism for the photoreduction of a Pt^{IV} diazido complex.[182]

In summary, the photochemistry of metal azido complexes is extensive and varied, so is not simple to predict. The nature of the leaving ligands and the solvent plays important role in determining the photochemical pathway. Therefore, care must be taken with investigations elucidating the pathway(s).

1.3.3 Photodynamic therapy

Photodynamic therapy (PDT) is a treatment using a photosensitive agent (called photosensitizer (PS)) and a particular wavelength of light. The PSs show low or no toxicity towards both tumour and healthy organs and tissues in the absence of irradiation. When the PS is exposed to a specific wavelength of light, the molecule is excited from ground state (singlet state) to excited state (triplet state).

The excited triplet state PS can undergo two types of energy transfer to return to the ground state. In the type I reaction, it can react directly with a substrate, such as the cell membrane or other molecule, and obtain a hydrogen atom (with one electron) to form radicals. These radicals interact with oxygen to produce oxygenated products.

In the type II reaction, energy is transferred from the triplet PS to the ground state oxygen (triplet state, $^3O_2$), and hence a highly reactive oxygen species (singlet oxygen, $^1O_2$) is generated.(**Figure 1.14**) The effects of almost all PSs are oxygen-dependent; photosensitization generally does not occur in anoxic areas of tissue.[183-185]

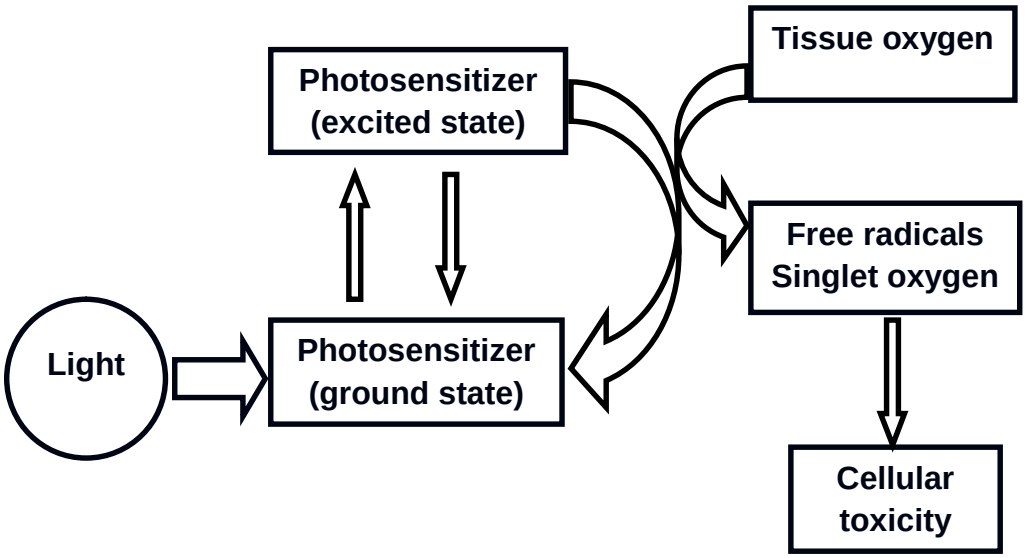

Figure 1.14 Mechanism of photodynamic therapy.[183]

Three main mechanisms are known for PDT-mediated tumour destruction. First, the ROS generated by PDT can directly kill cancer cells. PDT can also damage the vasculature associated with tumour, leading to tumour infarction. Finally, PDT can activate an immune response against tumour cells.[183]

A variety of light resources can be applied in the clinical therapy of PDT. Lamps give a wide spectrum and depending on the filter, various wavelengths can be obtained. LEDs are recently developed light resources, the choice of which range from UVA to infrared with a bandwidth of only 5 – 10 nm. The power output can be up to 150 mW/cm^2.[186] Lasers usually produce a very narrow bandwidth of wavelengths. Recent advances in laser and fibre optic technologies allow physicians

to irradiate internal organs with light of sufficient intensity for PDT. It is now possible to directly irradiate several areas of the body including the bladder, oesophagus, colon, cervix, lung, eyes, head (brain) and neck. By directing light to a localized tumour to selectively activate a photosensitive prodrug, the cytotoxic effects on the tumour can be specifically intensified, thus reducing the side-effects to the normal tissue.[187]

The effective wavelength for phototherapeutic purposes is in the range of *ca.* 600-800 nm (so called the phototherapeutic window). In general, the depth of penetration of light is inversely proportional to the wavelength within the spectrum of visible and near infrared (**Figure 1.15**).[187] For example, light of wavelength 600 – 800 nm is estimated to penetrate 1.5 – 3-fold deeper into tissues than light of 400 – 500 nm (~2 cm vs ~0.75 cm).[188] Near infrared (800 – 1100 nm) penetrates still further,[189] but such a long wavelength has insufficient energy to activate the necessary photochemical processes. Wavelengths shorter than 400 nm have been shown to damage the tissue.[190-192]

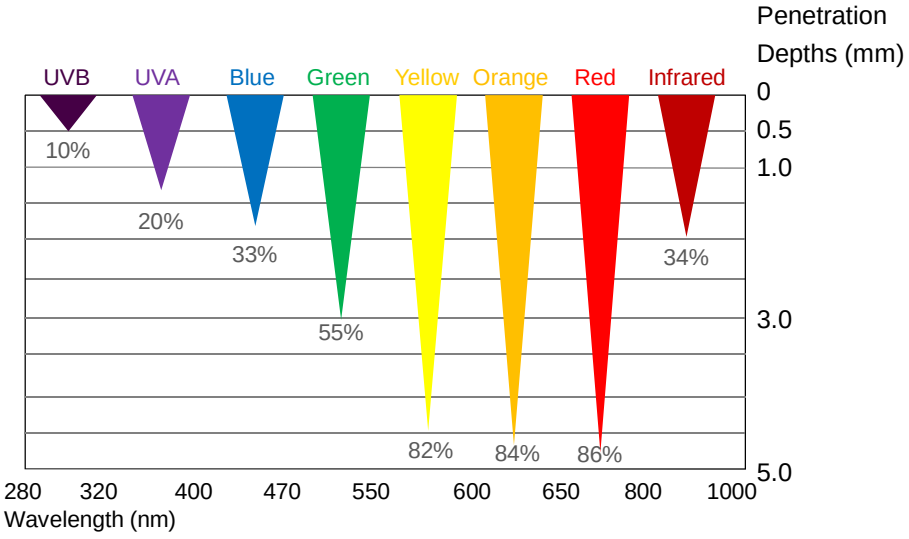

Figure 1.15 Light penetration in human tissues. Adapted from ref.[193]

One of the most important advantages of PDT is that the reactions only occur in the immediate locality of the light-absorbing area. Another major advantage is that it is relatively non-invasive, i.e., repeated dosing is possible and there is no total dose limitation.[135] However, the drawbacks of the photosensitizers seriously impact their usefulness for PDT.[194] The efficiency of PDT is dependent on a reasonably high level of oxygen in target tissue, but cancer cells are typically hypoxic owing to rapid growth.[195, 196] Sometimes the affinity of photosensitizer for selective accumulation in tumour cells is not as good as expected. Appreciable dark toxicity of the photosensitizer may cause nonspecific damage outside of the target tissue. Reactive oxygen species (ROS) can also damage blood components in normal tissue. Many of the synthetic porphyrins have long retention times in the skin. The slow excretion of photosensitizers prolongs the skin photosensitivity, which does extra harm to patients.

1.3.4 Photoactivatable platinum(IV) anticancer complexes

Based on knowledge of the photochemistry of Pt complexes and the idea of PDT, it is possible to design a class of Pt^{IV} anticancer prodrugs that are stable in the dark, but become active upon photoinduced reduction to active form with Pt^{II}. Compared to Pt^{II} species, Pt^{IV} complexes are much more inert to reaction in the ground electronic state but can be made to readily undergo photoinduced reduction and ligand substitution. Accordingly, a site-specific cancer therapy can be performed by exposure of the target tissue to light; the unirradiated drug will be kept intact and quickly excreted from the body without attacking healthy cells.

The first generation of photoactivatable Pt^{IV} anticancer prodrugs was designed and synthesized by Bednarski's group, a series of diiodo-Pt^{IV} complexes (**Figure**

1.16).[147] For examples, *trans*, *cis*-[Pt(OAc)$_2$I$_2$(en)] and *trans*, *cis*-[Pt(OH)$_2$I$_2$(en)] displayed broad ligand-to-metal charge-transfer (LMCT) bands centred at λ = 389 and 384 nm respectively, with a tail up to *ca.* 550 nm.[197] The LMCT (Pt-I) bands are of suitably low energy to give rise to photolytic reduction in the presence of visible light.

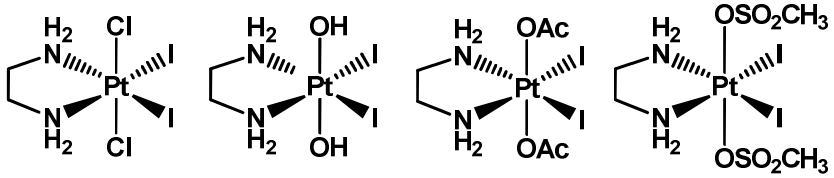

Figure 1.16 Photoactivatable diiodo-Pt^{IV} complexes.

However, the photo-induced anticancer activity and DNA platination level of these complexes are limited, and they were found to be easily reduced by thiols (e.g. glutathione, an intracellular reductant).[197, 198] Therefore, they have been deemed as unsuitable drug candidates.

The Sadler group developed the second generation of photoactivatable anticancer prodrugs: Pt^{IV} diazidodihydroxido complexes.[199-202] (**Figure 1.17**) These complexes possess strong LMCT bands ($N_3 \rightarrow Pt^{IV}$), with λ_{max} between 250 and 290 nm, and absorption tails extending to *ca.* 450 – 500 nm.

The dark stability, photoreactions, nucleotide/DNA binding and cell cytotoxicity for *trans*, *trans*, *trans*-[Pt(N$_3$)$_2$(OH)$_2$(NH$_3$)(Py)],[200] and *trans*, *trans*, *trans*-[Pt(N$_3$)$_2$(OH)$_2$(Py)$_2$],[201] (**Figure 1.17**) have been investigated and the results are promising. Both complexes were shown to have high stability in dark conditions, no reaction with nucleobases such as 5'-GMP and, more importantly, only a very slow reaction with glutathione (GSH) over a period of several weeks. By contrast, upon irradiation of these complexes with UVA (365 nm) or blue light (420/458 nm), these

complexes undergo rapid reductive N_3 ligand substitution, and form various hydrolysis products.[199, 200] In the presence of 5'-GMP in aqueous solution, these complexes can be rapidly reduced to Pt^{II} species upon irradiation with UVA/blue light, producing *trans* azido/guanine and *trans* diguanine Pt^{II} adducts.

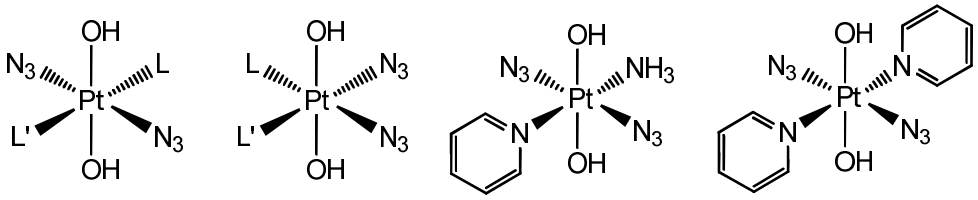

Figure 1.17 Photoactivatable Pt^{IV} diazidodihydroxido anticancer complexes containing either *cis* or *trans* diam(m)mies (L, L' = heterocyclic imines/aliphatic amines). Two examples *trans*, *trans*, *trans*-$[Pt(N_3)_2(OH)_2(NH_3)(Py)]$ and *trans*, *trans*, *trans*-$[Pt(N_3)_2(OH)_2(Py)_2]$ are presented.

Upon irradiation with UVA/blue light, these complexes display potent photocytotoxicity *in vitro* to a range of cancer cells by binding to DNA and thus causing cell death (**Figure 1.18**), despite other possible mechanisms may also be involved.[200, 201] A cytomorphology study showed that upon irradiation, dramatic changes occurred including rapid rounding up of the cells, then cellular shrinkage, loss of contact with neighbouring cells, and a large amount of nuclear packing.[203] These initial results suggest that the mechanism of action of photoactivatable Pt^{IV} dihydroxidodiazido complexes is different from that of cisplatin.

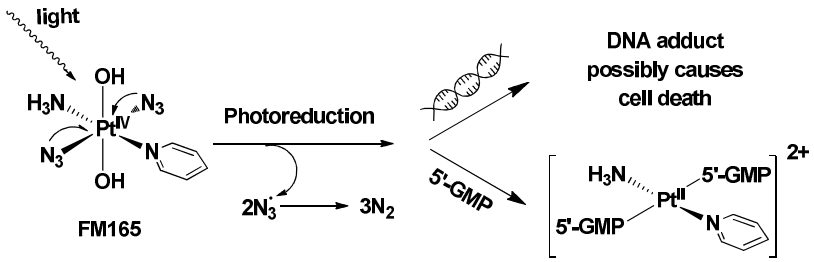

Figure 1.18 Proposed mechanism for photoinduced binding of *trans*, *trans*, *trans*-$[Pt(N_3)_2(OH)_2(NH_3)(Py)]$ to GMP or DNA.[204]

More importantly, it is thought that the DNA binding and anticancer activity are oxygen-independent. This is potentially advantageous compared to photodynamic therapy (PDT), because the PDT requires free oxygen at the target site, but the tumour cells can be hypoxic due to the rapid growth. This treatment is thus named photochemotherapy, which encompasses photodynamic therapy and also the chemotherapy with Pt-based complexes. Various light resources can be applied in the photoactivation, such as lamps, LEDs and lasers.

In recent years, Pt^{IV} tetrachlorido complexes [205] and dichloridodihydroxido complexes[206] have been found to be sensitive to light and undergo facile photoreaction with a range of biomolecules. However, it was later noticed that the thermolysis (323 K) of Pt^{IV} 2,2'-bipyridine complexes lead to identical Pt^{II}–DNA adducts as those from the photoreaction.[207] By contrast, the Pt^{IV} diazidodihydroxido complexes are very stable for at least several hours at 323 K. Also, it was found that Pt^{IV} complexes of the type *trans,trans,trans*-$[PtCl_2(OH)_2LL']$ (L and L' = different aliphatic amines) are toxic in the absence of irradiation with UVA.[148] These results stopped the further development of Pt^{IV} chlorido complexes in photochemotherapy.

Recently, the combination of photochemistry and platinum anticancer drugs has attracted increasing attention. Donzello and coworkers has reported a series of dichloridodipyrido Pt^{II} complexes externally appended to non-Pt metal-centred macrocycle photosensitizers as potential active photo/chemotherapeutic anticancer agents.[208] These complexes combine the features of PDT and chemotherapy by generating singlet oxygen as well as interacting with a G-quadruplex structure of the telomeric DNA.[209] Brewer and coworkers recently reported a Ru^{II}-Pt^{II} dinuclear complex that can be activated by red light in the therapeutic window. This "supramolecule" harvests energy of red light *via* MLCT excitation of the Ru^{II}

chromophore and the energy is imparted onto the *cis*-{$PtCl_2$} bioactive site where photoinduced binding to DNA occurs.[210]

1.3.5 Other metal-based photoactivatable anticancer complexes

A broad range of other metals has also been involved in the development of photoactivatable anticancer drugs.[211]

Ruthenium(II) arene organometallic complexes can exhibit potent anticancer activity.[212, 213] In recent years, Sadler and co-workers have reported the first Ru^{II} arene complex that can selectively photodissociate a pyridine ligand upon excitation with visible light and form a reactive aqua species, which hence can bind to nucleobases.[214] The structure-activity relationship was examined[215] and the photo-induced pyridine substitution for $[Ru^{II}(Bpy)_2(Py)_2]^{2+}$ has been studied by time-resolved X-ray solution scattering.[216] Marchan and coworkers have coupled this type of photoactivatable Ru^{II} arene complexes to a series of cancer cell targeting peptides, such as dicarba analogue of octreotide and RGD tripeptide.[217] Upon irradiation with visible light, reactive aqua species can be released from the conjugates, which reacted with DNA, forming an 1, 2-GpG intrastrand crosslinks.

In recent years, the Chakravarty group have developed a series of Fe^{III}, V^{IV} and Cu^{II} complexes with (derived) phenanthroline ligands, namely, 1,10-phenanthroline, dipyridoquinoxaline and dipyridophenazine, as photoactive anticancer agents. The common features of these complexes are as follows. They can be activated by visible light and even near-IR irradiation. They act as efficient photosensitizers, forming singlet oxygen ($^1O_2$) or hydroxyl radical (•OH) species. They show DNA photo-cleavage or photo-binding activity.[218-221] Very recently, the Chakravarty group reported a super multifunctional Fe^{III} complex[222] with a derived anthracene ligand, a

catechol ligand and nitrate as a leaving group. This complex exerts micro-molar cytotoxicity towards HeLa and MCF-7 cell lines upon irradiation with near-IR-light and negligible dark toxicity. It is also a powerful photosensitizer that photocleaves DNA by a hydroxyl radical pathway. It can also act as fluorophore for cellular imaging. The development of photoactive non-Pt metals anticancer complexes show promising future, and the application of cheap metals (such as Cu and Fe) into anticancer medicine may open a gate to reduce the cost of anti-tumour therapy.

Ideal photoactivable anticancer prodrugs should have the following features:

1. Good solubility in physiological media and efficient accumulation in tumour cells.
2. High stability and low systemic toxicity in the absence of irradiation.
3. Efficient photoactivation with light of as long wavelength as possible in the therapeutic window (600 – 800 nm).
4. Rapid cell death after photoactivation and lower cross-resistance by novel mechanisms of action.

Therefore, complexes with broader clinical utility (longer activation wavelength), greater potency (higher phototocytoxicity) and wider applicability (circumventing cisplatin cross-resistance) are still needed.

1.4 Aims of the thesis

The specific aims of the work carried out in this thesis were as follows:

1. To design and synthesize novel mixed amine ligands in complexes of the type *trans,trans,trans*-[$Pt(N_3)_2(OH)_2(amine_1)(amine_2)$] for more potent

photocytotoxicy, longer activation wavelength, with no compromise of dark stability, and study their photochemistry and photobiochemistry.

2. To investigate photodecomposition and photoreaction pathways of Pt^{IV} diazidodihydroxido complexes, in particular to detect the production of azide activation (e.g. N_3^-, N_3•, N_2), reactive oxygen species (e.g. $^1O_2$, H_2O_2) and adduct with various biomolecules, such as 5'-GMP and a DNA oligonucleotide.
3. To attempt to increase the wavelength of light activation of Pt^{IV} (di)azido complexes by suitable derivation of the amine ligands or by two-photon activation.

This work involves a wide range of techniques including ^1H, ^{14}N, ^{195}Pt NMR, UV-Vis, HPLC, MS, EPR and fluorescence, etc.

1.5 References

1. F. R. Hartley, *The chemistry of platinum and palladium: with particular reference to complexes of the elements*, Wiley, Weinheim, Germany, 1973.
2. N. N. Greenwood and A. Earnshaw, *Chemistry of the Elements, 2nd Edition*, Elsevier, Oxford, UK, 1997.
3. S. A. Cotton, *Chemistry of precious metals*, Blackie Academic & Professional, London, UK, 1997.
4. R. Shannon, *Acta Cryst. A*, 1976, **32**, 751-767.
5. I. M. Ismail, S. J. S. Kerrison and P. J. Sadler, *Polyhedron*, 1982, **1**, 57-59.
6. N. Turova, *Inorganic Chemistry in Tables*, Springer-Verlag Berlin Heidelberg 2011.
7. J. Reedijk, *Platinum Met. Rev.*, 2008, **52**, 2-11.
8. R. G. Pearson, *J. Chem. Educ.*, 1968, **45**, 581.

9. G. L. Miessler and D. A. Tarr, *Inorganic Chemistry, 3rd Edition*, Pearson Eduation, New Jersey, 2004.
10. F. A. Cotton, G. Wilkinson, C. A. Murillo and M. Bochmann, *Advanced Inorganic Chemistry, 6th Edition*, John Wiley and Sons, Inc., New York, NY, 1999.
11. F. A. Cotton and G. Wilkinson, *Advanced Inorganic Chemistry, 5th Edition*, John Wiley and Sons, New York, NY, 1988.
12. F. R. Hartley, *Chem. Soc. Rev.*, 1973, **2**, 163-179.
13. B. Rosenberg, L. Van Camp and T. Krigas, *Nature*, 1965, **205**, 698-699.
14. B. Rosenberg, L. Vancamp, J. E. Trosko and V. H. Mansour, *Nature*, 1969, **222**, 385-386.
15. L. Kelland, *Nat. Rev. Cancer*, 2007, **7**, 573-584.
16. S. C. Sweetman, *Martindale: The complete drug reference*, Pharmaceutical Press, London, 35th edn., 2007.
17. N. J. Wheate, S. Walker, G. E. Craig and R. Oun, *Dalton Trans.*, 2010, **39**, 8113-8127.
18. A. Eastman, in *Cisplatin:Chemistry and Biochemistry of a Leading Anticancer Drug*, ed. B. Lippert, Verlag Helvetica Chimica Acta, Zurich, 1999, pp. 111-134.
19. J. Reedijk, *Eur. J. Inorg. Chem.*, 2009, 1303-1312.
20. K. J. Barnham, M. I. Djuran, P. Del Socorro Murdoch, J. D. Ranford and P. J. Sadler, *Inorg. Chem.*, 1996, **35**, 1065-1072.
21. R. C. DeConti, B. R. Toftness, R. C. Lange and W. A. Creasey, *Cancer Res.*, 1973, **33**, 1310-1315.
22. D. P. Gately and S. B. Howell, *Br. J. Cancer*, 1993, **67**, 1171-1176.

23. S. Ishida, J. Lee, D. J. Thiele and I. Herskowitz, *Proc. Natl. Acad. Sci. USA*, 2002, **99**, 14298-14302.

24. S. J. Berners-Price and T. G. Appleton, in *Platinum-Based Drugs in Cancer Therapy*, eds. L. R. Kelland and N. P. Farrell, Humana Press, Totowa, New Jersey, USA, 2000, pp. 3 - 36.

25. M. S. Davies, S. J. Berners-Price and T. W. Hambley, *Inorg. Chem.*, 2000, **39**, 5603-5613.

26. D. P. Bancroft, C. A. Lepre and S. J. Lippard, *J. Am. Chem. Soc.*, 1990, **112**, 6860-6871.

27. S. J. Berners-Price, T. A. Frenkiel, U. Frey, J. D. Ranford and P. J. Sadler, *J. Chem. Soc., Chem. Commun.*, 1992, 789-791.

28. K. J. Barnham, S. J. Bernersprice, T. A. Frenkiel, U. Frey and P. J. Sadler, *Angew. Chem. Int. Ed.*, 1995, **34**, 1874-1877.

29. F. Legendre and J.-C. Chottard, in *Cisplatin:Chemistry and Biochemistry of a Leading Anticancer Drug*, ed. B. Lippert, Verlag Helvetica Chimica Acta, Zurich, 1999, pp. 223-245.

30. E. R. Jamieson and S. J. Lippard, *Chem. Rev.*, 1999, **99**, 2467-2498.

31. P. M. Takahara, A. C. Rosenzweig, C. A. Frederick and S. J. Lippard, *Nature*, 1995, **377**, 649-652.

32. H. Huang, L. Zhu, B. R. Reid, G. P. Drobny and P. B. Hopkins, *Science*, 1995, **270**, 1842-1845.

33. Y. Jung and S. J. Lippard, *Chem. Rev.*, 2007, **107**, 1387-1407.

34. Z. J. Guo and P. J. Sadler, *Adv. Inorg. Chem.*, 2000, **49**, 183-306.

35. D. R. Boer, A. Canals and M. Coll, *Dalton Trans.*, 2009, 399-414.

36. R. N. Bose, *Mini-Rev. Med. Chem.*, 2002, **2**, 103-101.

37. P. J. O'Dwyer, J. P. Stevenson and S. W. Johnson, in *Cisplatin:Chemistry and Biochemistry of a Leading Anticancer Drug*, ed. B. Lippert, Verlag Helvetica Chimica Acta, Zurich, 1999, ch. 2, pp. 29-69.

38. W. Hu, Q. Luo, K. Wu, X. Li, F. Wang, Y. Chen, X. Ma, J. Wang, J. Liu, S. Xiong and P. J. Sadler, *Chem. Commun.*, 2011, **47**, 6006-6008.

39. S. Kelley, A. Basu, B. Teicher, M. Hacker, D. Hamer and J. Lazo, *Science*, 1988, **241**, 1813-1815.

40. P. Mistry, L. R. Kelland, G. Abel, S. Sidhar and K. R. Harrap, *Br. J. Cancer*, 1991, **64**, 215-220.

41. H. Li, T.-Y. Lin, S. L. Van Orden, Y. Zhao, M. P. Barrow, A. M. Pizarro, Y. Qi, P. J. Sadler and P. B. O'Connor, *Anal. Chem.*, 2011, **83**, 9507-9515.

42. H. L. Li, Y. Zhao, H. I. A. Phillips, Y. L. Qi, T. Y. Lin, P. J. Sadler and P. B. O'Connor, *Anal. Chem.*, 2011, **83**, 5369-5376.

43. J. P. Williams, H. I. A. Phillips, I. Campuzano and P. J. Sadler, *J. Am. Soc. Mass. Spectrom.*, 2010, **21**, 1097-1106.

44. C. Sze, G. Khairallah, Z. Xiao, P. Donnelly, R. O'Hair and A. Wedd, *J. Biol. Inorg. Chem.*, 2009, **14**, 163-165.

45. F. Arnesano, S. Scintilla and G. Natile, *Angew. Chem. Int. Ed.*, 2007, **46**, 9062-9064.

46. F. Kratz, *Metal Complexes in Cancer Chemotherapy*, VCH, Weinheim, Germany, 1993.

47. A. I. Ivanov, J. Christodoulou, J. A. Parkinson, K. J. Barnham, A. Tucker, J. Woodrow and P. J. Sadler, *J. Biol. Chem.*, 1998, **273**, 14721-14730.

48. R. F. Borch and M. E. Pleasants, *Proc. Natl. Acad. Sci. USA*, 1979, **76**, 6611-6614.

49. E. L. M. Lempers and J. Reedijk, *Adv. Inorg. Chem.*, 1991, **37**, 175-217.

50. P. A. Andrews, W. E. Wung and S. B. Howell, *Anal. Biochem.*, 1984, **143**, 46-56.

51. A. R. Timerbaev, C. G. Hartinger, S. S. Aleksenko and B. K. Keppler, *Chem. Rev.*, 2006, **106**, 2224-2248.

52. L. R. Kelland, G. Abel, M. J. Mckeage, M. Jones, P. M. Goddard, M. Valenti, B. A. Murrer and K. R. Harrap, *Cancer Res.*, 1993, **53**, 2581-2586.

53. X. Wang, X. Du, H. Li, D. S.-B. Chan and H. Sun, *Angew. Chem. Int. Ed.*, 2011, **50**, 2706-2711.

54. K. R. Harrap, *Cancer Treat Rev.*, 1985, **12, Supplement A**, 21-33.

55. R. J. Knox, F. Friedlos, D. A. Lydall and J. J. Roberts, *Cancer Res.*, 1986, **46**, 1972.

56. L. R. Kelland, *Expert Opin. Inv. Drug*, 2000, **9**, 1373-1382.

57. L. R. Kelland, B. A. Murrer, G. Abel, C. M. Giandomenico, P. Mistry and K. R. Harrap, *Cancer Res.*, 1992, **52**, 822.

58. M. Dabholkar, F. Bostick-Bruton, C. Weber, V. A. Bohr, C. Egwuagu and E. Reed, *J. Natl. Cancer Ins.*, 1992, **84**, 1512-1517.

59. G. Gifford, J. Paul, P. A. Vasey, S. B. Kaye and R. Brown, *Clin. Cancer Res.*, 2004, **10**, 4420-4426.

60. S. B. Brown, E. A. Brown and I. Walker, *Lancet Oncol.*, 2004, **5**, 497-508.

61. M. J. Cleare and J. D. Hoeschele, *Bioinorg. Chem.*, 1973, **2**, 187-210.

62. G. Natile and M. Coluccia, *Coord. Chem. Rev.*, 2001, **216**, 383-410.

63. W. Liu, X. Chen, Q. Ye, Y. Xu, C. Xie, M. Xie, Q. Chang and L. Lou, *Inorg. Chem.*, 2011, **50**, 5324-5326.

64. M. Huxley, C. Sanchez-Cano, M. J. Browning, C. Navarro-Ranninger, A. G. Quiroga, A. Rodger and M. J. Hannon, *Dalton Trans.*, 2010, **39**, 11353-11364.

65. J. Ruiz, V. Rodríguez, N. Cutillas, A. Espinosa and M. J. Hannon, *J. Inorg. Biochem.*, 2011, **105**, 525-531.

66. P. Saha, C. Descôteaux, K. Brasseur, S. Fortin, V. Leblanc, S. Parent, É. Asselin and G. Bérubé, *Eur. J. Med. Chem.*, 2012, **48**, 385-390.

67. B. Liskova, L. Zerzankova, O. Novakova, H. Kostrhunova, Z. Travnicek and V. Brabec, *Chem. Res. Toxicol.*, 2012, **25**, 500-509.

68. S. Dhar and S. J. Lippard, *Proc. Natl. Acad. Sci. USA*, 2009.

69. E. Wong and C. M. Giandomenico, *Chem. Rev.*, 1999, **99**, 2451-2466.

70. K. S. Lovejoy and S. J. Lippard, *Dalton Trans.*, 2009, 10651-10659.

71. M. J. Cleare and J. D. Hoeschele, *Platinum Met. Rev.*, 1973, **17**, 2-13.

72. J.-M. Malinge and M. Leng, in *Cisplatin:Chemistry and Biochemistry of a Leading Anticancer Drug*, ed. B. Lippert, Verlag Helvetica Chimica Acta, Zurich, 1999, pp. 159-180.

73. M. Coluccia and G. Natile, *Anti-Cancer Agent Med. Chem.*, 2007, **7**, 111-123.

74. S. M. Aris and N. P. Farrell, *Eur. J. Inorg. Chem.*, 2009, **2009**, 1293-1302.

75. L. Cubo, A. G. Quiroga, J. Y. Zhang, D. S. Thomas, A. Carnero, C. Navarro-Ranninger and S. J. Berners-Price, *Dalton Trans.*, 2009, 3457-3466.

76. M. Van Beusichem and N. Farrell, *Inorg. Chem.*, 1992, **31**, 634-639.

77. N. Farrell, T. T. B. Ha, J. P. Souchard, F. L. Wimmer, S. Cros and N. P. Johnson, *J. Med. Chem.*, 1989, **32**, 2240-2241.

78. S. S. Lange, D. L. Mitchell and K. M. Vasquez, *Proc. Natl. Acad. Sci. USA*, 2008, **105**, 10320-10325.

79. Y. Najajreh, J. M. Perez, C. Navarro-Ranninger and D. Gibson, *J. Med. Chem.*, 2002, **45**, 5189-5195.

80. T. Suchankova, M. Vojtiskova, J. Reedijk, V. Brabec and J. Kasparkova, *J. Biol. Inorg. Chem.*, 2009, **14**, 75-87.

81. C. Bartel, A. Bytzek, Y. Scaffidi-Domianello, G. Grabmann, M. Jakupec, C. Hartinger, M. Galanski and B. Keppler, *J. Biol. Inorg. Chem.*, 2012, **17**, 465-474.

82. M. Leng, A. Schwartz and M. J. Giraud-Panis, in *Platinum-Based Drugs in Cancer Therapy*, eds. L. R. Kelland and N. P. Farrell, Humana Press, Totowa, New Jersey, USA, 2000, pp. 63-85.

83. C. Bauer, T. Peleg-Shulman, D. Gibson and A. H. J. Wang, *Eur. J. Biochem.*, 1998, **256**, 253-260.

84. X. Gao, X. Wang, J. Ding, L. Lin, Y. Li and Z. Guo, *Inorg. Chem. Commun.*, 2006, **9**, 722-726.

85. S. Wu, X. Wang, C. Zhu, Y. Song, J. Wang, Y. Li and Z. Guo, *Dalton Trans.*, 2011, **40**, 10376-10382.

86. K. S. Lovejoy, R. C. Todd, S. Zhang, M. S. McCormick, J. A. D'Aquino, J. T. Reardon, A. Sancar, K. M. Giacomini and S. J. Lippard, *Proc. Natl. Acad. Sci. USA*, 2008, **105**, 8902-8907.

87. D. Wang, G. Zhu, X. Huang and S. J. Lippard, *Proc. Natl. Acad. Sci. USA*, 2010, **107**, 9584-9589.

88. G. Zhu, M. Myint, W. H. Ang, L. Song and S. J. Lippard, *Cancer Res.*, 2012, **72**, 790-800.

89. N. P. Farrell, in *Platinum-Based Drugs in Cancer Therapy*, eds. L. R. Kelland and N. P. Farrell, Humana Press, Totowa, New Jersey, USA, 2000, pp. 321-338.

90. N. J. Wheate and J. G. Collins, *Coord. Chem. Rev.*, 2003, **241**, 133-145.
91. C. Gao, S. Gou, L. Fang and J. Zhao, *Bioorg. Med. Chem. Lett.*, 2011, **21**, 1763-1766.
92. C. Gao, G. Xu and S. Gou, *Bioorg. Med. Chem. Lett.*, 2011, **21**, 6386-6388.
93. S. Hochreuther, R. Puchta and R. van Eldik, *Inorg. Chem.*, 2011, **50**, 12747-12761.
94. M. Xie, W. Liu, L. Lou, X. Chen, Q. Ye, Y. Yu, Q. Chang and S. Hou, *Inorg. Chem.*, 2010, **49**, 5792-5794.
95. J. Zhu, Y. Zhao, Y. Zhu, Z. Wu, M. Lin, W. He, Y. Wang, G. Chen, L. Dong, J. Zhang, Y. Lu and Z. Guo, *Chem. Eur. J.*, 2009, **15**, 5245-5253.
96. C. Chopard, C. Lenoir, S. Rizzato, M. Vidal, J. Arpalahti, L. Gabison, A. Albinati, C. Garbay and J. i. Kozelka, *Inorg. Chem.*, 2008, **47**, 9701-9705.
97. C. Manzotti, G. Pratesi, E. Menta, R. Di Domenico, E. Cavalletti, H. H. Fiebig, L. R. Kelland, N. Farrell, D. Polizzi, R. Supino, G. Pezzoni and F. Zunino, *Clin. Cancer Res.*, 2000, **6**, 2626-2634.
98. C. Billecke, S. Finniss, L. Tahash, C. Miller, T. Mikkelsen, N. P. Farrell and O. Bögler, *Neuro-Oncol.*, 2006, **8**, 215-226.
99. G. Pratesi, P. Perego, D. Polizzi, S. C. Righetti, R. Supino, C. Caserini, C. Manzotti, F. C. Giuliani, G. Pezzoni, S. Tognella, S. Spinelli, N. Farrell and F. Zunino, *Br. J. Cancer*, 1999, **80**, 1912-1919.
100. J. D. Roberts, J. Peroutka, G. Beggiolin, C. Manzotti, L. Piazzoni and N. Farrell, *J. Inorg. Biochem.*, 1999, **77**, 47-50.
101. T. Servidei, C. Ferlini, A. Riccardi, D. Meco, G. Scambia, G. Segni, C. Manzotti and R. Riccardi, *Eur. J. Cancer*, 2001, **37**, 930-938.

102. J. Kasparkova, J. Zehnulova, N. Farrell and V. Brabec, *J. Biol. Chem.*, 2002, **277**, 48076-48086.

103. D. I. Jodrell, T. R. J. Evans, W. Steward, D. Cameron, J. Prendiville, C. Aschele, C. Noberasco, M. Lind, J. Carmichael, N. Dobbs, G. Camboni, B. Gatti and F. De Braud, *Eur. J. Cancer*, 2004, **40**, 1872-1877.

104. T. A. Hensing, N. H. Hanna, H. H. Gillenwater, M. Gabriella Camboni, C. Allievi and M. A. Socinski, *Anticancer Drugs*, 2006, **17**, 697-704.

105. J. Rautio, H. Kumpulainen, T. Heimbach, R. Oliyai, D. Oh, T. Jarvinen and J. Savolainen, *Nat. Rev. Drug Discov.*, 2008, **7**, 255-270.

106. F. Kratz, I. A. Müller, C. Ryppa and A. Warnecke, *Chemmedchem*, 2008, **3**, 20-53.

107. M. Mitsunaga, M. Ogawa, N. Kosaka, L. T. Rosenblum, P. L. Choyke and H. Kobayashi, *Nat. Med.*, 2011, **17**, 1685-1691.

108. S. S. Dharap, Y. Wang, P. Chandna, J. J. Khandare, B. Qiu, S. Gunaseelan, P. J. Sinko, S. Stein, A. Farmanfarmaian and T. Minko, *Proc. Natl. Acad. Sci. USA*, 2005, **102**, 12962-12967.

109. S. Mukhopadhyay, C. M. Barnés, A. Haskel, S. M. Short, K. R. Barnes and S. J. Lippard, *Bioconjugate Chem.*, 2008, **19**, 39-49.

110. M. W. Ndinguri, R. Solipuram, R. P. Gambrell, S. Aggarwal and R. P. Hammer, *Bioconjugate Chem.*, 2009, **20**, 1869-1878.

111. S. Hatakeyama, K. Sugihara, T. K. Shibata, J. Nakayama, T. O. Akama, N. Tamura, S.-M. Wong, A. A. Bobkov, Y. Takano, C. Ohyama, M. Fukuda and M. N. Fukuda, *Proc. Natl. Acad. Sci. USA*, 2011, **108**, 19587-19592.

112. H. Maeda, J. Wu, T. Sawa, Y. Matsumura and K. Hori, *J. Controlled Release*, 2000, **65**, 271-284.

113. H. Maeda, *Bioconjugate Chem.*, 2010, **21**, 797-802.

114. S. v. Zutphen and J. Reedijk, *Coord. Chem. Rev.*, 2005, **249**, 2845-2853.

115. S. Dhar, Z. Liu, J. Thomale, H. Dai and S. J. Lippard, *J. Am. Chem. Soc.*, 2008, **130**, 11467-11476.

116. S. Dhar, F. X. Gu, R. Langer, O. C. Farokhzad and S. J. Lippard, *Proc. Natl. Acad. Sci. USA*, 2008, **105**, 17356-17361.

117. S. Dhar, W. L. Daniel, D. A. Giljohann, C. A. Mirkin and S. J. Lippard, *J. Am. Chem. Soc.*, 2009, **131**, 14652-14653.

118. S. Dhar, N. Kolishetti, S. J. Lippard and O. C. Farokhzad, *Proc. Natl. Acad. Sci. USA*, 2011.

119. Y. Min, C. Mao, D. Xu, J. Wang and Y. Liu, *Chem. Commun.*, 2010, **46**, 8424-8426.

120. J. Della Rocca, R. C. Huxford, E. Comstock-Duggan and W. Lin, *Angew. Chem. Int. Ed.*, 2011, **50**, 10330-10334.

121. P. Brooks, R. Clark and D. Cheresh, *Science*, 1994, **264**, 569-571.

122. M. Friedlander, P. C. Brooks, R. W. Shaffer, C. M. Kincaid, J. A. Varner and D. A. Cheresh, *Science*, 1995, **270**, 1500-1502.

123. A. Erdreich-Epstein, H. Shimada, S. Groshen, M. Liu, L. S. Metelitsa, K. S. Kim, M. F. Stins, R. C. Seeger and D. L. Durden, *Cancer Res.*, 2000, **60**, 712-721.

124. R. Pasqualini, E. Koivunen, R. Kain, J. Lahdenranta, M. Sakamoto, A. Stryhn, R. A. Ashmun, L. H. Shapiro, W. Arap and E. Ruoslahti, *Cancer Res.*, 2000, **60**, 722-727.

125. S. S. Dharap and T. Minko, *Pharm. Res.*, 2003, **20**, 889-896.

126. C. Mamot, D. C. Drummond, K. Hong, D. B. Kirpotin and J. W. Park, *Drug Resist. Update*, 2003, **6**, 271-279.

127. R.-D. Hofheinz, S. U. Gnad-Vogt, U. Beyer and A. Hochhaus, *Anticancer Drugs*, 2005, **16**, 691-707.

128. T. Boulikas, *Expert Opin. Inv. Drug*, 2009, **18**, 1197-1218.

129. N. Mylonakis, A. Athanasiou, N. Ziras, J. Angel, A. Rapti, S. Lampaki, N. Politis, C. Karanikas and C. Kosmas, *Lung Cancer*, 2010, **68**, 240-247.

130. C. F. Jehn, T. Boulikas, A. Kourvetaris, K. Possinger and D. Lüftner, *Anticancer Res.*, 2007, **27**, 471-475.

131. D. P. Nowotnik and E. Cvitkovic, *Adv. Drug. Delivery Rev.*, 2009, **61**, 1214-1219.

132. D. P. Nowotnik, *Curr. Bioact. Compd.*, 2011, **7**, 21-26.

133. M. Serova, A. Ghoul, K. Rezaï, F. Lokiec, E. Cvitkovic, D. Nowotnik, S. Faivre and E. Raymond, eds. A. Bonetti, R. Leone, F. M. Muggia and S. B. Howell, Humana Press, 2009, pp. 41-47.

134. M. L. Tobe, *Inorganic Reaction Mechanisms*, Nelson, London, 1972.

135. P. J. Bednarski, F. S. Mackay and P. J. Sadler, *Anti-Cancer Agent Med. Chem.*, 2007, **7**, 75-93.

136. E. G. Talman, Y. Kidani, L. Mohrmann and J. Reedijk, *Inorg. Chim. Acta*, 1998, **283**, 251-255.

137. M. D. Hall and T. W. Hambley, *Coord. Chem. Rev.*, 2002, **232**, 49-67.

138. C. F. Chin, D. Y. Q. Wong, R. Jothibasu and W. H. Ang, *Curr. Top. Med. Chem.*, 2011, **11**, 2602-2612.

139. A. Nemirovski, Y. Kasherman, Y. Tzaraf and D. Gibson, *J. Med. Chem.*, 2007, **50**, 5554-5556.

140. M. D. Hall, S. Amjadi, M. Zhang, P. J. Beale and T. W. Hambley, *J. Inorg. Biochem.*, 2004, **98**, 1614-1624.

141. H. Choy, C. Park and M. Yao, *Clin. Cancer Res.*, 2008, **14**, 1633-1638.

142. S. Choi, C. Filotto, M. Bisanzo, S. Delaney, D. Lagasee, J. L. Whitworth, A. Jusko, C. Li, N. A. Wood, J. Willingham, A. Schwenker and K. Spaulding, *Inorg. Chem.*, 1998, **37**, 2500-2504.

143. M. R. Reithofer, A. K. Bytzek, S. M. Valiahdi, C. R. Kowol, M. Groessl, C. G. Hartinger, M. A. Jakupec, M. Galanski and B. K. Keppler, *J. Inorg. Biochem.*, 2011, **105**, 46-51.

144. U. Olszewski, E. Ulsperger, K. Geissler and G. Hamilton, *J. Exp. Pharmacol.*, 2011, **3**, 43-50.

145. J. Z. Zhang, E. Wexselblatt, T. W. Hambley and D. Gibson, *Chem. Commun.*, 2012.

146. M. D. Hall, H. R. Mellor, R. Callaghan and T. W. Hambley, *J. Med. Chem.*, 2007, **50**, 3403-3411.

147. N. A. Kratochwil and P. J. Bednarski, *Arch. Pharm.*, 1999, **332**, 279-285.

148. L. Cubo, T. W. Hambley, P. J. Sanz Miguel, A. Carnero, C. Navarro-Ranninger and A. G. Quiroga, *Dalton Trans.*, 2011, **40**, 344-347.

149. G. Stochel, M. Brindell, W. Macyk, Z. Stasicka and K. Szacilowski, *Bioinorganic Photochemistry*, John Wiley & Sons, Ltd., Chichester, United Kingdom, 2009.

150. W. Reusch, Photochemistry, http://www2.chemistry.msu.edu/faculty/reusch/VirtTxtJml/photchem.htm, Accessed 31, Mar, 2012.

151. J. Sýkora and J. Šima, *Coord. Chem. Rev.*, 1990, **107**, 1-212.

152. V. Balzani, G. Bergamini, S. Campagna and F. Puntoriero, in *Top. Curr. Chem.*, eds. V. Balzani and S. Campagna, Springer-Verlag, Berlin Heidelberg, 2007, vol. 280, pp. 1-36.
153. N. J. Farrer, L. Salassa and P. J. Sadler, *Dalton Trans.*, 2009, 10690-10701.
154. H. Phillips, PhD thesis, University of Warwick, 2011.
155. A. Gottlieb, *J. Am. Inst. Conserv.*, 1995, **34**, 11 - 32.
156. J. Šima, *Coord. Chem. Rev.*, 2006, **250**, 2325-2334.
157. A. L. Poznyak and V. I. Pavlovski, *Angew. Chem. Int. Ed.*, 1988, **27**, 789-796.
158. A. Villinger and A. Schulz, *Angew. Chem. Int. Ed.*, 2010, **49**, 8017-8020.
159. R. Haiges, J. A. Boatz and K. O. Christe, *Angew. Chem. Int. Ed.*, 2010, **49**, 8008-8012.
160. R. Haiges, J. A. Boatz, J. M. Williams and K. O. Christe, *Angew. Chem. Int. Ed.*, 2011, **50**, 8828-8833.
161. J. L. Reed, H. D. Gafney and F. Basolo, *J. Am. Chem. Soc.*, 1974, **96**, 1363-1369.
162. H. D. Gafney, J. L. Reed and F. Basolo, *J. Am. Chem. Soc.*, 1973, **95**, 7998-8005.
163. R. Ngai, Y. H. L. Wang and J. L. Reed, *Inorg. Chem.*, 1985, **24**, 3802-3807.
164. R. M. Dahlgren and J. I. Zink, *Inorg. Chem.*, 1979, **18**, 597-602.
165. G. Ferraudi and J. F. Endicott, *Inorg. Chem.*, 1973, **12**, 2389-2396.
166. M. Katz and H. D. Gafney, *Inorg. Chem.*, 1978, **17**, 93-99.
167. W. D. Wagner and K. Nakamoto, *J. Am. Chem. Soc.*, 1989, **111**, 1590-1598.
168. K. Meyer, E. Bill, B. Mienert, T. Weyhermüller and K. Wieghardt, *J. Am. Chem. Soc.*, 1999, **121**, 4859-4876.

169. C. A. Grapperhaus, B. Mienert, E. Bill, T. Weyhermüller and K. Wieghardt, *Inorg. Chem.*, 2000, **39**, 5306-5317.

170. A. Vogler and J. Hlavatsch, *Angew. Chem. Int. Ed.*, 1983, **22**, 154-155.

171. A. Vogler, C. Quett, A. Paukner and H. Kunkely, *J. Am. Chem. Soc.*, 1986, **108**, 8263-8265.

172. G. Ferraudi and J. F. Endicott, *J. Am. Chem. Soc.*, 1973, **95**, 2371-2372.

173. J. Strähle, *J. Organomet. Chem.*, 1995, **488**, 15-24.

174. A. Becalska, R. J. Batchelor, F. W. B. Einstein, R. H. Hill and B. J. Palmer, *Inorg. Chem.*, 1992, **31**, 3118-3123.

175. H. Kunkely and A. Vogler, *Inorg. Chem. Commun.*, 2003, **6**, 553-554.

176. V. M. Miskowski, G. L. Nobinger and G. S. Hammond, *Inorg. Chem.*, 1976, **15**, 2904-2907.

177. J. F. Endicott and G. J. Ferraudi, *J. Phys. Chem.*, 1976, **80**, 949-953.

178. H. Knoll, R. Stich, H. Hennig and D. J. Stufkens, *Inorg. Chim. Acta*, 1990, **178**, 71-76.

179. H. Hennig, K. Ritter, A. K. Chibisov, H. Görner, F.-W. Grevels, K. Kerpen and K. Schaffner, *Inorg. Chim. Acta*, 1998, **271**, 160-166.

180. S. Shukla, S. S. Kamath and T. S. Srivastava, *J. Photochem. Photobio. A*, 1988, **44**, 143-152.

181. V. Anbalagan, *J. Coord. Chem.*, 2003, **56**, 161-172.

182. A. Vogler, A. Kern and J. Hüttermann, *Angew. Chem. Int. Ed.*, 1978, **17**, 524-525.

183. D. E. J. G. J. Dolmans, D. Fukumura and R. K. Jain, *Nat. Rev. Cancer*, 2003, **3**, 380-387.

184. B. C. Wilson, *Can. J. Gastroenterol.*, 2002, **16**, 393-396.

185. A. P. Castano, P. Mroz and M. R. Hamblin, *Nat. Rev. Cancer*, 2006, **6**, 535-545.

186. L. Brancaleon and H. Moseley, *Laser Med. Sci.*, 2002, **17**, 173-186.

187. L. Carroll and T. R. Humphreys, *Clin. Dermatol.*, 2006, **24**, 2-7.

188. K. Szaciłowski, W. Macyk, A. Drzewiecka-Matuszek, M. Brindell and G. Stochel, *Chem. Rev.*, 2005, **105**, 2647-2694.

189. M. R. Detty, S. L. Gibson and S. J. Wagner, *J. Med. Chem.*, 2004, **47**, 3897-3915.

190. J. P. Pouget, T. Douki, M. J. Richard and J. Cadet, *Chem. Res. Toxicol.*, 2000, **13**, 541-549.

191. J. Cadet, S. Courdavault, J. L. Ravanat and T. Douki, *Pure Appl. Chem.*, 2005, **77**, 947-962.

192. S. Mouret, C. Baudouin, M. Charveron, A. Favier, J. Cadet and T. Douki, *Proc. Natl. Acad. Sci. USA*, 2006, **103**, 13765-13770.

193. Cosmetic Treatment Modules, by Q.Products AG., http://www.colourlight.ch/?q=en/node/219, Accessed 1st Apr, 2012.

194. R. R. Allison, G. H. Downie, R. Cuenca, X. H. Hu, C. J. H. Childs and C. H. Sibata, *J. Med. Chem.*, 2004, **47**, 3897.

195. A. L. Harris, *Nat. Rev. Cancer*, 2002, **2**, 38-47.

196. J. M. Brown and W. R. Wilson, *Nat. Rev. Cancer*, 2004, **4**, 437-447.

197. N. A. Kratochwil, M. Zabel, K.-J. Range and P. J. Bednarski, *J. Med. Chem.*, 1996, **39**, 2499-2507.

198. N. A. Kratochwil, Z. J. Guo, P. D. Murdoch, J. A. Parkinson, P. J. Bednarski and P. J. Sadler, *J. Am. Chem. Soc.*, 1998, **120**, 8253-8254.

199. F. S. Mackay, J. A. Woods, H. Moseley, J. Ferguson, A. Dawson, S. Parsons and P. J. Sadler, *Chem. Eur. J.*, 2006, **12**, 3155-3161.

200. F. S. Mackay, J. A. Woods, P. Heringova, J. Kasparkova, A. M. Pizarro, S. A. Moggach, S. Parsons, V. Brabec and P. J. Sadler, *Proc. Natl. Acad. Sci. USA*, 2007, **104**, 20743-20748.

201. N. J. Farrer, J. A. Woods, L. Salassa, Y. Zhao, K. S. Robinson, G. Clarkson, F. S. Mackay and P. J. Sadler, *Angew. Chem. Int. Ed.*, 2010, **49**, 8905-8908.

202. N. J. Farrer, J. A. Woods, V. P. Munk, F. S. Mackay and P. J. Sadler, *Chem. Res. Toxicol.*, 2010, **23**, 413-421.

203. P. J. Bednarski, R. Grunert, M. Zielzki, A. Wellner, F. S. Mackay and P. J. Sadler, *Chem. Biol.*, 2006, **13**, 61-67.

204. N. J. Farrer and P. J. Sadler, *Aust. J. Chem.*, 2008, **61**, 669-674.

205. Y. Nakabayashi, A. Erxleben, U. Létinois, G. Pratviel, B. Meunier, L. Holland and B. Lippert, *Chem. Eur. J.*, 2007, **13**, 3980-3988.

206. L. Cubo, A. M. Pizarro, A. G. Quiroga, L. Salassa, C. Navarro-Ranninger and P. J. Sadler, *J. Inorg. Biochem.*, 2010, **104**, 909-918.

207. C. Loup, A. Tesouro Vallina, Y. Coppel, U. Létinois, Y. Nakabayashi, B. Meunier, B. Lippert and G. Pratviel, *Chem. Eur. J.*, 2010, **16**, 11420-11431.

208. M. P. Donzello, D. Vittori, E. Viola, I. Manet, L. Mannina, L. Cellai, S. Monti and C. Ercolani, *Inorg. Chem.*, 2011, **50**, 7391-7402.

209. I. Manet, F. Manoli, M. P. Donzello, C. Ercolani, D. Vittori, L. Cellai, A. Masi and S. Monti, *Inorg. Chem.*, 2011, **50**, 7403-7411.

210. S. L. H. Higgins, A. J. Tucker, B. S. J. Winkel and K. J. Brewer, *Chem. Commun.*, 2012, **48**, 67-69.

211. K. Benjamin Garbutcheon-Singh, M. P. Grant, B. W. Harper, A. M. Krause-Heuer, M. Manohar, N. Orkey and J. R. Aldrich-Wright, *Curr. Top. Med. Chem.*, 2011, **11**, 521-542.

212. A. F. A. Peacock and P. J. Sadler, *Chem. Asian J.*, 2008, **3**, 1890-1899.

213. A. M. Pizarro, A. Habtemariam and P. J. Sadler, *Top. Organomet. Chem.*, 2010, **32**, 21-56.

214. S. Betanzos-Lara, L. Salassa, A. Habtemariam and P. J. Sadler, *Chem. Commun.*, 2009, 6622-6624.

215. S. Betanzos-Lara, L. Salassa, A. Habtemariam, O. Novakova, A. M. Pizarro, G. J. Clarkson, B. Liskova, V. Brabec and P. J. Sadler, *Organomet.*, 2012.

216. L. Salassa, E. Borfecchia, T. Ruiu, C. Garino, D. Gianolio, R. Gobetto, P. J. Sadler, M. Cammarata, M. Wulff and C. Lamberti, *Inorg. Chem.*, 2010, **49**, 11240-11248.

217. F. Barragán, P. López-Senín, L. Salassa, S. Betanzos-Lara, A. Habtemariam, V. Moreno, P. J. Sadler and V. Marchán, *J. Am. Chem. Soc.*, 2011, **133**, 14098-14108.

218. S. Roy, S. Saha, R. Majumdar, R. R. Dighe and A. R. Chakravarty, *Polyhedron*, 2010, **29**, 2787-2794.

219. B. Maity, M. Roy, B. Banik, R. Majumdar, R. R. Dighe and A. R. Chakravarty, *Organomet.*, 2010, **29**, 3632-3641.

220. S. Saha, R. Majumdar, M. Roy, R. R. Dighe and A. R. Chakravarty, *Inorg. Chem.*, 2009, **48**, 2652-2663.

221. P. K. Sasmal, S. Saha, R. Majumdar, S. De, R. R. Dighe and A. R. Chakravarty, *Dalton Trans.*, 2010, **39**, 2147-2158.

222. U. Basu, I. Khan, A. Hussain, P. Kondaiah and A. R. Chakravarty, *Angew. Chem. Int. Ed.*, 2012, **51**, 2658-2661.

Chapter 2

Experimental Methods

In this Chapter, an overview of major experimental methods and techniques used in this work is given. Some further specific details will also be outlined in each chapter.

2.1 Nuclear Magnetic Resonance (NMR) Spectroscopy

The application of NMR can be found in almost all the research field of chemistry and biology in unveiling information about the chemical environment of magnetically active nuclei. In this work, multinuclear NMR techniques were applied in characterizing new compounds, obtaining structure information and monitoring the reactions, etc.

The NMR relevant properties of some commonly studied nuclei are listed in **Table 2.1**. In this thesis, the main nuclei studied are ^{1}H, ^{13}C, ^{14}N and ^{195}Pt, although some experiments were performed on ^{15}N, ^{19}F and ^{31}P. Due to the relevance to this work, the NMR spectroscopy of ^{1}H, ^{13}C, ^{14}N, ^{15}N and ^{195}Pt nuclei and two-dimensional NMR techniques will be discussed further.

Table 2.1 NMR properties of common nuclides.[1]

Nucleus	Natural Abundance (%)	Sensitivity (relative to ^{13}C)	Gyromagnetic Ratio γ (10^7 rad T^{-1} s^{-1})	Spin quantum number I	Frequency at 14.092 T (MHz)
^{1}H	99.989	5870	26.75	½	600.00
^{13}C	1.070	1	6.73	½	150.87
^{14}N	99.634	1.0×10^{-3}	2.044	1	43.358
^{15}N	0.368	2.25×10^{-2}	-2.71	½	60.821
^{19}F	100.0	4900	25.18	½	564.56
^{31}P	100.0	391	10.84	½	242.89
^{195}Pt	33.83	20.7	5.839	½	128.98

2.1.1 ^{1}H-NMR

In organic solvents, e.g. acetone-d_6, the resonance of N$\underline{H_x}$ in ^{1}H NMR is usually broadened due to the quadrupole effect of ^{14}N. In this thesis, most of the NMR experiments of Pt am(m)ine complexes and their reactions were carried out in aqueous solutions, such as D_2O (99.9%), H_2O/D_2O (typically 90%/10%, v/v). In aqueous solvent, the exchange of N$\underline{H_x}$ with D may cause the disappearance of the signal. For Pt^{II} complexes, the exchange at physiological pH is sufficiently slow to follow the signal.[2, 3] However, for Pt^{IV} am(m)ine complexes, H_2O/D_2O (90%/10%, v/v) is used and also pH needs to be lowered to *ca.* 5 to slow down the rate of exchange as the amine ligands on Pt^{IV} have lower pK_a values. In addition, the pH may also need to be lowered to enable the detection of protonated amine released from platinum.

In addition, a water suppression strategy is necessary for experiments in aqueous solution especially in 90% H_2O/10% D_2O. Two main techniques were used in this thesis to suppress the H_2O/HOD signal: excitation sculpting (Shaka method)[4, 5] and pre-saturation.[6] The Shaka sequence applies pulsed-field gradients to excite from the opposite sides of the proton pulse but not the solvent peak. This strategy may lead to badly phased H_2O/HOD signal while the other signals are almost unaffected. Pre-saturation irradiates the solvent peak at exactly its resonance frequency during the delays of the pulse sequence. This approach gives perfect water suppression but it may cause considerable suppressions of signals close to the H_2O/HOD peak (±1 ppm). Therefore, the integration of signals close the H_2O/HOD peak is not reliable.

2.1.2 ^{13}C-NMR

^{13}C is the second most important nucleus after ^{1}H in elucidating chemical structures. The natural abundance of ^{13}C is 1.1%, the spin quantum number I = ½ and the magnetic moment *ca.* ¼ of that of ^{1}H (μ_{13C}/μ_{1H} = 0.252). This leads to *ca.* ¼ Larmor frequency of the ^{13}C nucleus as that for ^{1}H in the same external magnetic field. The sensitivity of ^{13}C nucleus for natural isotopes is only ~1.8×10^{-4} as that for ^{1}H, so acceptable signal can be obtained by isotope enrichment or accumulation of more acquisitions.

Also, a series of one dimensional multi-pulse sequences were applied to obtain intensified signal in this work. JMOD[7] (J Modulation) pulse sequences produce spectra in which the positive signals are from CH_2 or quaternary carbons and the negative signals are from CH and CH_3 groups.[8] Although the signals can be phased up or down, they can be phased relating to the solvent signal. Non-proton bearing ^{13}C nuclei give weak signals due to their longer spin-lattice relaxation time T_1 and smaller NOEs (Nuclear Overhauser Effect). DEPT (Distorsionless Enhancement by Polarization Transfer) was also used to gain an enhancement in signal intensity via polarization transfer from sensitive nuclei (^{1}H) to ^{13}C nuclei by a factor of γ_{1H}/γ_{13C}. However this method does not detect non-protonated ^{13}C nuclei, as there is no polarization transfer from ^{1}H to quaternary carbons. Therefore, a PENDENT[9] (Polarization Enhancement During Attached Nucleus Testing) pulse sequence was also used in which the sensitivity for CH, CH_2 and CH_3 groups are the same as that for DEPT and the non-protonated ^{13}C nucleus give stronger signals compared to that for JMOD.

In this thesis, the ^{13}C spectra reported have been broadband proton decoupled using a composite pulse sequence to generate simplified spectra. The integration of ^{13}C signals was not applied because of two reasons:

- The NOE effect from proton decoupling is not equal for all the carbons. In particular, quaternary carbons receive very little NOE, and hence their signals are usually weak.
- Some carbon nuclei have very long spin-lattice relaxation times T_1. For example, the T_1 value for quaternary carbons in styrene is 78 s as there are no close protons to relax it.[7]

2.1.3 ^{14}N NMR

Although ^{14}N (I = 1) has high natural abundant (99.63%), the detection of the ^{14}N resonances is never simple. The major problem is that in liquid samples, the bandwidths ^{14}N signals are often broad due to rapid quadrupolar relaxation (millisecond level),[10] especially when the chemical environment of ^{14}N has low symmetry. Nevertheless, large numbers of acquisitions can be acquired due to the short relaxation times. Therefore, it has been possible to follow the decomposition pathways of N_3 group in the photochemical reactions of Pt-azido complexes.[10-12]

Experimental parameters for ^{14}N NMR spectra (43.36 MHz): pulse sequences zgpg30 (proton broadband decoupled) was used and the digitization mode was in "baseopt" for improvement of baselines. The spectra were acquired with a relaxation delay (D1) of 0.25 s. Typical parameters were 32k data points and 64k scans. Data were processed using a line broadening of 20 Hz for EM window function unless otherwise stated. With the IUPAC recommended reference CH_3NO_2 (neat or 90% in $CDCl_3$) as δ = 0 for ^{14}N nucleus,[1] the typical chemical shift range is −400 to 400 ppm.

In this work, an external $^{14}NH_4Cl$ (1.5 M) in 1 M HCl was used as reference and a chemical shift range between −100 and 500 ppm was scanned. The chemical shift observed in this way can be converted to CH_3NO_2 standard by subtracting 380.5 ppm.

2.1.4 ^{15}N NMR

^{15}N NMR (I = ½) was also used in a few cases to characterize ^{15}N-labelled complexes in this thesis. The receptivity of ^{15}N is extremely low, 2.25×10^{-2} relative to ^{13}C, so ^{15}N-labelled derivatives need to be prepared.

The sensitivity of ^{15}N can be enhanced via inverse detection technique that has now been routinely used in detecting ^{15}N signals. This method is a two-dimensional correlation spectroscopy that detects the insensitive nuclei by detecting the sensitive nuclei attached to it (usually ^{1}H). Inverse detection techniques can, in principle, give a gain in sensitivity of nuclei X by $(\gamma_H/\gamma_X)^{5/2}$ over direct detection. For low γ value nuclei such as ^{15}N (**Table 2.1**), this method is even more dramatic. More information on two-dimensional correlation spectroscopy as well as the range of ^{15}N chemical shift can be found in **Section 2.1.6**.

Nevertheless, the direct detection of ^{15}N is still of advantage in some cases, if the ^{15}N nucleus has no H attached or there is rapid exchange of the N*H* proton.

2.1.5 ^{195}Pt NMR

^{195}Pt (natural abundance 33.8%) is the only NMR-active isotope of platinum and it has favourable properties for use in NMR, for example, nuclear spin quantum number I = ½, sensitivity 20 relative to ^{13}C, and gyromagnetic ratio $\gamma = 5.8 \times 10^7$ rad s^{-1} T^{-1}(**Table 2.1**). ^{195}Pt resonance is reasonably sensitive to observe and has been

routinely used in a wide variety of applications including structural elucidation, relaxation studies, kinetics and mechanistic studies and drug binding studies.[13]

The chemical shift range of ^{195}Pt is large (15k ppm) and is particularly sensitive to changes in the oxidation state, ligand substitution, stereochemistry, and even different isotopes around the ^{195}Pt nucleus.[14] For example, the ^{195}Pt chemical shift of *cis*-$[PtCl_2(Me_2NH)_2]$ in DMF-d_7 is −2188 ppm, while that of *trans*-$[PtCl_2(Me_2NH)_2]$ is −2181 ppm.[15] By contrast, the Pt chemical shifts of Pt^{IV} complexes $\{PtCl_2N_2O_2\}$ are *ca.* 900 ppm.[16] The ^{195}Pt chemical shift of $[PtCl_6]^{2-}$ is set up to 0 as reference, and δ of $[PtBrCl_5]^{2-}$ is −282 ppm.[17] Abbott et al reported 0.5 – 1.0 ppm shift between two isotopomers $K_2[Pt(^{16}OH)_2(Ox)_2]$ and $K_2[Pt(^{16}OH)(^{18}OH)(Ox)_2]$ (Ox = oxalate). The ^{195}Pt chemical shift difference for Pt-^{35}Cl and Pt-^{37}Cl is 0.17 ppm and for Pt-^{79}Br and Pt-^{81}Br is 0.03 ppm.[14]

However, such a small difference in ^{195}Pt NMR chemical shift is practically very difficult to observe due to the line width of the signals. First, the ^{195}Pt NMR resonance is strongly dependent on the temperature, *ca.* 1 ppm K^{-1}, so poor temperature control broadens the resonance.[14] Second, am(m)ine ligands containing ^{14}N (natural abundance 99.6%, $I = 1$) can also broaden the ^{195}Pt resonance by electric quadrupolar effects,[14] although this effect shortens the ^{195}Pt relaxation times and rapid pulsing can be used without saturation effects. Third, ^{195}Pt signal can also be broadened due to the chemical shift anisotropy (CSA) relaxation.[18]

The peak-widths of ^{195}Pt resonances (and also ^{195}Pt satellites, see **Chapter 3**) are dependent on the T_1 relaxation time of ^{195}Pt. The contribution to T_1 of ^{195}Pt from CSA is dependent on a number of factors:[14]

$$[T_1(\mathrm{Pt})]^{-1}\ (\mathrm{CSA}) = \frac{6}{7}[T_2(\mathrm{Pt})]^{-1}\ (\mathrm{CSA}) = \frac{2}{15} \times \gamma_{\mathrm{Pt}}^2 \times \boldsymbol{B}_0^2 \times \Delta\sigma^2 \times \tau_c$$

^{195}Pt resonances are broader in Pt^{II} complexes which are in square-planar geometry and hence are less symmetrical (larger anisotropy $\Delta\sigma$), in larger external magnetic field ($\boldsymbol{B}_0$) and in larger molecules where the correlation time τ_c is longer.

Experimental parameters for ^{195}Pt NMR spectra (129.4 MHz): Pulse sequences zg (non-proton-decoupled) was used and the digitization mode was in "baseopt" for improvement of baselines. The spectra were acquired with a relaxation delay (D1) of 0 s. Typical parameters were 2k data points and 10k acquisitions. Data were processed by using an exponential line broadening of 100 Hz unless otherwise stated.

2.1.6 Two-dimensional NMR Techniques

In 2D-NMR experiments, another frequency domain is involved to reveal structural correlations through various magnetic interactions between nuclei. For example, in a [^{1}H, ^{1}H] COSY (COrrelation SpectroscopY) experiment, two identical 1D spectra axes are plotted orthogonally, and all the spin-coupled protons are indicated by cross peaks placed along the diagonal. Usually, COSY spectra can only show the correlation between two- and three-bond coupled protons. NOESY (Nuclear Overhauser Effect SpectroscopY) can connect resonances of protons that are spatially close to each other. In TOCSY (TOtal Correlation SpectroscopY) experiments, the connectivity of all protons in a spin system is detected as cross peaks.[7]

Heteronuclear single (or multiple) quantum coherence (HSQC and HMQC) and HMBC (Heteronuclear multiple-bond correlation) spectroscopy are powerful inverse detection techniques that can detect insensitive nuclei (such as ^{13}C and ^{15}N) by

detecting the attached sensitive nuclei (such as ^{1}H, ^{31}P and ^{19}F).[19, 20] In HSQC, the sensitivity of ^{15}N can be improved by 306 ($(|\gamma^{1}H/\gamma^{15}N|)^{5/2}$) compared to directly detected ^{15}N. HSQC can detect heteronuclear correlations over one bond, where the spin-spin coupling to ^{1}H is measurable, e.g. in primary and secondary amines. For tertiary amines, HMBC is often applied to detect heteronuclear correlations over longer ranges of about 2 – 4 bonds.

Valuable information can be obtained from 2D [^{1}H, ^{15}N] HSQC spectra (**Figure 2.1A**), e.g., ^{15}N chemical shift and the $^{1}J(^{195}Pt\text{-}^{15}N)$ coupling constant, which are highly dependent on the nature of the ligand *trans* to ^{15}N ligand. As shown in **Figure 2.1B**, the observed ^{1}H and ^{15}N chemical shift ranges for a number of Pt^{II} and Pt^{IV} complexes have been defined.[19]

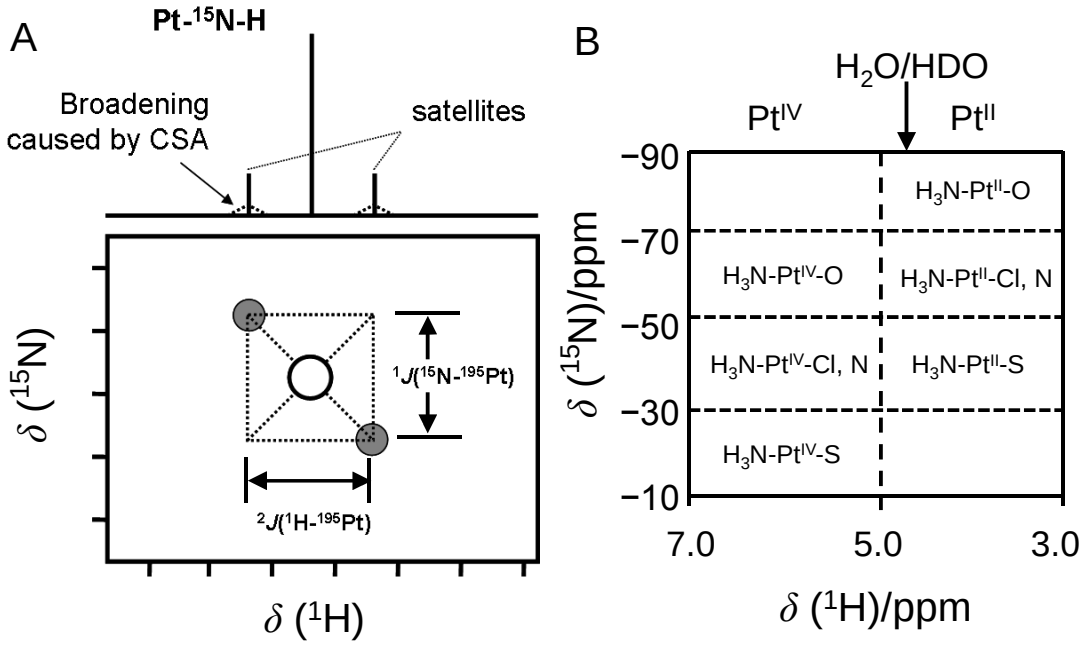

Figure 2.1 (**A**) Typical shape of Pt-^{15}N-*H* cross peak in a Pt ammine complex in 2D [^{1}H, ^{15}N] HSQC NMR spectrum. (**B**) Schematic representation illustrating the areas of positions of ^{1}H and ^{15}N cross peaks of 2D [^{1}H, ^{15}N] HSQC NMR spectra for various ligand *trans* to ^{15}N in Pt^{II} and Pt^{IV} complexes.[19, 20]

2.1.7 Experimental methods

NMR data were acquired by the author under the guidance from Dr. Nicola J. Farrer and Dr. Ivan Prokes (University of Warwick). NMR spectra were recorded on a Bruker DPX-400 (^{1}H: 400.03 MHz), a Bruker AV-400 (^{1}H: 399.10 MHz) or a Bruker AVIII-600 (^{1}H: 600.13 MHz) spectrometer. NMR chemical shifts were recorded in δ (ppm) and ^{1}H and ^{13}C chemical shifts were referenced to residual ^{1}H/^{13}C-solvent peaks from deuterated solvents $CDCl_3$ (^{1}H, δ = 7.26; ^{13}C, δ = 77.16), MeOD (^{1}H, δ = 3.31; ^{13}C, δ = 49.00), acetone-d_6 (^{1}H = δ 2.05; ^{13}C = δ 29.84, 206.26), DMSO-d_6 (^{1}H, δ = 2.50; ^{13}C, δ = 39.52), and DMF-d_7 (^{1}H, δ = 2.75, 2.92, 8.03; ^{13}C, δ = 29.76, 34.89, 163.15).[21] For D_2O or 90% H_2O/10% D_2O, chemical shifts were referenced internally to dioxane (^{1}H, δ = 3.75 in D_2O; δ = 3.764 for 90% H_2O/10% D_2O; ^{13}C, δ = 67.19 for both solvents).[22] ^{195}Pt NMR: chemical shifts were externally referenced to 15 mM K_2PtCl_6 in D_2O (δ = 0). ^{14}N and ^{15}N chemical shifts were referenced to external $^{14}NH_4Cl$ or $^{15}NH_4Cl$ (1.5 M) in 1 M HCl and ^{31}P to external H_3PO_4 85% in D_2O at δ = 0. Data processing was carried out by using Topspin 2.0 (Bruker) and MestReC version 4.9.9.9 (Mestrelab Research S.L.).

2.2 Mass Spectrometry (MS)

2.2.1 Electrospray Ionisation-Mass Spectrometry (ESI-MS)

ESI-MS is a soft-ionization mass spectrometric technique for the analysis of compounds in aqueous/organic solution. ESI-MS was used routinely in this work to characterise complexes and the products formed in photoreaction.

Electrospray Ionisation is induced by applying a strong field to a liquid passing through a nebuliser (capillary needle) at a rate level of microlitres per minute.[23] The

nebuliser is maintained at several kilovolts with respect to an electrode surrounding it (**Figure 2.2**). The resulting spray of charged fine droplets then passes through a space to evaporate the solvent and attach charge to the analyte molecules. As the size of the droplets decreases, the charge density increased. When the surface tension can no longer hold the charge, the droplets are torn apart into smaller droplets. The parameters can be adjusted so the desolvation process is repeated until all solvent is removed, leaving (multiply) charged analyte molecules. Ion analysis is then performed using various mass detectors, such as quadrupole, iontrap and time-of-flight (TOF) mass spectrometer.

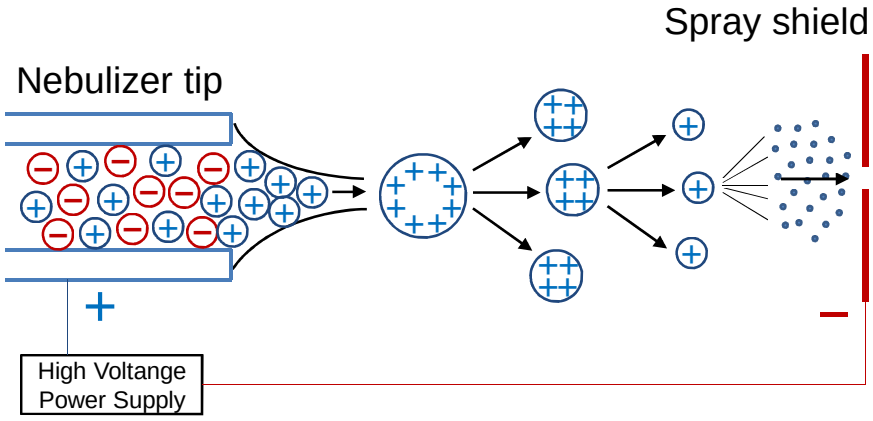

Figure 2.2 Schematic ionization mechanism for electrospray.[23]

The sample must be present in solution as ions and thus adjusting the pH to protonate (ESI positive) or deprotonate (ESI negative) the analyte molecule is sometimes necessary. Water, methanol, acetonitrile and isopropanol can be applied as solvent.

Positive/negative ion electrospray mass spectrometry (ESI-MS) was performed on a Bruker Esquire 2000 mass spectrometer coupled with an Agilent 1100 HPLC (without column) as an automatic sample delivery system. All samples were prepared in 80% acetonitrile/20% water.

2.2.2 High resolution (HR) ESI-MS

Positive/negative ion high resolution electrospray mass (HR-ESI-MS) spectra were recorded on a Bruker MaXis UHR-Qq-TOF mass spectrometer. The Bruker MaXis high resolution mass spectrometer offers ultra-high resolution of 40,000 – 60,000 over a broad mass range, theoretically MS and MS/MS mass accuracy 600 – 800 ppb for internal calibration, 1 – 3ppm for external calibration.

Platinum complexes samples were filtered with a 0.2 μm ionic membrane and then diluted to 10 μM scale in 80% acetonitrile/20% water before use. DNA samples were prepared 1.0 μM, in a solution of H_2O/isopropanol (50%/50%, v/v) with 50 mM ammonium acetate. The oligo concentrations of DNA were determined spectrophotometrically using the absorption coefficient ε_{260} = 132.52 $mM^{-1}cm^{-1}$, calculated by 'OligoCalc'.[24] A solution of HCOONa was also injected as an external calibration. Data processing and mass/isotope distribution simulation was carried out on Bruker Daltonics DataAnalysis.

2.2.3 HPLC coupled mass spectrometry (LC-MS)

HPLC-coupled mass spectrometry (LC-MS) was performed on a Bruker HCT-Ultra mass spectrometer coupled with an Agilent 1200 HPLC system with an Agilent ZORBAX Eclipse Plus C18 column (4.6 × 250 mm, 5 μm). Analytical separations for reaction mixtures of Pt complexes with 5′-GMP were carried out with detection at 254 nm. Mobile phases were A: 0.1% formic acid in HPLC grade water, and B: 0.1% formic acid in HPLC grade methanol. A 20-min linear gradient from 5% to 55.0% B was applied for all reaction mixtures of Pt complexes and 5′-GMP**.** The flow rate was 0.8 mL min^{-1}.

2.3 Inductively coupled plasma optical emission spectrometry (ICP-OES)

The platinum content of aqueous solutions was determined by ICP-OES (inductively coupled plasma optical emission spectrometry) or ICP-MS (mass spectrometry).

2.3.1 ICP-OES

ICP-OES experiments were carried out on a PerkinElmer Optima 5300 DV optical emission spectrometer with an AS-93 plus autosampler. The atoms/ions of elements can take up energy from an inductively coupled plasma (ICP), and are thereby promoted to an excited state. Then the atoms/ions emit a series of characteristic radiation while fall back into their ground state, so called optical emission spectrum. The intensity of radiation, in a certain range, is proportional to the concentration of the element, and is therefore quantitative.

In ICP-OES analysis, the liquid sample is introduced into the inductively generated argon plasma through a nebulizer system and get excited. The spectrum emitted is transferred into a spectrometer where it is decomposed into the individual wavelengths and evaluated. The emission wavelengths detected for Pt were 265.945, 214.423, 299.797, 204.937 and 193.700 nm. The intensities of the spectral lines are measured by CID semiconductor detectors. The ranges of detecting limit for different metals are quite different. For Pt in liquid samples, the theoretical lowest detecting limit on ICP-OES is 50ppb. Samples were calibrated with 5 – 7 standard Pt solutions (0.5 – 10 ppm) prepared from stock 1000 ppm Pt solutions (Sigma Aldrich). Data analysis was carried out on WinLab32 (version 3.4.1).

2.3.2 ICP-MS

ICP-MS was carried out on an Agilent 7500 Series ICP-MS spectrometer. Similar to ICP-OES, an inductively coupled plasma (ICP) is also used, but higher energy (higher temperature) is given to the sample to atomize and ionize the elements. The resulting ions are then passed through a series of apertures (cones) into the high vacuum mass analyser. The isotopes of the elements are identified by their mass-to-charge ratio (*m/z*) calibrated internally by standard samples of erbium. The concentration of an isotope (element) in the sample can be quantified by the intensity of the *m/z* peak in the mass spectrum. The theoretical lowest detecting limit for Pt samples in H_2O or 3% HNO_3 on ICP-MS is 0.5 ppt. Samples were calibrated with 5 – 7 standard Pt solutions (0.1 ppb – 500 ppb) prepared from stock 1000 ppm Pt solutions (Sigma Aldrich). Data acquisition was carried out on ICP-MS Top (version B.03.05) and analysis on Offline Data Analysis (version B.03.05).

2.4 Ultraviolet-Visible Absorption Spectroscopy

Ultraviolet-visible absorption spectroscopy (UV-Vis Spectroscopy, also known as electronic absorption spectroscopy) is a highly useful technique for studying electronic excitations of molecules.

UV-Vis spectrum records the transitions between the electronic energy levels of a molecule. The electrons in a molecule are excited from their ground electronic states to excited states, induced by the absorption of electromagnetic radiation (photons). The absorption bands generated from transition metal complexes are commonly based on three different transitions:

- ligand field transitions (LF), also known as d→d transition or metal centred transitions (MC): electron transfer from a lower to a higher energy metal-centred orbitals;
- Metal-to-Ligand Charge Transfer (MLCT) or Ligand-to-Metal Charge Transfer (LMCT): electron transfer from metal-centred orbitals to ligand-centred orbitals or *vice versa*;
- Intra-ligand transition (IL): electron transfer from lower to higher-energy ligand-centred orbitals.

These transitions and estimated extinction coefficients (ε) are further discussed in **Chapter 1**. The orbital energies involved in electronic transitions have fixed values, but practically, many available vibrational and rotational states in the molecule are associated to each electronic excited state. Therefore, each observed broad absorption band present in the UV-Vis spectrum often contains closely packed but discrete lines.

2.4.1 UV-Vis spectra

UV-Vis absorption spectra were recorded on a Varian Cary 300 UV-Vis spectrophotometer in 1cm path-length cuvettes. The spectral width was 200 – 800 nm and the bandwidth was 1.0 nm, the scan rate 600 nm/min. An Ocean Optics USB4000-UV-Vis spectrophotometer was also used to continuously follow UV-Vis spectra *in situ* with light irradiation. All spectra were referenced to neat solvent and data were processed with OriginLab Origin 7.0. Extinction coefficients (ε) were determined over a concentration range (A_{max} ~ 0.4 – 1.6 units) with at least 4 data points, using Pt concentrations determined by ICP-OES/MS.

2.5 pH measurement

pH values for NMR samples were measured at ambient temperature directly in the NMR tube with a Corning 145 pH-meter equipped with an Mettler Toledo U402-M3-S7/200 extra-long micro electrode, calibrated with standard buffer solutions at pH 4, 7 and 10 from Sigma Aldrich.

2.6 Irradiation methods and devices

Photoactivation of Pt complexes was carried out at 293 K by using a LZC-ICH2 photoreactor (Luzchem Research Inc.) (**Figure 2.3**) equipped with a temperature controller and 16 UVA lamps (Hitachi, λ_{max} = 361 nm) or 16 Luzchem LZC-420 lamps (λ_{max}= 420 nm) with no other sources of light filtration. ACULED® VHL™ LEDs were also used (λ_{max} = 450 nm) for irradiation of the samples (**Figure 2.4**). A modified Shimadzu RF-551 Fluorescence HPLC Monitor (**Figure 2.5**) was used as the light source to give low power monochromatic irradiation with PWHH (Peak Width at Half Height) of *ca.* 15 nm. A B&W® 72mm UV filter was used to eliminate the second/higher order diffraction of shorter wavelengths in the specified longer wavelength monochromatic light from the grating.[25]

Figure 2.3 LZC-ICH2 photoreactor (Luzchem Research Inc.) equipped with a temperature controller and 16 UVA lamps (Hitachi, λ_{max} = 365 nm) or 16 Luzchem LZC-420 lamps (λ_{max}= 420 nm)

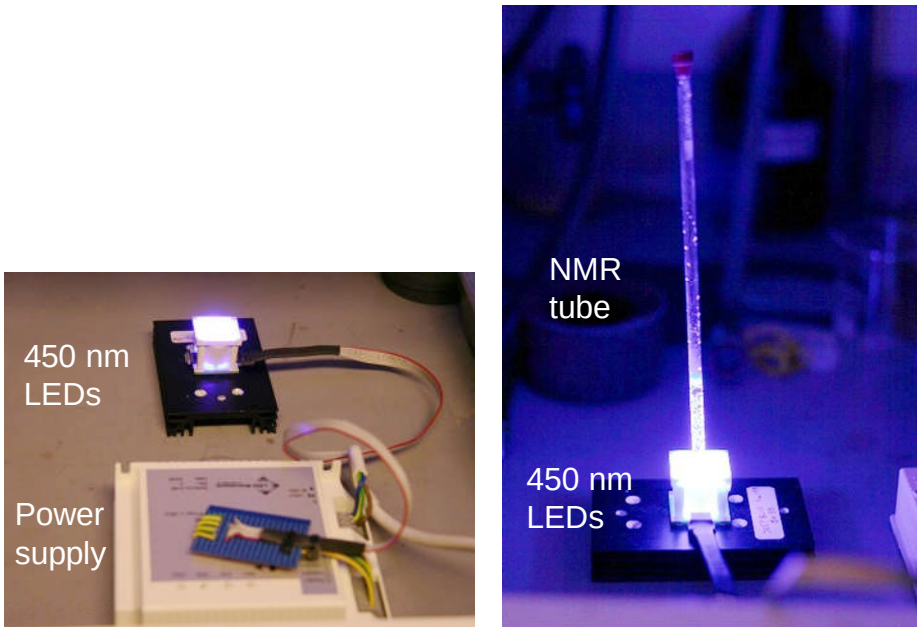

Figure 2.4 (A) ACULED® VHL™ LEDs (λ_{max} = 450 nm) and power supply; (B) a solution in an NMR tube being irradiated.

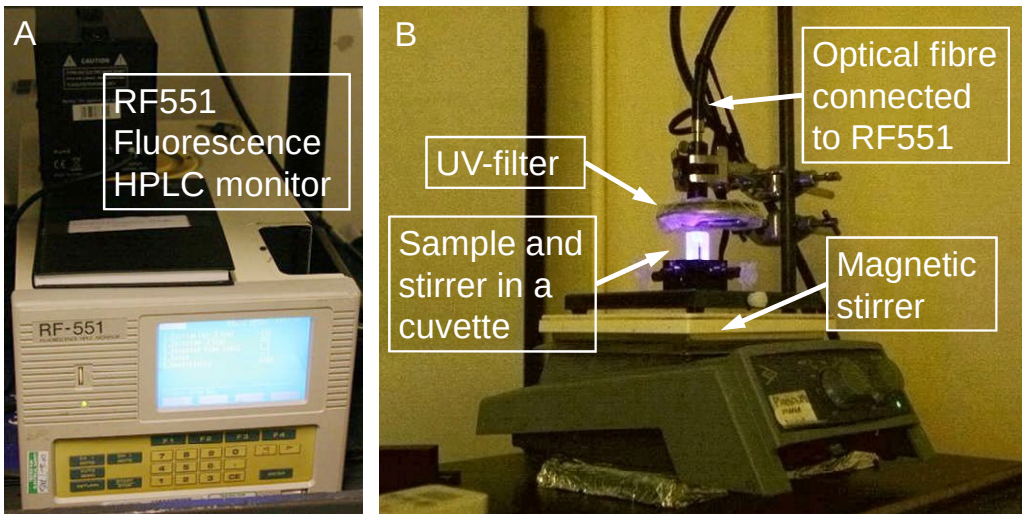

Figure 2.5 Irradiation set up using a modified Shimadzu RF-551 Fluorescence HPLC monitor (A). Light from an optical fibre was directed to the sample in a cuvette (B).

2.7 Light measurements

Power levels were measured with an International Light Technologies Powermeter (ILT1400-A) equipped with a SEL033 detector and either a UVA/TD filter (315-390 nm) for UVA irradiations or a flat response visible filter F/W (400-1064 nm) for visible wavelengths. The spectrum of each of the light sources was recorded on the Ocean Optics USB4000-UV-Vis spectrophotometer (see Appendix 2 for all the output spectra). The number of incident photons (einstein/s) was measured and calculated using a potassium ferrioxalate actinometer for the wavelength-dependent photodecomposition study.[26-29]

2.8 Electron Paramagnetic Resonance (EPR) spectroscopy

The EPR experiments and data analysis were carried out with the assistance of Jennifer S. Butler in University of Warwick. All EPR measurements were run on a Bruker EMX (X-band) spectrometer. The room temperature experiments (*ca*. 293 K) were recorded using the 1.0 mm quartz tubes. Typical instrument settings were: modulation amplitude 2.0 G and microwave power 0.63 mW. An aqueous solution of sample (5 mM) was added to an excess of spin trap, DMPO (5, 5-dimethyl-pyrroline-N-oxide), 10 mM. Known concentrations of the EPR standard TEMPO (2,2,6,6-Tetramethylpiperidine 1-oxyl) were run to obtain a standard calibration curve. From this curve, the concentration of spin adduct was determined. The 450 nm LED was used as the source of irradiation at a distance of *ca*. 30 cm from the EPR cavity. Samples were irradiated for 2 hours and signals were recorded every 5 min. Controls of both DMPO and sample, irradiated and non-irradiated were run as reference spectra. EPR spectra were analysed using the Bruker WINEPR software and simulations were run using the SIMFONIA.

2.9 X-ray crystallography

The data collection, structure determination and refinement were carried out by Dr Guy Clarkson of the University of Warwick. Structure analysis was performed by the author. Diffraction data for the complexes were collected with Mo-Kα radiation (λ = 0.71073 Å) on an Oxford Diffraction Gemini four-circle system with Ruby CCD area detector. The crystal was glued to a glass fibre and the data recorded at 296 K. The structure was solved by direct methods using SHELXS (Sheldrick, 1990) (TREF) with additional light atoms found by Fourier methods. Hydrogen atoms were added at calculated positions and refined using a riding model. Anisotropic displacement parameters were used for all non-H atoms; H-atoms were given isotropic displacement parameters equal to 1.2 (or 1.5 for OH hydrogen atoms) times the equivalent isotropic displacement parameter of the atom to which the H-atom is attached. ORTEP diagrams and for short contacts were generated using Mercury 2.3.

2.10 Cytotoxicity test for non-light-sensitive complexes

The cytotoxicity of non-light-sensitive platinum(II) dichlorido complexes was determined by Dr Ana Pizarro of the University of Warwick. The A2780 human ovarian cell line was obtained from the ECACC (European Collection of Animal Cell Culture, Salisbury, United Kingdom). The cells were maintained in RPMI 1640 media, which was supplemented with 10% foetal calf serum, 1% L-glutamine, and 1% penicillin/streptomycin. All cells were grown at 310 K in a humidified atmosphere containing 5% CO_2. Stock solutions of the Pt complexes were freshly prepared in DMSO to assist dissolution and then diluted into saline and medium (maximum final concentration of DMSO 1% and saline 6%). After plating 5000 A2780 cells per well on day 1, Pt complexes were added to the cancer cells on day 3 at concentrations

ranging from 0.01 to 100 μM, depending on the preliminary activity data obtained in screening assays. Cells were exposed to the complexes for 24 h, washed with PBS, supplied with fresh medium, and allowed to grow for three doubling times (72 h), and then the protein content (proportional to cell survival) was measured using the sulforhodamine B (SRB) assay.[30] The standard errors are based on two independent experiments of three replicates each. [31]

2.11 Photo/dark-cytotoxicity test for light-sensitive complexes

The photoactivated dose-dependent inhibition to cell viability for light-sensitive platinum(IV) diazidodihydroxido complexes was determined by Dr Julie A. Woods of the University of Dundee. Cell culture work was performed at ambient light levels below 1 lux (Solatell, UK). HaCaT cells were maintained in Dulbecco's modified Eagle's medium containing 5% foetal bovine serum (FBS). All other lines were maintained in RPMI medium containing 10% FBS. Cells were maintained in antibiotic-free culture in a humidified atmosphere of 95% air: 5% CO_2 and regularly screened for mycoplasma. Complexes were prepared in Earle's balanced salt solution just before use and filtered. Irradiations were performed using a bank of 2 × 6 ft Cosmolux RA Plus (Cosmedico; λ_{max}: 365 nm) 15500/100W light sources filtered to attenuate wavelengths below 320 nm; or 2 × 3 ft TL03 (Philips; λ_{max}: 420 nm) light sources filtered to attenuate wavelengths below 400 nm. Irradiance was measured with an International Light meter, fitted with the appropriate detector and diffuser and calibrated to each source using a double grating spectroradiometer (Bentham, UK) in the UKAS accredited optical physics laboratory (Photobiology Unit, Dundee). The delivered dose was 5 J/cm^2 for both sources, equivalent to about 1 hour or less sunlight exposure at midday on a summer day at 56º north (Dundee).

All experiments were controlled for solvent, test compound and irradiation. Cytotoxicity was measured using the neutral red uptake phototoxicity assay and DNA reactivity was measured using the single cell gel electrophoresis ('comet') assay as described in the literature.[32] For analysis of comet assay slides, the samples were coded so that their identity was unknown to the scorer. The concentration of complex required to inhibit dye uptake by 50% (IC_{50} value) was determined by curve fitting (Graphpad). Goodness of fit was assessed by R^2 values and the 95% confidence interval. All cell experiments were performed in duplicate/triplicate and repeated independently a minimum of two times. Where appropriate statistical analysis was performed using Anova followed by Dunnett's test.

2.12 References

1. R. K. Harris, E. D. Becker, S. M. C. de Menezes, R. Goodfellow and P. Granger, *Pure Appl. Chem.*, 2001, **73**, 1795-1818.
2. E. Koubek and D. A. House, *Inorg. Chim. Acta*, 1992, **191**, 103-107.
3. S. K. Miller and L. G. Marzilli, *Inorg. Chem.*, 1985, **24**, 2421-2425.
4. L. E. Kay, *Curr. Opin. Struct. Biol.*, 1995, **5**, 674-681.
5. T. L. Hwang and A. Shaka, *J. Magn. Reson. Ser. A*, 1995, **112**, 275-279.
6. H. Mo and D. Raftery, *J. Magn. Reson.*, 2008, **190**, 1-6.
7. J. W. Akitt and B. E. Mann, *NMR and Chemistry: An introduction to modern NMR spectroscopy*, Stanley Thornes Publishers Ltd., Cheltenham, UK, 2000.
8. N. T. McManus and A. Penlidis, *J. Appl. Polym. Sci.*, 2007, **103**, 2093-2098.
9. J. Homer and M. C. Perry, *J. Chem. Soc., Chem. Commun.*, 1994, 373-374.
10. N. J. Farrer, P. Gierth and P. J. Sadler, *Chem. Eur. J.*, 2011, **17**, 12059-12066.

11. H. I. A. Phillips, L. Ronconi and P. J. Sadler, *Chem. Eur. J.*, 2009, **15**, 1588-1596.
12. L. Ronconi and P. J. Sadler, *Dalton Trans.*, 2011, **40**, 262-268.
13. B. M. Still, P. G. A. Kumar, J. R. Aldrich-Wright and W. S. Price, *Chem. Soc. Rev.*, 2007, **36**, 665-686.
14. S. J. Berners-Price and P. J. Sadler, *Coord. Chem. Rev.*, 1996, **151**, 1-40.
15. F. D. Rochon and V. Buculei, *Inorg. Chim. Acta*, 2004, **357**, 2218-2230.
16. M. Watabe, M. Kai, S. Asanuma, M. Yoshikane, A. Horiuchi, A. Ogasawara, T. Watanabe, T. Mikami and T. Matsumoto, *Inorg. Chem.*, 2001, **40**, 1496-1500.
17. E. Penka Fowe, P. Belser, C. Daul and H. Chermette, *Phys. Chem. Chem. Phys.*, 2005, **7**, 1732-1738.
18. I. M. Ismail, S. J. S. Kerrison and P. J. Sadler, *Polyhedron*, 1982, **1**, 57-59.
19. S. J. Berners-Price, L. Ronconi and P. J. Sadler, *Prog. Nucl. Magn. Reson. Spectrosc.*, 2006, **49**, 65-98.
20. Y. Chen, Z. Guo and P. J. Sadler, in *Cisplatin:Chemistry and Biochemistry of a Leading Anticancer Drug*, ed. B. Lippert, Verlag Helvetica Chimica Acta, Zurich, 1999, pp. 293-318.
21. H. E. Gottlieb, V. Kotlyar and A. Nudelman, *J. Org. Chem.*, 1997, **62**, 7512-7515.
22. Z. J. Guo and P. J. Sadler, *Adv. Inorg. Chem.*, 2000, **49**, 183-306.
23. J. H. Gross, *Mass spectrometry: a textbook*, Springer Verlag, Heidelberg, Germany, 2004.
24. W. A. Kibbe, *Nucleic Acids Res.*, 2007, **35**, W43-W46.
25. L. A. Mackenzie and W. Frain-Bell, *Br. J. Dermatol.*, 1973, **89**, 251-264.

26. H. J. Kuhn, S. E. Braslavsky and R. Schmidt, *Pure Appl. Chem.*, 2004, **76**, 2105-2146.

27. S. L. Murov, G. L. Hug and I. Carmichael, *Handbook of Photochemistry*, M. Dekker, New York, 1993.

28. C. G. Hatchard and C. A. Parker, *Proc. R. Soc. London, Ser. A*, 1956, **235**, 518-536.

29. C. A. Parker, *Proc. R. Soc. London, Ser. A*, 1953, **220**, 104-116.

30. P. Skehan, R. Storeng, D. Scudiero, A. Monks, J. McMahon, D. Vistica, J. T. Warren, H. Bokesch, S. Kenney and M. R. Boyd, *J. Natl. Cancer Ins.*, 1990, **82**, 1107-1112.

31. Z. Liu, A. Habtemariam, A. M. Pizarro, S. A. Fletcher, A. Kisova, O. Vrana, L. Salassa, P. C. A. Bruijnincx, G. J. Clarkson, V. Brabec and P. J. Sadler, *J. Med. Chem.*, 2011, **54**, 3011-3026.

32. F. S. Mackay, J. A. Woods, P. Heringova, J. Kasparkova, A. M. Pizarro, S. A. Moggach, S. Parsons, V. Brabec and P. J. Sadler, *Proc. Natl. Acad. Sci. USA*, 2007, **104**, 20743-20748.

Chapter 3

Synthesis and Characterization of Novel Photoactivatable Platinum Complexes and Their Anticancer Activity

3.1 Introduction

Platinum-based anticancer drugs (*e.g.* cisplatin, *cis*-$[PtCl_2(NH_3)_2]$) are amongst the most important anti-tumour agents currently available in the clinic, which have proved to be highly effective towards a variety of solid tumours[1-4] (also see **Chapter 1**). However, severe toxic and dose-limiting side-effects, including nausea, vomiting and nephrotoxicity accompany the treatment, which limits their application.[5] In addition, intrinsic or acquired resistance of tumours and cross-resistance with other platinum-based drugs with similar structures reduces their efficacy.[6, 7] To overcome these drawbacks a vast number of new strategies have been investigated, such as structural modifications,[8-10] varying *trans/cis* geometries,[11, 12] different binding modes[13-15] and the strategy of prodrugs.[16, 17]

Prodrugs are pharmacologically inactive precursors, which undergo chemical and/or biological transformation to generate (or release) the active drug at the site of action.[18] Apart from reducing the platinum(IV) anticancer prodrugs with biological molecules, photochemical reduction is also an efficient way to activate them.[19] Photoactivatable Pt^{IV} diazidodihydroxido anticancer complexes (**Figure 3.1**) are a group of prodrugs that are inert and non-toxic in a biological environment in the dark. Upon irradiation with light these complexes can be selectively activated to become potently cytotoxic against a number of cancer cell lines.[20-24]

Metal azides have long been known to be sensitive to light.[25] The introduction of azido ligands into platinum anticancer complexes plays a major role in tuning the photoactivity of this family of compounds. Apart from the azido ligands, the selection of the other leaving groups is also of great importance. Previous studies have shown that Pt^{IV} complexes with dihydroxido ligands have lower reduction

potentials compared to corresponding Pt^{IV} complexes with dichlorido ligands[26, 27] or diacetato ligands.[28] This decrease in the reduction potential of dihydroxido complexes makes them stable in the presence of reductive biomolecules.[17, 29] In other words, the Pt^{IV} complexes with dihydroxido ligands are stable in the absence of irradiation, which lowered the potential of side effects. Furthermore, the addition of dihydroxido group substantially increased the solubility of Pt^{IV} complexes in aqueous solutions. Therefore, in this work, diazidodihydroxido ligands are used with the aim of developing novel Pt^{IV} anticancer prodrugs that are more potent upon irradiation with light and have low toxicity in the dark.

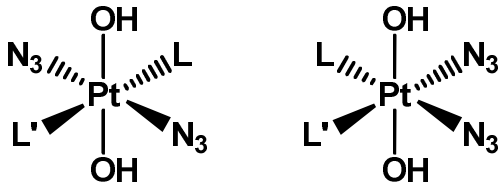

Figure 3.1 *Trans*- and *cis*- photoactivatable platinum(IV) diazidodihydroxido anticancer complexes. L, L′ = heterocyclic imines/aliphatic amines.

Although this class of complex exhibits very good photoactivated anti-tumour activity, there are still several hurdles to overcome. Ideally the complexes would be activated with light of the longest possible wavelength in the so-called therapeutic window (up to 600 − 800 nm[30, 31]) to allow treatment of larger tumours given that tissue-penetration of light is wavelength-dependent (**Chapter 1**). In addition, cross-resistance to cisplatin-resistant cells was also observed.[21, 24] By changing the ligands on the Pt^{IV} complexes, compounds with broader clinically utility (longer activation wavelength), greater potency (higher phototoxicity) and wider applicability (circumventing cisplatin cross-resistance) can be developed.

It was previously demonstrated that *trans* isomers of complexes containing aliphatic or heterocyclic imines are more photocytotoxic than their *cis* isomers.[20, 23] Also, replacing NH_3 ligands with pyridine (Py) in *trans,trans,trans*-$[Pt(N_3)_2(OH)_2(NH_3)(Py)]$[21] to form *trans,trans,trans*-$[Pt(N_3)_2(OH)_2(Py)_2]$[24] lead to higher photocytoxicity for visible light activation. This study reviews that replacing the NH_3 with aliphatic amine or replacing the pyridine by thiazole (Tz) which are other approaches to obtain potent photocytoxicity and in turn more efficient anticancer complexes.

Replacing NH_3 ligands with aliphatic amines such as methylamine (MA), dimethylamine (DMA) and isopropylamine (IPA) (**Scheme 3.1**) or aromatic imines such as pyridine and thiazole will affect the hydrophilicity/lipophilicity of this type of complex. This will vary the cellular uptake of the complex and the steric hinderance of the platinum fragment on platinated DNA. Therefore, it is possible to obtain higher cytotoxicity by improved cellular accumulation or reduced DNA repair rate.

Thiazole (Tz) (**Scheme 3.1**), is a five-membered aromatic ring. The sulfur atom in Tz is sp^2 hybridized, leaving one lone pair in the π system and the other in the plane of the ring. Tz is aromatic and very stable to a broad range of reaction conditions.[32] Tz ring is widely present in a variety of biomolecules, such as vitamin B1, and it also exists as a functional group in epothilone, a new cancer drug.[33] By replacing the Py by Tz, it is possible to vary the bulkiness of the molecule and its optical absorption properties. This in turn will hopefully lead to more efficient platinum complexes and different activation wavelengths.

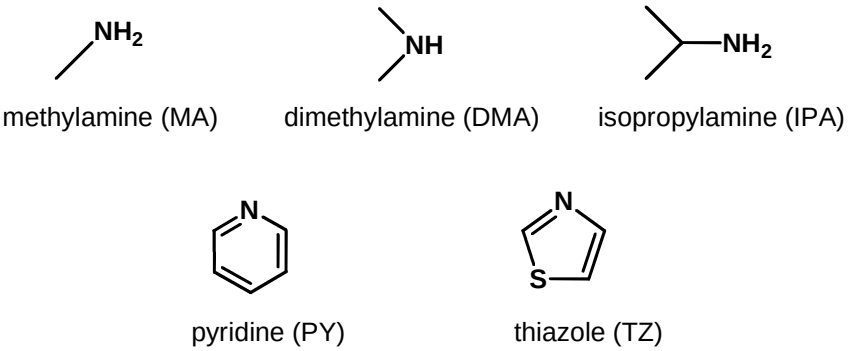

Scheme 3.1 Aliphatic amine/heterocyclic imine ligands used in this Chapter.

This chapter reports the synthesis, characterisation and (photo) cytoxicity of a series of novel Pt^{IV} diazidodihydroxido complexes and their *trans* platinum(II) dichlorido precursors. Their toxicities toward several carcinoma cell lines in the presence and absence of light are reported.

3.2 Experimental

Caution! While no problems were encountered during this work, heavy metal azides are known to be shock sensitive detonators,[34-36] therefore it is *essential* that any Pt azido compound is handled with care.

3.2.1 Materials

All materials were used as obtained from commercial sources unless otherwise stated. K_2PtCl_4 was obtained from Precious Metal Online and Alfa Aesar, KI, KOH, and NaCl from Fisher Scientific, $AgNO_3$ from Fluka, NaN_3, H_2O_2 (30%) and all other chemicals from Sigma-Aldrich. All solvents for common use were analytical reagent grade from Fisher Scientific and were used as supplied. Distilled water was purified using a Millipore water purification system. Water used in ICP-OES was purified using Purelab UHQ water purification system.

3.2.2 Synthesis and Characterisation

3.2.2.1 *Cis*-$[PtI_2(MA)_2]$ (1)

Cis-$[PtI_2(MA)_2]$ (**1**) was synthesized according to a reported method.[37] $K_2[PtCl_4]$ (2.08 g, 5.0 mmol) was dissolved in H_2O (30 mL) and KI (8.30 g, 50 mmol) added. After stirring for 30 min, 40% MA aqueous solution (0.78 mL, 10 mmol) was added. The mixture was stirred for a further 30 min after which the yellow precipitate was collected by filtration, washed with cold water, ethanol and diethyl ether and dried under vacuum.

Yield: 2.18 g (85 %)

^{1}H NMR (400 MHz, MeCN-d_3): δ (ppm) 3.90 (broad, N$\underline{H}_2$, 4H), 2.49 (t, CH_3, $^3J(^{195}Pt, ^1H)$ = 48 Hz, 6H).

Elemental Analysis: $C_2H_{10}I_2N_2Pt$, Calc. C 4.70%, H 1.97%, N 5.48%, I 49.67%, Found: C 4.61%, H 1.87%, N 5.23%, I 49.78%.

3.2.2.2 *Cis*-$[PtCl_2(MA)_2]$ (2)

Cis-$[PtI_2(MA)_2]$ (1.02 g, 2.0 mmol) was suspended in H_2O (30 mL) to this $AgNO_3$ (0.76 g, 4.0 mmol) was added. The mixture was stirred at 328 K overnight. AgI precipitate was filtered off with celite followed by an inorganic membrane filter (Sartorius, Minisart, 0.2 µm). NaCl (0.47 g, 8.0 mmol) was added and the mixture was stirred for a further 30 min after which the yellow precipitate was collected by filtration, washed with minimal cold water, ethanol and diethyl ether then dried under vacuum.

Yield: 0.61 g (93 %)

^{1}H NMR (400 MHz, MeCN-d_3): δ (ppm) 3.90 (broad, N$\underline{H}_2$, 4H), 2.44 (t, C$\underline{H}_3$, $^3J(^{195}Pt, ^1H)$ = 48 Hz, 6H).

Elemental Analysis: $C_2H_{10}Cl_2N_2Pt$, Calc. C 7.32%, H 3.07%, N 8.54%, Cl 21.61%, Found: C 7.16%, H 2.94%, N 8.46%, Cl 21.73%.

From this point on all syntheses were carried out under controlled (dim) lighting conditions.

3.2.2.3 *Trans*-[Pt(Cl)$_2$(MA)(Py)] (3)

Cis-[$PtCl_2(MA)_2$] (0.33 g, 1 mmol) was suspended in 9 mL H_2O, then pyridine (240 mg, 3 mmol) was added. The reaction was heated to 353 K with stirring and kept at this temperature for 90 min. The solution was allowed to cool to room temperature and HCl (12M, 1 mL) was added and stirred at 368 K for 65h.The flask was cooled on ice and the product was filtered, washed successively with minimal cold H_2O, ethanol, and diethyl ether and then dried under vacuum. The yellow product was further purified by recrystallized from 0.1 M HCl.

Yield: 0.306 g (81.3%)

^{1}H NMR (400 MHz, Acetone-d_6): δ (ppm) 8.83 (dd, $\underline{H_{2,6}}$, ^{3}J (^{195}Pt, ^{1}H) = 32 Hz, 2H), 7.98 (tt, $\underline{H_4}$, 1H), 7.45 (ddd, $\underline{H_{3,5}}$, 2H), 4.31 (broad, N$\underline{H_2}$, 2H), 2.49 (t, C$\underline{H_3}$, ^{3}J (^{195}Pt, ^{1}H) = 35 Hz, 3H).^{13}C NMR (150.9 MHz, Acetone-d_6): δ (ppm) 154.1 ($\underline{C_{2,6}}$), 139.3 ($\underline{C_4}$), 126.2 ($\underline{C_3}$), 33.7 ($\underline{C}H_3$). ^{195}Pt NMR (129.4 MHz, Acetone-d_6): δ = −2085.3 ppm. ESI-MS: $[M - 2Cl - H]^+$ (*m/z*) Calc., 304.0, Found, 304.1.

Elemental Analysis: $C_6H_{10}Cl_2N_2Pt$, Calc., C, 19.16%; H, 2.68%; N, 7.45%; Found, C, 19.26%; H, 2.60%; N, 7.37%.

3.2.2.4 *Trans*-[Pt(N$_3$)$_2$(MA)(Py)] (4)

Trans-[$Pt(Cl)_2(MA)(Py)$] (0.188 g, 0.5 mmol) was suspended in H_2O 50 mL, and $AgNO_3$ (0.17g, 1.0 mmol) added and the solution stirred at 323 K for 16 h. AgCl precipitate was filtered off with celite followed by an inorganic membrane filter

(Sartorius, Minisart, 0.2 µm). NaN_3 (0.65g, 10 mmol) was added and the solution stirred (323 K, 6h) and the volume of the solution was reduced under vacuum to *ca.* 3 mL and cooled to 277 K overnight. The yellow precipitate was filtered using a Buchner funnel, washed with minimal ice cold H_2O, EtOH, and ether then dried under vacuum.

Yield: 0.153 g (78.7%)

^{1}H NMR (400 MHz, Acetone-d_6): δ (ppm) 8.79 (dd, $\underline{H_{2,6}}$, ^{3}J (^{195}Pt, ^{1}H) = 34 Hz, 2H), 8.08 (tt, $\underline{H_4}$, 1H), 7.61 (t, $\underline{H_{3,5}}$, 2H), 4.43 (broad, N$\underline{H_2}$, 2H), 2.50 (t, C$\underline{H_3}$, ^{3}J (^{195}Pt, ^{1}H) = 41 Hz, 3H). ^{13}C NMR (150.9 MHz, Acetone-d_6): δ (ppm) 153.5 ($\underline{C_{2,6}}$), 139.9 ($\underline{C_4}$), 127.3 ($\underline{C_3}$), 33.2 ($\underline{C}H_3$). ^{195}Pt NMR (129.4 MHz, Acetone-d_6): δ = −2202.4 ppm.

ESI-MS: $[M + Na]^+$ (*m/z*) Calc., 421.06; Found, 421.0.

3.2.2.5 *Trans,trans,trans*-$[Pt(N_3)_2(OH)_2(MA)(Py)]$ (5)

Trans-$[Pt(N_3)_2(MA)(Py)]$ (39 mg, 0.1 mmol) was suspended in H_2O_2 (20 mL, 30%) and stirred at 323 K for 1 h. The volume of the solution was reduced using rotary evaporation to *ca.* 4 mL, to form a bright yellow solution (usually takes 1~2 hours). *It was important to maintain the temperature below 323 K.* Water (50 mL) was added and the solution was lyophilised. Crystals suitable for X-ray analysis were obtained via crystallisation in water-ethanol with ether diffusion. The solution was filtered (Buchner) to collect the product which was washed with minimal ether and dried under vacuum.

Yield: 21 mg (50 %)

^{1}H NMR (400 MHz, 90% H_2O / 10% D_2O, pH~5): δ (ppm) 8.72 (d, $\underline{H_{2,6}}$, ^{3}J (^{195}Pt, ^{1}H) = 22 Hz, 2H), 8.30 (t, $\underline{H_4}$, 1H), 7.84 (t, $\underline{H_{3,5}}$, 2H), 6.65 (broad, N$\underline{H_2}$, 2H), 2.42 (s, C$\underline{H_3}$, ^{3}J(^{195}Pt, ^{1}H) = 28 Hz, 3H). ^{13}C NMR (100.6 MHz, D_2O): δ (ppm) 149.60 ($\underline{C_{2,6}}$),

142.77 (*C4*), 127.62 (*C3, 5*, $^{3}J(^{195}Pt, ^{13}C)$ = 25 Hz), 30.50 (*C*H_3). ^{195}Pt NMR (129.4 MHz, D_2O): δ = 888.66 ppm.

ESI-MS: $[M + Na]^+$ (*m/z*) Calc., 446.1; Found, 446.0.

Elemental Analysis: $C_6H_{12}N_8O_2Pt$, Calc., C, 17.02%; H, 2.86%; N, 26.47%; Found, C, 16.87%; H, 2.65%; N, 26.87%.

$\varepsilon_{max(289)}$ = 16200 L mol^{-1} cm^{-1} (H_2O)

3.2.2.6 *Trans*-[Pt(Cl)$_2$(MA)(Tz)] (6)

Cis-[$PtCl_2(MA)_2$] (0.33 g, 1 mmol) was suspended in 9 mL H_2O, then thiazole (255 mg, 3 mmol) was added. The reaction was heated to 353 K and stirred for 2 h. The solution was allowed to cool to room temperature and HCl (12M, 1 mL) was added. The solution was heated at 368 K and stirred overnight (~16 h). The solution was cooled on ice and the yellow product was filtered, washed successively with minimal cold H_2O, ethanol, and diethyl ether and then dried under vacuum. The product was recrystallized from a minimal amount of 0.1 M HCl.

Yield: 0.280 g (73.5%)

^{1}H NMR (400 MHz, Acetone-d_6): δ (ppm) 9.50 (d, *H2*, $^{3}J(^{195}Pt, ^{1}H)$ = 26 Hz, 1H), 8.26 (d, *H4*, $^{3}J(^{195}Pt, ^{1}H)$ = 15 Hz, 1H), 7.81 (dd, *H5*, 1H), 4.37 (broad, N*H*$_2$, 2H), 2.50 (t, C*H*$_3$, $^{3}J(^{195}Pt, ^{1}H)$ = 36 Hz, 3H). ^{13}C NMR (150.9 MHz, Acetone-d_6): δ (ppm) 157.8 (*C2*), 144.7 (*C4*), 120.9 (*C5*), 33.6 (C*H*$_3$). ^{195}Pt NMR (129.4 MHz, Acetone-d_6): δ = −2111.6 ppm.

ESI-MS: $[M - 2Cl - H]^+$ (*m/z*) Calc., 310.0; Found, 310.0.

Elemental Analysis: $C_4H_8Cl_2N_2PtS$, Calc., C, 12.57%; H, 2.11%; N, 7.33%; Found, C, 12.68%; H, 2.04%; N, 7.46%.

3.2.2.7 *Trans*-[Pt(N_3)$_2$(MA)(Tz)] (7)

Trans-[Pt(Cl)$_2$(MA)(Tz)] (0.190 g, 0.5 mmol) was suspended in H_2O 50 mL, to this $AgNO_3$ (0.17g, 1.0 mmol) was added and the solution stirred at 323 K for 24 h. AgCl precipitate was filtered off with celite followed by an inorganic membrane filter (Sartorius, Minisart, 0.2 µm). NaN_3 (0.65g, 10 mmol) was added, the solution stirred (323 K, 6h) and the solvent reduced under vacuum to *ca.* 3 mL. The solution was then cooled before to 277 K overnight. The yellow precipitate was filtered with a Buchner funnel, washed with minimal ice cold H_2O, EtOH, and ether then dried under vacuum.

Yield: 0.182 g (92%)

^{1}H NMR (400 MHz, Acetone-d$_6$): δ (ppm) 9.44 (d, $\underline{H_2}$, ^{3}J(^{195}Pt, ^{1}H) = 28 Hz, 1H), 8.14 (d, $\underline{H_4}$, ^{3}J(^{195}Pt, ^{1}H) = 20 Hz 1H), 7.98 (dd, $\underline{H_5}$, 1H), 4.54 (broad, N$\underline{H_2}$, 2H), 2.52 (t, C$\underline{H_3}$, ^{3}J(^{195}Pt, ^{1}H) = 44 Hz, 3H). ^{13}C NMR (150.9 MHz, Acetone-d$_6$): δ (ppm) 158.0 ($\underline{C_2}$), 144.3 ($\underline{C_4}$), 122.7 ($\underline{C_5}$), 33.4 ($\underline{C}H_3$). ^{195}Pt NMR (129.4 MHz, Acetone-d$_6$): δ (ppm) −2203.0 ppm.

ESI-MS: $[M+Na]^+$ (*m/z*) Calc., 418.0; Found, 417.9.

3.2.2.8 *Trans,trans,trans*-[Pt(N_3)$_2$(OH)$_2$(MA)(Tz)] (8)

Trans-[Pt(N_3)$_2$(MA)(Tz)] (20 mg, 0.05 mmol) was suspended in H_2O_2 (10 mL, 30%) and stirred at 323 K for 1 h. The volume of the solution was reduced to *ca.* 2 mL, forming a bright yellow solution (usually takes 1~2 hours). *It was important to maintain the temperature below 323 K.* Water (50 mL) was added and the solution was lyophilised. Crystals suitable for X-ray diffraction were obtained via slow diffusion of ether into water-ethanol. The solution was filtered under vacuum

yielding a yellow precipitate which was washed with minimal ether and dried under vacuum.

Yield: 12 mg (56 %)

^{1}H NMR (400 MHz, 90% H_2O/10% D_2O): δ (ppm) 9.59 (d, $\underline{H_2}$, $^{3}J(^{195}Pt, ^{1}H)$ = 16 Hz, 1H), 8.27 (d, $\underline{H_4}$, $^{3}J(^{195}Pt, ^{1}H)$ = 14 Hz, 1H), 8.12 (d, $\underline{H_5}$, 1H), 6.66 (broad, N$\underline{H_2}$, 2H), 2.37 (s, C$\underline{H_3}$, $^{3}J(^{195}Pt, ^{1}H)$ = 29 Hz, 3H). ^{13}C NMR (150.9 MHz, D_2O): δ (ppm) 149.6 ($\underline{C_2}$), 140.4 ($\underline{C_4}$), 123.6 ($\underline{C_5}$), 30.39 ($\underline{C}H_3$).^{195}Pt NMR (129.4 MHz, D_2O): δ (ppm) 906.71.

ESI-MS: $[M+Na]^+$ (*m/z*) Calc., 452.0; Found, 451.9.

Elemental Analysis: $C_4H_{10}N_8O_2PtS$, Calc., C, 11.19%; H, 2.35%; N, 26.10%; Found, C, 10.95%; H, 2.26%; N, 25.71%.

$\varepsilon_{max(289)}$ = 18600 L mol^{-1} cm^{-1} (H_2O)

3.2.2.9 *Cis*-[$PtI_2(DMA)_2$] (9)

$K_2[PtCl_4]$ (2.075 g, 5.0 mmol) was dissolved in H_2O (30 mL) and KI (8.300 g, 50 mmol) added. After stirring for 30 min at room temp., DMA (25% in H_2O, 1.9 mL, 10.0 mmol) was added. The mixture was stirred for a further 3 h after which the brown precipitate was collected by filtration, washed with minimal cold water, ethanol and diethyl ether and dried under vacuum.

Yield: 2.59 g (96.1 %)

^{1}H NMR (400 MHz, Acetone-d_6): δ (ppm) 4.95 (broad, N$\underline{H}$, 2H), 2.78 (d, C$\underline{H_3}$, $^{3}J(^{195}Pt, ^{1}H)$ = 46 Hz, 12H).

Elemental Analysis: $C_4H_{14}I_2N_2Pt$, Calc., C, 8.91%; H, 2.62%; I, 47.08%, N, 5.20%; Found, C, 8.75%; H, 2.35%; I, 46.95%, N, 5.12%.

3.2.2.10 *Cis*-[$PtCl_2(DMA)_2$] (10)

Cis-[$PtI_2(DMA)_2$] (0.539 g, 1 mmol) was suspended in H_2O (50 mL) and $AgNO_3$ (340 mg, 2 mmol) was added. The mixture was stirred at 328 K overnight. AgI precipitate was filtered off with celite followed by an inorganic membrane filter (Sartorius, Minisart, 0.2 µm). NaCl (234 mg, 4 mmol) was added and the solution stirred overnight, after which the volume was reduced to 10 mL and the yellow precipitate was collected by filtration, washed with minimal cold water, ethanol and diethyl ether and dried under vacuum. The product was recrystallized from a minimal amount of 0.1 M HCl.

Yield: 278 mg (77 %)

^1H NMR (400 MHz, MeCN-d_3): δ (ppm) 4.60 (broad, NH, 2H), 2.62 (d, CH_3, ^3J (^{195}Pt, ^1H) = 41 Hz, 12H).

ESI-MS: $[M + Na]^+$ (*m/z*): Calc., 378.0; Found, 378.0.

Elemental Analysis: $C_4H_{14}Cl_2N_2Pt$, Calc., C, 13.49%; H, 3.96%; N, 7.87%; Found, C, 13.16%; H, 3.84%; N, 7.72%.

3.2.2.11 *Trans*-[$PtCl_2$(DMA)(Tz)] (11)

Cis-[$PtCl_2(DMA)_2$] (106 mg, 0.3 mmol) was suspended in 5 mL H_2O, then Tz (92 mg, 1.08 mmol) was added. The reaction was heated to 353 K with stirring and kept at this temperature for 90 min. *N.B. This intermediate is light sensitive!* The solution was allowed to cool to room temperature and HCl (12M, 0.5 mL) was added and the solution was heated at 368 K over the weekend (~65h). The flask was cooled on ice and the product was filtered, washed successively with minimal cold H_2O, ethanol, and diethyl ether and then dried under vacuum.

Yield: 97.5 mg (82.3%)

^{1}H NMR (400 MHz, acetone-d_6): δ (ppm) 9.48 (d, $\underline{H_2}$, ^{3}J (^{195}Pt, ^{1}H) = 27 Hz, 1H), 8.23 (d, $\underline{H_4}$, 1H), 7.81 (dd, $\underline{H_5}$, 1H), 4.99 (broad, N$\underline{H}$, 1H), 2.64 (d, C$\underline{H_3}$, ^{3}J (^{195}Pt, ^{1}H) = 31 Hz, 6H). ^{13}C NMR (150.9 MHz, acetone-d_6): δ (ppm) 158.3 ($\underline{C_2}$), 145.0 ($\underline{C_4}$), 121.1 ($\underline{C_5}$), 43.8 ($\underline{C}H_3$). ^{195}Pt NMR (129.4 MHz, acetone-d_6): δ (ppm) −2086.1.

ESI-MS: $[M - 2Cl - H]^+$ (*m/z*) Calc., 324.0, Found, 324.1.

Elemental Analysis: $C_5H_{10}Cl_2N_2PtS$, Calc., C, 15.16%; H, 2.54%; N, 7.07%; Found, C, 15.12%; H, 2.39%; N, 7.01%.

3.2.2.12 *Trans*-[Pt(N$_3$)$_2$(DMA)(Tz)] (12)

Trans-[$PtCl_2$(MA)(Tz)] (40 mg) was suspended in H_2O 25 mL, and $AgNO_3$ (34 mg) was added and the solution stirred at 333K for 16 h. AgCl precipitate was filtered off with celite followed by an inorganic membrane filter. NaN_3 (65 mg, 10 molar equivalents) was added and the solution stirred at room temperature for 6h before cooling to 277 K overnight. The yellow precipitate was filtered, washed successively with minimal cold H_2O, ethanol, and diethyl ether and then dried under vacuum.

Yield: 35 mg (84%)

^{1}H NMR (400 MHz, acetone-d_6): δ (ppm) 9.48 (d, $\underline{H_2}$, ^{3}J (^{195}Pt, ^{1}H) = 22 Hz, 1H), 8.17 (d, $\underline{H_4}$, 1H), 8.01 (dd, $\underline{H_5}$, 1H), 4.98 (broad, N$\underline{H}$, 1H), 2.63 (d, C$\underline{H_3}$, ^{3}J (^{195}Pt, ^{1}H) = 36 Hz, 6H). ^{13}C NMR (150.9 MHz, acetone-d_6): δ (ppm) 158.3 ($\underline{C_2}$), 144.5 ($\underline{C_4}$), 122.9 ($\underline{C_5}$), 43.6 ($\underline{C}H_3$). ^{195}Pt NMR (129.4 MHz, acetone-d_6): δ (ppm) −2193.2.

ESI-MS: $[M - 2N_3 - H]^+$ (*m/z*) Calc., 324.0, Found, 324.1.

Elemental Analysis: $C_5H_{10}N_8PtS$, Calc., C, 14.67%; H, 2.46%; N, 27.37%; Found, C, 14.57%; H, 2.28%; N, 27.13%.

3.2.2.13 *Trans, trans, trans*-[$Pt(N_3)_2(OH)_2(DMA)(Tz)$] (13)

Trans-[$PtCl_2(MA)(Tz)$] (20 mg) was dissolved in H_2O_2 (10 mL, 30%) and stirred at 323 K for 1 h. The volume of the solution was reduced to *ca.* 3 mL, forming a dark yellow solution. *It was important to keep the temperature below 323 K.* Water (50 mL) was added and the solution was lyophilised. Crystals suitable for X-ray diffraction were obtained by diffusion of diethyl ether into a solution of product in water-ethanol.

Yield: 11 mg (51%).

^{1}H NMR (400 MHz, D_2O): δ (ppm) 9.54 (d, $\underline{H_2}$, ^{3}J (^{195}Pt, ^{1}H) = 16 Hz, 1H), 8.26 (d, $\underline{H_4}$, 1H), 8.04 (d, $\underline{H_5}$, 1H), 2.49 (s, C$\underline{H_3}$, ^{3}J (^{195}Pt, ^{1}H) = 27 Hz, 6H). ^{13}C NMR (150.9 MHz, D_2O): δ (ppm) 157.9 ($\underline{C_2}$), 140.5 ($\underline{C_4}$), 123.7 ($\underline{C_5}$), 42.11 ($\underline{C}H_3$, ^{2}J (^{195}Pt, ^{13}C) = 14.5 Hz).^{195}Pt NMR (129.4 MHz, D_2O): δ (ppm) 941.1.

ESI-MS: $[M + Na]^+$ (*m/z*) Calc., 466.0; Found, 465.9.

Elemental Analysis: $C_5H_{12}N_8O_2PtS$, Calc., C, 13.55%; H, 2.73%; N, 25.27%; Found, C, 13.32%; H, 2.62%; N, 25.62%.

3.2.2.14 *Trans*-[$PtCl_2(DMA)(Py)$] (14)

Trans-[$PtCl_2(DMA)(Py)$](**14**) was synthesized by a similar procedure as for *trans*-[$PtCl_2(DMA)(Tz)$] (**11**) using Py instead of Tz.

Yield: 81%

^{1}H NMR (400 MHz, acetone-d_6): δ (ppm) 8.79 (d, $\underline{H_{2,6}}$, ^{3}J (^{195}Pt, ^{1}H) = 32 Hz, 2H), 7.98 (t, $\underline{H_4}$, 1H), 7.45 (t, $\underline{H_{3,5}}$, 2H), 4.90 (broad, N$\underline{H}$, 1H), 2.63 (d, C$\underline{H_3}$, ^{3}J (^{195}Pt, ^{1}H) = 30 Hz, 6H).^{13}C NMR (150.9 MHz, acetone-d_6): δ (ppm) 154.3 ($\underline{C_{2,6}}$), 139.4 ($\underline{C_4}$), 126.2 ($\underline{C_{3,5}}$), 43.7 ($\underline{C}H_3$). ^{195}Pt NMR (129.4 MHz, acetone-d_6): δ (ppm) −2062.2.

ESI-MS: $[M + Na]^+$ (*m/z*) Calc., 412.0; Found, 412.1.

Elemental Analysis: $C_7H_{12}Cl_2N_2Pt$, Calc., C, 21.55%; H, 3.10%; N, 7.18%; Found, C, 21.72%; H, 3.04%; N, 7.18%.

3.2.2.15 *Trans*-[Pt(N$_3$)$_2$(DMA)(Py)] (15)

Trans-[Pt(N$_3$)$_2$(DMA)(Py)] (**15**) was synthesized by a similar procedure as for *trans*-[Pt(N$_3$)$_2$(DMA)(Tz)] using complex **14**.

Yield: 78.2%

^{1}H NMR (400 MHz, acetone-d$_6$): δ (ppm) 8.81 (d, $\underline{H_{2,6}}$, ^{3}J (^{195}Pt, ^{1}H) = 34 Hz, 2H), 8.08 (tt, $\underline{H_4}$, 1H), 7.64 (t, $\underline{H_{3,5}}$, 2H), 4.84 (broad, N$\underline{H}_2$, 2H), 2.61 (d, C$\underline{H}_3$, ^{3}J (^{195}Pt, ^{1}H) = 35 Hz, 6H).^{13}C NMR (150.9 MHz, acetone-d$_6$): δ (ppm) 153.9 ($\underline{C_{2,6}}$), 140.1 ($\underline{C_4}$), 127.5 ($\underline{C_{3,5}}$), 43.5 ($\underline{C}$H$_3$). ^{195}Pt NMR (129.4 MHz, acetone-d$_6$): δ (ppm) −2201.0.

ESI-MS: $[M + H]^+$ (*m/z*) Calc., 404.1; Found, 404.0.

3.2.2.16 *Trans, trans, trans*-[Pt(N$_3$)$_2$(OH)$_2$(DMA)(Py)] (16)

Trans, trans, trans-[Pt(N$_3$)$_2$(OH)$_2$(DMA)(Py)] (**16**) was synthesized by a similar procedure as for *trans, trans, trans*-[Pt(N$_3$)$_2$(OH)$_2$(DMA)(Tz)] using complex **15**.

Yield: 37%

^{1}H NMR (600 MHz, D$_2$O): δ (ppm) 8.75 (d, $\underline{H_{2,6}}$, ^{3}J (^{195}Pt, ^{1}H) = 24 Hz, 2H), 8.23 (t, $\underline{H_4}$, 1H), 7.77 (t, $\underline{H_{3,5}}$, 2H), 2.53 (s, C$\underline{H}_3$, ^{3}J (^{195}Pt, ^{1}H) = 26 Hz, 6H). ^{13}C NMR (150.9 MHz, D$_2$O): δ (ppm) 149.9 ($\underline{C_{2,6}}$), 142.8 ($\underline{C_4}$), 127.7 ($\underline{C_{3,5}}$, ^{3}J (^{195}Pt, ^{13}C) = 25 Hz), 42.2 ($\underline{C}$H$_3$). ^{195}Pt NMR (129.4 MHz, D$_2$O): δ (ppm) 926.4.

ESI-MS: $[M + H]^+$ (*m/z*) Calc., 438.1; Found, 438.0.

Elemental Analysis: $C_7H_{14}N_8O_2Pt$, Calc., C, 19.22%; H, 3.23%; N, 25.62%; Found, C, 19.28%; H, 3.00%; N, 25.93%.

3.2.2.17 *Cis*-[$PtCl_2(IPA)_2$] (17)

Cis-[$PtCl_2(IPA)_2$] (**17**) was synthesized by a similar procedure as for *cis*-[$PtCl_2(MA)_2$] (**2**), using IPA instead of MA.

Yield: 76%

^{1}H NMR (400 MHz, dmso-d_6): δ (ppm) 4.75 (broad, N$\underline{H}_2$, 2H), 3.11 (septet, C$\underline{H}$, 1H), 1.21 (d, C$\underline{H}_3$, 6H).

Elemental Analysis: $C_6H_{18}Cl_2N_2Pt$, Calc., C, 18.76%; H, 4.72%; N, 7.29%; Found, C, 18.50%; H, 4.48%; N, 7.06%.

3.2.2.18 *Trans*-[$PtCl_2$(IPA)(Tz)] (18)

Trans-[$PtCl_2$(IPA)(Tz)] (**18**) was synthesized by a similar procedure as for *trans*-[$PtCl_2$(DMA)(Tz)] (**11**) using *cis*-[$PtCl_2(IPA)_2$](**17**).

Yield: 69%

^{1}H NMR (400 MHz, acetone-d_6): δ (ppm) 9.52 (d, $\underline{H_2}$, ^{3}J (^{195}Pt, ^{1}H) = 24 Hz, 1H), 8.28 (d, $\underline{H_4}$, 1H), 7.81 (dd, $\underline{H_5}$, 1H), 4.27 (broad, N$\underline{H}$, 2H), 3.34 (septet, C$\underline{H}$, 1H), 1.38 (d, C$\underline{H}_3$, 6H).

ESI-MS: $[M - 2Cl - H]^+$ (*m/z*) Calc., 338.0, Found, 338.1.

$[M + Na]^+$ (*m/z*) Calc., 433.0, Found, 432.9.

3.2.2.19 *Trans*-[$PtCl_2$(IPA)(Py)] (19)

Trans-[$PtCl_2$(IPA)(Py)] (**19**) was synthesized by a similar procedure as for *trans*-[$PtCl_2$(DMA)(Tz)] (**11**) using Py and *trans*-[$PtCl_2(IPA)_2$] (**17**).

Yield: 83%

^{1}H NMR (400 MHz, acetone-d_6): δ (ppm) 8.84 (dd, $\underline{H_{2,6}}$, ^{3}J (^{195}Pt, ^{1}H) = 30 Hz, 2H), 7.98 (t, $\underline{H_4}$, 1H), 7.45 (t, $\underline{H_{3,5}}$, 2H), 4.21 (broad, N$\underline{H}_2$, 2H), 3.34 (septet, C$\underline{H}$, 1H),

1.39 (d, C*H*$_3$, 6H).^{13}C NMR (150.9 MHz, acetone-d$_6$): δ (ppm) 154.1 (*C*$_{2,6}$), 139.2 (*C*$_4$), 126.2 (*C*$_{3,5}$), 49.3 (*C*H), 23.8 (*C*H$_3$). ^{195}Pt NMR (129.4 MHz, acetone-d$_6$): δ (ppm) −2088.2.

ESI-MS: [M − 2Cl − H] (*m/z*) Calc., 332.1, Found, 332.2.

Elemental Analysis: $C_8H_{14}Cl_2N_2Pt$, Calc., C, 23.77%; H, 3.49%; N, 6.93%; Found, C, 23.53%; H, 3.36%; N, 6.93%.

3.2.2.20 *Trans*-[Pt(N$_3$)$_2$(IPA)(Py)] (20)

Trans-[Pt(N$_3$)$_2$(IPA)(Py)] (**20**) was synthesized by a similar procedure as for *trans*-[Pt(N$_3$)$_2$(DMA)(Tz)] (**12**) using *trans*-[PtCl$_2$(IPA)(Py)](**19**).

Yield: 98%

^{1}H NMR (400 MHz, acetone-d$_6$): δ (ppm) 8.80 (dd, H$_{2,6}$, ^{3}J (^{195}Pt, ^{1}H) = 30 Hz, 2H), 8.08 (tt, H$_4$, 1H), 7.62 (t, H$_{3,5}$, 2H), 4.34 (broad, NH$_2$, 2H), 3.19 (septet, CH,1H), 1.42 (d, CH$_3$, 6H).^{13}C NMR (150.9 MHz, acetone-d$_6$): δ (ppm) 152.5 (C$_{2,6}$), 139.0 (C$_4$), 126.3 (C$_{3,5}$), 48.3 (CH), 22.8 (CH$_3$). ^{195}Pt NMR (129.4 MHz, acetone-d$_6$): δ (ppm) −2205.0.

ESI-MS: [M − 2Cl − H]$^+$ (*m/z*) Calc., 332.1, Found, 332.1.

[M + Na]$^+$ (*m/z*) Calc., 440.1, Found, 440.1.

3.2.2.21 *Trans, trans, trans*-[Pt(N$_3$)$_2$(OH)$_2$(IPA)(Py)] (21)

Trans, trans, trans-[Pt(N$_3$)$_2$(OH)$_2$(IPA)(Py)] (**21**) was synthesized by a similar procedure as for *trans, trans, trans*-[Pt(N$_3$)$_2$(OH)$_2$(DMA)(Tz)] (**13**) using *trans*-[PtCl$_2$(IPA)(Py)] (**19**).

Yield: 34%.

^{1}H NMR (400 MHz, D$_2$O): δ (ppm) 8.75 (d, *H*$_{2,6}$, ^{3}J (^{195}Pt, ^{1}H) = 24 Hz, 2H), 8.23 (t, *H*$_4$, 1H), 7.78 (t, *H*$_{3,5}$, 2H), 3.29 (septet, C*H*, 1H), 1.38 (d, C*H*$_3$, 6H). ^{13}C NMR

(150.9 MHz, D_2O): δ (ppm) 149.5 ($\underline{C_{2,6}}$), 142.8 ($\underline{C_4}$), 127.6 ($\underline{C_{3,5}}$, ^3J (^{195}Pt, ^{13}C) = 25 Hz), 48.4 ($\underline{C}H$), 22.44 ($\underline{C}H_3$, ^3J (^{195}Pt, ^{13}C) = 16.6 Hz). ^{195}Pt NMR (129.4 MHz, D_2O): δ (ppm) 935.9.

ESI-MS: $[M + Na]^+$ (m/z) Calc., 474.1. Found, 474.0.

Elemental Analysis: $C_8H_{16}N_8O_2Pt$, Calc., C, 21.29%; H, 3.57%; N, 24.83%; Found, C, 21.69%; H, 3.39%; N, 24.51%.

3.2.3 NMR acquisition

NMR data was acquired by the author with the guidance from Dr. Nicola Farrer and Dr. Ivan Prokes (University of Warwick). Specific parameters, along with other general parameters for acquisition are found in **Chapter 2**.

3.2.4 Elemental analysis

Elemental analysis for general samples was performed on an EAI CE440 Elemental Analyser by the Warwick Analytical Service. For potentially explosive samples (Pt^{IV}-diazido complexes), they were analysed by MEDAC Ltd. in Surrey, UK.

3.2.5 X-ray crystallography

The data collection and analysis were carried out by Dr Guy Clarkson in University of Warwick. Structures were also analysed by the author. Instrumentation, acquisition parameters and data processing can be found in **Chapter 2**.

3.2.6 Cell culture and cytotoxicity for Pt complexes

The photoactivated dose-dependent inhibition to cell viability for light-sensitive Pt^{IV} diazidodihydroxido complexes was determined by Dr Julie A. Woods (University of Dundee). Cell culture and cytotoxicity for non-light-sensitive Pt^{II} dichlorido

complexes were determined by Dr Ana Pizarro (University of Warwick). Details can be found in **Chapter 2**.

3.3 Results and discussion

3.3.1 Synthesis

The platinum(IV)-diazidodihydroxido complexes were synthesized via oxidation of the respective *trans*-Pt^{II} diazido complexes using a revised reported method.[21, 38] All the new compounds synthesised are listed in **Appendix 1**. As pictured in **Scheme 3.2**, *cis*-$[PtCl_2(MA)_2]$, *cis*-$[PtCl_2(DMA)_2]$ and *cis*-$[PtCl_2(IPA)_2]$ were synthesized following the method described previously for cisplatin.[37, 39] In this step, direct replacement of Cl^- with aliphatic amine ligands L from $K_2[PtCl_4]$. This produces relatively low yields and are often contaminated with impurities such as "Magnus"green salt $[PtL_4][PtCl_4]$.[40,41] In 1970, Dhara published the procedure for synthesis of cisplatin which is adapted here.[39, 42] The *trans* effect (see **Chapter 1**) of the I^- ligand is higher than Cl^-. Therefore, excess I^- was used in the synthesis to form $[PtI_4]^{2-}$ before the ligand L (e.g. NH_3) is added. *cis*-$[PtI_2L_2]$ is formed cleanly without any significant tendency for $[PtL_4]^{2+}$.[43] The next step is the removal of iodido ligands using $AgNO_3$, forming *cis*-$[PtL_2(OH_2)_2]$ and insoluble AgI. This precipitate is fine powder and thus is filtered off through celite followed by an inorganic membrane filter (Sartorius, Minisart, 0.2 µm). After that, NaCl was added to form *cis*-$[PtCl_2L_2]$.

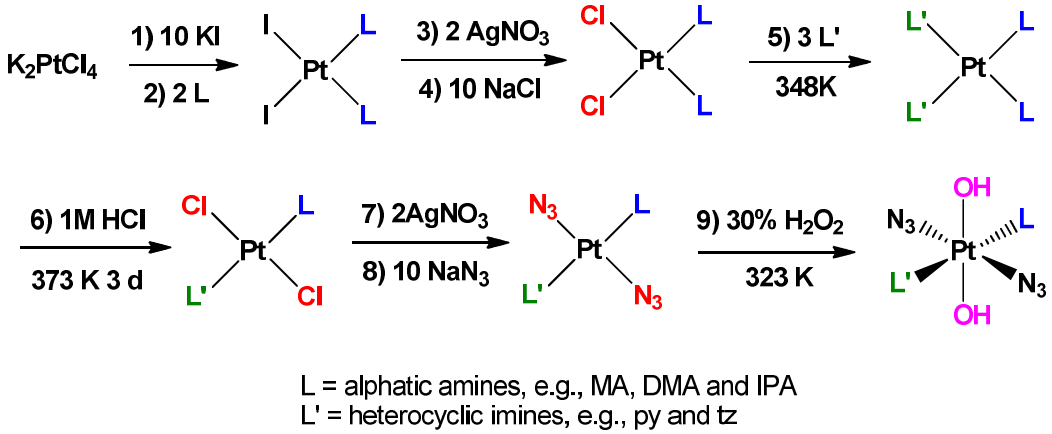

Scheme 3.2 Synthesis of platinum(IV) diazidodihydroxido complexes.

The synthesis of *trans*-[$PtCl_2LL'$] was carried out according to the method developed by Kauffman and Cowan in 1963.[11, 44-46] The basis of this method is that the *trans* effect of Cl^- is slightly stronger than that of heterocyclic imines and aliphatic amine ligands. In step 5 in **Scheme 3.2**, the two Cl^- in *cis*-[$PtCl_2L_2$] were replaced with L', forming *cis*-$[PtL'_2L_2]^{2+}$, which is kinetically favoured. In the step 6, the reaction mixture was refluxed in 1 M HCl at 373 K; this will substitute one of the N-ligands randomly. Subsequently, the second Cl^- substitutes the N-ligand preferentially on the *trans* position due to the larger *trans*-effect of Cl^-. Interestingly, the *trans*-[$PtCl_2LL'$] molecule is neutral and so tends to precipitate in aqueous solution, while the intermediates *cis*-$[PtL'_2L_2]^{2+}$ and $[PtClL_2L']^+$ and any additional side products (e.g., $[PtCl_3L']^-$) are quite soluble. The replacement of Cl^- with an N-ligand is an equilibrium, and disassociation of an N-ligand from Pt^{II} is kinetically much slower than that of Cl^-; thus excess acid must be used to protonate the N-ligand to push this equilibrium forward.

However, in some cases, step 6 produces the corresponding tetrachloro Pt^{IV} species, *trans*-[$PtCl_4LL'$], as a side product. Although the facile oxidation of Pt^{II} to Pt^{IV} in

aqueous HCl has been observed previously,[47-49] the mechanism of oxidation is still not fully understood.

There is a simplified synthetic route to make such mixed-ligand *trans* platinum(II) complexes (**Scheme 3.3**).[10, 46, 48] Silver nitrate was added to *cis*-[$PtCl_2L_2$] to remove the Cl^- and the L' was added immediately after that. The disadvantage of this route is that the nitrate can act as an oxidative reagent, especially after HCl is added in the next step. The reduction potential of HNO_3 is +0.96 V, which is much higher than the reduction potential of *cis*-[$Pt^{IV}Cl_4L_2$] (*ca.* −40 mV).[50, 51] Therefore, this reaction tends to generate more Pt^{IV} products.[46] In this work, this reaction route produced almost all Pt^{IV} tetrachloridoproducts. For this reason, all the *trans* Pt^{II} dichloridocomplexes were synthesized according to the route described in **Scheme 3.2**.

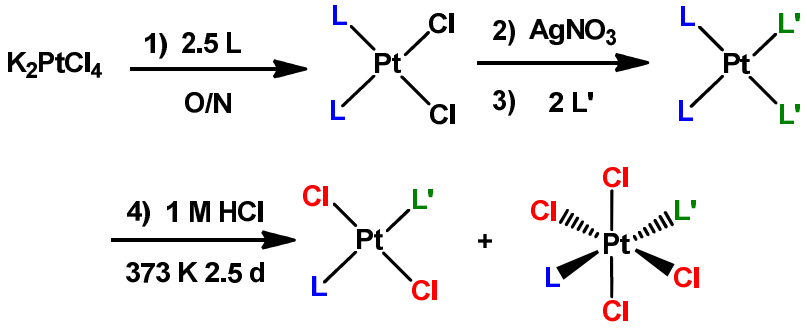

Scheme 3.3. Alternative synthetic routes to mixed-ligand *trans* Pt^{II} complexes. L=heterocyclic imine ligand, L'=aliphatic amine ligand.

In attempting to synthesize *trans*-[$PtCl_2$(IPA)(Tz)] (**18**), great difficulty was encountered to obtain a pure product. Only after three recrystallizations, could a satisfactory purity be obtained. A number of attempts were made to optimize the reaction conditions to increase the purity, including changing the molar equivalent of Tz, the reaction time and temperature. However, the purity could not be substantially improved. Therefore, the synthesis of diazido species was not attempted.

It is important to note at this stage that metal azides and high concentrations of H_2O_2 are dangerous, so care must be taken when handling them. Metal azides are also heat sensitive, and thus during the oxidation reactions the temperature should be carefully optimized. In this chapter, 333K is safe for most of the platinum azido complexes

3.3.2 NMR chemical shifts

The ^{1}H (NH_x) and ^{195}Pt NMR chemical shifts for Pt^{II} dichlorido/diazido and Pt^{IV} diazidodihydroxido complexes are summarized in **Table 3.1**. The ^{1}H NMR signal for amine groups in Pt^{II} complexes can be easily observed in acetone-d_6, as N-H solvent exchange is sufficiently slow. However, it is often not possible to observe the NH_x signal of Pt^{IV} complexes in D_2O, due to H-D exchange at ambient temperature ($t_{1/2}$ *ca.* a few minutes).[52, 53] It is possible to slow down the H-D exchange rate by lowering the pH. This approach was used to observe amine protons in aqueous solution. The ^{1}H NMR experiments for Pt^{IV} complexes in this work were carried out in H_2O:D_2O = 90%:10%, and the pH was adjusted to < 5. In general, the ^{1}H NMR chemical shifts for NH_x in all the Pt^{II} complexes are in the range of 4 – 5 ppm, and are 6 – 7 ppm for the Pt^{IV} complexes. Compared to the MA complexes, the ^{1}H chemical shifts of all DMA complexes shift downfield by 0.5 – 0.6 ppm and all IPA complexes shift upfield by 0.1 ppm.

The assignments of ^{195}Pt NMR spectra are consistent with published data.[54, 55] The ^{195}Pt NMR chemical shifts for the *trans*-[$Pt^{II}Cl_2L_2$], *trans*-[$Pt^{II}(N_3)_2L_2$] and *trans, trans, trans*-[$Pt^{IV}(N_3)_2(OH)_2LL'$] complexes are close to −2100 ppm, −2200 ppm and 900 ppm, respectively. In the literature, the ^{195}Pt chemical shifts of *trans*-{$Pt^{II}Cl_2N_2$} range from −1950 to −2250 ppm; *trans*-{$Pt^{II}N_4$} from −2150 to −2650 ppm; *trans, trans*-[$Pt^{IV}N_4O_2$] from 800 to 1200 ppm.[56] In general the resonances for Pt^{IV}

complexes appear at lower field than those for their Pt^{II} precursors. The chemical shifts of ^{195}Pt nuclei are very sensitive to the coordinated ligands. Generally speaking, the order of increased shielding effects of ^{195}Pt for coordinating atoms is: O < Cl^-< N (imine) < Br^- <N (amine) < S ~ I^- < As < P.[54, 55] For example, in the results presented in **Table 3.1** of this thesis, the shielding effect of N_3^- to ^{195}Pt nuclei is slightly higher than that for Cl^-.

In the formation of the Pt-N σ-bond, the extent of the electron donation of the heterocyclic imine ligands is smaller than that of the amine ligands leading to a less electron shielding on the Pt nucleus. The electron density on the Pt nucleus is thus reduced, resulting in deshielding of ^{195}Pt nucleus. For instance, the δ(Pt) of *trans*-[$Pt^{II}Cl_2MA_2$] and *trans*-[$Pt^{II}Cl_2Py_2$] are −2181 and −1948,[56] respectively, and the mixed ligand *trans*-[$Pt^{II}Cl_2LL'$] complexes in **Table 3.1** fall in between.

In the *trans*-[$Pt^{II}Cl_2LL'$] complexes, the ^1H chemical shifts of N$\underline{H}_x$ in Tz complexes are at lower field (*ca.* 0.09 ppm) than the corresponding Py complexes, while the ^{195}Pt chemical shifts are at higher field (*ca.* 25 ppm). In the *trans*-[$Pt^{II}(N_3)_2LL'$] the changes in aliphatic amine or heterocyclic imine ligands do not alter the chemical shifts of ^{195}Pt very much, but the chemical shifts of N$\underline{H}_x$ are different. In the *trans, trans, trans*-[$Pt^{IV}(N_3)_2(OH)_2LL'$] complexes, the Tz ligand shift the chemical shifts of ^{195}Pt nuclei downfield by ca. 20 ppm when compared to the corresponding Py complexes. Therefore, the shielding effect of Py and Tz vary in different types of Pt complexes.

In summary, a definite relationship between the structures and the amine (imine) ^1H and the ^{195}Pt NMR chemical shifts has been established. The chemical shifts can

therefore be considered as an unambiguous probe to distinguish the Pt^{II} and Pt^{IV} diazidodihydroxido complexes.

Table 3.1 ^{1}H (imine/amine) and ^{195}Pt NMR chemical shifts for platinum(II) dichlorido/diazido and Pt^{IV} diazidodihydroxido complexes.

General structures of complexes	Compound Number	L'	L	δ (^{1}H) (N$\underline{H}_x$) (ppm)	δ (^{195}Pt) (ppm)
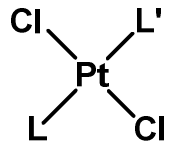	**3**	Py	MA	4.31	−2085.3
	14	Py	DMA	4.90	−2062.5
	19	Py	IPA	4.21	−2088.2
	6	Tz	MA	4.37	−2111.6
	11	Tz	DMA	4.99	−2086.1
	18	Tz	IPA	4.27	−2113.9
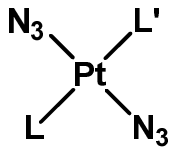	**4**	Py	MA	4.43	−2202.4
	15	Py	DMA	4.84	−2201.0
	20	Py	IPA	4.34	−2205.0
	7	Tz	MA	4.54	−2203.0
	12	Tz	DMA	4.98	−2193.2
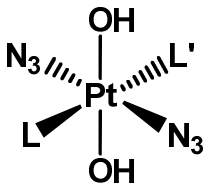	**5**	Py	MA	6.65	888.7
	16	Py	DMA	NT	926.4
	21	Py	IPA	NT	935.9
	8	Tz	MA	6.66	906.7
	13	Tz	DMA	NT	941.1

NT: not tested.

Last but not least, line broadening of the ^{195}Pt coupled ^{1}H NMR signals due to chemical shift anisotropy (CSA) relaxation was observed in the ^{1}H NMR spectra of platinum complexes. **Figure 3.2** shows the differences in the shape of ^{195}Pt satellites of ^{1}H NMR signals for $\underline{H_{2,6}}$ of the Py ligand of Pt^{II} and Pt^{IV} complexes at different magnetic fields. The effect of CSA relaxation for a particular nucleus is correlated

with the range of chemical shift for the nucleus. It turns out that ^{195}Pt, which has a large chemical shift range, also has a large CSA effect.[54] Also, the Pt^{II} complexes have square-planar geometry and so a large chemical shift anisotropy. By contrast, Pt^{IV} complexes with higher symmetry (octahedral geometry) are expected to have smaller anisotropy. The CSA effect influences the proton nucleus coupled to Pt nucleus. Due to the lower symmetry of the Pt^{II} species, their ^{195}Pt satellites are much broader compared to those in the Pt^{IV} complexes.(**Figure 3.2**) Also, CSA relaxation increases with the square of the applied magnetic field, nuclear screening anisotropy, molecular weight and lowering of the temperature.[57] As shown in **Figure 3.2**, at higher ^{1}H resonance frequency (600 MHz), the Pt satellites on either side of the proton signal for $\underline{H_{2,6}}$ are broader than at lower frequency (400 MHz).[57, 58] This effect is more significant for the Pt^{II} complexes compared to the Pt^{IV} complexes, as the Pt^{II} complexes have larger CSA. The CSA relaxation is also discussed in **Chapter 2**.

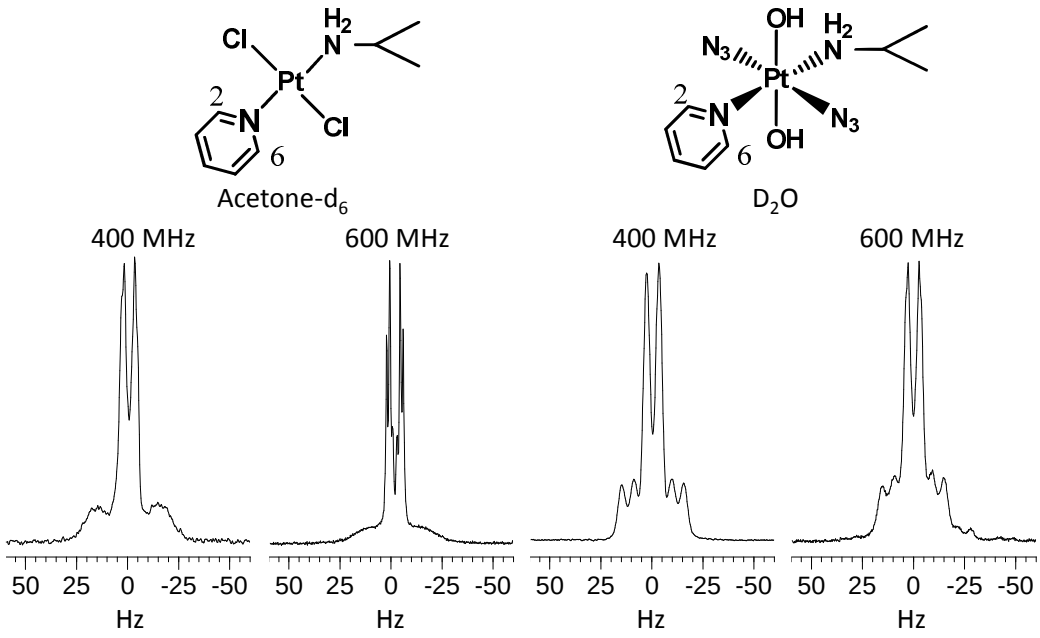

Figure 3.2 The ^{1}H NMR signal of the $\underline{H_{2,6}}$ in the Py ligand of complexes *trans*-[$Pt(N_3)_2$(IPA)(Py)] and *trans*, *trans*, *trans*-[$Pt(N_3)_2(OH)_2$(IPA)(Py)] recorded in different frequencies (400 MHz and 600 MHz).

3.3.3 X-ray structures

Crystals for X-ray diffraction studies of *trans, trans, trans*-[$Pt(N_3)_2(OH)_2(MA)(Py)$] (**5**), *trans, trans, trans*-[$Pt(N_3)_2(OH)_2(MA)(Tz)$] (**8**), *trans, trans, trans*-[$Pt(N_3)_2(OH)_2(DMA)(Tz)$] (**13**) and *trans, trans, trans*-[$Pt(N_3)_2(OH)_2(DMA)(Py)$] (**16**) were obtained by diffusion of diethyl ether into an ethanolic solution of the product at 298 K. The crystallographic data are summarized in **Table 3.2**.

Table 3.2 Crystallographic data for complex **5p**, **5q, 8, 13** and **16**.

Complex	**5p**	**5q**	**8**	**13**	**16**
Chemical structure	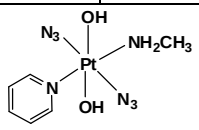		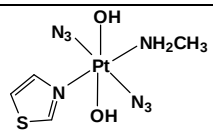	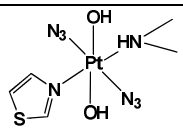	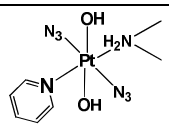
Empirical formula	$C_6H_{12}N_8O_2Pt$	$C_6H_{12}N_8O_2Pt$	$C_4H_{10}N_8O_2PtS$	$C_5H_{12}N_8O_2PtS$	$C_7H_{14}N_8O_2Pt$
Formula weight	423.33	423.33	429.35	443.38	437.35
Crystal description	Block	Block	Block	Block	Block
Crystal colour	Yellow	Yellow	Yellow	Yellow	Yellow
Crystal system	Triclinic	Monoclinic	Orthorhombic	Triclinic	Monoclinic
Space group	*P*-1	*C*2/*c*	*P*2(1)2(1)2(1)	*P*-1	*P*2(1)/*c*
a (Å)	8.0249(5)	17.4032(5)	6.84656(14)	7.9713(13)	18.2758(7)
b (Å)	8.2392(5)	5.7967(2)	12.5237(2)	8.9621(17)	13.7047(5)
c (Å)	8.6317(5)	22.7173(8)	12.9730(3)	9.1501(17)	10.2777(4)
α (°)	84.236(5)	90	90	75.237(16)	90
β (°)	79.453(5)	93.863(3)	90	78.152(15)	90.026(4)
γ (°)	83.981(5)	90	90	84.912(15)	90
Volume ($Å^3$)	556.05(6)	2286.54(13)	1112.36(4)	618.18(19)	2574.20(17)
Z	2	8	4	2	8

D_{calcd} (g/cm^3)	2.528	2.459	2.564	2.382	2.257
F (000)	396	1584	800	416	1648
μ_{calcd} (mm^{-1})	12.624	12.280	12.804	11.524	10.912
Measurement temp. (K)	100(2)	100(2)	100(2)	296(2)K	100(2)
θ Range (°)	<32.74	<32.76	<32.65	<31.06	<29.40
Reflections collected	11442	13569	14240	10824	9565
Independent reflections	3781	3836	3812	3574	5619
Goodness-of-fit F^2	1.104	0.971	1.030	0.994	1.093
Conventional *R1*	0.0224	0.0249	0.0216	0.0453	0.0398
wR_2	0.0579	0.0556	0.0467	0.1087	0.0999

3.3.3.1 *Trans, trans, trans*-[Pt(N$_3$)$_2$(OH)$_2$(MA)(Py)] (5)

Two different crystal structures were isolated and analysed for complex **5** (**Figure 3.3** for **5p** and **5q**), which were the first polymorphs found for Pt^{IV}-diazido complexes. The two structures have identical formulae, with the Pt^{IV} adopting octahedral geometry, but their lattice system, space group and the dimensions of unit cells are different. The structure **5p** adopts the triclinic lattice system, the space group is *P*-1 and the unit cell has two molecules, whereas the structure **5q** adopts the monoclinic lattice system, the space group is *C*2/*c* and the unit cell has eight molecules. It is of interest that their azido groups adopt different orientations. The dihedral angles of N_{Py}–Pt–N_9–N_{10} and N_{Py}–Pt–N_{12}–N_{13} are −34° and 97°, respectively, in the structure of **5p**, whereas the corresponding angles in the structure of **5q** are −6° and −23°.

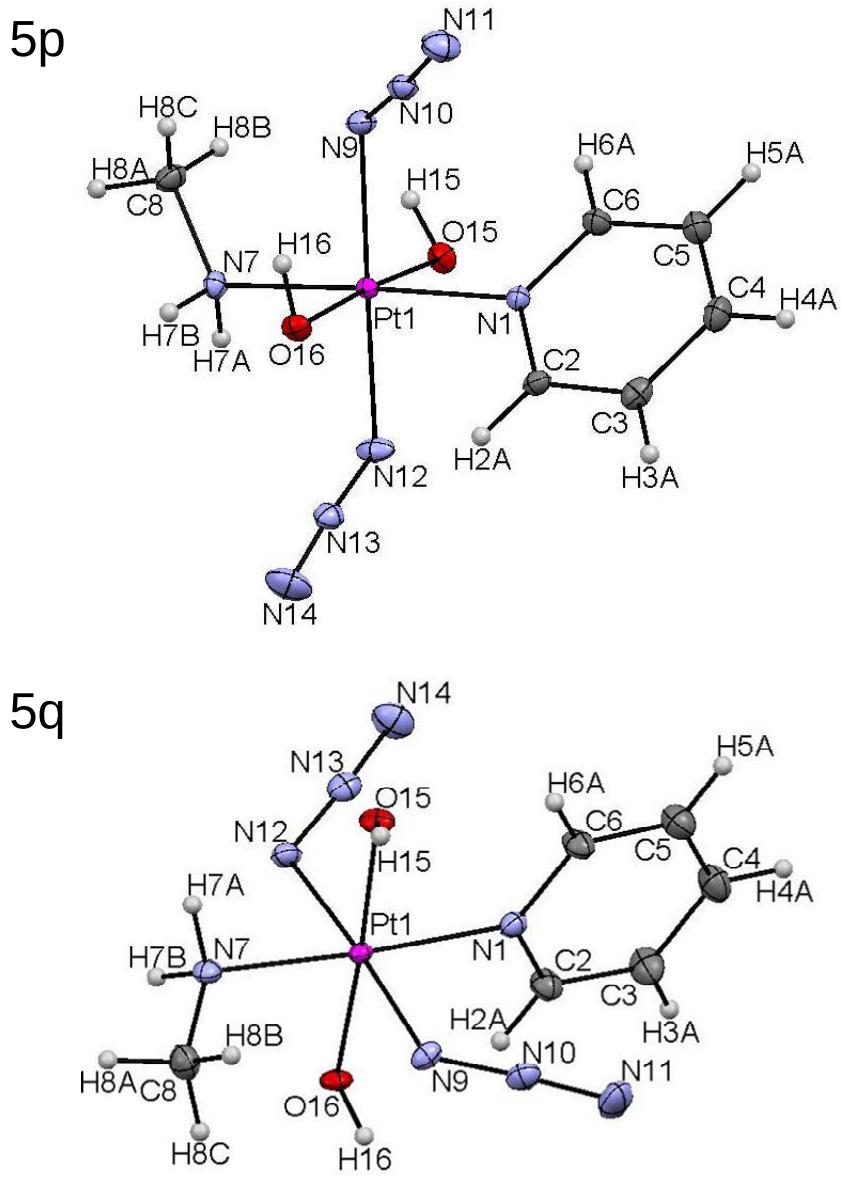

Figure 3.3 X-ray crystallographic structure of complexes **5p** and **5q** with ellipsoids set at 50% probability. (100 K)

The different orientations of the azido ligands are influenced by the intra- and intermolecular H-bonds (see **Figure 3.4** and **3.5**). It is widely acknowledged that the hydrogen bond is an attractive interaction between a hydrogen atom from a molecule or a molecular fragment D–H in which D (donor) is more electronegative than H, and an atom A (acceptor) or a group of atoms in the same or a different molecule (D−H···A).[59] Generally, the H···A lengths below 1.5 Å, from 1.5 to 2.2 and from 2.2

to 3.2 are regarded to be strong, medium and weak H-bonds respectively.[60] The preferred donor (D) and acceptor (A) atoms are F, O and N, etc. C−H can also form weak H-bonds in the presence of strong acceptors. As shown in **Figure 3.4** and **3.5**, in the crystal structures of **5p** and **5q**, medium H-bonds are in many cases formed with the types of O−H···N, N−H···O and O−H···O, while weak H-bonds are formed as intramolecular O−H···N, C−H···N and intermolecular C−H···N. The angles of D−H···A are between 90° and 180°.

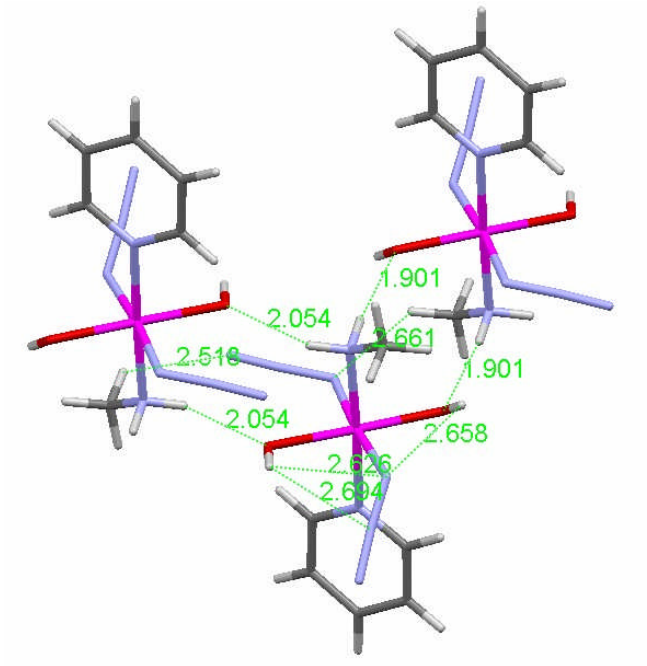

Figure 3.4 Extensive intra- and inter- molecular H-bonds network formed by azido and hydroxido ligands in the structure of **5p** which determines the orientation of the azido ligands.

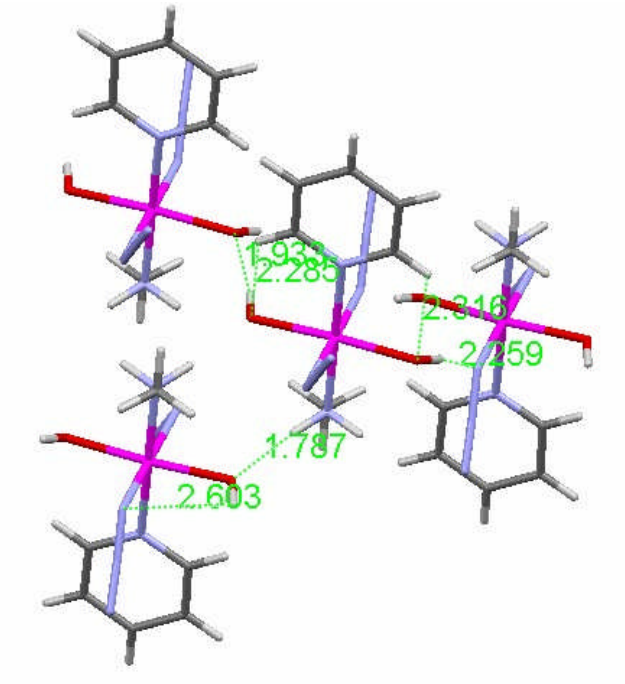

Figure 3.5 Extensive intra- and inter-molecular H-bonds network involving azido and hydroxido ligands in the structure of **5q** which determine the orientation of the azido ligands.

In the structures of **5p** and **5q**, Pt–N and Pt–O bond lengths are similar to those of related published complexes, e.g., *trans*, *trans*, *trans*-$[Pt(N_3)_2(OH)_2(NH_3)(Py)]$ (**22**),[21] *trans*, *trans*, *trans*-$[Pt(N_3)_2(OH)_2(NH_3)(Tz)]$(**23**)[38] and *trans*, *trans*, *trans*-$[Pt(N_3)_2(OH)_2(Py)_2]$(**24**),[24] and the azido groups are approximately linear (N–N–N angles 174° − 175°). Selected bond length and angles are listed in **Table 3.3**.

Table 3.3 Selected bond lengths [Å] and angles [°] for structures **5p** and **5q**.

Bond/angle	**5p**	**5q**
Pt(1)-O(16)	2.006(2)	2.005(2)
Pt(1)-O(15)	2.013(2)	2.011(2)
Pt(1)-N(12)	2.044(3)	2.026(3)
Pt(1)-N(7)	2.048(3)	2.056(3)
Pt(1)-N(9)	2.049(3)	2.063(3)
Pt(1)-N(1)	2.055(3)	2.068(3)
O(16)-Pt(1)-O(15)	176.41(8)	176.65(10)
N(12)-Pt(1)-N(9)	174.90(10)	176.43(13)
N(7)-Pt(1)-N(1)	177.38(9)	176.10(11)
N(10)-N(9)-Pt(1)	118.7(2)	115.4(2)
N(11)-N(10)-N(9)	174.6(3)	174.9(4)
N(13)-N(12)-Pt(1)	117.1(2)	116.2(2)
N(14)-N(13)-N(12)	174.6(4)	175.5(4)

In the structures of **5p**, an offset $\pi - \pi$ stacking interaction between two neighbouring pyridines was observed (**Figure 3.6**). The $\pi - \pi$ stacking interactions adopt a "face-to-face" geometry and the two pyridine planes have a centroid-centroid distance of 3.95 Å. These rings are parallel as they are related by an inversion centre. According to a search in Cambridge Structural Database (CSD) to the reported $\pi - \pi$ stacking between metal coordinated pyridines,[61] up to the year of 2000, the relative maximum of the centroid–centroid contacts between two pyridine fragments in the number of examples was found around 3.8 Å. Therefore, the $\pi - \pi$ interaction in **5p** is medium-weak. Generally, there are two conformation of $\pi - \pi$ stacking: face-to-face and T-shape. Face-to-face stacking does not necessarily have to be a perfect face-to-face alignment of the aromatic rings but can also be offset or slipped packing. As shown

in **Figure 3.6** for structure **5p**, the parallel displacement of two centroids is *ca.* 2.4 Å, which is a relative large value.

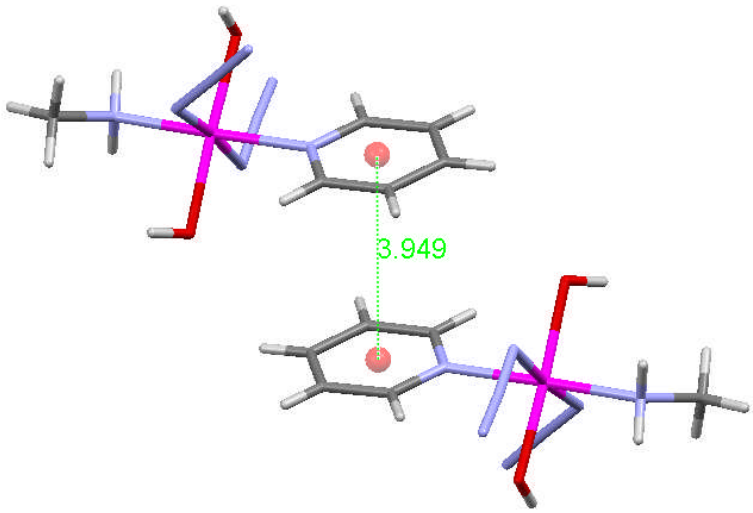

Figure 3.6 The "face-to-face" π–π stacking interactions in structure of **5p** between two parallel Py ligands in adjacent molecules (centroid-centroid distance, 3.949 Å).

In the structure of **5q**, a *zigzag* chain of Py fragments was found along the *a* axis (**Figure 3.7**). The centroid-centroid distances between neighbouring Py rings are 4.89 and 5.43Å, respectively and the angle of the two Py planes is 60.2°. These centroid-centroid distances and the inter-plane angles are too large to classify this as π–π stacking. Previous studies[61] have shown that the majority of intermolecular metal coordinated-pyridine plane contacts are close to parallel with a certain amount of displacement. Also, centroid-centroid distances over 4.6 Å are not considered to be π–π stacking.

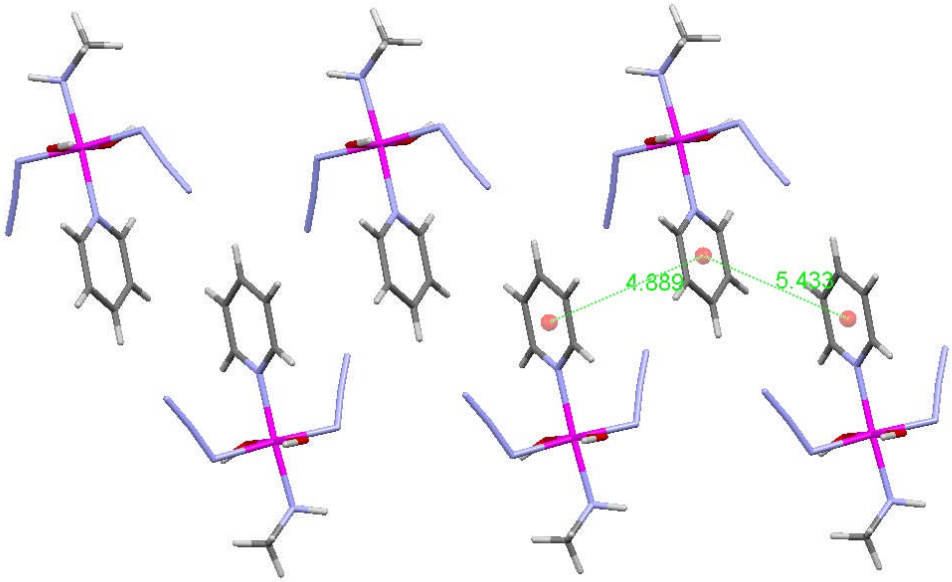

Figure 3.7 A *zigzag* chain of pyridines along the *a* axis in structure of **5q.** The centroid-centroid distances between neighbouring Py rings are 4.889 and 5.433 Å, respectively. The angles of two Py planes are 60.20°.

3.3.3.2 *Trans, trans, trans*-[$Pt(N_3)_2(OH)_2(MA)(Tz)$] (8)

In the structure of *trans, trans, trans*-[$Pt(N_3)_2(OH)_2(MA)(Tz)$]**(8)**, Pt^{IV} adopts an octahedral geometry (**Figure 3.8**). In previous published X-ray crystal structures of Pt^{II} and Pt^{IV} thiazole complexes *trans*-[$PtCl_2(Tz)_2$],[62] *trans*-[$PtCl_2(NH_3)(Tz)$][63] and *trans, trans, trans*-[$Pt(N_3)_2(OH)_2(NH_3)(Tz)$],[38] platinum is always bound to the nitrogen atom of thiazole. Calculations on the electron density of thiazole have shown that the net charge of the thioether-type sulphur is positive,[63] whereas the negative charge is located on the nitrogen and it is therefore a much better donor to platinum. For this reason, in complex **8**, it was assigned that thiazole bind through the nitrogen. Various levels of intra- and inter-molecular H-bonds were also found between N_α and N_γ in azido group and adjacent protons of hydroxido ligands. The extensive H-bonds network is depicted in **Figure 3.9**, in which the shortest contact is 1.84Å. In the structure of **8**, Pt–N and Pt–O bond lengths are similar to those of

published complexes,[21, 24, 38] and the azido groups are approximately linear (N–N–N angles 173° – 174°) (**Table 3.4**).

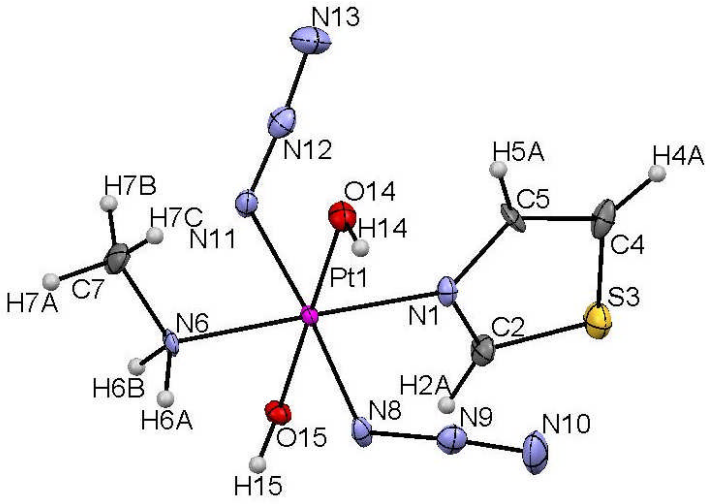

Figure 3.8 X-ray crystal structure of *trans*, *trans*, *trans*-$[Pt(N_3)_2(OH)_2(MA)(Tz)]$ (**8**) with ellipsoids set at 50% probability. (100 K)

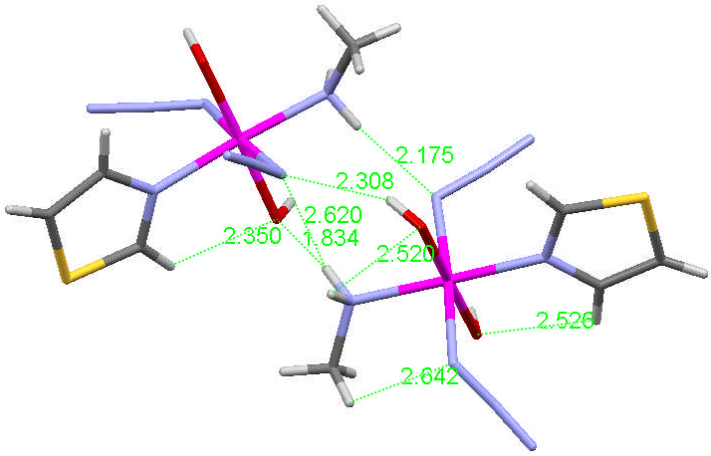

Figure 3.9 Extensive intra- and inter-molecular H-bonds networks involving azido and hydroxido ligands in the crystal structure of *trans*, *trans*, *trans*-$[Pt(N_3)_2(OH)_2(MA)(Tz)]$ (**8**).

Table 3.4 Selected bond lengths [Å] and angles [°] for *trans, trans, trans*-[$Pt(N_3)_2(OH)_2(MA)(Tz)$] (**8**).

Bond/angle	Å/°
Pt(1)-O(14)	2.010(3)
Pt(1)-O(15)	2.021(2)
Pt(1)-N(6)	2.032(3)
Pt(1)-N(8)	2.041(3)
Pt(1)-N(1)	2.049(3)
Pt(1)-N(11)	2.061(3)
O(14)-Pt(1)-O(15)	178.40(12)
N(6)-Pt(1)-N(1)	176.99(13)
N(8)-Pt(1)-N(11)	175.70(13)
N(9)-N(8)-Pt(1)	117.5(3)
N(10)-N(9)-N(8)	174.6(5)
N(12)-N(11)-Pt(1)	116.6(3)
N(13)-N(12)-N(11)	173.7(4)

3.3.3.3 *Trans, trans, trans*-[$Pt(N_3)_2(OH)_2(DMA)(Tz)$] (13)

In the crystal structure of *trans, trans, trans*-[$Pt(N_3)_2(OH)_2(DMA)(Tz)$] **(13)**, Pt^{IV} again adopts an octahedral geometry (**Figure 3.10**). The thiazole was refined as disordered over two positions by rotation of 180 degrees about the Tz N-Pt bond in a ratio of 70:30. Similar to complex **8**, it was assigned that Tz bonding was through the nitrogen atom. Various levels of intra- and inter- molecular H-bonds were found between N_α of the azido group and adjacent NH or OH protons, (**Figure 3.11**) in which the shortest contact is 1.89 Å. In this structure, there are also very weak π–π stacking interactions adopting "face-to-face" geometry and the centroid-centroid distance of the rings is 4.455 Å (**Figure 3.12**). In the structures of **13**, Pt–N and Pt–O bond lengths are similar to those of related published complexes,[21, 24, 38] and the

azido groups are close to linear (N–N–N angles 173° – 175°). Selective bond length and angles are listed in **Table 3.5**.

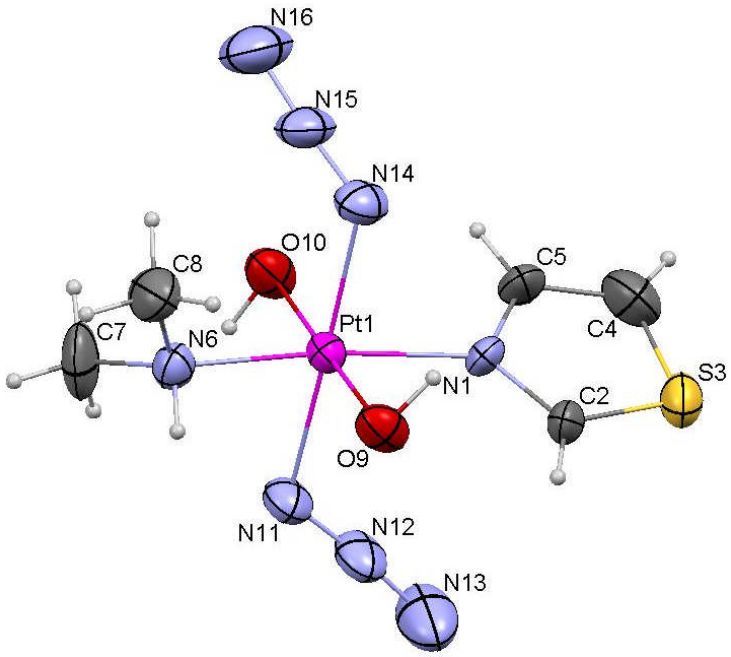

Figure 3.10 X-ray crystal structure of *trans, trans, trans*-[$Pt(N_3)_2(OH)_2$(DMA)(Tz)](**13**) with atom numbering. The minor disordered component of the thiazole ring has been removed for clarity. Ellipsoids are set at 50% probability. (296 K)

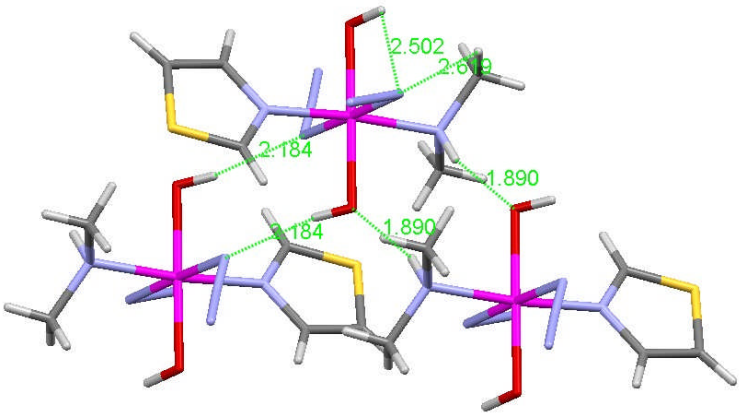

Figure 3.11 Intra- and inter- molecular H-bonds in the X-ray crystal structure of *trans, trans, trans*-[$Pt(N_3)_2(OH)_2$(DMA)(Tz)] (**13**)

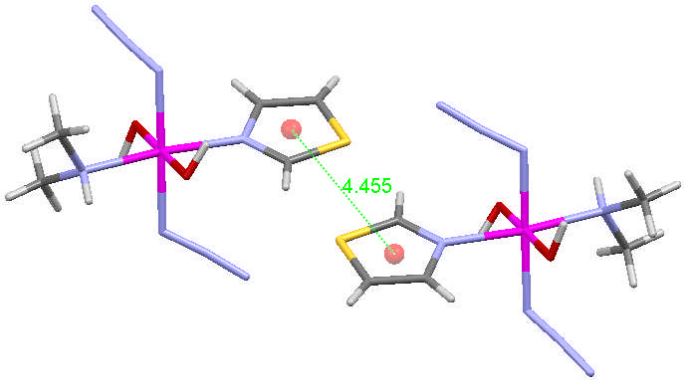

Figure 3.12 The weak "face-to-face" π–π stacking interactions in structure of **13** between two parallel Tz ligands in neighbouring molecules (centroid-centroid distance, 4.455 Å).

Table 3.5 Selected bond lengths [Å] and angles [°] for *trans*, *trans*, *trans*-$[Pt(N_3)_2(OH)_2(DMA)(Tz)]$ (**13**).

Bond/angle	Å/°
Pt(1)-O(10)	2.021(6)
Pt(1)-O(9)	2.022(5)
Pt(1)-N(14)	2.050(6)
Pt(1)-N(6)	2.059(7)
Pt(1)-N(11)	2.064(6)
Pt(1)-N(1)	2.071(18)
O(10)-Pt(1)-O(9)	178.6(2)
N(1A)-Pt(1)-N(6)	179.1(12)
N(14)-Pt(1)-N(11)	178.0(3)
N(6)-Pt(1)-N(1)	172.9(4)
N(12)-N(11)-Pt(1)	117.2(5)
N(13)-N(12)-N(11)	174.9(9)
N(15)-N(14)-Pt(1)	116.9(6)
N(16)-N(15)-N(14)	173.1(9)

3.3.3.4 *Trans, trans, trans*-[Pt(N$_3$)$_2$(OH)$_2$(DMA)(Py)] (16)

The crystal *trans, trans, trans*-[Pt(N$_3$)$_2$(OH)$_2$(DMA)(Py)] (**16**) chosen was refined as monoclinic with a beta angle very close to 90° (90.026°) emulating orthorhombic. The asymmetric unit contains two molecules. The Pt^{IV} adopts an octahedral geometry (**Figure 3.13**) and the Pt–N and Pt–O bond lengths are similar to those of related published complexes (**Table 3.6**).[20,23,36] Various levels of intra- and inter-molecular H-bonds were found between N$_\alpha$ of the azido group and adjacent NH or OH protons are depicted in **Figure 3.14**, in which the shortest contact is 1.83 Å. There is no observed π–π stacking interaction between the pyridine rings in this structure as the closest contact is >5 Å away.

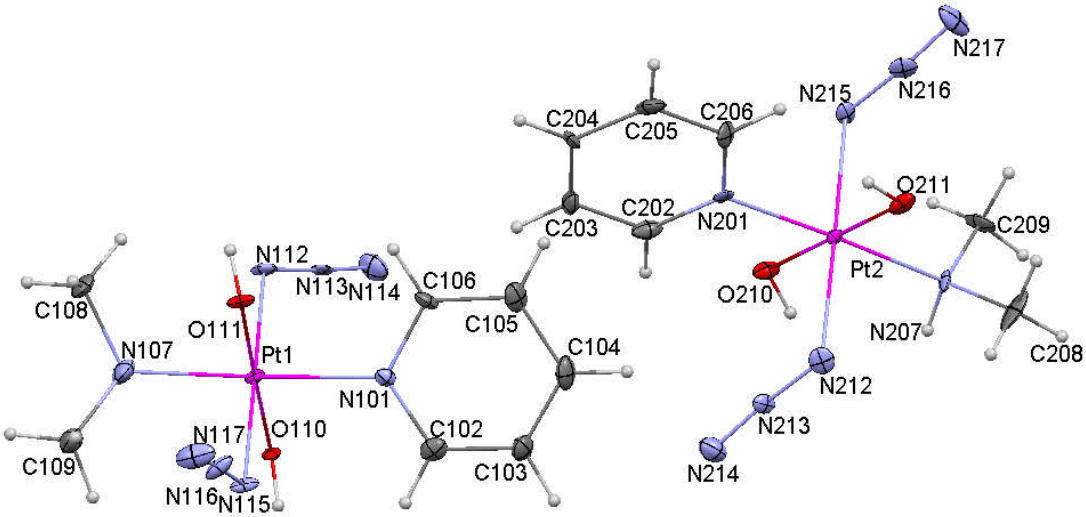

Figure 3.13 X-ray crystal structure of *trans, trans, trans*-[Pt(N$_3$)$_2$(OH)$_2$(DMA)(Py)](**16**) with atom numbering. The asymmetric unit contains two molecules. Ellipsoids are set at 50% probability. (100 K)

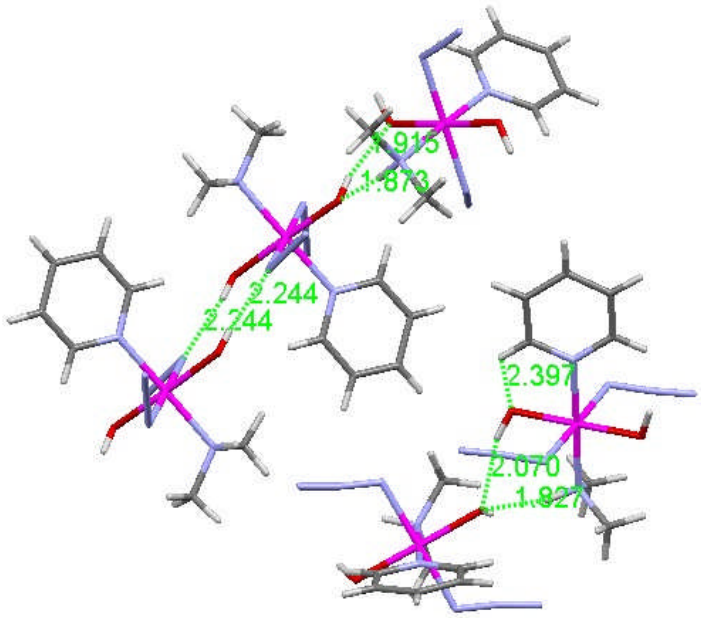

Figure 3.14 Intra- and inter-molecular H-bond network in the X-ray crystal structure of *trans*, *trans*, *trans*-[Pt(N_3)$_2$(OH)$_2$(DMA)(Py)] (**16**)

Table 3.6 Selected bond lengths [Å] and angles [°] for *trans*, *trans*, *trans*-[Pt(N_3)$_2$(OH)$_2$(DMA)(Py)] (**16**). A comparison is made between the two molecules in the asymmetric unit Pt(1) and Pt(2).

Bond/angle	Å/°	Bond/angle	Å/°
Pt(1)-O(210)	2.003(5)	Pt(2)-O(110)	2.020(5)
Pt(1)-O(211)	2.008(5)	Pt(2)-O(111)	2.000(5)
Pt(1)-N(215)	2.052(7)	Pt(2)-N(115)	2.069(7)
Pt(1)-N(212)	2.059(7)	Pt(2)-N(112)	2.036(6)
Pt(1)-N(201)	2.062(7)	Pt(2)-N(101)	2.031(7)
Pt(1)-N(207)	2.074(6)	Pt(2)-N(107)	2.057(8)
O(210)-Pt(1)-O(211)	179.3(3)	O(111)-Pt(2)-O(110)	178.6(2)
N(215)-Pt(1)-N(212)	179.2(3)	N(112)-Pt(2)-N(115)	179.5(3)
N(201)-Pt(1)-N(207)	178.0(3)	N(101)-Pt(2)-N(107)	176.6(3)
N(213)-N(212)-Pt(1)	116.1(6)	N(113)-N(112)-Pt(2)	116.4(5)
N(214)-N(213)-N(212)	174.2(9)	N(114)-N(113)-N(112)	176.6(9)
N(216)-N(215)-Pt(1)	115.7(5)	N(116)-N(115)-Pt(2)	112.7(5)
N(217)-N(216)-N(215)	174.2(9)	N(117)-N(116)-N(115)	176.3(9)

3.3.4 Photocytotoxicity of platinum(IV) diazidodihydroxido complexes

The photoactivated dose-dependent inhibitions to cell viability (IC_{50} values against a number of human cell lines) for complexes **5** and **8** are summarised in **Table 3.7**. The corresponding data for cisplatin, *trans*, *trans*, *trans*-$[Pt(N_3)_2(OH)_2(NH_3)(Py)]$ (**22**),[21] *trans*, *trans*, *trans*-$[Pt(N_3)_2(OH)_2(NH_3)(Tz)]$ (**23**)[38] and *trans*, *trans*, *trans*-$[Pt(N_3)_2(OH)_2(Py)_2]$ (**24**),[24] are also listed for comparison. In the absence of light, complexes **5** and **8** were not substantially cytotoxic to HaCaT (human keratinocytes), A2780 (cisplatin sensitive ovarian adenocarcinoma cells), A2780cis (the cisplatin-resistant subline of A2780) or OE19 (oesophageal adenocarcinoma cells) under the experimental conditions used. However, upon irradiation with UVA (λ_{max} = 365 nm), the cytotoxicities of complexes **5** and **8** towards the above cells were increased and were observed to be greater than that of cisplatin (50 – 65-fold) under the experimental conditions used (light dose 5 J/cm^2). It is notable that towards HaCaT cells, complexes **5** and **8** were more potent with activation by UVA or blue light (TL03 lamp, λ_{max} = 420 nm) than complexes **22** and **23**. Although complexes **5** and **8** were slightly less photocytotoxic against A2780 cells upon irradiation with UVA than the previously reported complexes **22** and **24**, they were *ca*. 3-fold more toxic towards the cisplatin-resistant subline A2780cis. The resistance factor (RF, IC_{50} resistant/parent line)[9] for complexes **5** and **8** are about 1.9 and 1.6, respectively, much lower than that for complexes **22**, **23** and **24** (8.9, 2.9 and 10.3). Upon irradiation with TL03, complexes **5** and **8** were still highly cytotoxic against A2780, A2780cis and OE19 cell lines, although they were generally less potent than upon irradiation with UVA. Remarkably, the photocytotoxicity of complex **5** against OE19 cell lines and complex **8** against A2780 cell lines upon irradiation with blue light was comparable to the cytotoxicity upon irradiation with UVA. When

comparing complexes **5** and **8**, it was observed that **5** was slightly more active against HaCaT, A2780 and A2780cis cell lines upon irradiation with UVA and against OE19 cell lines with TL03, while complex **8** was more active towards OE19 cells upon irradiation with UVA and towards HaCaT, A2780 cell lines upon irradiation with TL03.

Table 3.7 Phototoxicity (IC_{50} value[a]/μM) of *trans, trans, trans*-$[Pt(N_3)_2(OH)_2(MA)(Py)]$ (**5**) and *trans, trans, trans*-$[Pt(N_3)_2(OH)_2(MA)(Tz)]$ (**8**), with comparison to cisplatin, complexes **22**, **23** and **24**.

Complex	HaCaT			A2780			A2780cis			OE19		
	UVA	TL03[b]	sham[e]	UVA	TL03	sham	UVA	TL03	sham	UVA	TL03	sham
5	2.6	15.0	>236.3[c]	2.3	34.3	>236.3	4.4	14.1	>236.3	10.1	13.9	>236.3
8	3.5	11.2	>232.9	3.2	2.2	>232.9	5.3	14.0	>232.9	6.2	19.3	>232.9
22[21]	6.8	85.9	>244.4	1.9	NT[d]	>244.4	16.9	NT	>244.4	10.0	NT	>244.4
23[64]	4.5	19.8	>241.0	5.5	NT	186.9	16.2	NT	>241.0	NT	NT	NT
24[24]	2.2	6.8	>212.3	1.4	NT	>212.3	14.5	NT	>212.3	4.7	8.4	>212.3
Cisplatin (**26**)	144.0	NT	173.3	151.3	NT	152.0	261.0	NT	229.0	NT	NT	NT

[a] IC_{50} is the concentration of complex that inhibited cell growth by 50%. The lower value indicates higher toxicity to cells. Each value is mean of two or three independent experiments.

[b] TL03 is a blue light lamp (λ_{max} = 420 nm).

[c] > indicates IC_{50} greater than the concentration range used.

[d] not tested.

[e] sham: dark control.

By comparing complexes **5**, **8** and **22** – **24**, several structure-activity relationships can be established. (a) Substituting pyridine by thiazole can improve the photocytotoxicity towards HaCaT and A2780 cell lines upon irradiation with blue light. (b) Changing NH_3 to MA can in many cases increase the cytotoxicity upon

irradiation with UVA towards HaCaT, A2780, A2780cis and OE19 cell lines, and the phototoxicity towards HaCaT cell lines upon irradiation with TL03 was substantially increased. (c) The complexes with MA were very potent towards A2780cis cells upon irradiation with UVA, with a resistance factor < 2. Even upon irradiation with blue light, the IC_{50} values were still smaller than the other compounds upon irradiation with UVA.

The differences in photocytotoxicity values may depend on a number of factors. The cells are very sensitive towards even very tiny changes in the structures of complexes. Firstly, different aliphatic amine and heterocyclic imine groups have effects on the photochemistry of the complexes. The extinction coefficient, photochemical reaction rate and extent can be very different. A study to explore this difference is carried out in **Chapter 4**. Secondly, different aliphatic amine and heterocyclic imine groups also change the hydrophilicity/lipophilicity of the complexes and the shape of the molecules which can impact on their cellular uptake and accumulation within the cell. Furthermore, if the complexes bind to DNA and this plays a role in the mechanism of action then the ligands will affect DNA distortions, such as bending, kinking and unwinding. Experiments related to these possibilities are currently being carried by our collaborators. Thirdly, it was of interest to discover that complexes **5** and **8** exhibit lower cross-resistance to cisplatin towards A2780cis cell lines than the other complexes. A2780cis is an acquired cisplatin-resistant subline derived from A2780 ovarian carcinoma cells.[65] One or more of the following mechanisms may correspond to the resistance: insufficient platinum may reach and bind to the target DNA (by reduced accumulation or increased cytoplasmic detoxification by cellular thiols); increased DNA repair/tolerance of platinum-DNA adducts may lead to failure to achieve cell death.[6,

[66] Experiments designed to explore these possibilities are also being carried by our collaborators.

3.3.5 Cytotoxicity of platinum(II) precursors

In *trans, trans, trans*-[$Pt(N_3)_2(OH)_2LL'$], N_3^- and OH^- are leaving groups upon irradiation with light, and the L and L' groups can be regarded as non-leaving groups.[67, 68] After binding to DNA, L and L' remain with the Pt on the DNA lesion (also see **Chapter 4**). Therefore, it is reasonable to assume that the Pt^{II} complexes with the formula *trans*-[$PtCl_2LL'$] may partly have similar properties as the Pt^{IV} diazidodihydroxido complexes. In other words, the Pt^{IV} diazidodihydroxido complexes can act to a certain extent as the prodrugs of the corresponding *trans*-[$PtCl_2LL'$] complexes.

Although transplatin is not active towards cancer cells, a number of novel platinum complexes with *trans*-geometry have been found to be very toxic to cancer cells.[69-71] More importantly, these complexes often act with mechanisms different from that for cisplatin, so as to circumvent cisplatin resistance. If the DNA binding behaviour of complexes **5** and **8** is different from cisplatin, but similar to transplatin or other *trans* platinum complexes, this would contribute to their lower resistance factors.

In order to investigate the similarity and difference between the Pt^{IV} diazidodihydroxido complexes and their Pt^{II} dichlorido analogues *trans*-[$PtCl_2LL'$], the cytotoxicities of complexes *trans*-[$PtCl_2$(MA)(Py)] (**3**), *trans*-[$PtCl_2$(MA)(Tz)] (**6**), *trans*-[$PtCl_2$(DMA)(Tz)] (**11**), *trans*-[$PtCl_2$(DMA)(Py)] (**14**) and *trans*-[$PtCl_2$(IPA)(Py)] (**17**) were determined. The toxicity was not photoinduced, as they are not photoactive. To the best of the author's knowledge, no cytotoxicity data for this class of *trans*-Pt^{II} complexes with mixed aliphatic amine/heterocyclic imine

ligands has been previously reported. The data and comparison with cisplatin are listed in below (**Table 3.8**). Although the cell-line examined in this experiment was limited to A2780 only, some useful results and conclusions can be obtained. This class of complexes is very potent tytotoxic towards the A2780 cells compared to the published *trans*-Pt^{II} compounds.[72-75] The IC_{50} values of complex **3**, **11** and **14** are comparable to cisplatin despite having a *trans* geometry. The details of mechanism of action have yet to be fully elucidated. Complex **3** is *ca.* three times more cytotoxic compared to complex **6** against A2780 cells. However, the difference in photocytotoxicity of corresponding Pt^{IV} diazidodihydroxido complexes **5** and **8** is small. The difference can be attributed to their photochemistry, as will be explored in **Chapter 4**.

Table 3.8 Cyototoxicity data for a series of *trans*-[$PtCl_2LL'$] complexes towards the A2780 cell line[a] in comparison with cisplatin.

Compound No.	L/L'	$IC_{50}/\mu M$[b] (A2780)
3	MA/Py	2.4±0.7
6	MA/Tz	6.9±2.3
11	DMA/Tz	2.1±0.3
14	DMA/Py	2.3±0.3
17	IPA/Py	5.9±0.9
Cisplatin	–	1.5±0.3

[a] This experiment was carried out in ambient light conditions.

[b] Each value is mean of two independent experiments.

In summary, complexes **3** and **6**, as the precursors of complexes *trans*, *trans*, *trans*-[$Pt(N_3)_2(OH)_2$(MA)(Py)] (**5**) and *trans*, *trans*, *trans*-[$Pt(N_3)_2(OH)_2$(MA)(Tz)] (**8**), are also highly cytotoxic to cancer cells (**Table 3.8**). The IC_{50} values of complexes **11**, **14** and **17** towards A2780 cells are also within the micromolar range. Although

cytotoxicity testing for all Pt^{IV} complexes is on-going, there appears to be a relationship between the photocytotoxicity of the Pt^{IV} complexes and the cytotoxicity of their Pt^{II} precursors.

3.4 Conclusion

A series of platinum(IV) diazidodihydroxido complexes has been synthesized and characterized and their activities as photoactivatable anticancer prodrugs has been determined. Their X-ray crystal structures have been determined and interesting H-bond and π-π stacking effects have been found. The ^{195}Pt NMR chemical shifts and chemical shift anisotropy (CSA) relaxation in the ^{1}H NMR spectra for the new platinum complexes have been studied. The replacement of NH_3 by methylamine dramatically improved the photocytotoxicity against A2780 cisplatin-resistant ovarian cancer cells upon irradiation with UVA**.** When they were irradiated with blue light (420 nm), the photocytotoxicity against the A2780, A2780cis, OE19 and HaCaT cell lines are still potent. These results suggest that these complexes are promising candidates for use in the cancer photochemotherapy of thin-walled organs.

3.5 References

1. P. J. O'Dwyer, J. P. Stevenson and S. W. Johnson, in *Cisplatin:Chemistry and Biochemistry of a Leading Anticancer Drug*, ed. B. Lippert, Verlag Helvetica Chimica Acta, Zurich, 1999, ch. 2, pp. 29-69.
2. N. J. Wheate, S. Walker, G. E. Craig and R. Oun, *Dalton Trans.*, 2010, **39**, 8113-8127.
3. J. Reedijk, *Eur. J. Inorg. Chem.*, 2009, 1303-1312.
4. J. R. Aldrich-Wright, B. W. Harper, A. M. Krause-Heuer, M. P. Grant, M. Manohar and K. B. Garbutcheon-Singh, *Chem. Eur. J.*, 2010, **16**, 7064-7077.

5. T. Boulikas, *Expert Opin. Inv. Drug*, 2009, **18**, 1197-1218.
6. L. Kelland, *Nat. Rev. Cancer*, 2007, **7**, 573-584.
7. Z. H. Siddik, *Oncogene*, 2003, **22**, 7265-7279.
8. L. R. Kelland, *Am. J. Cancer*, 2002, **1**, 247-255.
9. J. Holford, S. Y. Sharp, B. A. Murrer, M. Abrams and L. R. Kelland, *Br. J. Cancer*, 1998, **77**, 366-373.
10. L. Cubo, A. G. Quiroga, J. Y. Zhang, D. S. Thomas, A. Carnero, C. Navarro-Ranninger and S. J. Berners-Price, *Dalton Trans.*, 2009, 3457-3466.
11. N. Farrell, L. R. Kelland, J. D. Roberts and M. Vanbeusichem, *Cancer Res.*, 1992, **52**, 5065-5072.
12. J. Kasparkova, O. Novakova, V. Marini, Y. Najajreh, D. Gibson, J. M. Perez and V. Brabec, *J. Biol. Chem.*, 2003, **278**, 47516-47525.
13. N. Farrell, *Comments Inorg. Chem.*, 1995, **16**, 373-389.
14. C. Manzotti, G. Pratesi, E. Menta, R. Di Domenico, E. Cavalletti, H. H. Fiebig, L. R. Kelland, N. Farrell, D. Polizzi, R. Supino, G. Pezzoni and F. Zunino, *Clin. Cancer Res.*, 2000, **6**, 2626-2634.
15. D. Fan, X. Yang, X. Wang, S. Zhang, J. Mao, J. Ding, L. Lin and Z. Guo, *J. Biol. Inorg. Chem.*, 2007, **12**, 655-665.
16. A. M. Krause-Heuer, R. Grunert, S. Kuhne, M. Buczkowska, N. J. Wheate, D. D. Le Pevelen, L. R. Boag, D. M. Fisher, J. Kasparkova, J. Malina, P. J. Bednarski, V. Brabec and J. R. Aldrich-Wright, *J. Med. Chem.*, 2009, **52**, 5474-5484.
17. M. D. Hall and T. W. Hambley, *Coord. Chem. Rev.*, 2002, **232**, 49-67.
18. F. Kratz, I. A. Muller, C. Ryppa and A. Warnecke, *Chemmedchem*, 2008, **3**, 20-53.

19. O. Horváth and K. L. Stevenson, *Charge Transfer Photochemistry of Coordination Compounds*, VCH, Weinheim, Germany, 1993.
20. F. S. Mackay, J. A. Woods, H. Moseley, J. Ferguson, A. Dawson, S. Parsons and P. J. Sadler, *Chem. Eur. J.*, 2006, **12**, 3155-3161.
21. F. S. Mackay, J. A. Woods, P. Heringova, J. Kasparkova, A. M. Pizarro, S. A. Moggach, S. Parsons, V. Brabec and P. J. Sadler, *Proc. Natl. Acad. Sci. USA*, 2007, **104**, 20743-20748.
22. N. J. Farrer and P. J. Sadler, *Aust. J. Chem.*, 2008, **61**, 669-674.
23. N. J. Farrer, J. A. Woods, V. P. Munk, F. S. Mackay and P. J. Sadler, *Chem. Res. Toxicol.*, 2010, **23**, 413-421.
24. N. J. Farrer, J. A. Woods, L. Salassa, Y. Zhao, K. S. Robinson, G. Clarkson, F. S. Mackay and P. J. Sadler, *Angew. Chem. Int. Ed.*, 2010, **49**, 8905-8908.
25. J. Šima, *Coord. Chem. Rev.*, 2006, **250**, 2325-2334.
26. P. J. Bednarski, R. Grunert, M. Zielzki, A. Wellner, F. S. Mackay and P. J. Sadler, *Chem. Biol.*, 2006, **13**, 61-67.
27. P. J. Bednarski, F. S. Mackay and P. J. Sadler, *Anti-Cancer Agent Med. Chem.*, 2007, **7**, 75-93.
28. F. S. Mackay, N. J. Farrer, L. Salassa, H. C. Tai, R. J. Deeth, S. A. Moggach, P. A. Wood, S. Parsons and P. J. Sadler, *Dalton Trans.*, 2009, 2315-2325.
29. M. D. Hall, H. R. Mellor, R. Callaghan and T. W. Hambley, *J. Med. Chem.*, 2007, **50**, 3403-3411.
30. L. Brancaleon and H. Moseley, *Laser Med. Sci.*, 2002, **17**, 173-186.
31. M. R. Detty, S. L. Gibson and S. J. Wagner, *J. Med. Chem.*, 2004, **47**, 3897-3915.
32. A. Dondoni and A. Marra, *Chem. Rev.*, 2004, **104**, 2557-2600.

33. K. C. Nicolaou, A. Ritzen and K. Namoto, *Chem. Commun.*, 2001, 1523-1535.
34. R. Haiges, J. A. Boatz and K. O. Christe, *Angew. Chem. Int. Ed.*, 2010, **49**, 8008-8012.
35. P. Portius, A. C. Filippou, G. Schnakenburg, M. Davis and K.-D. Wehrstedt, *Angew. Chem. Int. Ed.*, 2010, **49**, 8013-8016.
36. A. Villinger and A. Schulz, *Angew. Chem. Int. Ed.*, 2010, **49**, 8017-8020.
37. S. Wimmer, F. Wimmer, J. Jaud, N. P. Johnson and P. Castan, *Inorg. Chim. Acta*, 1988, **144**, 25-30.
38. F. S. Mackay, S. A. Moggach, A. Collins, S. Parsons and P. J. Sadler, *Inorg. Chim. Acta*, 2009, **362**, 811-819.
39. R. A. Alderden, M. D. Hall and T. W. Hambley, *J. Chem. Educ.*, 2006, **83**, 728-734.
40. R. N. Keller, T. Moeller and J. V. Quagliano, *Inorg. Synth.*, 2007, 250-253.
41. M. Atoji, J. W. Richardson and R. E. Rundle, *J. Am. Chem. Soc.*, 1957, **79**, 3017-3020.
42. S. C. Dhara, *Indian J. Chem.*, 1970, **8**, 193.
43. S. J. Berners-Price and T. G. Appleton, in *Platinum-Based Drugs in Cancer Therapy*, eds. L. R. Kelland and N. P. Farrell, Humana Press, Totowa, New Jersey, USA, 2000, pp. 3 - 36.
44. G. B. Kauffman and D. O. Cowan, *Inorg. Synth.*, 1963, **7**, 239-245.
45. U. Bierbach, M. Sabat and N. Farrell, *Inorg. Chem.*, 2000, **39**, 3734-3734.
46. A. G. Quiroga, J. M. Perez, C. Alonso, C. Navarro-Ranninger and N. Farrell, *J. Med. Chem.*, 2006, **49**, 224-231.
47. A. M. Pizarro, V. P. Munk, C. Navarro-Ranninger and P. J. Sadler, *Angew. Chem. Int. Ed.*, 2003, **42**, 5339-5342.

48. M. J. Macazaga, J. Rodriguez, A. G. Quiroga, S. Peregina, A. Carnero, C. Navarro-Ranninger and R. M. Medina, *Eur. J. Inorg. Chem.*, 2008, 4762-4769.

49. S. Shamsuddin, M. S. Ali, S. Huang and A. R. Khokhar, *J. Coord. Chem.*, 2002, **55**, 659-665.

50. M. D. Hall, S. Amjadi, M. Zhang, P. J. Beale and T. W. Hambley, *J. Inorg. Biochem.*, 2004, **98**, 1614-1624.

51. L. Ellis, H. Er and T. Hambley, *Aust. J. Chem.*, 1995, **48**, 793-806.

52. E. Koubek and D. A. House, *Inorg. Chim. Acta*, 1992, **191**, 103-107.

53. S. K. Miller and L. G. Marzilli, *Inorg. Chem.*, 1985, **24**, 2421-2425.

54. B. M. Still, P. G. A. Kumar, J. R. Aldrich-Wright and W. S. Price, *Chem. Soc. Rev.*, 2007, **36**, 665-686.

55. P. S. Pregosin, *Coord. Chem. Rev.*, 1982, **44**, 247-291.

56. J. R. L. Priqueler, I. S. Butler and F. D. Rochon, *Appl. Spectrosc. Rev.*, 2006, **41**, 185-226.

57. I. M. Ismail, S. J. S. Kerrison and P. J. Sadler, *Polyhedron*, 1982, **1**, 57-59.

58. C. G. Anklin and P. S. Pregosin, *Magn. Reson. Chem.*, 1985, **23**, 671-675.

59. E. Arunan, G. R. Desiraju, R. A. Klein, J. Sadlej, S. Scheiner, I. Alkorta, D. C. Clary, R. H. Crabtree, J. J. Dannenberg, P. Hobza, H. G. Kjaergaard, A. C. Legon, B. Mennucci and D. J. Nesbitt, *Pure Appl. Chem.*, 2011, **83**, 1637-1641.

60. J. W. Steed and J. L. Atwood, *Supramolecular Chemistry*, Wiley-VCH, Weinheim, Germany, 2009.

61. C. Janiak, *J. Chem. Soc., Dalton Trans.*, 2000, 3885-3896.

62. M. Van Beusichem and N. Farrell, *Inorg. Chem.*, 1992, **31**, 634-639.

63. U. Bierbach, Y. Qu, T. W. Hambley, J. Peroutka, H. L. Nguyen, M. Doedee and N. Farrell, *Inorg. Chem.*, 1999, **38**, 3535-3542.

64. Y. Zhao, N. J. Farrer, J. A. Woods, L. Salassa, J. S. Butler, K. S. Robinson, F. S. Mackay, G. Clarkson, L. Song and P. J. Sadler, unpublished work.

65. K. J. Scanlon and M. Kashani-Sabet, *Proc. Natl. Acad. Sci. USA*, 1988, **85**, 650-653.

66. L. R. Kelland, G. Abel, M. J. Mckeage, M. Jones, P. M. Goddard, M. Valenti, B. A. Murrer and K. R. Harrap, *Cancer Res.*, 1993, **53**, 2581-2586.

67. R. Guddneppanavar, J. R. Choudhury, A. R. Kheradi, B. D. Steen, G. Saluta, G. L. Kucera, C. S. Day and U. Bierbach, *J. Med. Chem.*, 2007, **50**, 2259-2263.

68. J.-L. Butour, P. Alvinerie, J.-P. Souchard, P. Colson, C. Houssier and N. P. Johnson, *Eur. J. Biochem.*, 1991, **202**, 975-980.

69. G. Natile and M. Coluccia, *Coord. Chem. Rev.*, 2001, **216**, 383-410.

70. M. Coluccia and G. Natile, *Anti-Cancer Agent Med. Chem.*, 2007, **7**, 111-123.

71. S. M. Aris and N. P. Farrell, *Eur. J. Inorg. Chem.*, 2009, **2009**, 1293-1302.

72. Y. Najajreh, J. M. Perez, C. Navarro-Ranninger and D. Gibson, *J. Med. Chem.*, 2002, **45**, 5189-5195.

73. J. Kasparkova, V. Marini, Y. Najajreh, D. Gibson and V. Brabec, *Biochemistry*, 2003, **42**, 6321-6332.

74. R. Prokop, J. Kasparkova, O. Novakova, V. Marini, A. M. a. Pizarro, C. Navarro-Ranninger and V. Brabec, *Biochem. Pharmacol.*, 2004, **67**, 1097-1109.

75. F. P. Intini, A. Boccarelli, V. C. Francia, C. Pacifico, M. F. Sivo, G. Natile, D. Giordano, P. De Rinaldis and M. Coluccia, *J. Biol. Inorg. Chem.*, 2004, **9**, 768-780.

Chapter 4

Photochemistry of Platinum Diazidodihydroxido Complexes

4.1 Introduction

The photochemical properties of Pt compounds were first recognized in photographic processes during the 1850s.[1] In the 1970s, the earliest examinations of the photoreduction and photo-solvation of platinum(IV) complexes, namely $[Pt(CN)_4Cl_2]^{2-}$ and $[Pt(CN)_4(N_3)_2]^{2-}$, were reported.[2] In the cases of chlorido Pt^{IV} complexes, photoisomerisations, photosubstitutions and photoaquations are common, whereas for Pt^{IV} azido and nitrito complexes, photoreductions prevail. For example, irradiation into the LMCT bands of $[Pt(CN)_4(N_3)_2]^{2-}$ leads to $[Pt(CN)_4]^{2-}$ and two $\bullet N_3$ radicals, via a simultaneous two-electron reduction avoiding a Pt^{III} intermediate.[3]

The charge transfer transition from orbitals of the ligand to the *d* orbitals of the metal (LMCT) can cause reductive eliminations whereby the leaving ligand(s) is (are) oxidized.[4] In addition, LMCT can also cause ligand substitutions, the pathway of which depends significantly on the nature of the leaving ligand and the solvent. Usually, a mixture of photo-reductions and photo-substitution occurs. Thus, the photochemistry of Pt complexes is not easily predictable and the photoproducts must be investigated carefully to establish the pathway(s).

The photochemistry of photoactivatable Pt^{IV} diazidodihydroxido anticancer complexes, namely, *trans,trans,trans*-$[Pt(N_3)_2(OH)_2(NH_3)_2]$, *cis,trans,cis*-$[Pt(N_3)_2(OH)_2(NH_3)_2]$ and *trans,trans,trans*-$[Pt(N_3)_2(OH)_2(NH_3)(Py)]$(**22**), has been studied during the last six years.[5-10] On the one hand, in the absence of light, these complexes exhibit minor or very low cytotoxicity towards cancer cells. In cell-free media or aqueous solutions, they do not react with biological reductants, e.g., glutathione (GSH), neither do they react with 5'-guanosine monophosphate (5'-GMP) or DNA. On the other hand, upon irradiation with UVA or blue light, these

complexes undergo rapid N_3 ligand substitution and form various hydrolysis products.[5, 6] The photodecomposition of complexes *trans,trans,trans*-$[Pt(N_3)_2(OH)_2(NH_3)_2]$ or *cis,trans,cis*-$[Pt(N_3)_2(OH)_2(NH_3)_2]$ was reported to involve the generation of N_3^- anions, $N_3^{\bullet}$ radicals, nitrogen gas and oxygen gas.[7, 8] Some platinum(III) and nitrene intermediates can also be captured during the photolysis of *trans,trans,trans*-$[Pt(N_3)_2(OH)_2(NH_3)(Py)]$(**22**).[9, 11] It was also reported that upon irradiation with UVA, this type of complex may also generate oxygen gas (O_2),[7, 8] but no direct evidence has been previously reported for the energy state of the released oxygen. In the presence of 5'-GMP in aqueous solution, these complexes can be rapidly reduced to Pt^{II} species upon irradiation with UVA/blue light, producing *trans* azido/guanine and *trans* diguanine Pt^{II} adducts. *In vitro*, upon irradiation with UVA/blue light, these complexes display potent photocytotoxicity to a range of cancer cells by binding to DNA and thus causing cell death (other possible mechanisms may also be involved).

In **Chapter 3**, it was demonstrated that replacing the NH_3 ligand by aliphatic amine in *trans,trans,trans*-$[Pt(N_3)_2(OH)_2(NH_3)(Py)]$(**22**) can produce potent photocytotoxicity (especially to cisplatin-resistant cancer cells) and higher activity by blue light. In this Chapter, the photochemistry of the complexes with a methylamine and a heterocyclic imine group (pyridine/thiazole) is explored by ^{1}H NMR, ^{14}N NMR, UV-Vis, electron paramagnetic resonance (EPR) spectroscopy and gas phase chromatography (GC). The photoreactions of these complexes with 5'-GMP were also studied by ^{1}H NMR, ^{195}Pt NMR, HPLC-MS and high-resolution mass spectrometry (HR-MS). Their photoreactions with a single strand DNA short oligonucleotide were investigated by HR-MS.

Also in this Chapter, the energy state of the oxygen gas released from the photodecomposition of Pt^{IV} diazidodihydroxido complexes was studied by a singlet oxygen ($^1O_2$) fluorescence probe. Singlet oxygen is a very reactive and toxic species and it reacts with various biomolecules, including several amino acids, and some DNA bases (preferentially guanosine).[12-14] It has been proved to be an important source of oxidative DNA damage[15] and the major cytotoxic species in photodynamic therapy (PDT).[16] The most common method to generate $^1O_2$ is photosensitization, which produces $^1O_2$ by energy transfer from a photo-excited sensitizer to ground state oxygen (triplet state, $^3O_2$).[17] The reaction of hydrogen peroxide with hypochlorite in water can also generate $^1O_2$.[18] It has been reported that platinum complexes can work as $^1O_2$ photosensitizers and generate $^1O_2$ by energy transfer processes involving Pt^{II} complexes in their MLCT excited states.[19, 20] These strategies require the availability of oxygen at the target site. However, tumour cells can be hypoxic due to the rapid growth. In this Chapter, it was discovered that $^1O_2$ was released intrinsically, independent of dissolved O_2, from the photoreaction of *trans,trans,trans*-[$Pt(N_3)_2(OH)_2$(MA)(Py)](**5**), which may partly contribute to its high photocytotoxicity. This is the first discovery of a Pt^{IV} diazidodihydroxido complex which release singlet oxygen upon irradiation with UVA or blue light in the absence of any exogenous source of oxygen gas.

4.2 Experimental

4.2.1 Materials

All chemicals used were obtained from Sigma-Aldrich or Fisher Scientific, if unspecified. The water used in the experiments was deionised water from a Millipore water purification system. D_2O and 5'-guanosine monophosphate (5'-GMP) were

obtained from Sigma-Aldrich, ^{15}N-labelled NaN_3 (1-^{15}N, >98%) from Cambridge Isotopes Lab, 5, 5-dimethyl-pyrroline-N-oxide (DMPO) from Enzo Life Sciences (≥ 98%). Quartz tubes (1.0 mm ID × 1.2 mm O.D) were purchased from Wilmad Labglass. A 50 μL Hamilton HPLC syringe needle was purchased from Hamilton Company and used to fill the quartz tubes. T-Blu Tac® was used to seal the quartz tubes. The dodecamer $d(TATGGTACCATA)_2$ sodium salt (**I**) was obtained from DNA Technology A/S (Aarhus, DK) as an HPLC-purified oligonucleotides. Singlet Oxygen Sensor Green (SOSG) was obtained from Molecular Probes®, Inc. Quantofix® Peroxide 25 Test Sticks was obtained from Sigma-Aldrich, with a detection limit of 0.5 ~ 25 mg/L. All chemicals were used as received without any further purification, unless specified.

4.2.2 Methods and Instruments

Photochemical reactions of Pt complexes with or without 5'-GMP were carried out at 298 K by using a LZC-ICH2 photoreactor (Luzchem Research Inc.) equipped with a temperature controller and 8 UVA lamps (Hitachi, λ_{max} = 365 nm, 3.5 mW/cm^2) or 8 Luzchem LZC-420 lamps (λ_{max}= 420 nm, 4.3 mW/cm^2) with no other sources of light filtration. ACULED® VHL™ LEDs were also used (λ_{max} = 450 nm, 50 mW/cm^2) for irradiation of the samples.

NMR spectra were recorded on either a Bruker AV-600 (^1H, 600.13 MHz; ^{13}C, 150.9MHz; ^{195}Pt, 129.4 MHz; ^{15}N, 60.8 MHz; ^{14}N, 43.4MHz) or a Bruker DPX-400 spectrometer (^1H, 400.03 MHz).

ESI-MS was performed on a Bruker Esquire 2000 mass spectrometer, HPLC-ESI-MS on a Bruker HCT-Ultra mass spectrometer coupled with an Agilent 1200 HPLC system with an Agilent ZORBAX Eclipse Plus C18, 5 μm, 4.6 × 150 mm column for

experiments in **Section 4.3.3.3** or a 4.6 × 250 mm column for experiments in **Section 4.3.4.1**. Flow rate, 1.0 ml/min; detecting wavelength, 254 nm; mobile phase A, H_2O with 0.1% formic acid (FA); mobile phase B, MeOH with 0.1% FA. A linear gradient from 5% to 55% B over 15 min was applied to separate the photoreaction mixture of Pt complexes with GMP. ESI-HR-MS and CID (collision-induced disassociation) tandem MS/MS was performed on a Bruker MaXis UHR-Qq-TOF high resolution ESI-MS spectrometer in positive-ion mode. Samples containing 50.0 μM Pt were prepared in 20% H_2O/80% methanol.

UV-Vis electronic absorption spectra were recorded on a Varian Cary 300 UV-Vis spectrophotometer in a 1 cm path-length quartz cuvette. All spectra were referenced to neat solvent and data were processed with OriginLab Origin 7.0. Extinction coefficients (ε) were determined over a concentration range (A_{max} ~ 0.4 – 1.6) with at least 4 data points, using Pt concentrations determined by ICP-MS.

The EPR spectra were recorded on a Bruker EMX (X-band) spectrometer by Jennifer S. Butler in University of Warwick. Specific details, along with other general methods and parameters for acquisition are found in **Chapter 2**.

The intensity of fluorescence was measured on a Jasco FP-6500 fluorometer. The output light was used for both excitation and irradiation by adjusting to the wavelength required. The excitation and the emission slit widths were set to 3 nm. Filters were used to eliminate second order diffraction of shorter wavelengths from the specified longer wavelength monochromatic light. Power of individual wavelengths: 365 nm, 21 μW/cm^2; 420 nm, 0.85 mW/cm^2; 450 nm, 0.80 mW/cm^2. Fluorescence response time was 0.1 second and sensitivity was medium. Power levels were measured with an International Light Technologies Powermeter

(ILT1400-A) equipped with a SEL033 detector and either a UVA/TD filter (315-390 nm) for UVA irradiations or a flat response visible filter F/W (400-1064 nm) for visible wavelengths.

4.2.3 Photo-induced DNA platination

For platination of the single strand DNA dodecamer (ss-DNA, **I**), Pt^{IV} complex (100 or 200 μM) and ss-DNA **I** (100 μM) were mixed in 500 μL H_2O to make up a solution of 1:1 or 2:1 molar ratios of complex to ss-DNA **I**. The mixtures were incubated with irradiation at 450 nm for 1 h at 298 K. The mixture was desalted and diluted 100-fold in a solution of H_2O/isopropanol (50%/50%) with 50 mM ammonium acetate for direct injection to ESI-HR-MS. The *m/z* of Pt-DNA adducts were calibrated internally with the *m/z* of the ss-DNA **I** species. The oligo concentrations of aqueous stock solutions of **I** were determined spectrophotometrically using the absorption coefficient ε_{260} = 132.52 $mM^{-1}cm^{-1}$, calculated by 'OligoCalc'.[21]

4.2.4 Synthesis and characterisation

4.2.4.1 Platinum(IV) diazidodihydroxido complexes

The complexes *trans,trans,trans*-$[Pt(N_3)_2(OH)_2(MA)(Py)]$ (**5**) (MA = methylamine , Py = pyridine) and *trans,trans,trans*-$[Pt(N_3)_2(OH)_2(MA)(Tz)]$ (**8**) (Tz = thiazole) were synthesized as described in **Chapter 3**.

4.2.4.2 *Trans,trans,trans*-$[Pt(^{15}N_3)_2(OH)_2(MA)(Py)]$ (5*)

^{15}N-N_3 labelled *trans,trans,trans*-$[Pt(^{15}N_3)_2(OH)_2(MA)(Py)]$ (**5***), was synthesized by the same method as for complex *trans,trans,trans*-$[Pt(N_3)_2(OH)_2(MA)(Py)]$ (**5**) (see **Chapter 3**) except with the use of ^{15}N-labelled NaN_3 (99% $Na[^{15}N=^{14}N=^{14}N]$).

^{195}Pt NMR (D_2O, 129.4 MHz): δ = 898.8 ppm. ^{15}N NMR (D_2O, 60.8 MHz): δ ($\underline{N_\gamma}$) = 165.6 ppm ($^3J_{Pt\text{-}N}$ = 24 Hz); δ ($\underline{N_\alpha}$) = 51.4 ppm ($^1J_{Pt\text{-}N}$ = 222 Hz).

4.2.4.3 *Trans*-[Pt(MA)(Py)(5'-GMP)$_2$ − 2H] (5a)

Trans-[Pt(MA)(Py)(5'-GMP)$_2$ − 2H] (**5a**) was synthesized with a slight revised reported method.[6] *Trans*-[$PtCl_2$(MA)(Py)] (3.76 mg, 10 μmol) was suspended in D_2O (3 mL) and $AgNO_3$ (3.4 mg, 20 μmol) added. After stirring for 24 h at 333 K, the insoluble AgCl was filtered off. An NMR sample was prepared using 0.54 mL of the above solution and 60 μl of D_2O, 5'-GMP (2.6 mg, 40 μmol) was added. The ^{1}H and ^{195}Pt NMR spectra were acquired after 24 h and then the sample was analyzed by ESI-MS. ^{1}H NMR (600 MHz, D_2O): δ (ppm) 8.64 (d, $\underline{H_{2,6}}$, 2H), 8.81 (s, $\underline{H_8}$ 5'-GMP, 1H), 7.86 (t, $\underline{H_4}$, 1H), 7.38 (t, $\underline{H_{3,5}}$, 2H), 2.17 (s, C$\underline{H}_3$, ^{3}J (^{195}Pt, ^{1}H) = 13 Hz, 3H). ^{195}Pt NMR (129.4 MHz, D_2O): δ = −2398 ppm. ESI-MS: $[M + H]^+$ (*m/z*) Calc., 1030.2; Found, 1030.3.

4.2.4.4 (*SP*-4-2)-[Pt(N_3)(MA)(Py)(5'-GMP) − H] (5b)

(*SP*-4-2)-[Pt(N_3)(MA)(Py)(5'-GMP) − H] (**5b**) was synthesized with a slight revised reported method.[6] *Trans*-[$PtCl_2$(MA)(Py)] (3.76 mg, 10 μmol) was added to a D_2O solution of NaN_3 (3 mL, 3.3 mM), and left stirring at 303 K for 24 h. 5'-GMP (10 μmol, 3.63 mg) was added and the solution stirred for another 24 h at 298 K. Signals due to *trans*-[Pt(N_3)(MA)(Py)(5'-GMP) − H] were present in both the NMR and mass spectra. ^{1}H NMR (600 MHz, D_2O): δ (ppm) 8.70 (s, $\underline{H_8}$, 5'-GMP, 1H), 8.69 (d, $\underline{H_{2,6}}$, 2H), 7.91 (t, $\underline{H_4}$, 1H), 7.46 (t, $\underline{H_{3,5}}$, 2H), 2.26 (s, C$\underline{H}_3$, 3H). ^{195}Pt NMR (129.4 MHz, D_2O): δ = −2328 ppm. ESI-MS: $[M + H]^+$ (*m/z*) Calc., 710.1; Found, 710.1.

4.2.4.5 *Trans*-[Pt(MA)(Py)$(H_2O)_2$]$(BF_4)_2$ (5g)

Trans-[$Pt(Cl)_2$(MA)(Py)] (0.85 mg) was suspended in 1 mL H_2O, and $AgBF_4$ (8.7 mg, 2.1 mol equiv) was added and stirred at 333 K for 24 h. AgCl precipitate was filtered off by an inorganic membrane filter (Sartorius, Minisart, 0.2 μm).The filtrate was transferred to an NMR tube with 10% D_2O for NMR experiments. This aqua product was not isolated but only used for NMR spectroscopic experiments. ^{1}H NMR (600 MHz): δ (ppm) 8.66 (d, $\underline{H_{2,6}}$, 2H), 8.03 (t, $\underline{H_4}$, 1H), 7.61 (t, $\underline{H_{3,5}}$, 2H), 2.35 (s, C$\underline{H}_3$, ^{3}J (^{195}Pt, ^{1}H) = 13 Hz, 3H). ^{195}Pt NMR (129.4 MHz): δ = −1498 ppm.

4.2.4.6 *Trans*-[Pt(MA)(Tz)(5'-GMP)$_2$ − 2H] (8a)

Trans-[$PtCl_2$(MA)(Tz)] (3.82 mg, 10 μmol) was suspended in D_2O (3 mL) and $AgNO_3$ (3.4 mg, 20 μmol) added. After stirring for 24 h at 333 K, the AgCl precipitate was filtered off. An NMR sample was prepared using 0.54 mL of the above solution and 60 μl of D_2O, 5'-GMP (4 mol equiv, 2.6 mg) was added. ^{1}H and ^{195}Pt NMR spectra were acquired after 24 h and then the sample was analyzed by ESI-MS. δ (ppm) 9.20 (d, $\underline{H_2}$, 1H), 8.84 (s, $\underline{H_8}$, 5'-GMP, 1H), 7.92 (d, $\underline{H_4}$, 1H), 7.65 (d, $\underline{H_5}$, 1H), 2.15 (s, C$\underline{H}_3$, 3H). ^{195}Pt NMR (129.4 MHz, D_2O): δ = –2356 ppm. ESI-MS: $[M + H]^+$ (*m/z*) Calc., 1036.1; Found, 1036.1.

4.2.4.7 (*SP*-4-3)-[Pt(N_3)(MA)(Tz)(5'-GMP) − H] (8b)

Trans-[$PtCl_2$(MA)(Tz)] (3.82 mg, 10 μmol) was added to a D_2O solution of NaN_3 (3 mL, 3.3 mM), and left stirring at 303 K for 24 h. 5'-GMP (10 μmol, 3.63 mg) was added and the solution stirred for another 24 h at 298 K. Signals due to (*SP*-4-3)-[Pt(N_3)(MA)(Tz)(5'-GMP) − H] were present in both the NMR and mass spectra. δ (ppm) 9.28 (d, $\underline{H_2}$, 1H), 8.65 (s, $\underline{H_8}$, 5'-GMP, 1H), 8.00 (d, $\underline{H_4}$, 1H), 7.75 (d, $\underline{H_5}$, 1H),

2.26 (s, C*H*$_3$, 3H). ^{195}Pt NMR (129.4 MHz, D_2O): δ = −2294 ppm. ESI-MS: [M + H]$^+$ (*m/z*) Calc., 716.1; Found, 716.2.

4.3 Results

4.3.1 Photochemistry

4.3.1.1 Dark stability

Complexes *trans,trans,trans*-[Pt(N$_3$)$_2$(OH)$_2$(MA)(Py)] (**5**) and *trans,trans,trans*-[Pt(N$_3$)$_2$(OH)$_2$(MA)(Tz)] (**8**) have very good aqueous solubility (>40 mM) and are very stable in water and in EBSS (Eagle's balanced salt, a biological cell culture medium) for >7 months in the dark, as monitored by ^{1}H NMR. They do not react with two equivalents of 5'-GMP or L-ascorbic acid (VC) in the dark, observed by ^{1}H NMR for three days. Those complexes react with glutathione (GSH, reduced form) very slowly, only 2% of complex **5** and 10% of **8**, respectively, were consumed after incubation for three days.

4.3.1.2 Photolysis study by UV-Vis spectroscopy

Complexes **5** and **8** exhibit similar absorption maxima (azido ligand-to-metal-charge-transfer band) at 289 nm and the absorption extends up to *ca.* 500 nm (for their extinction coefficients at various wavelengths, see **Table 4.1**).

Table 4.1 Extinction coefficients (ε, M^{-1} cm^{-1}) for complexes *trans,trans,trans*-[Pt(N$_3$)$_2$(OH)$_2$(MA)(Py)] (**5**) and *trans,trans,trans*-[Pt(N$_3$)$_2$(OH)$_2$(MA)(Tz)] (**8**) at various wavelengths.

Complex	**5**	**8**
ε_{289} (max)	16200	18600
ε_{365}	496	607
ε_{420}	129	138
ε_{450}	66	65

Irradiation of an aqueous solution of **5** or **8** at 365 nm (2.35 mW/cm^2) or 420 nm (5.10 mW/cm^2) or 450 nm (50 mW/cm^2) resulted in a decrease in intensity of absorption at 289 nm (**Figure 4.1**), indicating loss of the Pt^{IV}-N_3 bond(s), i.e., the LMCT band. A lower dose of 365 nm irradiation induced the decomposition of complexes faster than a *ca.* twice higher dose of 420 nm light, which is consistent with their different extinction coefficients at these wavelengths.

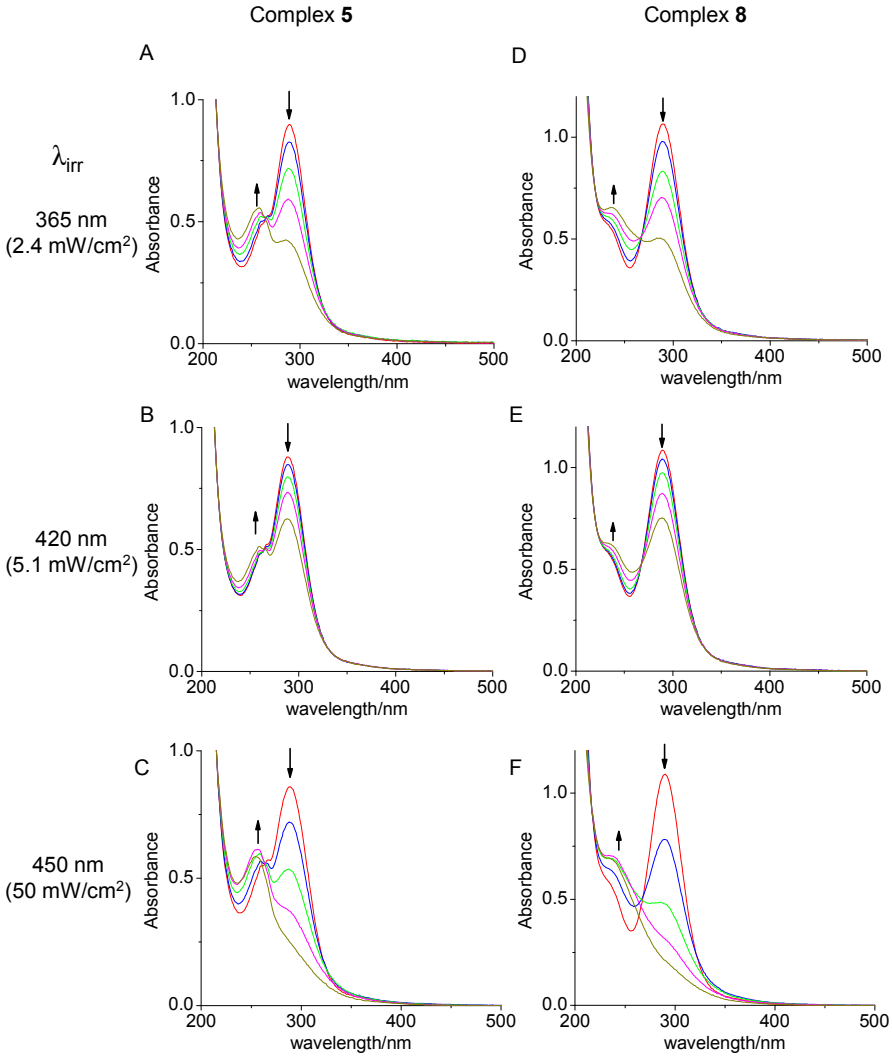

Figure 4.1 UV-Vis spectra recorded for complexes **5** (*trans,trans,trans*-[$Pt(N_3)_2(OH)_2(MA)(Py)$], 50 µM) and **8** (*trans,trans,trans*-[$Pt(N_3)_2(OH)_2(MA)(Tz)$], 60 µM) in H_2O upon irradiation at 365 nm (light dose 0, 0.7, 2.1, 4.2, 8.4 J/cm^2), 420 nm (light dose 0, 1.5, 4.6, 9.2, 18.4 J/cm^2) and 450 nm (light dose 0, 15, 45, 90, 18 J/cm^2).

4.3.1.3 ^{1}H NMR spectroscopy

When a solution of complexes **5** (*trans,trans,trans*-[$Pt(N_3)_2(OH)_2$(MA)(Py)]) or **8** (*trans,trans,trans*-[$Pt(N_3)_2(OH)_2$(MA)(Tz)]) (10 mM in 90% H_2O/10% D_2O) was irradiated at 450 nm light (50 mW/cm^2), gas bubbles and a yellow precipitate were observed within *ca.* 30 min. The gas generated was assumed to be a mixture of O_2 and N_2 gas, as they were observed in the previous work in Sadler's group on related complexes.[7, 8] The precipitate from the irradiated complex **5** was filtered off, dried and the weight was found to be 1.3 mg, the yield of which was indeed high with respect to the 2.6 mg starting material dissolved in the NMR sample. The precipitate was poorly soluble in H_2O, MeOH, EtOH, acetone or acetonitrile, but could be dissolved in DMF, giving a dark brown solution. No ^{195}Pt NMR resonance was found for the precipitate in DMF-d_7 between −6200 and 6200 ppm.

^{1}H NMR spectroscopy was used to follow the photoreaction. Although every signal would not be assigned due to the overlap of signals, some useful information could still be obtained. Taking complex **5** *trans,trans,trans*-[$Pt(N_3)_2(OH)_2$(MA)(Py)] as an example, the methylamine (MA) group exhibits a triplet for the C$\underline{H}_3$ group in ^{1}H NMR (**Figure 4.2**) due to the coupling with the NH_2 group, for which the protons were hardly exchanged by deuterium under the experiment conditions (90% H_2O/10% D_2O, pH 4 ± 0.5). A number of new species were formed after irradiation at 450 nm for only 15 min. After irradiation for 1 hour, < 17% of the starting material was still left, and after 4 hours, the starting material had all reacted. Three new species containing Pt-MA moiety were generated, probably by isomerization, ligand substitution or reduction. In the reaction mixture, a very tiny amount of free methylamine (MA) was found after irradiation at 450 nm in ^{1}H NMR (δ (C$\underline{H}_3$) = 2.60 ppm). < 0.5% and < 3% MA release was observed after irradiation for 1 hour

(180 J/cm^2) and 4 hours (540 J/cm^2), respectively. (**Figure 4.2**) The chemical shift of free MA was confirmed by adding 1 mol equiv free MA to the final irradiated NMR sample, and adjust the pH value to 4 ± 0.5. Free MA exhibit a singlet as the H-D exchange rate for the NH_2 group is much faster than for MA coordinated to Pt, as the pK_a value of MAH^+ is 10.62.[22] Also, an independent series of experiments showed that the pH decreased from 6.22 to 5.88 after irradiation at 450 nm for 1 hour. Since a significant release of free MA should increase the pH, it is confirmed that MA group remains strongly bound to Pt in the photo-reactions.

^{195}Pt satellites for Pt^{II} species in high frequency ^{1}H NMR spectra are broadened due to the effects of chemical shift anisotropy (CSA) relaxation.[23] But in highly symmetrical platinum(IV) complexes, the satellites are still sharp in the 600 MHz ^{1}H NMR spectrum. For example, in the aromatic area of the ^{1}H NMR spectrum of complex **5** (*trans,trans,trans*-[$Pt(N_3)_2(OH)_2(MA)(Py)$]), the resonance for $\underline{H_{2,6}}$ in pyridine has sharp satellites. After irradiation at 450 nm for 15 min, a series of new species appeared with satellites, which suggests that the new species are largely Pt^{IV} complexes from photo-induced ligand substitution and isomerization. After irradiation at 450 nm for 1 hour, more new signals appeared with no satellites, which indicate that Pt^{II} species were generated by photo-induced reduction. After 4 hours, all the resonances with satellites disappeared, so all the Pt^{IV} species were consumed. At least four new species were formed. The noise level of the ^{1}H NMR spectra increased during the photoreaction, which is probably due to the lowered concentration of the sample by generation of precipitate.

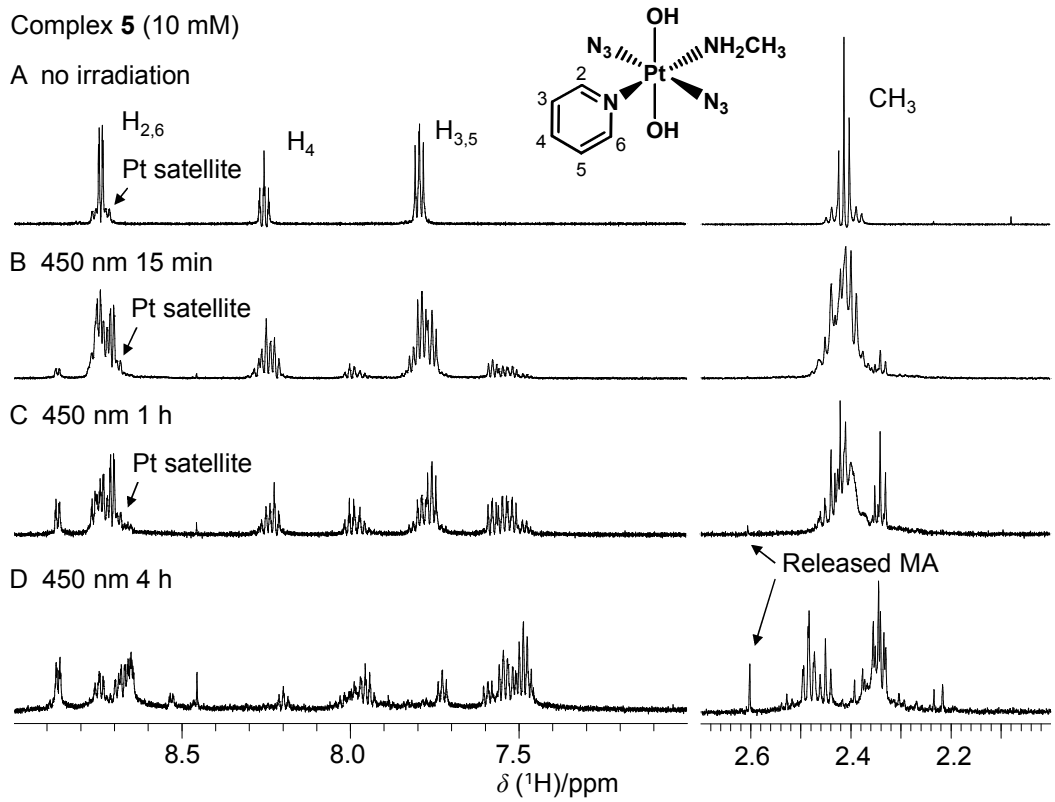

Figure 4.2 Time-dependent 600 MHz ^{1}H-NMR spectra (aliphatic and aromatic area) of complex **5** complexes **5** (*trans,trans,trans*-[$Pt(N_3)_2(OH)_2(MA)(Py)$], 10 μM) in 90% H_2O/10% D_2O upon irradiation at 450 nm (50 mW/cm^2, 298 K). The pH value of the sample was adjusted to 4 ± 0.5 before every NMR experiment. A, no irradiation; B, 15 min; C, 1 h; D, 4 h.

The detailed photochemistry of complex **5** in aqueous solution was then studied.

4.3.1.4 ^{14}N NMR spectroscopy

^{14}N NMR spectroscopy was used to probe the photolysis of complex **5** (*trans,trans,trans*-[$Pt(N_3)_2(OH)_2(MA)(Py)$]) in aqueous solution. First, the 1D ^{14}N NMR spectrum of complex **5** in 90% H_2O and 10% D_2O was recorded (**Figure 4.3A**). The assignments of the signals listed in **Table 4.2** are made according to the ^{14}N NMR studies of the authentic samples or published data for related complexes.[7,

[8, 24] It is theoretically possible to quantify these peaks by integration, as the T_1 relaxation times of ^{14}N nucleus are quite short (millisecond level).[24] However, practically the signals are often badly overlapped and the bandwidths are very broad. Therefore, quantification was performed for some of the distinguishable sharp peaks only.

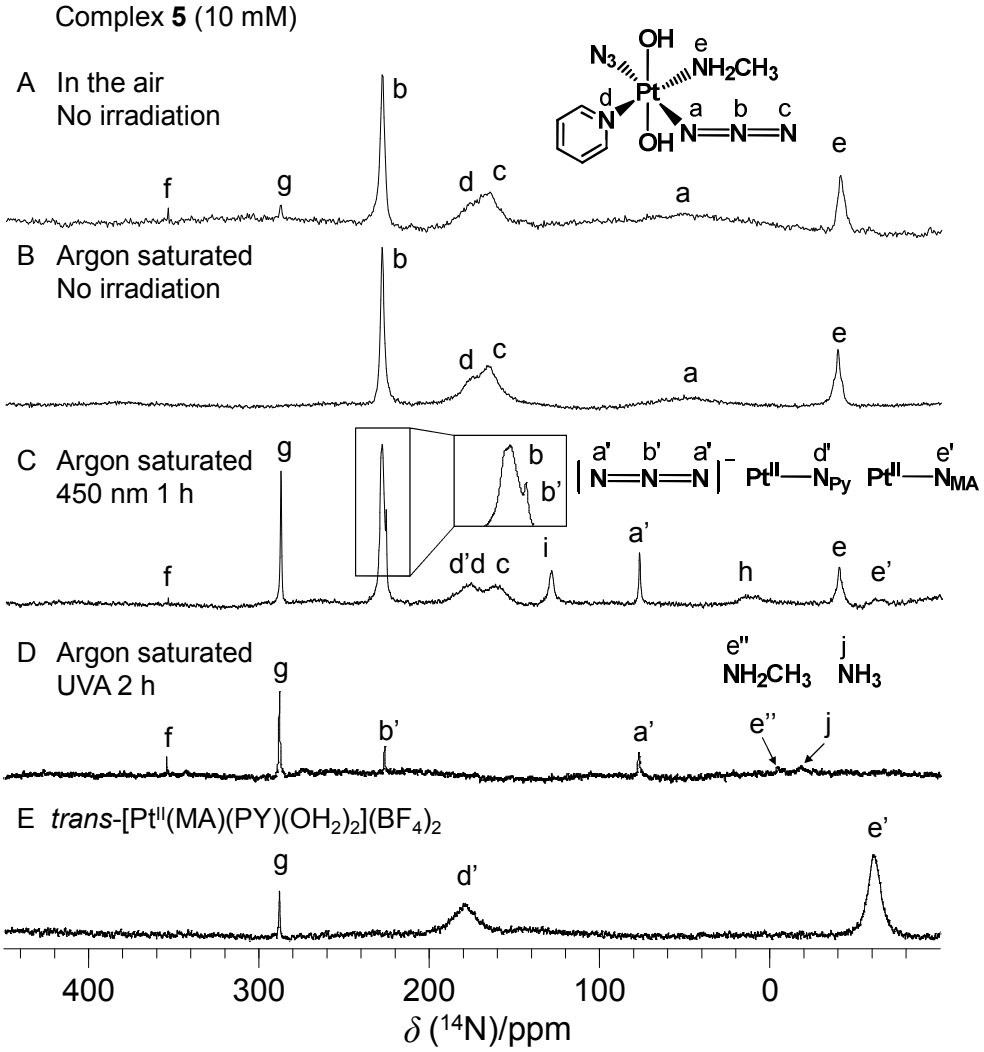

Figure 4.3 ^{14}N NMR (43.4 MHz) spectrum of complex **5** (*trans,trans,trans*-$[Pt(N_3)_2(OH)_2(MA)(Py)]$, 10 mM in 90% H_2O:10% D_2O, pH adjusted to 7.4 ± 0.5). (**A**) sample prepared in air and kept in the dark; (**B**) sample saturated with argon, (**C**) sample **B** irradiated at 450 nm for 60 min; (**D**) sample **B** irradiated with UVA for 2 h; (**E**) *trans*-$[Pt(MA)(Py)(OH_2)_2](BF_4)_2$ (**5g**) (10 mM in 90% H_2O:10% D_2O).

The signal at 288 ppm (peak **g**) was assigned as dissolved nitrogen gas. The signal disappeared after saturating the solution with argon (**Figure 4.3B**). Peaks **b** (228 ppm) **c** (165 ppm) and the broad signal **a** (~ 80 ppm) correspond to the central, unbound terminal and Pt-bound terminal N atoms, respectively, of coordinated N_3^- ligands. The resonance of Pt^{IV} bound N atoms (**a**) in azido ligands is exceptionally broad due to an highly asymmetric electric field gradient at the ^{14}N nucleus.[24] Peaks **d** (174 ppm) and **e** (−39 ppm) correspond to the N atoms of the Py and MA, respectively. The integrations of the peaks **b** : (**c**+**d**) : **e** = 2 : 3.05 : 0.93, which is *ca.* 2 : 3 :1, consistent with the numbers of ^{14}N atoms in the molecule.

After irradiation at 450 nm (50 mW/cm^2) at 298 K for 1 hour, new ^{14}N signals appeared (**Figure 4.3C**). Peaks **b'** (226 ppm) and **a'** (78 ppm) are assignable to the terminal and central nitrogen atoms of free azide (N_3^-). This assignment was confirmed regarding the ^{14}N NMR spectrum of NaN_3 in D_2O and also by literature data.[7, 25] Other new peaks **d'** (δ = 179 ppm) and **e'** (δ = −60 ppm) are assigned as the Pt^{II}-coordinated Py and MA ligands, respectively. Their assignment was confirmed by the ^{14}N NMR spectrum of the di-aqua species of *trans*-[Pt(MA)(Py)$(OH_2)_2$]$(BF_4)_2$ (**5g**) synthesized independently (**Figure 4.3E**). Peaks **b** (228 ppm) and **c** (165 ppm) for the coordinated N_3^- ligand of complex **5** were still present, but with reduced intensities. The integration of (**b** + **b'**) : **a'** = 8.7 : 1, and theoretically **a'** : **b'** =2 : 1. Therefore, **b** : **b'** = 16.4 : 1, which means a large amount of N_3^- ligand remained bound to Pt. Some was on intact starting materials (~17% from ^1H NMR), and the remainder is possibly N_3^- mono-coordinated Pt complexes. The signals **d** and **d'** were both very broad due to the quadrupolar effect of ^{14}N, but they could still be distinguished in **Figure 4.3C**.

Remarkably, the sharp peak **g** corresponding to nitrogen gas (N_2) was also observed. By integration, the ratio of peak **g** : **a'**= 2.0 : 1, so the ratio of released N_2 molecules to N_3^- anions in aqueous phase was 2.0 as well. Considering that part of the N_2 gas was liberated as bubbles from the solvent (solubility of N_2 in H_2O at 298 K is *ca.* 17 μg/g) and the NMR tube was kept sealed, the actual amount of generated N_2 gas was much more than the free N_3^- anions. Peak **f** is assigned as free nitrate NO_3^- in solution, arising as a side-product of the photodecomposition of the azido ligand. [7, 8] The other new peaks **h** and **i** were not identified. If ignore the evolved N_2 gas, the molar ratio of the following molecules/ions in the solution is *ca.*:

$$Pt\text{-}N_3 : N_3^- : N_2 = 16.4 : 1 : 2$$

After irradiation of an argon-saturated solution of complex **5** with UVA (3.46 mW/cm^2) for 2 hours, gas bubbles and a lot of precipitate were again observed. Almost no peaks assignable as coordinated azides were detected, and intriguingly, the signals for coordinated Py and MA were not observed either (**Figure 4.3D**). It is likely that most of the Py and MA ligands were present in the precipitate. Three new signals **b'** (226 ppm), **c'** (78 ppm) and **g** (δ = 288 ppm) were again assignable as the terminal and central nitrogen atoms of free azide ($\underline{N_3}^-$) and nitrogen gas, respectively. A very small amount of free MA ($\underline{N}H_2CH_3$) **e"** (δ = −3 ppm) and free ammonia $\underline{N}H_3$ **j** (δ = −18 ppm) was detected. These signals were confirmed by ^{14}N NMR experiments for authentic samples and also by literature data.[8] The existence of MA is consistent with the ^1H NMR result for this photoreaction. However, it was surprising to find the signal of free NH_3. With the assistance of the following results and literature report, the source of free NH_3 was identified. Upon irradiation with light, N_2 gas may be released directly from the $Pt\text{-}N_3$, forming a nitrene intermediate {Pt-N}.[9] This intermediate can thus convert to $Pt\text{-}NH_3$, (*vide infra*) followed by

photo-disassociation to give free NH_3.[7, 8, 27, 28] Free N_3^- anion can also undergo this series of photoreactions and give free NH_3.[29] If we ignore the evolved N_2 gas, the molar ratio of the following molecules/ions in the solution is *ca.*:

$$Pt\text{-}N_3 : N_3^- : N_2 : NO_3^- = 0.59 : 1 : 2.55 : 0.58$$

This result indicates that upon photoactivation, the azido ligands in the Pt^{IV} complex in aqueous solution are converted to both free azide (N_3^-) and N_2 gas. The nitrogen gas was probably formed from the combination of the N_3• radicals released in this photoreaction (*vide infra*).[30] The N_2 gas may also be released directly from the Pt bound N_3^- ligand on forming a nitrene intermediate (*vide infra*).[9] Upon irradiation at 450 nm for 1 hour, the major pathways of azido ligand are either formation of N_2 gas or new Pt-N_3 compounds, while upon irradiation with UVA for 2 hours, the major products for the azido ligands is N_2 gas.

Table 4.2 Assignments of ^{14}N NMR signals in **Figure 4.3**.

Peak	δ/ppm	Assignment
a	70 – 80	Pt^{IV}–<u>*N*</u>NN
b	228	Pt^{IV}–N<u>*N*</u>N
c	165	Pt^{IV}–NN<u>*N*</u>
a'	78	<u>*N*</u>N<u>*N*</u>$^-$
b'	226	N<u>*N*</u>N$^-$
d	174	Pt^{IV}–$\underline{N}_{Py}$
d'	179	Pt^{II}–$\underline{N}_{Py}$
e	−39	Pt^{IV}–$\underline{N}_{MA}$
e'	60	Pt^{II}–$\underline{N}_{MA}$
e"	−3	<u>*N*</u>H_2CH_3
f	354	<u>*N*</u>O_3^-
g	288	$\underline{N_2}$ gas
h	~15	n.a.
i	130	n.a.
j	−18	<u>*N*</u>H_3

n.a. = not assigned.

4.3.1.5 Azidyl radicals (N_3•) detected by EPR

An unambiguous method to identify the N_3• radicals is electron paramagnetic resonance (EPR) using spin traps, developed by Rehorek.[31] The hyperfine splitting patterns of the EPR signal and the g-factor are the "finger print" of trapped radicals. In this work, the generation of azidyl radicals (N_3•) was confirmed by EPR experiment using 5,5-dimethyl-pyrroline-N-Oxide (DMPO) as the spin trap.[32, 33] DMPO can effectively capture O-, N-, S- and C-centered radicals and form stable products which can be studied by EPR.

To detect the N_3• radicals, complex **5** (*trans,trans,trans*-[$Pt(N_3)_2(OH)_2(MA)(Py)$], 5 mM) with 2 mol equiv of DMPO in aqueous solution was irradiated at 450 nm (50 mW/cm^2) at 293 K. The resulting EPR spectrum which is compatible with the adduct DMPO•-$^{14}N_3$ is shown in **Figure 4.4A**. The simulation of hyperfine splittings and the ratios of integrations are illustrated in **Figure 4.4B**, which consists of a quartet of triplets (1:1:1:2:2:2:2:2:2:1:1:1). This results from overlap of the hyperfine splitting constants (HFSC) of the proton ($^1H_2$) and the nitroxyl nitrogen ($^{14}N_1$), with further splitting by the azide nitrogen ($^{14}N_\alpha$). The EPR signal was observed in the first spectrum recorded within 5 minutes, (**Figure 4.4C**) and is in good agreement with the simulation and previously reported data for N_3•.[33, 34] The hyperfine splitting constants (HFSC) were: a($^{14}N_1$) = 14.4 G, a($^1H_2$) = 14.6 G, a($^{14}N_\alpha$) = 3.2 G and the g-factor = 2.011, (reported results: a($^{14}N_1$) = 14.8 G, a($^1H_2$) = 14.2 G and a($^{14}N_\alpha$) = 3.1 G).[34] The decay time of DMPO•-$^{14}N_3$ spin adduct was *ca.* 25 min.

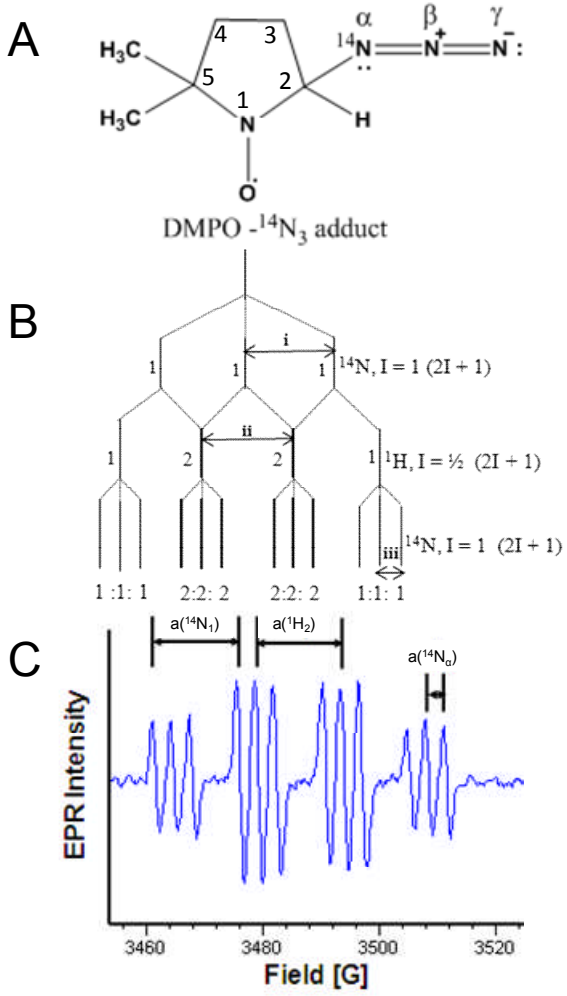

Figure 4.4 (**A**), Structure of spin adduct DMPO•-$^{14}N_3$; (**B**), Illustrated hyperfine splittings and the ratios of peaks; (**C**), EPR spectrum of irradiated (450 nm, 10 mW/cm^2, 5 min) sample of complex **5** (*trans,trans,trans*-[$Pt(N_3)_2(OH)_2(MA)(Py)$], 5 mM) with DMPO (10 mM) in deionised water (293 K). Spectrum was recorded by Miss J. Butler.

The hydroxyl radical OH• can also be captured by DMPO, and the EPR signal of DMPO•-OH should have the hyperfine splitting pattern of 1:2:2:1.[33, 35] However, in this work, no signal corresponding to DMPO•-OH was found. Therefore, it can be concluded that OH• radicals are not generated in the photolysis of complex **5** under the conditions used.

In addition, another experiment was conducted on complex **5** and DMPO in the presence of 2 equivalents of 5'-GMP, other conditions being identical to above. The EPR spectrum was identical to above too, indicating that excess 5'-GMP did not affect the generation or trapping of N_3• radical or the spin trap DMPO reacts with the N_3• radical faster than 5'-GMP.

4.3.2 Singlet oxygen ($^1O_2$) detection

It has been reported that upon irradiation with UVA, two platinum(IV) diazidodihydroxido complexes, namely *cis,trans,cis*-$[Pt(N_3)_2(OH)_2(NH_3)_2]$ and *trans,trans,trans*-$[Pt(N_3)_2(OH)_2(NH_3)_2]$ generated oxygen gas (O_2),[7, 8] but no direct evidence has been previously obtained for the energy state of the released oxygen. In this work, the nature of the released oxygen was investigated using a fluorescence probe for singlet oxygen: Singlet Oxygen Sensor Green (SOSG®). SOSG is a highly selective sensor for $^1O_2$ without any appreciable response to hydroxyl radicals or superoxides, marketed by Invitrogen/Molecular Probes.[36] The structure of SOSG has not been disclosed, but it is believed to contain a fluorescein bond to a dimethylanthracene derivative as a fluorescence quencher via charge transfer (**Figure 4.5**).[37] In the absence of $^1O_2$, SOSG exhibits weak blue fluorescence, but in the presence of $^1O_2$, the charge transfer is blocked and the fluorescein moiety emits strong green fluorescence with excitation and emission maxima at 504 nm and 525 nm, respectively.[38] Although it was reported that SOSG can itself sensitize the production of singlet oxygen,[39] under our experimental conditions, this fluorescence probe was stable to light between 365 – 504 nm, with no change in the intensity of fluorescence.

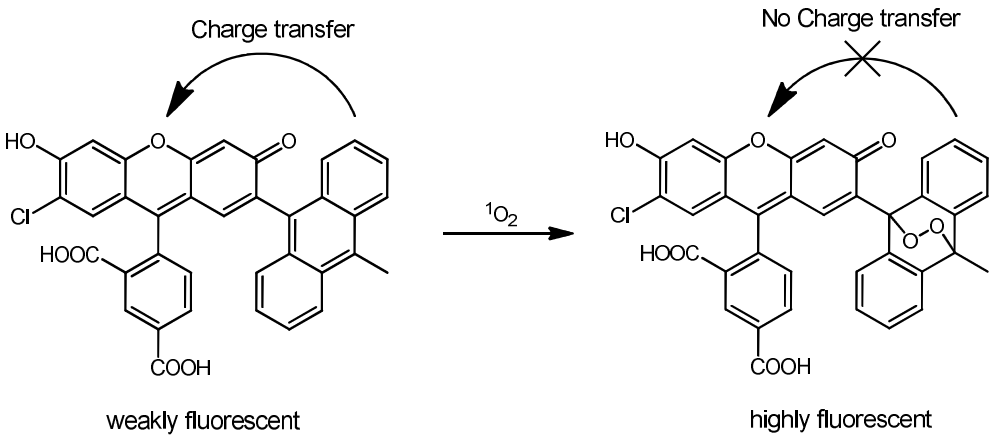

Figure 4.5 Formation of the endoperoxide of SOSG (denoted SOSG-EP) upon reaction of SOSG with singlet oxygen. Adapted from ref.[37]

A sample of complex **5** (*trans,trans,trans*-$[Pt(N_3)_2(OH)_2(MA)(Py)]$, 50 μM) and SOSG (1 μM) was prepared in deionized water with 3% methanol. MeOH was always added to maintain the solubility of SOSG. The pH of the mixture was *ca.* 7, as measured by pH paper. This solution was stable in the dark or even upon irradiation at 504 nm, which is important because 504 nm is the excitation wavelength for fluorescence. When it was exposed to very weak 365 nm light (21 $\mu W/cm^2$), the intensity of the fluorescence at 525 nm (λ_{ex} = 504 nm) increased rapidly, at was recorded at certain time intervals as shown in **Figure 4.6**. The *ca.* 10-times increase in the fluorescence after irradiation for 15 min suggested that $^1O_2$ was generated upon irradiation at 365 nm. The pH of the final solution was still *ca.* 6, preventing the SOSG from being activated at alkaline pH.[36] A control sample saturated with argon was irradiated at 365 nm and the fluorescence was even higher. This result again proved that the $^1O_2$ was not from the dissolved O_2 via energy transfer from a photosensitizer. It also ruled out the possibility that SOSG can act as photosensitizer. It was very interesting to note that with argon saturation, the intensity of fluorescence increased faster. Argon alone could not trigger the fluorescence of SOSG, verified by a blank test with SOSG saturated with argon.

Also, when a sample of complex **5** and SOSG was saturated with N_2, the intensity of the fluorescence after irradiation was similar to that of the sample saturated with Ar.

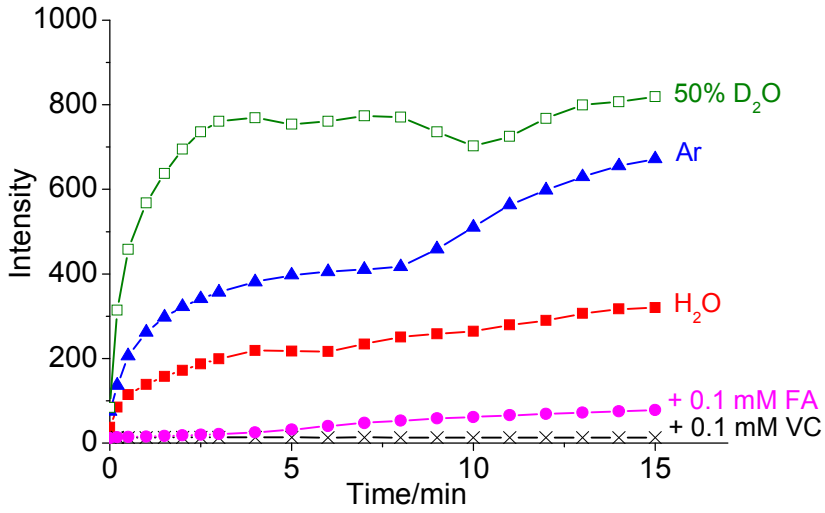

Figure 4.6 The time dependent intensity of the fluorescence (λ_{ex} = 504 nm, λ_{em}= 525 nm) of complex **5** (*trans,trans,trans*-[$Pt(N_3)_2(OH)_2(MA)(Py)$], 50 μM) and SOSG (1 μM) in 97% H_2O/3% MeOH upon a weak irradiation at 365 nm (3 nm slit width, 21 $\mu W/cm^2$). T = 293 K. Solid squares, no additive; hollow squares, 50% D_2O added; triangles, saturated with argon; solid circles, 0.1 mM formic acid (FA) added; crosses, 0.1 mM L-ascorbic acid (VC) added. All the data points were the average of 2 ~ 4 independent experiments.

As the life time of $^1O_2$ in D_2O is much longer than in H_2O, the oxidation reaction by $^1O_2$ may be greatly potentiated in D_2O.[40, 41] This experiment was carried out in 50% D_2O to confirm the existence of $^1O_2$. Upon irradiation at 365 nm, the intensity of fluorescence was 3 – 4-fold higher than that of the reaction carried out in H_2O (**Figure 4.6**). In order to distinguish between the generation of $^1O_2$ and •OH, appropriate scavengers were used. Two independent groups of experiments with 100 μM L-ascorbic acid (VC) as $^1O_2$ scavenger or 100 μM formic acid (FA) as •OH scavenger were carried out. The data are plotted in **Figure 4.6**. Complex **5** does not

react with VC in the absence of light (see **Section 4.3.1.1**), given VC is a strong reductant. In the presence of VC, the fluorescence was totally quenched, whereas in presence of FA, the fluorescence slightly increased upon irradiation at 365 nm, although the intensity of the fluorescence was lower than that of the sample without FA.

More experiments were carried out to compare the efficiency of $^1O_2$ generation with different irradiation wavelengths and dark or blank controls. As depicted in **Figure 4.7**, fluorescence was still observed upon irradiation at 420 or 450 nm. Owing to the higher power densities of 420 and 450 nm light compared to that of 365 nm, the dose-dependent efficiency of generating $^1O_2$ upon irradiation at 365 nm was still higher than that with the longer wavelengths. The dark control experiment (with sham irradiation) for the solution of complex **5**/SOSG (50 μM/1 μM) showed very low intensity of fluorescence (data not shown). The blank control experiment (in the absence of complex **5**) showed low intensity of fluorescence, too.

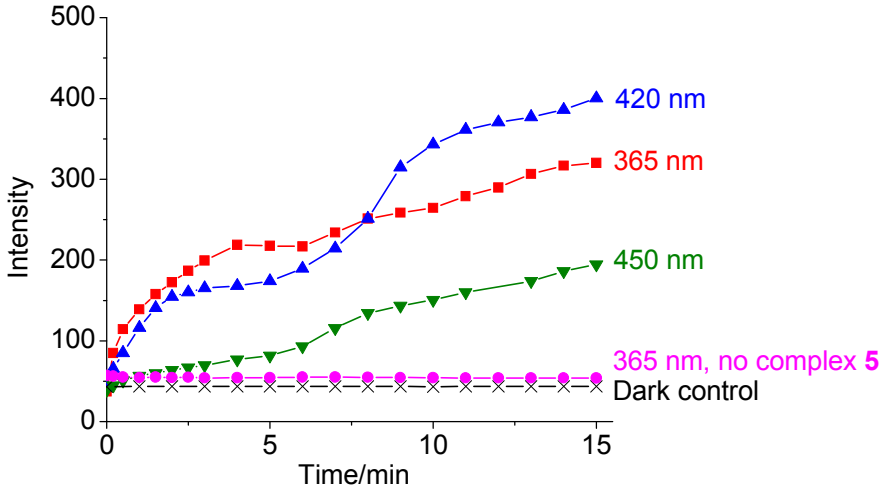

Figure 4.7 The time dependent intensity of the fluorescence (λ_{ex} = 504 nm, λ_{em} = 525 nm) of complex **5** (*trans,trans,trans*-[$Pt(N_3)_2(OH)_2(MA)(Py)$], 50 μM) and SOSG (1 μM) in H_2O (3% MeOH) upon irradiation at various wavelengths. T = 290 – 295 K. Squares, λ_{irr} = 365 nm, 21 μW/cm^2; triangles, λ_{irr} = 420 nm, 850 μW/cm^2; inverted triangles, λ_{irr} = 450 nm, 800 μW/cm^2; crosses, dark control; circles, no complex **5** was added, λ_{irr} = 365 nm. All the data points were the average of 2 ~ 4 independent experiments.

The detailed mechanism for the generation of $^1O_2$ could involve the recombination of released hydroxyl radicals. When hydroxyl radicals are generated at high local concentrations, they readily dimerize to give H_2O_2, [42] which is known to decompose by disproportionation to water and gaseous dioxygen upon irradiation with UV light.[43] In order to investigate this pathway under our reaction conditions, a mixture of 500 μM H_2O_2 and 1 μM SOSG was irradiated at 365 nm for 15 min, but no change in the intensity of the fluorescence was observed. However, when a solution of complex **5** (50 μM) and SOSG (1 μM) was added to 500 μM H_2O_2, the intensity of fluorescence upon irradiation at 365 nm was much higher than that of without H_2O_2 (**Figure 4.8**). Therefore, it is reasonable to postulate that one or more than one Pt-containing species can catalyse the photolysis of H_2O_2 and give $^1O_2$, upon

irradiation with light. In order to verify this, K_2PtCl_6 or *trans*-[$PtCl_2$(MA)(Py)] (50 μM) was added to a mixture of H_2O_2 and SOSG before irradiating, but still no increase of intensity of fluorescence was observed (**Figure 4.8**). These results indicate that only certain Pt-containing intermediate(s) in the photo-reaction mixture can catalyse the photolysis of H_2O_2 upon irradiation of light and generate $^1O_2$.

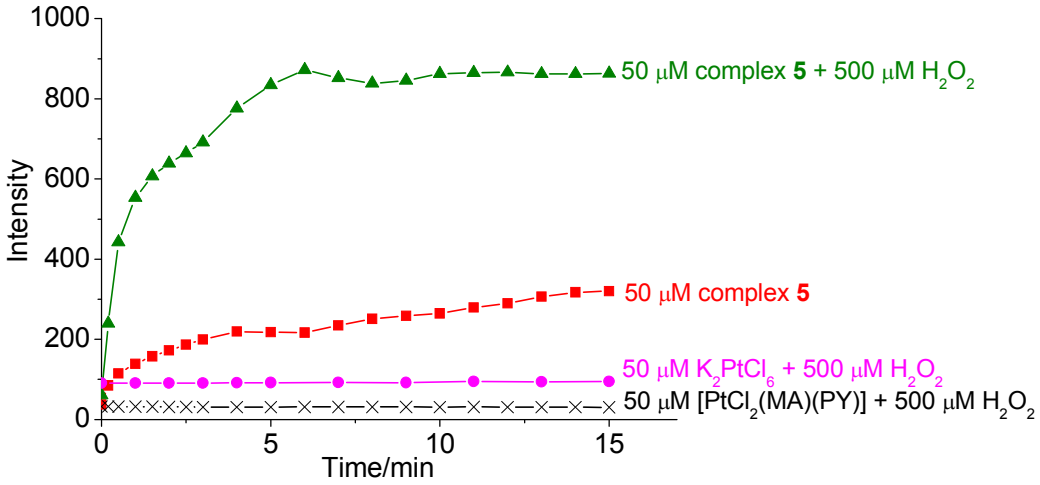

Figure 4.8 The time dependent intensity of the fluorescence (λ_{ex} = 504 nm, λ_{em} = 525 nm) of Pt complexes (50 μM) and SOSG (1 μM) in H_2O (3% MeOH) upon irradiation at 365 nm. Squares, complex **5** (*trans,trans,trans*-[$Pt(N_3)_2(OH)_2$(MA)(Py)], 50 μM); triangles, complex **5** (50 μM) and 500 μM H_2O_2; circles, K_2PtCl_6 (50 μM) and 500 μM H_2O_2; crosses, [$PtCl_2$(MA)(Py)] (50 μM) and 500 μM H_2O_2. All the data points were the average of 2 ~ 4 independent experiments.

Finally, an attempt was made to detect the H_2O_2 with a peroxide test stick (Quantofix® Peroxide 25) while the solution of complex **5** was irradiated with light. The paper zone of the test stick is originally white and turns blue upon exposure of aqueous peroxide. A small amount (2 μL) of a high concentration complex **5** (20 mM in H_2O) was dropped on the paper zone of the test stick; no colour change was observed. Assuming that each complex molecule releases one molecule of peroxide,

the theoretical maximum amount of H_2O_2 released is 20 mM, which is 680 mg/L. This number is far above the minimum detection limit for the peroxide test sticks. Therefore, the generation of peroxide under these conditions should be detectable. Then 2 μL of the complex **5** solution was irradiated with light (450 nm, 30 s – 15 min) and was immediately dropped onto the paper zone of the test stick, there was still no colour change. However, when the paper zone was stained with an intact solution of complex **5** and then irradiated at 450 nm, the stained area turned blue (**Figure 4.9**). The concentration of H_2O_2 was semi-quantitively measured as 10 ~ 25 mg/L by comparing to the colour scale.

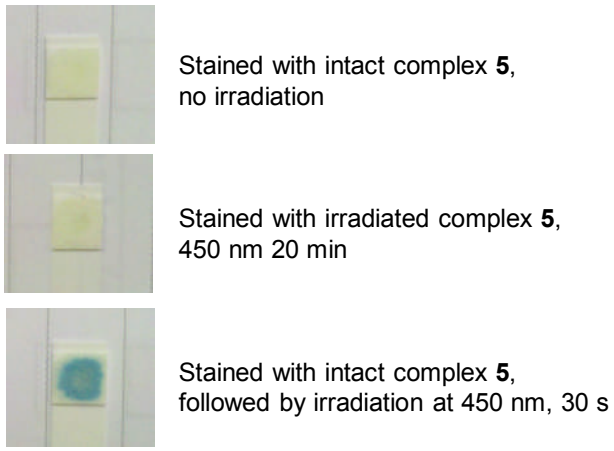

Figure 4.9 Colour change in the aqueous solution of complex **5** (20 mM) stained area on the paper zone of the Peroxide 25 Test Sticks (Quantofix®) under various irradiation conditions. (450 nm, 50 mW/cm^2).

Apparently, the peroxide test sticks were activated by some very short lived oxidative species. According to the product information from the supplier, other strong oxidative agents may cause false-positive results.[44] This experiment leads to two possibilities. First, the photodecomposition of complex **5** does not involve peroxide (H_2O_2) as an intermediate, but some other kinds of strong oxidative species (e.g., $^1O_2$, nitrenium ion, etc.) can activated the test stick. Second, the peroxide

(H_2O_2) was still generated but quickly decomposed upon irradiation with UVA or through the catalytic effect of the Pt-containing species in the solution. However, according to the measured concentration of peroxide, if it was, 10 ~ 25 mg/L, it would not be fully decomposed within only a few seconds. Therefore, it is concluded that H_2O_2 itself is not an intermediate in the photodecomposition of complex **5**.

4.3.3 Photoreaction with 5'-guanosine monophosphate

The photochemical reaction of Pt complexes with 5'-guanosine monophosphate (5'-GMP) in aqueous solution was investigated, since guanine is a preferred target for DNA platination of Pt^{II} complexes such as cisplatin.[45, 46] The reactions with 5'-GMP may mimic the platination of DNA in cells.

4.3.3.1 ^{1}H NMR spectroscopy

Complexes **5** (*trans,trans,trans*-$[Pt(N_3)_2(OH)_2(MA)(Py)]$) and **8** (*trans,trans,trans*-$[Pt(N_3)_2(OH)_2(MA)(Tz)]$) (2 mM) did not react with 5'-GMP (2 mol equiv) in water in the absence of light over a period of three days, as judged by ^{1}H NMR spectroscopy. The photo-induced reactions of complex **5** or **8** (3.9 mM in D_2O) in the presence of 2 equivalents of 5'-GMP were monitored by ^{1}H, ^{195}Pt NMR spectroscopy and HPLC-ESI-MS. During the photoreaction of complex **5** and 5'-GMP upon irradiation at 450 nm, the yellow colour of the solution grew deeper and darker, and gas bubbles formed. (**Figure 4.10**) Interestingly, no precipitate was observed. Before irradiation, in the ^{1}H NMR spectrum, signals at δ = 8.72, 8.30, 7.84 and 2.42 ppm correspond to $\underline{H_{2,6}}$, $\underline{H_4}$ and $\underline{H_{3,5}}$ of the Py ligand and C$\underline{H_3}$ of the MA ligand, respectively. δ = 8.12 ppm corresponds to $\underline{H_8}$ of free 5'-GMP. (**Figure 4.11**) After irradiation at 450 nm for 1 hour, the signal of complex **5** nearly vanished and a new major product was formed with δ = 2.25 and 8.86 ppm, which was assigned as

C$\underline{H}_3$ of MA and $\underline{H_8}$ of Pt coordinated 5'-GMP in (*SP*-4-2)-[Pt(N_3)(MA)(Py)(5'-GMP) − H] (**5b**). The identical chemical shift was exhibited by an authentic sample of **5b**. Other characterization methods (^{195}Pt NMR spectroscopy and HPLC-ESI-MS) also confirmed the assignment of this compound (see **Section 4.3.3.3** and **4.3.3.4**). According to the ^{1}H NMR spectra, the reaction between complex **5** and 5'-GMP had almost finished after irradiation for one hour, and longer exposure to light caused no obvious change to the major product but only the decomposition of the other photoproducts. After irradiation of a sample of complex **5** and 5'-GMP at 450 nm, very little amount of MA was released (1% after 1 hour and 4% after 3 hours of irradiation), as monitored by ^{1}H NMR (δ (C$\underline{H}_3$) = 2.59 ppm). The chemical shift of MA was confirmed by spiking the irradiated NMR sample with free MA.

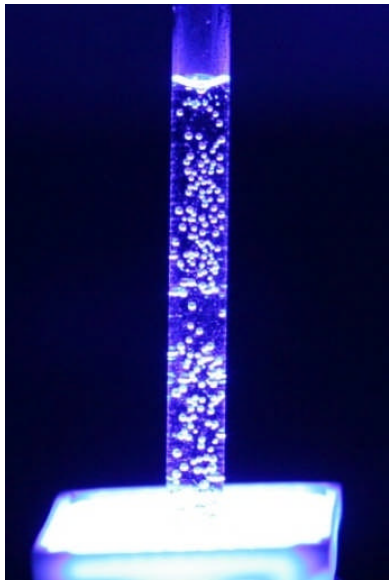

Figure 4.10 Gas bubbles observed in NMR tube while a D_2O solution of complex **5** (3.9 mM)/5'-GMP (7.8 mM) was irradiated with a 450 nm LED over 30 min (298 K).

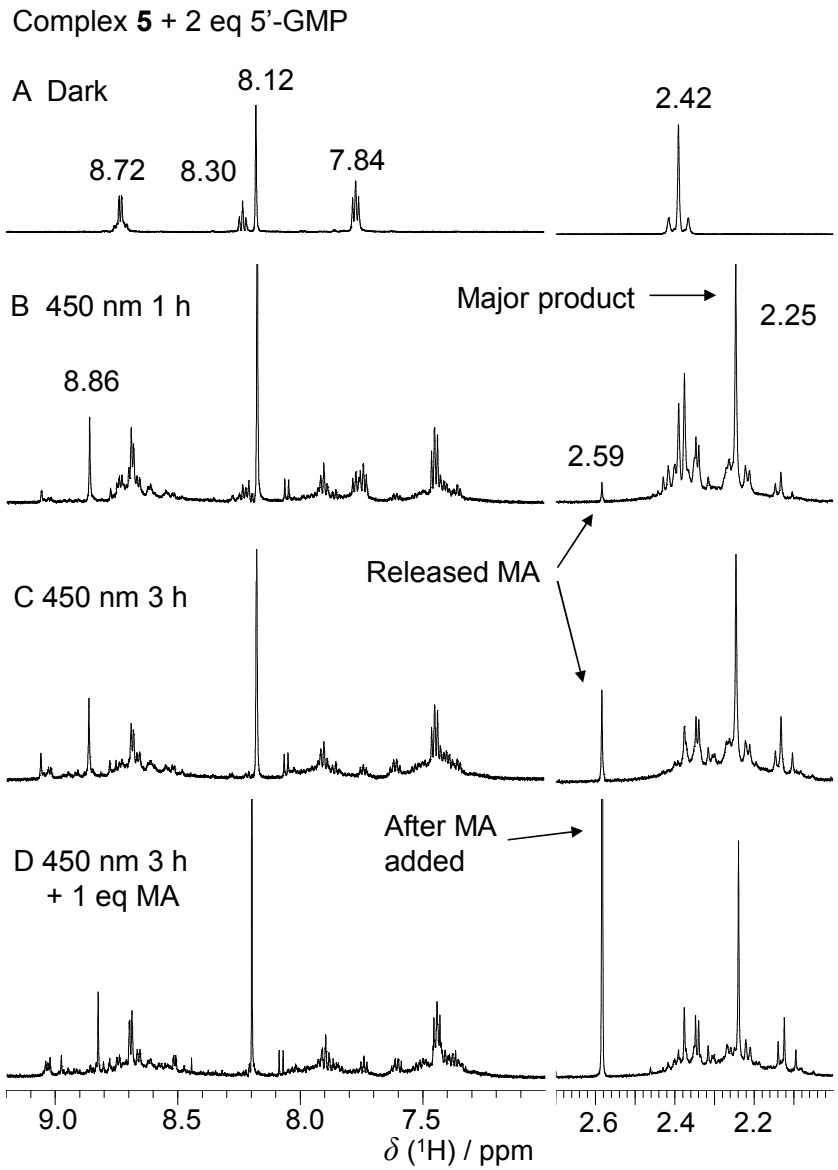

Figure 4.11 ^{1}H-NMR spectra of complex **5** (3.9 mM) with 5'-GMP (7.8 mM) in D_2O upon irradiation at 450 nm (50 mW/cm^2, 298 K) for (**A**) 0 h; (**B**) 1 h (180 J/cm^2); (**C**) 3 h (540 J/cm^2); (**D**) after irradiation, the NMR sample was spiked with 1 mol equivalent of free MA.

Similar experiments were performed for complex **8** with two equivalent of 5'-GMP. Before irradiation, in the ^{1}H NMR spectrum, signals at δ = 9.51, 8.23, 8.02 and 2.34 ppm correspond to $\underline{H_2}$, $\underline{H_4}$ and $\underline{H_5}$ of the Tz ligand and C$\underline{H_3}$ of the MA ligand, respectively. δ = 8.17 ppm corresponds to $\underline{H_8}$ of free 5'-GMP. (**Figure 4.12**) After

irradiation at 450 nm for only 15 min, the reaction was nearly finished and a new major product formed with peaks at δ = 8.82 and 2.25 ppm, which were assigned as C$\underline{H}_3$ of MA and $\underline{H_8}$ of Pt coordinated 5'-GMP in (*SP*-4-3)-[Pt(N_3)(MA)(Tz)(5'-GMP) − H] (**8b**). Identical chemical shifts were exhibited by an authentic sample of **8b**. Other characterization methods (^{195}Pt NMR spectroscopy and HPLC-ESI-MS) also confirmed the assignment of this compound (*vide infra*). According to the ^{1}H NMR signals, the released MA was <1% after 15 min and *ca.* 2% after 1 hour irradiation at 450 nm.

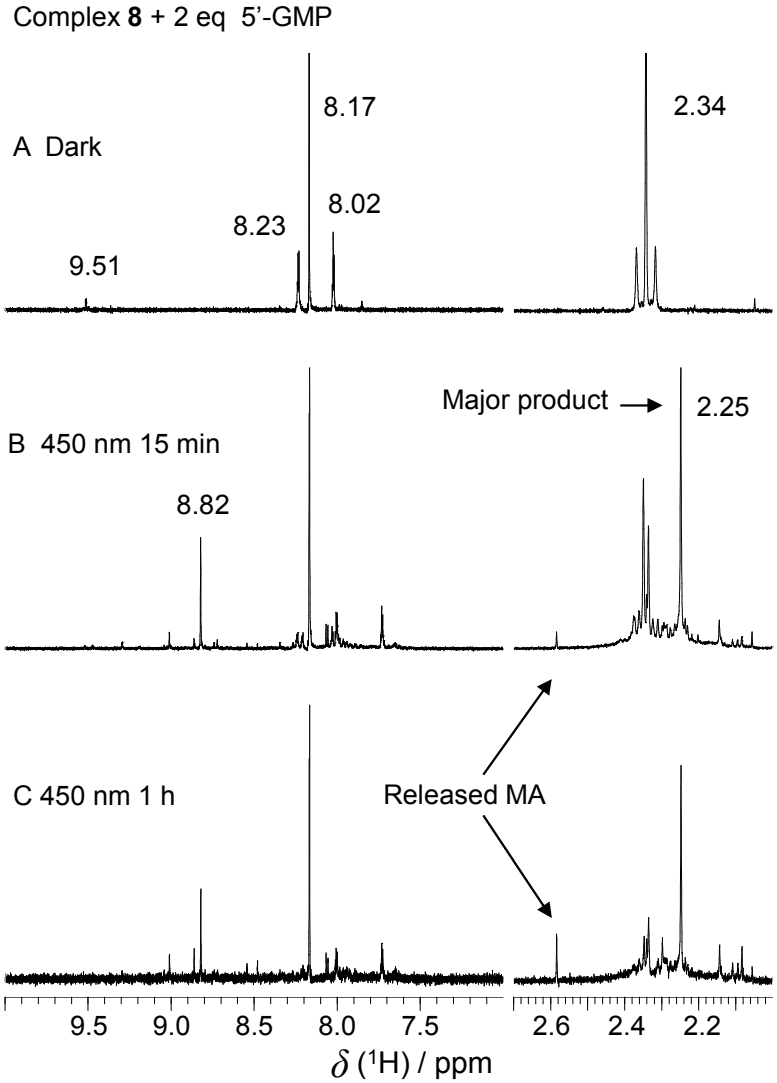

Figure 4.12 ^{1}H-NMR spectra of complex **8** (3.9 mM) with 5'-GMP (7.8 mM) in D_2O upon irradiation at 450 nm (50 mW/cm^2, 298 K) for (**A**) 0 min; (**B**) 15 min (45 J/cm^2); (**C**) 1h (180 J/cm^2).

4.3.3.2 UV-Vis spectroscopy

The photoreaction of complex **5** (*trans,trans,trans*-$[Pt(N_3)_2(OH)_2(MA)(Py)]$) with 5'-GMP was also followed by UV-Vis spectroscopy. In the UV-Vis spectrum of complex **5**, the absorption band maximum at 289 nm corresponds to the N_3-Pt^{IV} LMCT (Ligand-to-Metal-Charge-Transfer) transition. This absorption diminished upon irradiation with light, e.g., 450 nm (**Figure 4.13A**) The UV-Vis spectrum of 5'-GMP was also recorded (**Figure 4.13B**). 5'-GMP was very stable upon irradiation at 450 nm. Then the UV-Vis spectrum of a mixture of complex **5** with 5'-GMP was recorded (black line in **Figure 4.13C**); this curve is approximately equal to the overlap spectra of complex **5** and 5'-GMP. The mixture was stable in the dark for over 16 hours, as followed by UV-Vis. This mixture was then irradiated at 450 nm and the UV-Vis spectra in **Figure 4.13C** were recorded. Finally, the rate of decrease in A_{289} was plotted in **Figure 4.13D**. According to the slops of the two curves, the loss of Pt^{IV}-N_3 bond from complex **5** in the presence of 5'-GMP was *ca.* 1.5 times faster than in its absence upon irradiation at 450 nm.

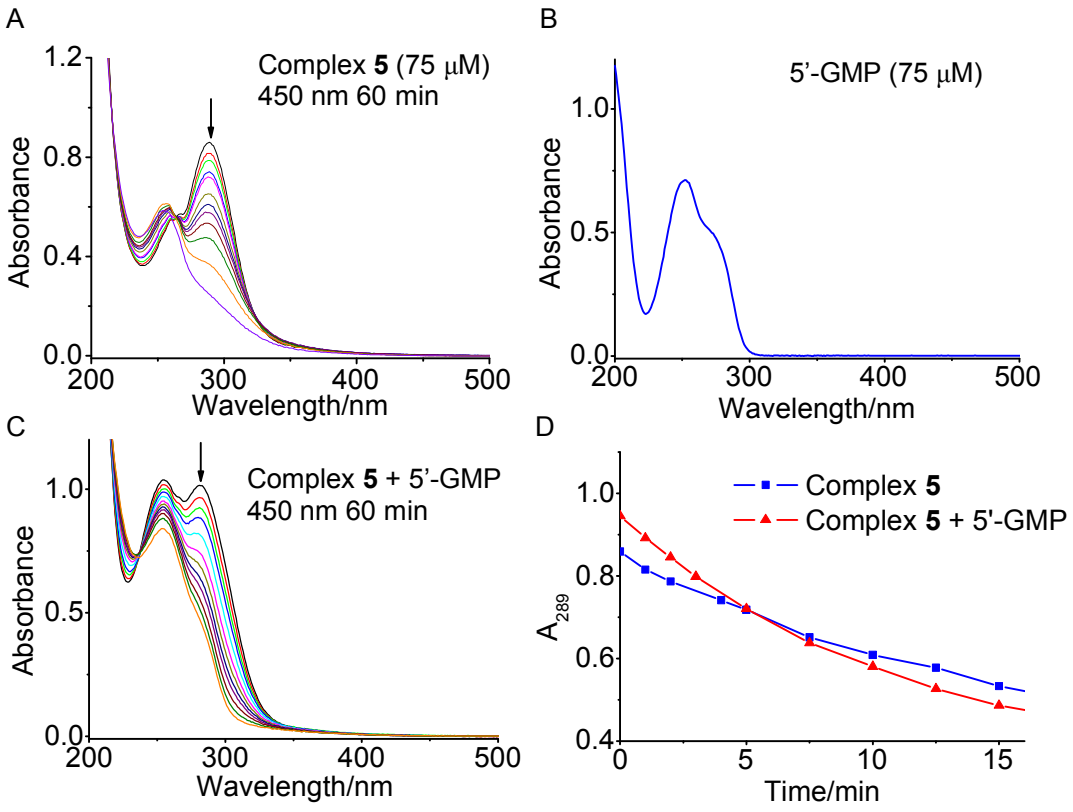

Figure 4.13 UV-Vis spectra for the photoreaction of complex **5** (*trans,trans,trans*-$[Pt(N_3)_2(OH)_2(MA)(Py)]$) with 5'-GMP in aqueous solution. (**A**) Complex **5** (75 μM) irradiated at 450 nm (50 mW/cm^2) for 60 min; (**B**) 5'-GMP (75 μM); (**C**) complex **5** (75 μM) and 5'-GMP (75 μM) irradiated at 450 nm for 60 min; (**D**) comparison of the decrease in rate of A_{289} in (**A**) and (**C**).

4.3.3.3 HPLC-ESI-MS study

In order to examine the products of the photochemical reaction of complexes **5** (*trans,trans,trans*-$[Pt(N_3)_2(OH)_2(MA)(Py)]$) and **8** (*trans,trans,trans*-$[Pt(N_3)_2(OH)_2(MA)(Tz)]$) with 5'-GMP in more detail, the reaction was studied by HPLC-ESI-MS. A solution of complex **5** (0.5 mM) and 5'-GMP (1.0 mM) in H_2O was irradiated at 450 nm for one hour at room temperature (298 K), and the reaction mixture was diluted 10-fold and then injected into HPLC-ESI-MS. The chromatogram is shown in **Figure 4.14A** and all the major peaks were identified by

coupled ESI-MS. The peak with a retention time t_r = 3.46 min was assigned as 5'-GMP; t_r = 11.10 min was assigned as *trans*-[Pt(MA)(Py)(5'-GMP)$_2$ − 2H] (**5a**); t_r = 11.47 min was assigned as (*SP*-4-2)-[Pt(N_3)(MA)(Py)(5'-GMP) − H] (**5b**). The identical retention times and absorption spectra were verified by the synthesis of authentic samples of these species. The MS isotope distributions agreed very well with their corresponding simulations. (**Figure 4.15**) This result indicated that one azido ligand and two Pt^{IV} bound hydroxyl groups were released during irradiation, while the Pt^{IV} was reduced to Pt^{II} and binds to 5'-GMP. Very small amounts of the complex **5** lost the second azido ligand to form a bis-GMP adduct. Then irradiation at 450 nm of the reaction mixture was continued for another 2 hours, the HPLC chromatogram is shown in **Figure 4.14B**. The difference between the two chromatograms (**Figure 4.14A** and **B**) is very small; the intensity of the peak for **5a** increased slightly. This result indicates that the mono-GMP/N_3^- adduct can slowly lose N_3^- and form the bis-GMP adduct. Then this resulting reaction mixture was irradiated with UVA for 1 hour and again HPLC-ESI-MS was performed (**Figure 4.14C**). In this chromatogram, the signal corresponding to **5b** completely disappeared, and the signal for **5a** increased a little. Some unidentified Pt-containing species was found, as shown by the coupled ESI-MS. Therefore, **5b** is not stable to irradiation with UVA; it may lose the N_3^- and form some new species such as **5a**, which is stable to UVA (**Scheme 4.1**).

A similar sample of complex **5** (0.5 mM) and 5'-GMP (1.0 mM) in H_2O was irradiated with UVA for 60 min. As expected, the chromatogram in **Figure 4.14D** was similar to that in **Figure 4.14C**, **5a** being the major product (**Scheme 4.1**). This result indicated that irradiation with UVA induced the loss of two hydroxido ligands and two azido ligands and Pt binds to two 5'-GMP molecules to form **5a**, during

which the Pt^{IV} was reduced to Pt^{II}. By contrast, irradiation at 450 nm released two hydroxido ligands but only one azido ligand, and Pt binds to one 5'-GMP to form **5b**. Thereafter, only a small portion of **5b** lost the remaining azido ligand upon irradiation with UVA and formed **5a**. The possible photodecomposition pathways of **5b** and the other unidentified products will be discussed in **Section 4.3.4**.

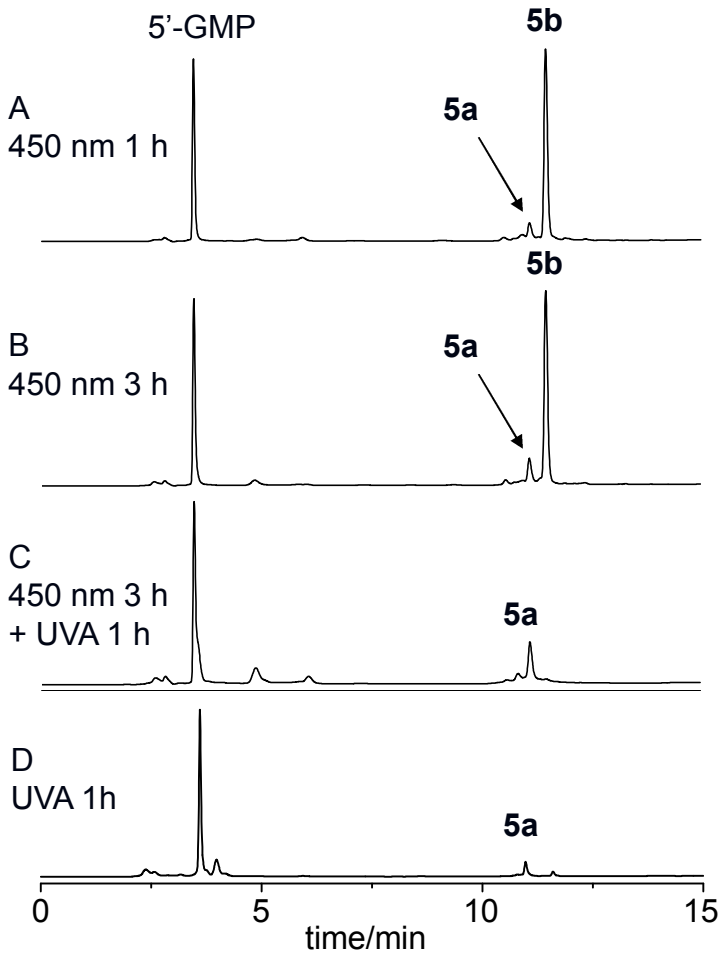

Figure 4.14 HPLC chromatograms of the photoreaction of complex **5**, *trans,trans,trans*-[$Pt(N_3)_2(OH)_2(MA)(Py)$] (0.5 mM) with 5'-GMP (1.0 mM) upon irradiation at (**A**) 450 nm 1 h; (**B**) 450 nm 3 h; (**C**) 450 nm 3 h and UVA 1 h successively; (**D**) UVA 1 h only. (298 K) Retention times and assignments: 3.46 min, 5'-GMP; 11.10 min, *trans*-[Pt(MA)(Py)(5'-GMP)$_2$ − 2H] (**5a**); 11.47 min, (*SP*-4-2)-[$Pt(N_3)$(MA)(Py)(5'-GMP) − H] (**5b**).

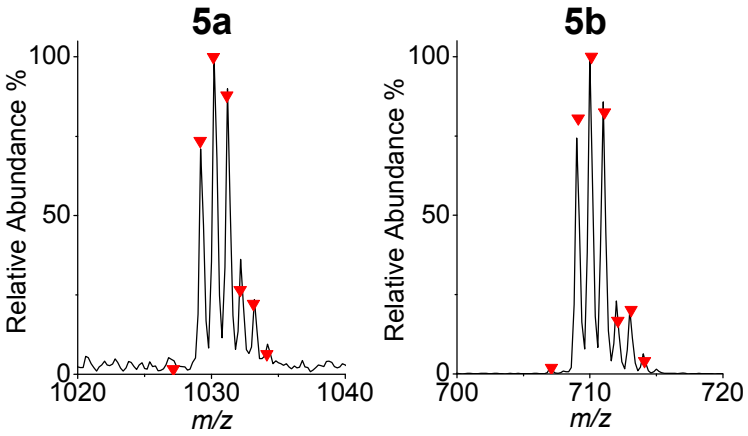

Figure 4.15 Mass spectrum isotope distributions of **5a** (*trans*-[Pt(MA)(Py)(5'-GMP)$_2$ − 2H], *m/z* for [M + H], calc. 1030.2; found, 1030.3) and **5b** (*SP*-4-2)-[Pt(N$_3$)(MA)(Py)(5'-GMP) − H], *m/z* for [M + H], calc. 710.1; found, 710.0. Their corresponding simulated isotope distributions are labelled with reversed red triangles.

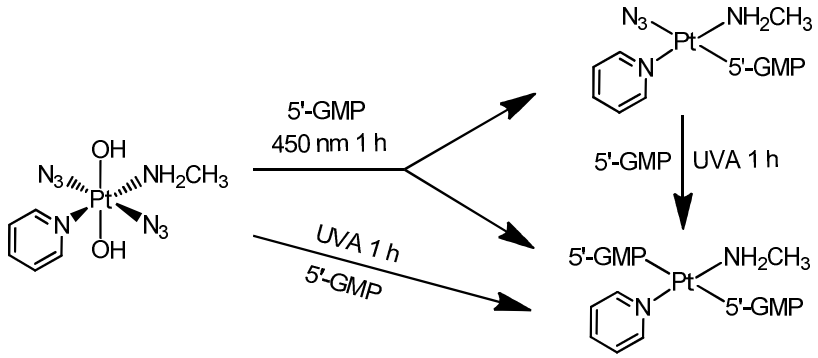

Scheme 4.1 Photoreaction scheme of complex **5** with 5'-GMP upon irradiation with UVA or 450 nm light.

The photoreaction of complex **8** with 5'-GMP followed a course very similar to that of complex **5**. Irradiation at 450 nm of a mixture of **8** and 5'-GMP (0.5 : 1.0 mM in H_2O) for one hour produced **8b** (t_r = 10.69, (*SP*-4-3)-[Pt(N$_3$)(MA)(Tz)(5'-GMP) − H]) as the major product and **8a** (t_r = 10.82 *trans*-[Pt(MA)(Tz)(5'-GMP)$_2$ − 2H]) as minor product (for HPLC chromatogram, see **Figure 4.16A**). The identical retention time and absorption spectrum were verified by the synthesized authentic samples of **8a** and **8b**. Their isotope distributions agree with the simulations. (**Figure 4.17**)

Compounds **8a** and **8b** possessed very similar retention times on the HPLC chromatogram, but they could be clearly identified as two products by coupled mass spectrometry. The photoproducts in **Figure 4.16A** did not change much over 2 hours of additional irradiation at 450 nm (**Figure 4.16B**), and after irradiation with UVA for one hour, almost all the mono-N_3^- adduct **8b** was destroyed, leaving **8a** only (**Figure 4.16C**). The reaction with irradiation of UVA gave **8a** as a major product (**Figure 4.16D**), similar to **Figure 4.16C**.

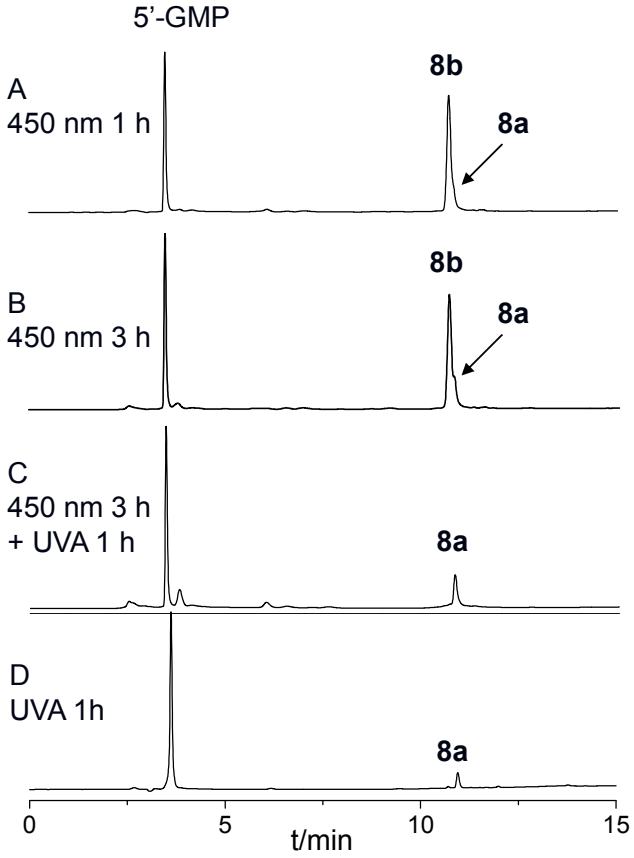

Figure 4.16 HPLC chromatography of the photoreaction of complex **8**, *trans,trans,trans*-[$Pt(N_3)_2(OH)_2(MA)(Tz)$] (0.5 mM) and 5'-GMP (1.0 mM) upon irradiation with (**A**) 450 nm light 1 h; (**B**) 450 nm light 3 h; (**C**) 450 nm 3 h and UVA 1h successively; (**D**) UVA 1 h only. (298 K) Retention times and assignments: 3.46 min, 5'-GMP; 10.82 min, *trans*-[Pt(MA)(Tz)(5'-GMP)$_2$ − 2H] (**8a**); 10.69 min, (*SP*-4-3)-[$Pt(N_3)$(MA)(Tz)(5'-GMP) − H] (**8b**).

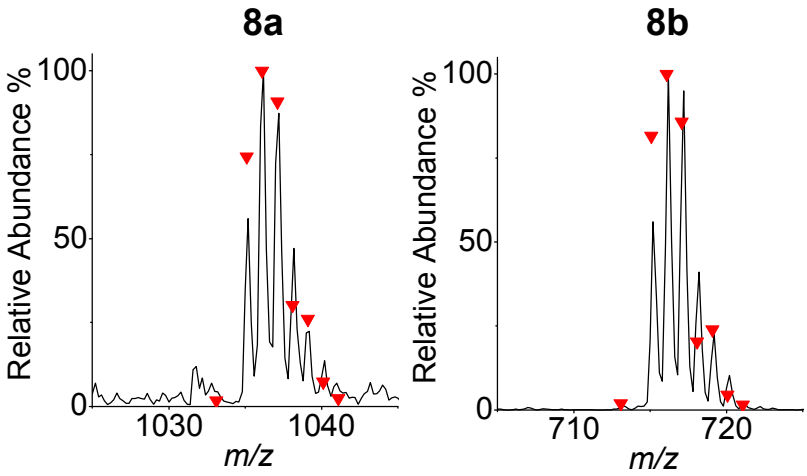

Figure 4.17 Mass spectrum isotope distribution of **8a** (*trans*-[Pt(MA)(Tz)(5'-GMP)$_2$ − 2H], *m/z* for [M + H], calc. 1036.1; found, 1036.1) and **8b** (*SP*-4-3)-[Pt(N$_3$)(MA)(Tz)(5'-GMP) − H], *m/z* for [M + H], calc. 716.1; found, 716.2. Their corresponding simulated isotope distributions are labelled with reversed red triangles.

4.3.3.4 ^{195}Pt NMR spectroscopy

The products from photoreaction of complexes **5** (*trans,trans,trans*-[Pt(N$_3$)$_2$(OH)$_2$(MA)(Py)]) and **8** (*trans,trans,trans*-[Pt(N$_3$)$_2$(OH)$_2$(MA)(Tz)]) with 5'-GMP were monitored by ^{195}Pt NMR and the chemical shifts were assigned in accordance with published data.[47, 48] A solution of complex **5** (3.9 mM) and 5'-GMP (7.8 mM) in D$_2$O was irradiated at 450 nm in an NMR tube and the ^{195}Pt NMR spectrum was recorded at various time intervals (**Figure 4.18 A – C**). Before irradiation, there was only one ^{195}Pt NMR peak (at δ = 892 ppm) corresponding to complex **5**. During the first 30 min of irradiation, this peak decreased in intensity and a new signal (δ = −2328 ppm) in Pt^{II} region appeared, which was assigned as **5b**, (*SP*-4-2)-[Pt(N$_3$)(MA)(Py)(5'-GMP) − H]. The assignment of the new signal was confirmed by the ^{195}Pt NMR chemical shift of a synthesized authentic sample. The signal of complex **5** completely disappeared after irradiation of the sample for 1 hour,

while the signal of **5b** was still present. The NMR spectrum did not change much over the following two hours' irradiation (data not shown). This photoproduct was quite stable and was not re-oxidized to Pt^{IV} species after one week of storing in dark at room temperature.

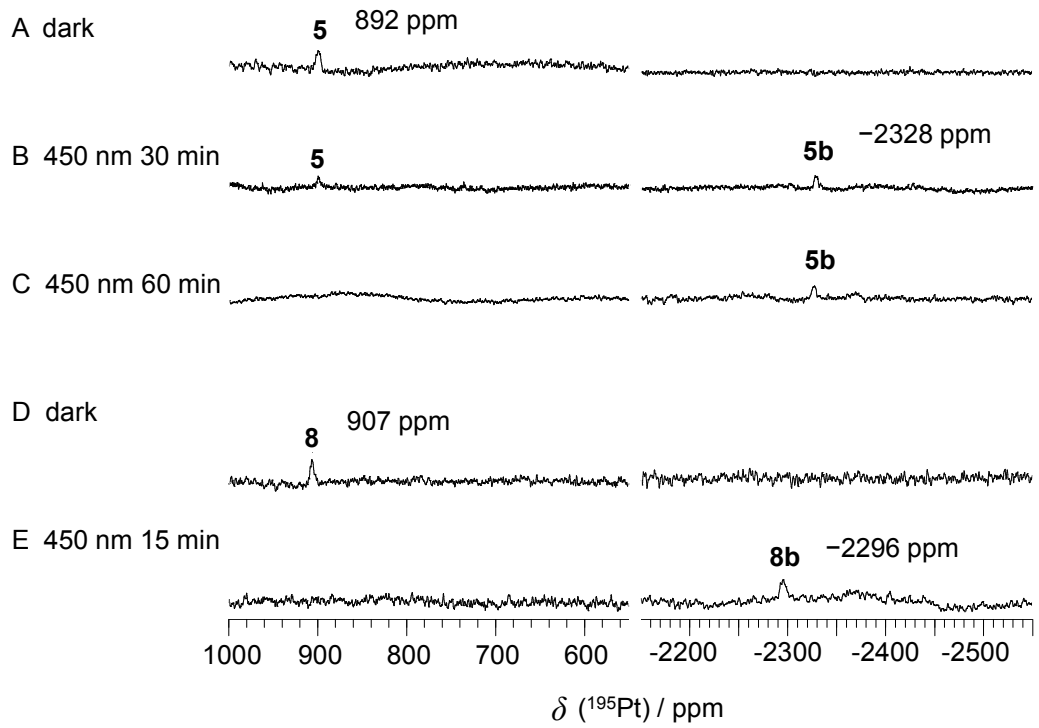

Figure 4.18 ^{195}Pt NMR (129.4 MHz, 298 K) spectra of complex **5** or **8** (3.9 mM) with 5'-GMP (7.8 mM) in D_2O after irradiation at 450 nm (298 K). Complex **5** with 5'-GMP irradiated (**A**) 0 min, (**B**) 30 min and (**C**) 1 h. Complex **8** with 5'-GMP irradiated for (**D**) 0 min and (**E**) 15 min.

Similar ^{195}Pt NMR experiments were performed for complex **8** as well to follow its photoreaction with 5'-GMP (**Figure 4.18 D** and **E**). The peak for complex **8** (δ = 907 ppm) completely disappeared during only 15 min of irradiation at 450 nm. The new signal (δ = −2296 ppm) was assigned as **8b** (*SP*-4-3)-[Pt(N_3)(MA)(Tz)(5'-GMP) − H] and was confirmed by the ^{195}Pt NMR spectrum of a synthesized authentic sample.

4.3.4 Nitrene intermediates and guanine oxidation

4.3.4.1 Discovery of the side products generated by UVA irradiation

As shown in **Section 4.3.3.3**, in the photoreaction of complex **5** (*trans,trans,trans*-$[Pt(N_3)_2(OH)_2(MA)(Py)]$, 0.5 mM) with 5'-GMP (1.0 mM), *trans*-$[Pt(N_3)(MA)(Py)(5'\text{-GMP}) - H]$ (**5b**) was the major product upon irradiation at 450 nm for 1 hour, but *trans*-$[Pt(MA)(Py)(5'\text{-GMP})_2 - 2H]$ (**5a**) was the major product upon irradiation with UVA for 1 hour. The reaction conditions and the HPLC conditions were both optimized to examine the other side photo-products generated by UVA irradiation. When the ratio of complex **5** : 5'-GMP was changed to 2 : 3 and irradiation with UVA (3.5 mW/cm^2) was shortened to 15 minutes, some new species were found by HPLC (**Figure 4.19C**, where a new C18 reverse-phase column was used in the HPLC analysis). Apart from unreacted 5'-GMP, bis-adduct *trans*-$[Pt(MA)(Py)(5'\text{-GMP})_2 - 2H]$ (**5a**) and mono-adduct (*SP*-4-2)-$[Pt(N_3)(MA)(Py)(5'\text{-GMP}) - H]$ (**5b**), compound **5c** (*m/z*=718.1), **5d** (*m/z*=684.1), **5e** (*m/z*=700.1) and **5f** (*m/z*=685.1) were identified as new Pt-containing species by their isotope distributions in LC-coupled mass spectrometry (detailed characterization will be carried out later in this chapter). When the mixture of 0.67 mM complex **5** and 1.0 mM 5'-GMP was irradiated at 420 nm for 30 min or 450 nm for 60 minutes, some of the side products were also observed (**Figure 4.19A**, **B** and **C**) This clearly shows that with photons of higher energy, more new species are generated. A control experiment of 1.0 mM 5'-GMP in the absence of complex **5** was irradiated with UVA for 15 min and the product was analysed with HPLC as shown in **Figure 4.19D**. There was no reaction and only 5'-GMP was found. This result suggested that 5'-GMP in aqueous solution is very stable upon irradiation with UVA. The photoreaction of complex **5** with 5'-GMP was repeated under the protection of argon,

and identical result was found by HPLC. Therefore, the generation of compounds **5c**, **5d**, **5e** and **5f** are all caused by the Pt complex **5**.

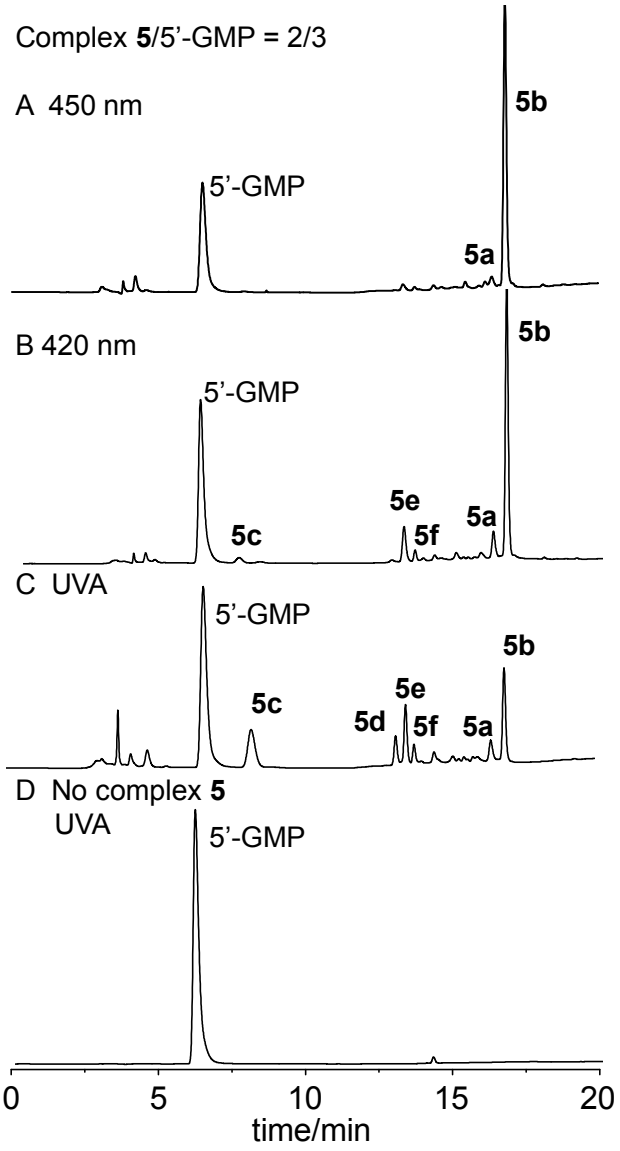

Figure 4.19 High performance liquid chromatograms (HPLC) of photoreactions of complex **5** (0.67 mM) with 5'-GMP (1.0 mM) in aqueous solution upon irradiation with (**A**) 450 nm light, 50 mW/cm^2, 60 min; (**B**) 420 nm, 4.3 mW/cm^2, 30 min; (**C**) UVA, 3.5 mW/cm^2, 15 min; (**D**) 5'-GMP (1.0 mM) in aqueous solution irradiated with UVA for 15 min.

4.3.4.2 Analysis of the side products by HR-MS and MS/MS

In order to examine the structures of species **5c**, **5d** and **5e**, electrospray ionization high resolution mass spectra (ESI-HR-MS) and tandem mass (MS/MS) spectra for these species, as well as for **5b**, were obtained (**Figure 4.20**). Those species were assigned as listed in **Table 4.3**. Their MS/MS spectra are in **Figure 4.21** and fragmentations and assignments are listed in **Table 4.4** – **Table 4.7**.

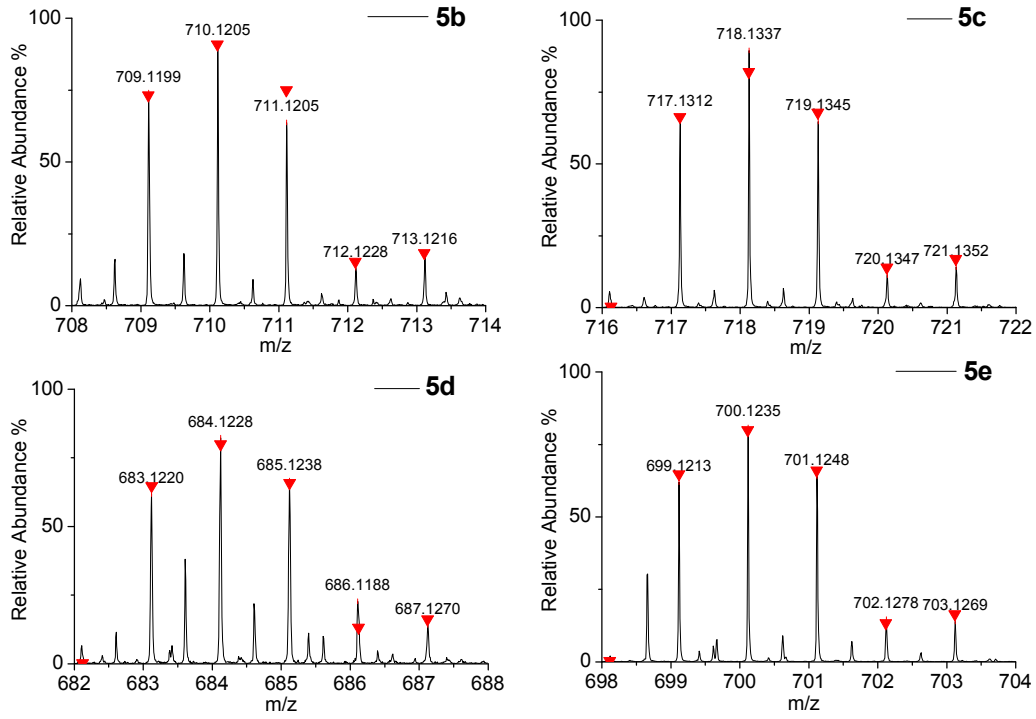

Figure 4.20 High resolution mass spectrometry (HRMS) for compounds **5b**, **5c**, **5d** and **5e**. The major calc. isotope distributions of each species (reversed red triangles) are consistent with the peaks found in HRMS spectra (labelled with numbers).

Table 4.3 HRMS and assignments of compounds **5b**, **5c**, **5d** and **5e**.

Masses found *m/z*	Assigned chemical structures	Assigned chemical formula	Model *m/z*	Error ppm
710.1205	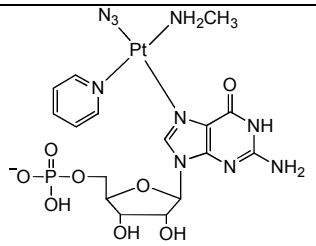 [$Pt(N_3)$(MA)(Py)(5'-GMP) − H] (**5b**)	$C_{16}H_{24}N_{10}O_8PPt$ for $[M + H]^+$	710.1164	5.8
718.1337	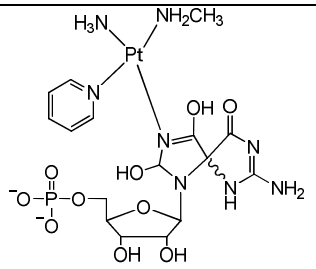 [$Pt(NH_3)$(MA)(Py)(5'-(RedSp)MP) − 2H] (**5c**)	$C_{16}H_{28}N_8O_{10}PPt$ for $[M + H]^+$	718.1314	3.2
684.1228	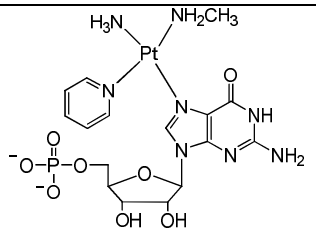 [$Pt(NH_3)$(MA)(Py)(5'-GMP) − 2H] (**5d**)	$C_{16}H_{26}N_8O_8PPt$ for $[M + H]^+$	684.1260	4.7
700.1235	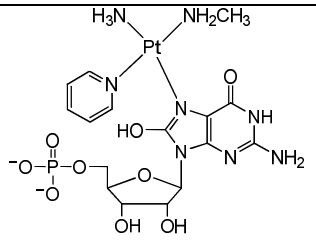 [$Pt(NH_3)$(MA)(Py)(5'-(8-oxo-G)MP) − 2H] (**5e**)	$C_{16}H_{26}N_8O_9PPt$ for $[M + H]^+$	700.1209	3.7

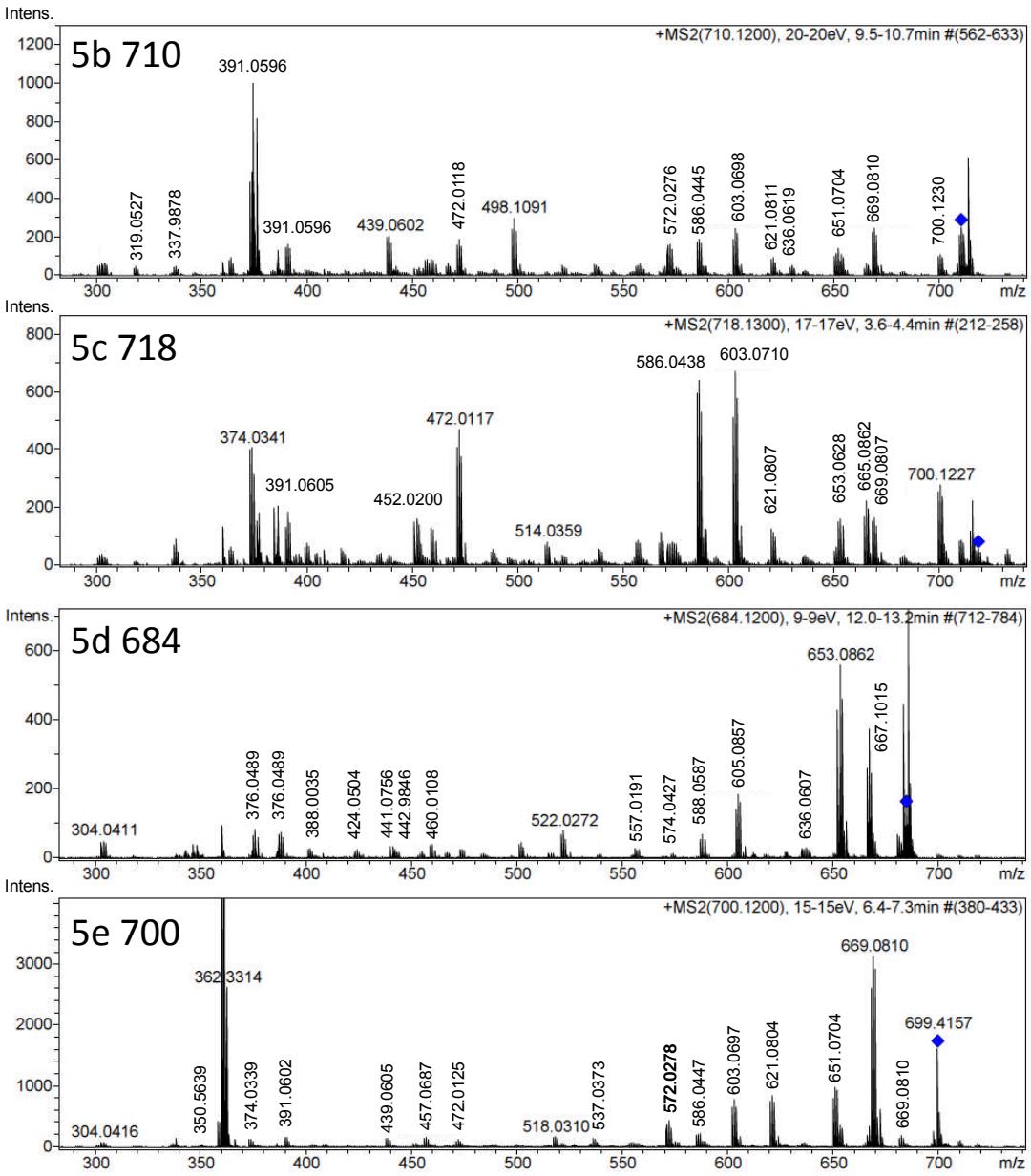

Figure 4.21 MS/MS spectra (CID) of the species with *m/z* 710.12 (**5b**), 718.13 (**5c**), 684.12 (**5d**) and 700.12 (**5e**).

The species with *m/z* 684.1228 is assigned as [Pt(NH_3)(MA)(Py)(5'-GMP) − 2H] (**5d**) with an error between found and calculated *m/z* for $[M + H]^+$ of 4.7 ppm. The fragments in the MS/MS analysis assignable as $[M - NH_3 + H]^+$ (667.1015), $[M - MA + H]^+$ (653.0862), $[M - Py + H]^+$ (605.0857) and $[Pt(GMP) + H]^+$ (557.0191) were found, which confirmed the assignment of [Pt(NH_3)(MA)(Py)(5'-GMP) − 2H] (**5d**). The other fragments were all reasonably assigned as Pt with certain

combinations of NH_3, MA, Py, GMP, phosphate and sugar moiety. It was surprising to find an NH_3 ligand in this molecule, as it does not belong to any of the reactants. A reasonable source of the NH_3 ligand is N_3^-, which can lose N_2 upon irradiation of Pt^{IV}-N_3 with light to form a {Pt-N^-} (nitrene) intermediate. The nitrene intermediate is electron-deficient so it tends to gain two electrons from reductants. For example, N^- can insert into a C-H or O-H bonds,[49, 50] capture an H^- and react with one or two H^+, forming R-NH_2 or NH_3.[28] The 5'-GMP was not oxidized in this molecule, probably because it coordinated after NH_3 was formed. However, an oxidized form of guanine in 5'-GMP was observed in this work (*vide infra*).

Table 4.4 MS/MS analysis for [Pt(NH_3)(MA)(Py)(5'-GMP) − 2H] (**5d**) $[M + H]^+$ *m/z* = 684.12 and assignment of fragments.

Found *m/z*	Assigned structure	Formula	Calc. *m/z*	Error ppm
667.1015	$[M - NH_3 + H]^+$	$C_{16}H_{23}N_7O_8PPt$	667.0994	3.1
653.0862	$[M - MA + H]^+$	$C_{15}H_{21}N_7O_8PPt$	653.0838	3.7
636.0607	$[M - MA - NH_3 + H]^+$	$C_{15}H_{18}N_6O_8PPt$	636.0572	5.5
605.0857	$[M - Py + H]^+$	$C_{11}H_{21}N_7O_8PPt$	605.0837	3.3
588.0587	$[M - Py - NH_3 + H]^+$	$C_{11}H_{18}N_6O_8PPt$	588.0572	2.6
574.0427	$[M - Py - MA + H]^+$	$C_{10}H_{16}N_6O_8PPt$	574.0415	2.1
557.0191	$[M - Py - MA - NH_3 + H]^+$ ($[Pt(GMP) - H]^+$)	$C_{10}H_{13}N_5O_8PPt$	557.0150	7.4
522.0272	$[Pt(Py)(G) + H_2PO_4]^+$	$C_{10}H_{12}N_6O_5PPt$	522.0255	3.3
460.0108	$[Pt(NH_3)(G) + H_2PO_4]^+$	$C_5H_{10}N_6O_5PPt$	460.0098	2.2
442.9846	$[Pt(G) + H_2PO_4]^+$	$C_5H_7N_5O_5PPt$	442.9833	2.9
441.0756	$[Pt(NH_3)(Py)(G) - H]^+$	$C_{10}H_{12}N_7OPt$	441.0751	1.1
424.0504	$[Pt(Py)(G) - H]^+$	$C_{10}H_9N_6OPt$	424.0486	4.2
388.0035	$[Pt(NH_3)(Py) + H_2PO_4]^+$	$C_5H_{10}N_2O_4PPt$	388.0026	2.3
376.0489	$[Pt(MA)(G) - H]^+$	$C_6H_9N_6OPt$	376.0485	1.1
304.0411	$[Pt(MA)(Py) - H]^+$	$C_6H_9N_2Pt$	304.0414	1.0

The species with *m/z* 700.1235 is assignable as [Pt(NH_3)(MA)(Py)(5'-(8-oxo-G)MP) − 2H] (**5e**) with an error between found and calculated *m/z* for $[M + H]^+$ of only 3.7 ppm, where 5'-(8-oxo-G)MP is 8-oxoguanosine 5'-phosphate. It has an 8-oxo-G (8-oxo-guanine or 8-hydroxyguanine) moiety in the molecule, which is one of the most common DNA lesions resulting from reactive oxidants.[13, 14, 51] The oxidation of guanine possibly occurred by the nitrene intermediate. Reactions of nitrene intermediates in inorganic compounds are rarely reported, however, it is still possible to find clues from such reactions in organic chemistry.[49, 52] A possible mechanism is proposed in **Scheme 4.2**, Mechanism 1. The {Pt-N_3^-} loses N_2 upon irradiation with UVA to form the {Pt-N^-} intermediate. Two electrons are transferred from the guanine moiety to the nitrene and guanine is oxidized to form 8-oxo-guanine, with the addition of an H_2O molecule. The nitrene is reduced and finally forms {Pt-NH_3}. Another possible oxidant is singlet oxygen. As demonstrated in **Section 4.3.2** in this Chapter, the photolysis of complex **5** could release $^1O_2$, which can then oxidize guanine to 8-oxo-G via a direct [4+2] cycloaddition of $^1O_2$ (**Scheme 4.2**, Mechanism 2).[14]

The MS/MS analysis for **5e** was performed. A number of fragments corresponding to the loss of H_2O were found, e.g., *m/z* 682.1123, which is assignable to the formation of Pt coordinated cyclic phosphodiester (8-hydroxyguanosine 5',8 cyclic phosphodiester) or cGMP (**Figure 4.22**).[53, 54] The fragments with *m/z* 537.0373 and 472.0125, assignable as 8-hydroxyguanosine phosphodiester, support the formation of the cyclic phosphodiester. Other assignable fragments such as $[M - MA + H]^+$ (*m/z* 669.0810), $[M - Py + H]^+$ (*m/z* 621.0804) and $[M - Py - H_2O - NH_3 + H]^+$ (*m/z* 586.0447) confirm the structure assignment of [Pt(NH_3)(MA)(Py)(5'-(8-oxo-G)MP) − 2H] (**5e**). It is interesting to note that during the MS/MS, the OH group of the 8-

OH-G can lose together with a proton to form a dehydrogenated guanine (*m/z* 374.0339).

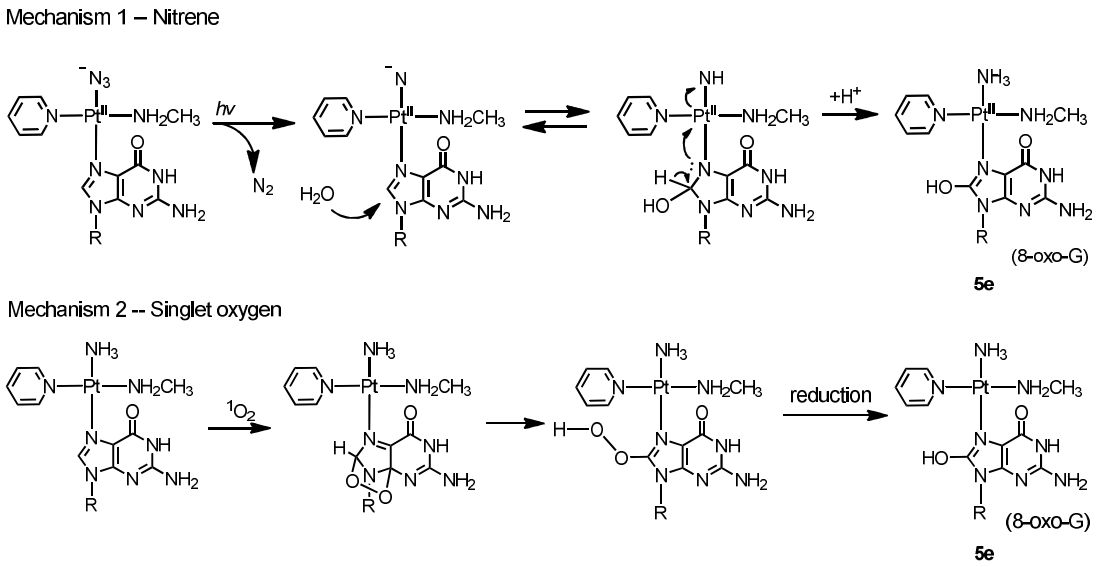

Scheme 4.2 Two possible mechanisms for the oxidation of 5'-GMP.

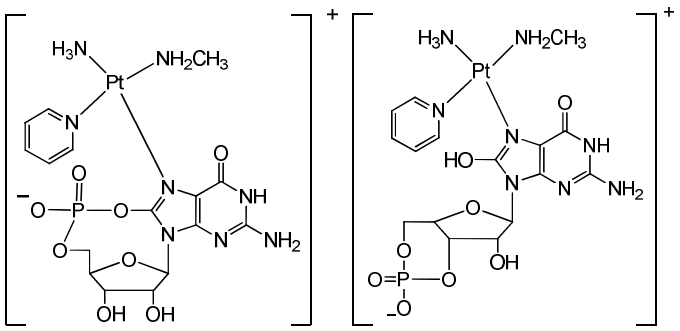

Figure 4.22 Possible Pt coordinated cyclic phosphodiester (8-hydroxyguanosine 5',8 cyclic phosphodiester) and cGMP[53, 54] intermediates for m/z = 682.1123.[53, 54]

Table 4.5 MS/MS analysis for [Pt(NH_3)(MA)(Py)(5'-(8-oxo-G)MP) − 2H] (**5e**) $[M + H]^+$ *m/z* = 700.12 and assignment of fragments.

Found *m/z*	Assigned structure	Formula	Calc. *m/z*	Error ppm
682.1123	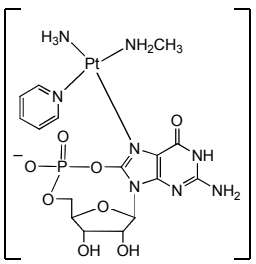 $[M - H_2O + H]^+$	$C_{16}H_{24}N_8O_8PPt$	682.1103	2.9
669.0810	$[M - MA + H]^+$	$C_{15}H_{21}N_7O_9PPt$	669.0787	3.4
651.0704	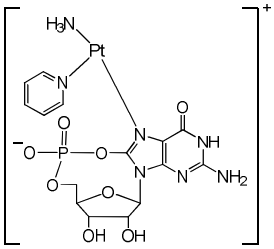 $[M - MA - H_2O + H]^+$	$C_{15}H_{19}N_7O_8PPt$	651.0681	3.5
621.0804	$[M - Py + H]^+$	$C_{11}H_{21}N_7O_9PPt$	621.0786	2.9
603.0697	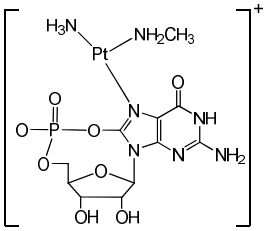 $[M - Py - H_2O + H]^+$	$C_{11}H_{19}N_7O_8PPt$	603.0681	2.7
586.0447	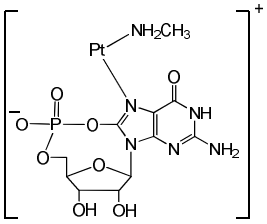 $[M - Py - H_2O - NH_3 + H]^+$	$C_{11}H_{16}N_6O_8PPt$	586.0415	5.5

572.0278	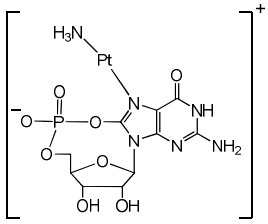 [M − MA − Py − H_2O + H]$^+$	$C_{10}H_{14}N_6O_8PPt$	572.0259	3.3
537.0373	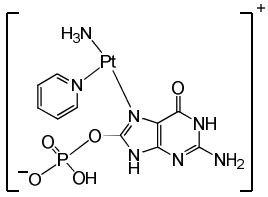	$C_{10}H_{13}N_7O_5PPt$	537.0364	1.7
518.0310	Unspecified			
472.0125	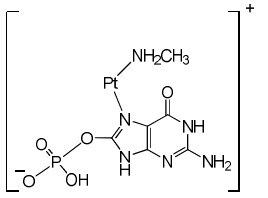	$C_6H_{10}N_6O_5PPt$	472.0098	5.7
457.0687	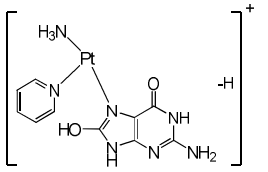	$C_{10}H_{12}N_7O_2Pt$	457.0700	2.8
439.0605	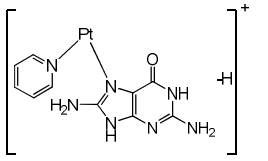	$C_{10}H_{10}N_7OPt$	439.0595	2.3
391.0602	Unspecified			
374.0339	Unspecified			
360.3218	Contamination. Also appeared in blank.			
350.5639	[M + 2H]$^{2+}$	$C_{16}H_{27}N_8O_9PPt$	350.5638	0.3
304.0416	[Pt(MA)(Py) − H]$^+$	$C_6H_9N_2Pt$	304.0408	2.6

The species with *m/z* 710.1205 is assignable as [Pt(N_3)(MA)(Py)(5'-GMP) − H] (**5b**) with the error between found and calculated *m/z* for [M + H]$^+$ of 5.8 ppm. The observed peaks with *m/z* 700.1230, 669.0810 and 621.0811 are assigned as

$[Pt(NH_3)(MA)(Py)(5'\text{-}(8\text{-oxo-G})MP - H)]^+$, $[Pt(NH_3)(Py)(5'\text{-}(8\text{-oxo-G})MP - H)]^+$ and $[Pt(NH_3)(MA)(5'\text{-}(8\text{-oxo-G})MP - H)]^+$, respectively. The loss of N_2 from M-N_3 forming Pt-N in MS/MS has been reported previously and the reaction is described in **Equation 1** and **2**. [27, 55]

$$[Pt(L)N_3]^+ \rightarrow [Pt(L)N]^+ + N_2 \quad (\mathbf{1})$$

$$[Pt(L)N]^+ + H_2O \rightarrow [Pt(L - 2H + OH)NH_3]^+ \quad (\mathbf{2})$$

The peaks with *m/z* 651.0704, 572.0276, 439.0602, 391.0596, 337.9878 and 319.0527 are assignable as $[Pt(N)(MA)(GMP)]^+$, $[Pt(N)(GMP)]^+$, $[Pt(N)(Py)(G)]^+$, $[Pt(N)(MA)(G)]^+$, $[Pt(N)(MA) + H_3PO_4]^+$ and $[Pt(N)(MA)(Py)]^+$, respectively, corresponding to the $[Pt(L)N]^+$ species in **Equation 1**. Other assignable fragments such as $[Pt(Py)(GMP) - H]^+$ (636.0619) and $[Pt(N_3)(Py)(MA)(G)]^+$ (498.1091) again confirm the structure assignment of **5b**. The oxidation of guanine may have happened during the MS/MS process, as the peaks with *m/z* 586.0447 and 472.0118 were found and assigned as Pt coordinated cyclic phosphodiester. Also, the loss of H_2O of the 8-OH-G was also found, resulting in a dehydrogenated guanine (*m/z* 374.0336).

Table 4.6 MS/MS analysis for [Pt(N_3)(MA)(Py)(5'-GMP) − H] (**5b**) $[M + H]^+$ *m/z* = 710.12 and assignment of fragments.

Found *m/z*	Assigned structure	Formula	Calc. *m/z*	Error ppm
700.1230	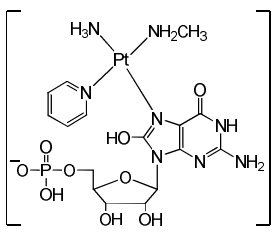	$C_{16}H_{26}N_8O_9PPt$	700.1203	3.9
669.0810	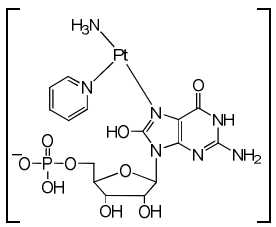	$C_{15}H_{21}N_7O_9PPt$	669.0781	4.3
651.0704	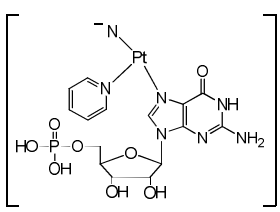 $[Pt(N)(Py)(GMP)]^+$	$C_{15}H_{19}N_7O_8PPt$	651.0676	4.3
636.0619	$[Pt(Py)(GMP) - H]^+$	$C_{15}H_{18}N_6O_8PPt$	636.0571	7.5
621.0811	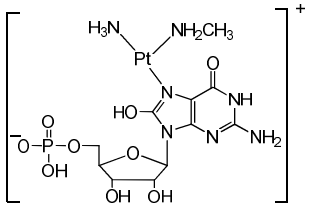	$C_{11}H_{21}N_7O_9PPt$	621.0781	4.8
603.0698	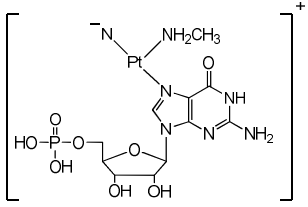 $[Pt(N)(MA)(GMP)]^+$	$C_{11}H_{19}N_7O_8PPt$	603.0675	3.8
586.0445	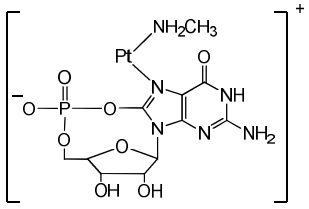	$C_{11}H_{16}N_6O_8PPt$	586.0410	6.0

572.0276	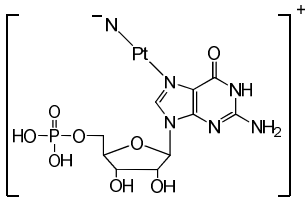 $[Pt(N)(GMP)]^+$	$C_{10}H_{14}N_6O_8PPt$	572.0253	4.0
498.1091	$[Pt(N_3)(Py)(MA)(G)]^+$	$C_{11}H_{15}N_{10}OPt$	498.1072	3.8
472.0118	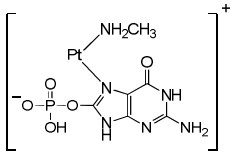	$C_6H_{10}N_6O_5PPt$	472.0092	5.5
439.0602	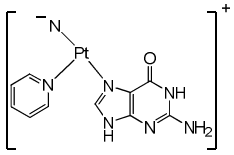 $[Pt(N)(Py)(G)]^+$	$C_{10}H_{10}N_7OPt$	439.0589	3.0
391.0596	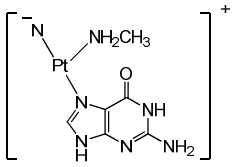 $[Pt(N)(MA)(G)]^+$	$C_6H_{10}N_7OPt$	391.0589	1.8
374.0336	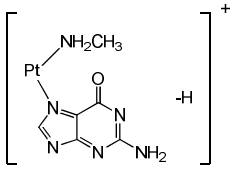 $[Pt(MA)(G) - H]^+$	$C_6H_7N_6OPt$	374.0323	3.5
337.9878	$[Pt(N)(MA) + H_3PO_4]^+$	$CH_8N_2O_4PPt$	337.9864	4.1
319.0527	$[Pt(N)(MA)(Py)]^+$	$C_6H_{10}N_3Pt$	319.0517	3.1

The species with *m/z* 718.1337 is assignable as $[Pt(NH_3)(MA)(Py)(5'\text{-}(RedSp)MP) - 2H]$ (**5c**) (RedSp = N-formylamidoiminohydantoin) with an error between found and calculated *m/z* for $[M + H]^+$ of 3.2 ppm. Compound **5c** is assigned as compound **5e** with hydrolysed 8-oxo-G — RedSp (N-formylamidoiminohydantoin). The hydrolysis reaction of 8-oxo-G has been reported[14] and is shown in **Scheme 4.3**. Compound **5c** is much more hydrophilic than **5d**, **5e**, and **5b**, so the retention time in

HPLC for **5c** is much shorter. In MS/MS analysis, compound **5c** could lose one or two water molecules, which could lead to the formation of either an 8-cyclic phosphodiester or a 8-oxo-G (**Scheme 4.4**), but it is not possible to determine which water is lost first. For instance, peaks with *m/z* 700.1227, 683.1052, 669.0807, 665.0862, 621.0807, 603.0710 and 586.0438 can be assigned as $[M - H_2O + H]^+$, $[M - H_2O - NH_3 + H]^+$, $[M - H_2O - MA + H]^+$, $[M - 2H_2O - NH_3 + H]^+$, $[M - Py - H_2O + H]^+$, $[M - Py - 2H_2O + H]^+$ and $[M - Py - 2H_2O - NH_3 + H]^+$, respectively. These fragments also confirm the presence of MA, MH_3 and Py groups in the molecule. The loss of H_2O from 8-OH-G (*m/z* 374.0341) was again found here.

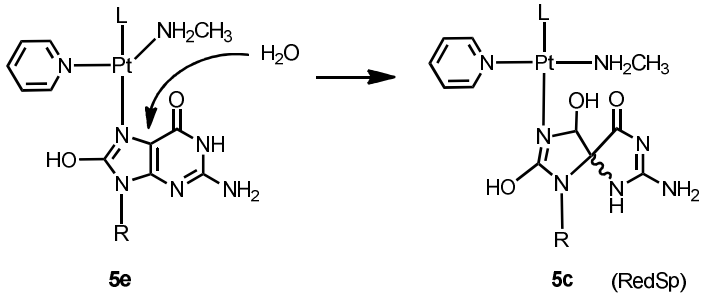

Scheme 4.3 Reaction mechanism for RedSp (N-formylamidoiminohydantoin).

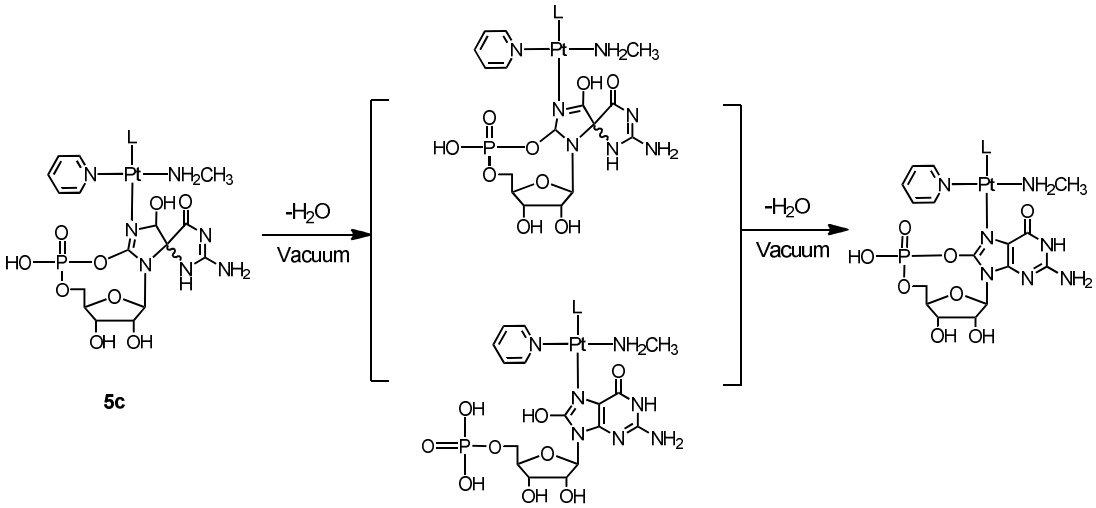

Scheme 4.4 Two steps of dehydrolization of complex **5c** in MS/MS, forming an 8-cyclic phosphodiester or and an 8-oxo-G.

Table 4.7 MS/MS analysis for $[Pt(NH_3)(MA)(Py)(5'\text{-}(RedSp)MP) - 2H]$ (**5c**) $[M + H]^+$ *m/z* = 718.13 and assignment of fragments.

Found *m/z*	Assigned structure	Formula	Calc. *m/z*	Error ppm
700.1227	$[M - H_2O + H]^+$	$C_{16}H_{26}N_8O_9PPt$	700.1203	3.4
669.0807	$[M - H_2O - MA + H]^+$	$C_{15}H_{21}N_7O_9PPt$	669.0781	3.9
665.0862	$[M - 2H_2O - NH_3 + H]^+$	$C_{16}H_{21}N_7O_8PPt$	665.0832	4.5
653.0628	Unspecified			
621.0807	$[M - Py - H_2O + H]^+$	$C_{11}H_{21}N_7O_9PPt$	621.0781	4.2
603.0710	$[M - Py - 2H_2O + H]^+$	$C_{11}H_{19}N_7O_8PPt$	603.0675	5.8
586.0438	$[M - Py - 2H_2O - NH_3 + H]^+$	$C_{11}H_{16}N_6O_8PPt$	586.0410	4.8
472.0117	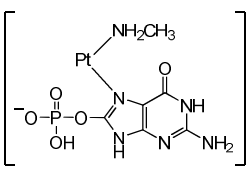	$C_6H_{10}N_6O_5PPt$	472.0092	5.3
452.0200	Unspecified			
391.0605	Unspecified			
374.0341	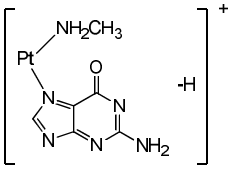	$C_6H_7N_6OPt$	374.0323	4.8

4.3.4.3 Direct evidence for the conversion from Pt-N_3 to Pt-NH_3

More than 40 years ago, the conversion of $[Ir(NH_3)_5(N_3)]^{2+}$ to the chloramine complex $[Ir(NH_3)_5(NH_2Cl)]^+$ was reported, and was believed to involve the nitrene intermediate $[Ir(NH_3)_5(N)]^{2+}$.[56] Also, the formation of NH_3 in the photodecomposition of free N_3^- via a nitrene intermediate has been reported.[28, 29] In recent years, electrospray ionization MS studies of $[Pt(L)N_3]^+$ type of coordination compounds in the gas-phase has revealed the existence of the following species $[Pt(L)N]^+$, $[Pt(L - 2H)NH_2]^+$ and $[Pt(L - 3H)]^+ + NH_3$ formed under collision-induced dissociation (CID).[27, 55] However, stable species of the type $[Pt(L)_n(NH_3)]$

generated from the corresponding azido species has not been reported yet. In order to confirm that the NH_3 group was formed from the N_3^- group, ^{15}N end-labelled NaN_3 was used to synthesize *trans,trans,trans*-[Pt($^{15}N_3$)$_2$(OH)$_2$(MA)(Py)] (**5***), where $^{15}N_3$ = [^{15}N=^{14}N=^{14}N]$^-$. Then the photoreaction of complex **5*** with 5'-GMP upon irradiation with UVA was carried out under identical conditions as those in **Section 4.3.4.1**. LC-MS analysis was performed afterwards and an identical chromatogram was recorded. The MS spectra for species **5b***, **5c*** **5d*** and **5e*** corresponding to identical retention time as **5b**, **5c**, **5d** and **5e** were recorded in **Figure 4.23**. If the molecule contains the intact end-labelled $^{15}N_3$ ligand, the *m/z* of each peak of the isotope distributions should be 1 Da larger than that of the unlabelled molecule. If the molecule contains an NH_3 group converted from the end-labelled $^{15}N_3$ ligand, the N atom should be a 50%/50% mixture of ^{15}N and ^{14}N. Therefore, the resultant isotope distributions should be a 50%/50% mixture of M and M + 1. As it was expected, compound **5b*** was 1 Da larger than **5b**, which confirms that it has an N_3 ligand. The isotope distributions of the other three species **5c***, **5d*** and **5e*** are all 50%/50% mixture of M and M + 1, so they are all considered as {Pt-NH_3} moieties derived from {Pt-N_3} moieties. Therefore, the species in **Figure 4.23** are assigned as [Pt($^{15}N_3$)(MA)(Py)(5'-GMP) − H] (**5b***), [Pt(NH_3^*)(MA)(Py)(5'-(RedSp)MP) − 2H] (**5c***), [Pt(NH_3^*)(MA)(Py)(GMP) − 2H] (**5d***) and [Pt(NH_3^*)(MA)(Py)(5'-(8-oxo-G)MP) − 2H] (**5e***) (NH_3^*= 50% $^{15}NH_3$/50% $^{14}NH_3$).

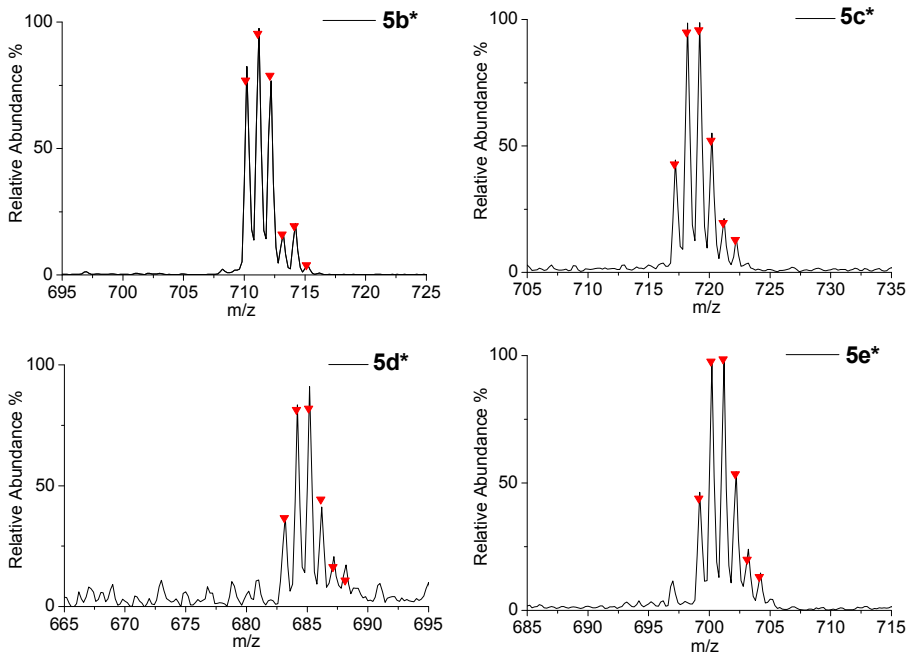

Figure 4.23 MS spectra for compounds **5b***, **5c*** **5d*** and **5e*** obtained from LC-MS. The major calc. isotope distributions of each species are labelled with reversed red triangles.

4.3.5 Photo-induced binding with DNA oligonucleotide

A preliminary DNA binding experiment was carried out since the DNA is regarded as the major target for platinum based anticancer drugs. A self-complementary single strand DNA d(TATGGTACCATA) (**I**) was selected for study since it contains a GG sequence which is usually the preferred binding site for platinum drugs.[57]

The photoreaction of complex **5** (*trans,trans,trans*-$[Pt(N_3)_2(OH)_2(MA)(Py)]$, 100 μM) with the ss-DNA **I** in a 1:1 mol ratio was irradiated for 1 hour with 450 nm light at 298 K, and the products were characterized by ESI-HR-MS. The major species in the reaction mixture was found to be unreacted ss-DNA **I** (**Figure 4.24**), and their *m/z* were used as internal calibration in linear mode. A series of platinated products were also found, assignable as a mono-functional platinum-DNA adduct with one N_3

group remaining on Pt, [**I** + $Pt(N_3)(MA)(Py)$ − H]. The MS peaks detected are listed and assigned in **Table 4.8.** Interestingly, a series of weak signals corresponding the loss of the second N_3 group was also found, assignable as [**I** + Pt(MA)(Py) − 2H]. This species is probably a bifunctional DNA intrastrand crosslink.

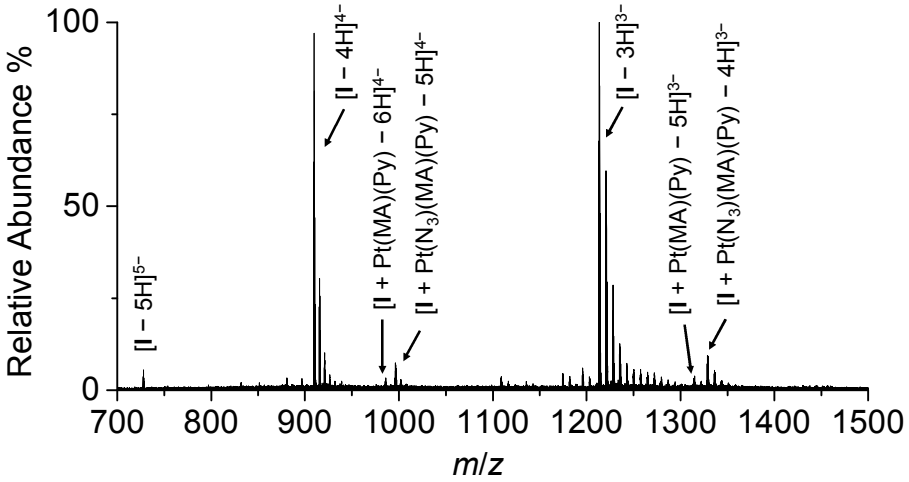

Figure 4.24 ESI-HR-MS (negative mode) spectrum for the photoreaction of complex **5** (100 μM) with ss-DNA **I** (1:1, in H_2O, 450 nm, 1 hour, 298 K). Assignments are labelled on the spectrum and the species may also be found as nNa^+ adducts in the spectrum.

Table 4.8 Negative ions *m/z* detected by ESI-HR-MS for the photoreaction of complex **5** (100 μM) with ss-DNA **I** (100 μM) (in H_2O, 450 nm, 1 hour, 298 K)

Species assignment	Found *m/z*	Calculated *m/z*	Error/ppm
$[\mathbf{I} - 5H]^{5-}$	727.7234	727.7235	- [a]
$[\mathbf{I} - 4H]^{4-}$	909.9067	909.9065	-
$[\mathbf{I} - 3H]^{3-}$	1213.5446	1213.5447	-
$[\mathbf{I} + Pt^{II}(N_3)(MA)(Py) - 5H]^{4-}$	996.4165	996.4190	2.5
$[\mathbf{I} + Pt^{II}(N_3)(MA)(Py) - 4H]^{3-}$	1328.8916	1328.8948	2.4
$[\mathbf{I} + Pt^{II}(MA)(Py) - 6H]^{4-}$	985.6627	985.6647	2.0
$[\mathbf{I} + Pt^{II}(MA)(Py) - 5H]^{3-}$	1314.5458	1314.5558	7.6

[a] The *m/z* of **I** are used for internal calibration with linear mode.

When the molar ratio of complex **5** : ss-DNA **I** was changed to 2:1, the signal for [**I** + $Pt(N_3)(MA)(Py)$ − H] increased, and another product was identified: [**I** + $2Pt(N_3)(MA)(Py)$ − 2H] (**Figure 4.25** and **Table 4.9**). The signals assignable to bifunctional DNA intrastrand crosslink [**I** + Pt(MA)(Py) − 2H] and [**I** + 2Pt (MA)(Py) + N_3 − 3H] were again found. The sample was stored in dark at room temperature for 3 months after irradiation and was analysed by ESI-HR-MS spectrometry again (**Figure 4.26**). The mono-functional adduct [**I** + $Pt(N_3)(MA)(Py)$ − H] was still found. It is notable that the intensity of the signals corresponding to possible bifunctional DNA intrastrand crosslinks [**I** + Pt(MA)(Py) − 2H] increased, even higher than for the mono-functional DNA adduct. This suggests that the DNA binding with platinum is very stable, and the mono-functional adducts was possibly converted to bifunctional adducts slowly in aqueous solution. The isotopic distributions of the observed DNA adducts [**I** + $Pt(N_3)(MA)(Py)$ − H] and [**I** + Pt(MA)(Py) − 2H] are shown in **Figure 4.27**, and are consistent with their simulation.

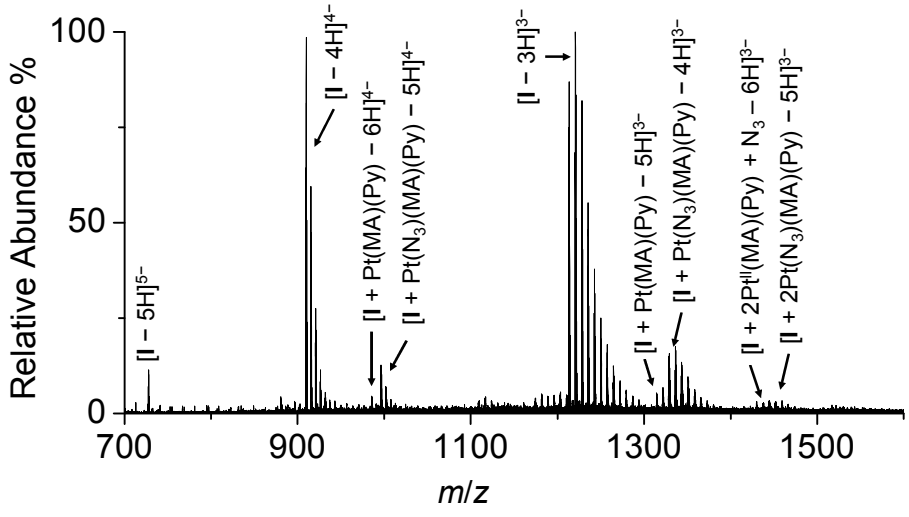

Figure 4.25 ESI-HR-MS (negative mode) spectrum for the photoreaction of complex **5** (200 μM) with ss-DNA **I** (100 μM) (in H_2O, 450 nm, 1 hour, 298 K). Assignments are labelled on the spectrum and the species may also be found as nNa^+ adducts in the spectrum.

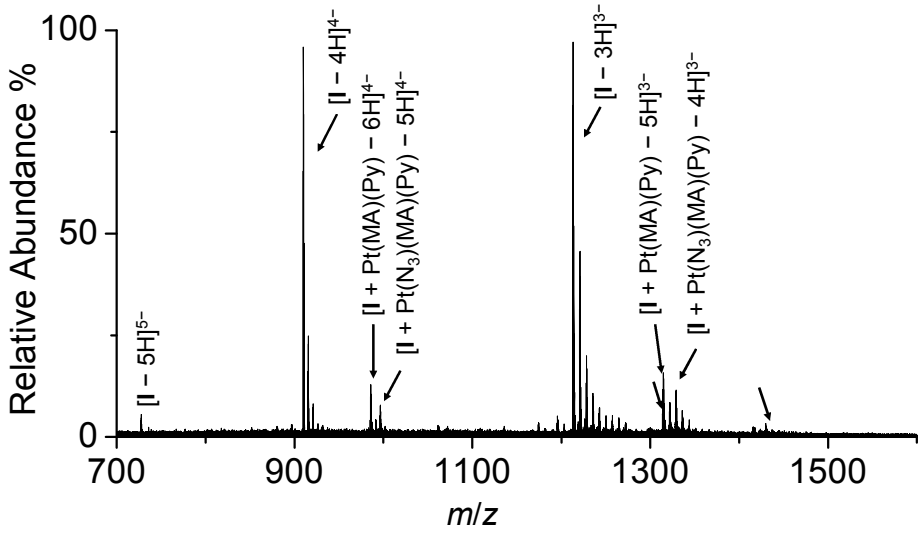

Figure 4.26 ESI-HR-MS (negative mode) spectrum for the photoreaction of complex **5** (200 μM) with ss-DNA **I** (100 μM) 100 days after irradiation (in H_2O, 450 nm, 1 hour, 298 K). Assignments are labelled on the spectrum and the species may also be found as nNa^+ adducts in the spectrum.

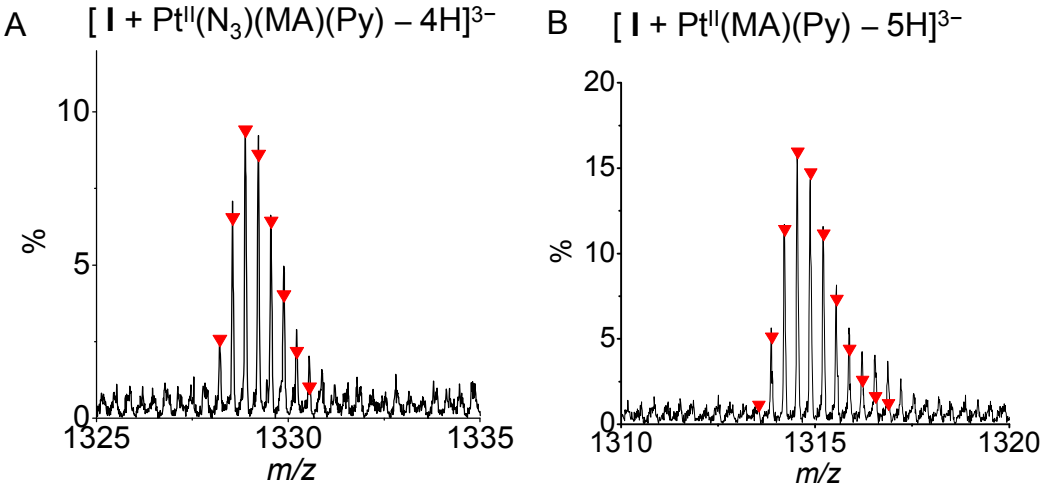

Figure 4.27 Mass spectrum isotope distributions for photoproducts of complex **5** with ss-DNA **I** (A): $[\mathbf{I} + Pt(N_3)(MA)(Py) - 4H]^{3-}$, *m/z* calc. 1328.8948, found, 1328.8892 and (B) $[\mathbf{I} + Pt(MA)(Py) - 5H]^{3-}$, *m/z* calc. 1314.5558; found, 1314.5474. Their corresponding simulations are labelled with red reversed triangles.

Table 4.9 Negative ions *m/z* detected by ESI-HR-MS for the photoreaction of complex **5** (200 μM) with ss-DNA **I** (100 μM) (in H_2O, 450 nm, 1 hour, 298 K)

Species assignment	Found *m/z*	Calculated *m/z*	Error/ppm
$[\mathbf{I} - 5H]^{5-}$	727.7234	727.7235	- [a]
$[\mathbf{I} - 4H]^{4-}$	909.9067	909.9065	-
$[\mathbf{I} - 3H]^{3-}$	1213.5446	1213.5447	-
$[\mathbf{I} + Pt^{II}(N_3)(MA)(Py) - 5H]^{4-}$	996.4176	996.4190	1.4
$[\mathbf{I} + Pt^{II}(N_3)(MA)(Py) - 4H]^{3-}$	1328.8892	1328.8948	4.2
$[\mathbf{I} + Pt^{II}(MA)(Py) - 6H]^{4-}$	985.6617	985.6647	3.0
$[\mathbf{I} + Pt^{II}(MA)(Py) - 5H]^{3-}$	1314.5474	1314.5558	6.4
$[\mathbf{I} + 2Pt^{II}(N_3)(MA)(Py) - 5H]^{3-}$	1444.5578	1444.5787	14.5
$[\mathbf{I} + 2Pt^{II}(MA)(Py) + N_3 - 6H]^{3-}$	1430.2275	1430.2397	8.5

[a] The *m/z* of **I** are used for internal calibration with linear mode.

A similar reaction of complex **8** (*trans,trans,trans*-$[Pt(N_3)_2(OH)_2(MA)(Tz)]$) and ss-DNA **I** (2:1) was also carried out, monitored by ESI-HR-MS (**Figure 4.28**). As expected, apart from the signal of the ss-DNA (**I**), a signal corresponding to mono-functional Pt-DNA adduct $[\mathbf{I} + Pt(N_3)(MA)(Tz) - (n + 1)H]^{n-}$ was detected. Also, another signal possibly corresponding to bifunctional DNA intrastrand crosslink $[\mathbf{I} + Pt(MA)(Tz) - (n + 2)H]^{n-}$ was found (see **Table 4.10**). The isotopic distributions correlated well with the simulations and are summarized in **Figure 4.29**.

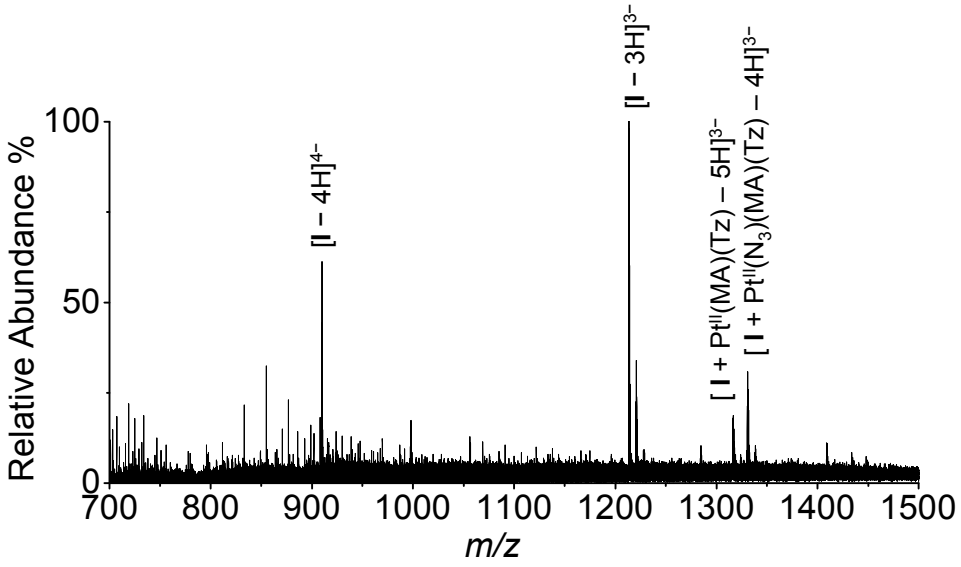

Figure 4.28 ESI-HR-MS (negative mode) spectrum of complex **8** (200 μM) with ss-DNA **I** (2:1 in H_2O, irradiated at 450 nm light for 1 hour at 298 K). Assignments are labelled on the spectrum and the species may also be found as Na^+ adducts in the spectrum.

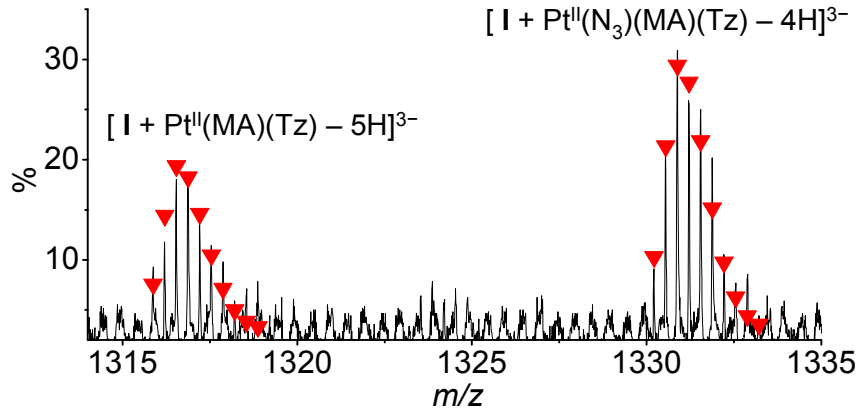

Figure 4.29 Mass spectrum isotope distribution of photo-adducts of complex **8** with ss-DNA **I**: $[\mathbf{I} + Pt(N_3)(MA)(Tz) - 4H]^{3-}$, *m/z* calc. 1330.8813, found, 1330.8879 and $[\mathbf{I} + Pt(MA)(Tz) - 5H]^{3-}$, *m/z* calc. 1316.5412; found, 1316.5373. Their corresponding simulations are labelled with red reversed triangles.

Table 4.10 Negative ions *m/z* detected by ESI-HR-MS for the photoreaction between complex **8** (200 μM) and ss-DNA **I** (100 μM) (in H_2O, irradiated at 450 nm for 1 hour at 298 K)

Species assignment	Found *m/z*	Calculated *m/z*	Error/ppm
$[\mathbf{I} - 4H]^{4-}$	909.9065	909.9065	- [a]
$[\mathbf{I} - 3H]^{3-}$	1213.5447	1213.5447	-
$[\mathbf{I} + Pt^{II}(N_3)(MA)(Tz) - 4H]^{3-}$	1330.8879	1330.8813	5.0
$[\mathbf{I} + Pt^{II}(MA)(Tz) - 5H]^{3-}$	1316.5373	1316.5412	3.0

[a] The *m/z* of **I** are used for internal calibration with linear mode.

These results suggested that complexes **5** (*trans,trans,trans*-$[Pt(N_3)_2(OH)_2(MA)(Py)]$) and **8** (*trans,trans,trans*-$[Pt(N_3)_2(OH)_2(MA)(Tz)]$) can quickly form DNA adducts upon irradiation with blue light, and that the major adducts are mono-functional and bi-functional adducts were possibly formed. (**Figure 4.30**) Complex **8** seems to be able to generate more bi-functional adduct within a short period of time than complex **5**. The binding site cannot be identified at this stage, but is to be determined in the future work. As the photoreaction took place very rapidly, the Pt complexes may bind not only to guanine, but also possibly to cytosine and adenine.[6, 58] Further experiments must be carried out to determine the binding sites.

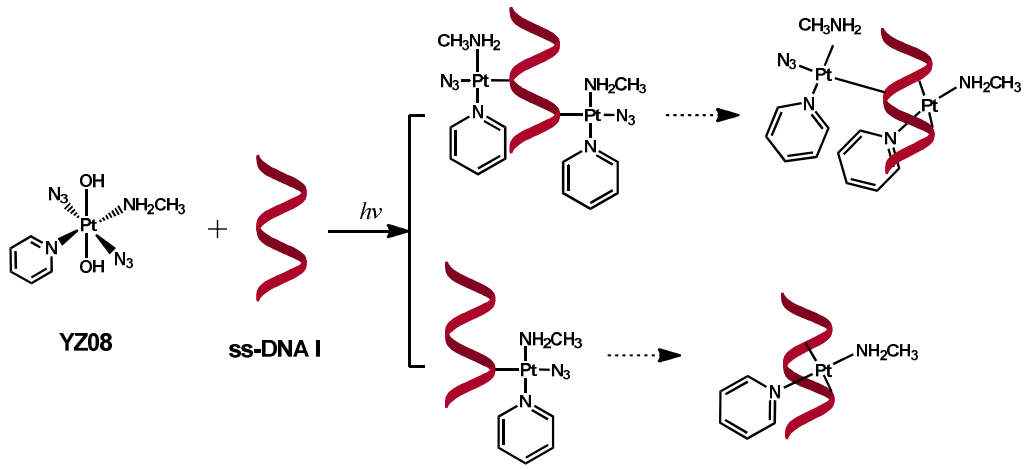

Figure 4.30 Photoinduced DNA binding for complex **5** with ss-DNA **I**. The reaction of complex **8** occurs in a similar way.

4.4 Discussion

4.4.1 Dark stability and reduction potential

Complexes **5** (*trans,trans,trans*-$[Pt(N_3)_2(OH)_2(MA)(Py)]$) and **8** (*trans,trans,trans*-$[Pt(N_3)_2(OH)_2(MA)(Tz)]$) are very stable in aqueous solution and do not react with 5'-GMP and the biological reductants such as L-ascorbic acid, and their reactions with glutathione were very slow. It is generally accepted that for Pt^{IV} complexes, the ease of reduction is determined mainly by their reduction potentials, which are closely related to the nature of the ligands. The empirical sequence for the ease of reduction affected by the axial ligands in *cis,trans,cis*-$[PtCl_2X_2N_2]$ complexes (N = N-donor ligands) follows this order of X: $OH^- < OAc^- < Cl^- < I^-$.[59-61] Therefore, the Pt^{IV} *trans*-dihydroxido complexes are harder to be reduced than the diiodo, dichlorido and the diacetato complexes.

4.4.2 Stability of non-leaving groups

Reports from Sadler's group [6-9] and Bednarski's group [11] have previously examined the photoproducts of Pt^{IV} diazido complexes. The loss of ammine ligand (NH_3) was observed at a considerable level during the irradiation towards complex *trans,trans,trans*-$[Pt(N_3)_2(OH)_2(NH_3)_2]$ and *cis,trans,cis*-$[Pt(N_3)_2(OH)_2(NH_3)_2]$.[7, 8] On the other hand, the loss of pyridine from Pt^{IV} complexes such as *trans,trans,trans*-$[Pt(N_3)_2(OH)_2(Py)_2]$ was very low.[10] It is widely accepted that the non-leaving groups, also called "carrier ligands", e.g., aliphatic imines and aromatic imines, play a very important role in the anticancer activity.[62] The existence of these ligands may affect the distortion of damaged DNA and enzyme recognition in DNA repair synthesis. Taking cisplatin as an example, the loss of ammine may partly account for the deactivation and resistance to the drug in cancer cells.[63, 64] Therefore,

in this work, special attention was paid on the stability of the MA ligand in Pt complexes. ^{1}H and ^{14}N NMR were both used to examine this issue, and it was found that the MA ligand was very stable during irradiation at 450 nm. Also, in the presence of 5'-GMP, little loss of MA was observed. The high stability of MA ligand after photoactivation indicates that it may largely remain on Pt if the reaction takes place on DNA. As a result, the high stability of Pt-MA bonds in complexes **5** (*trans,trans,trans*-$[Pt(N_3)_2(OH)_2(MA)(Py)]$) and **8** (*trans,trans,trans*-$[Pt(N_3)_2(OH)_2(MA)(Tz)]$) may contribute to their potent photocytotoxicity to cancer cells.

4.4.3 Photodecomposition pathways of Pt diazidodihydroxido complexes

The photodecomposition pathways for *cis* or *trans* platinum(IV) diazidodihydroxido complexes with one or two NH_3 ligand have been investigated previously. [6-9, 11] The formation of Pt^{II} and Pt^{IV} products, Pt^{III} and nitrene intermediates, and the release of N_3^- anions and free NH_3, evolution of N_2 gas and O_2 gas have been observed. The release of N_3• radicals was postulated but no evidence was given yet. In the current work, Pt^{IV} diazidodihydroxido complexes were designed with methylamine replacing the NH_3 ligand. Also, direct evidence for N_3• radicals and nitrene intermediates were obtained. More importantly, the energy state of the released O_2 gas was examined.

4.4.3.1 Azido ligands

For complex **5**, *trans,trans,trans*-$[Pt(N_3)_2(OH)_2(MA)(Py)]$, which was studied extensively in this work, the photodecomposition pathways for the azido ligands are very versatile. There are a number of known photoproducts according to this work:

- In the absence of nucleophiles, such as 5'-GMP,
  - Free azide anion N_3^-
  - Azidyl radical N_3•
  - Nitrogen gas N_2
  - Mono-azido Pt moiety {Pt-N_3}
  - In the precipitate
  - Nitrene intermediate {Pt-N} followed by forming {Pt-NH_3}
- In the presence of nucleophiles (5'-GMP)
  - Free azide anions N_3^-
  - Azidyl radical N_3•
  - Mono-azido Pt complex moiety {Pt-N_3}
  - Very low nitrogen gas N_2 release
  - No precipitate
  - Nitrene intermediate {Pt-N} followed by forming {Pt-NH_3} and oxidation of GMP

The importance and impact of each pathway are discussed as follows.

The photo-induced generation of azidyl radicals N_3• has been reported for a wide range of metal azido complexes, including cobalt(III), molybdenum(IV), platinum(II), ion(III) and gold(III) azides.[28] The formation of azidyl radicals N_3• is initiated by a LMCT transition followed by a one-electron reduction of the central atom. The general expression for the homolytic cleavage of the M-N_3 bond is as follows:

$$[L_xM^n(N_3)] \xrightarrow{h\nu\ (\text{LMCT})} [L_xM^{n-1}] + N_3^{\bullet}$$

In the present work, upon the release of an azidyl radical N_3•, Pt^{IV} is reduced to a Pt^{III} intermediate $[Pt^{III}(OH)_2(N_3)LL']$. The Pt^{III} is not stable so it must obtain or lose one electron to form a Pt^{II} or Pt^{IV} species. The Pt^{III} intermediate $[Pt^{III}(OH)_2(N_3)LL']$ tends to lose another azidyl radical N_3• or a hydroxyl radical OH• and form Pt^{II} species. In older work, the N_3• and OH• radicals were proved by initiating the polymerization of ethyl acrylate or acrylonitrile via the free-radical chain mechanism.[65-67] Alternatively, the radical N_3• and radical OH• can both be identified by EPR using spin traps, such as 5,5-dimethylpyrroline-1-oxide (DMPO).[33, 68] Since the radical OH• was not detected by EPR in this work, the Pt^{III} intermediate $[Pt^{III}(OH)_2(N_3)LL']$ should lose the azidyl radical N_3• and form $[Pt^{II}(OH)_2LL']$. Therefore, a photodecomposition pathway for complex **5** via azidyl radical N_3• formation is postulated, as in **Scheme 4.5**.

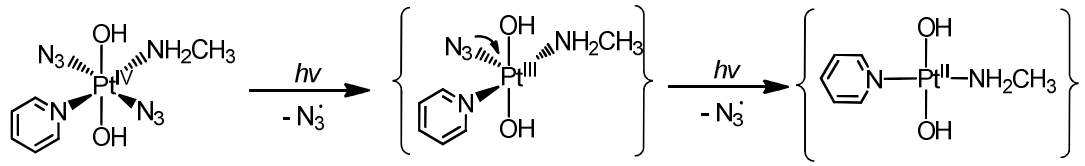

Scheme 4.5 Photodecomposition pathway for complex **5** via the formation of N_3• radical.

Since the N_3• radical may be formed in one of the major pathways of the photodecomposition of Pt^{IV} diazidodihydroxido complexes, its reactions in biological systems are of great interest. On the one hand, it was demonstrated as early as in 1970 that the N_3• radical generated from the photolysis of $[Au(N_3)_4]^-$, $[Pb(N_3)_6]^{2-}$ and NaN_3 can recombine to form N_2 gas: [30, 65, 69]

$$N_3^{\bullet} + N_3^{\bullet} \xrightarrow{k_1} 3N_2\,(g)$$

where the $k_1 = 8.8 \pm 0.5 \times 10^9\ M^{-1}\ s^{-1}$. On the other hand, the azidyl radical N_3• is a relatively mild and selective oxidant reported to oxidize aromatic oxyanions and amines directly by electron transfer,[30, 70, 71] in general:

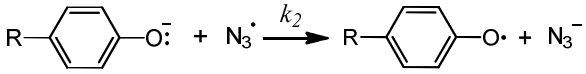

For a range of phenols, $k_2 \sim 4 \times 10^9\ M^{-1}\ s^{-1}$. Oxidation reactions of tryptophan and tyrosine by N_3• radicals have also been reported.[72] As a result, it is reasonable to conclude that N_3• holds potential ability to damage proteins in the cells.

Photoinduced release of free azide anions N_3^- is often accompanied by photosubstitution with, e.g. a solvent molecule, in general: [28]

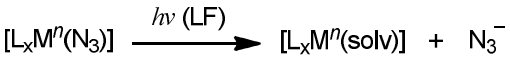

While this process does not involve any redox reaction of the metal or the ligand, the photoelimination is usually part of more complicated simultaneously-occurring decomposition process. For example, in the photodecomposition of complexes $[Pt(N_3)_4]^{2-}$, $[Au(N_3)_2]^-$ and $[Hg(N_3)_3]^-$, release of N_3^- is accompanied by the elimination of N_2. For example: [73]

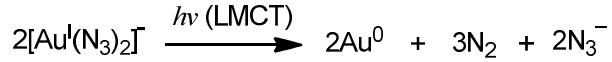

This involves formation of the N_3• radicals transformed into nitrogen molecules as a final product and associated with central atom reduction (*vide supra*). Nevertheless, azide anion N_3^- is generally considered to be an acutely toxic species. It is a potent vasodilator and inhibitor of platelet aggregation.[74] In the cells, it is regarded as a mitochondrial inhibitor [75-78] and myeloperoxidase and catalase inhibitor.[34] Therefore, although the N_3^- anion is not the main pathway in the photodecomposition of Pt^{IV} diazidodihydroxido complexes, even very low concentration of N_3^- could greatly contribute to the photocytotoxic effect of the Pt^{IV} diazidodihydroxido complexes.

The release of N_2 gas found by ^{14}N NMR has been reported recently for $[Pt(N_3)_2(OH)_2(NH_3)_2]$ type of complexes.[7, 8] Apart from recombination of two N_3• radicals (*vide supra*), N_2 gas was also released directly from the {Pt-N_3} moiety, forming a {Pt-N} nitrene intermediate. The release of N_2 gas in targeted tissues or cells might potentially cause symptoms similar to decompression sickness, as gas bubbles may block circulation and cause infarction.

Nitrene is a very reactive intermediate that can be quickly formed by the thermolysis or photolysis of either metal azides or the free N_3^- anion.[28] It has 6 valence electrons, which, lacking two electrons, is an electrophile and a powerful oxidant. It tends to capture two electrons via insertion in to C-H or O-H bond.[49, 50] In aqueous solution, it is responsible for a wide range of DNA lesions.[52, 79-82] In 1968, it was reported that the photodecomposition of $Ba(N_3)_2$ produced OH^-, NH_3 and N_2 gas and small amounts of H_2.[29] It was also described that the transformation from M-N_3^- to M-NH_3 or free NH_3 was found in CID (collision-induced dissociation).[27, 55] Also, as was reported by Ronconi etc.,[8] after irradiation of *trans,trans,trans*-$[Pt(N_3)_2(OH)_2(^{15}NH_3)_2]$ with UVA, signal corresponding to free $^{14}NH_3$ was found by ^{14}N NMR as a photoproduct of azido ligand. To sum up, the discovery of photogenerated {Pt-NH_3} species in this work is again direct and unambiguous evidence of inorganic nitrene intermediates arising from the photodecomposition of Pt-N_3 complexes. This intermediate exhibits a very strong oxidative property, which possibly causes oxidative DNA damage.

Last but not least, it was discovered that two azido ligands of Pt^{IV} diazidodihydroxido complexes can be released step by step from Pt. upon irradiation at 450 nm, the photodecomposition stopped at the first step, releasing only one azido ligand. After the release of the first azido group, the extinction coefficient of the

band from the mono-Pt-N_3 residual at 450 nm may decrease due to the change in the structure of the molecule and the oxidation state of Pt. At this point, the second azido ligand could only undergo photolysis with higher energy irradiation, e.g. UVA (λ_{max} = 365 nm).

4.4.3.2 Hydroxido ligands

Compared to the azido ligands, the decomposition behaviour of the hydroxido ligands is still poorly understood. It has been previously reported that upon irradiation with UVA, $[Pt(N_3)_2(OH)_2(NH_3)_2]$ type complexes can generate oxygen gas (O_2),[7, 8], as detected by an oxygen electrode. However, the source and the energy state of the evolved O_2 are not clear.

It was previously postulated that upon irradiation with UVA, the dihydroxido ligands are released as hydroxyl radicals OH•. When hydroxyl radicals are generated at high local concentrations, they readily dimerize to give H_2O_2,[42] which is known to decompose by disproportionation to water and gaseous dioxygen on irradiation with UV light.[43] However, OH• radical and H_2O_2 were not detected in this work. The OH• radical scavenger formic acid (FA) did not fully quench the fluorescence of the singlet oxygen sensor (SOSG) and the spin trapping experiment by EPR did not observe the signal of OH• radicals. Also, peroxide test stick did not detect H_2O_2 unless the solution was irradiated on the stick (*in situ*). The stability of H_2O_2 in aqueous solution is influenced primarily by temperature and pH value. The decomposition of H_2O_2 increases sharply with the pH value over 5, and trace amount of impurities may induce the decomposition. Nevertheless, assuming that H_2O_2 is the intermediate, the concentration of which found by the peroxide test stick was > 10 mg/L (see **Section 4.3.2**), it was not possible for H_2O_2 at such level fully

decomposed in a few seconds. Other strong oxidants (e.g., $^1O_2$), although short lived, may have activated the test stick when the solution was irradiated *in situ*. Therefore, it is reasonable to conclude that H_2O_2 does not exist as an intermediate in the photo-decomposition of the Pt^{IV} diazidodihydroxido complexes studied in this work.

Singlet oxygen ($^1O_2$) is a very reactive and toxic species to biological systems. It causes oxidative stress and is responsible for various types of oxidative DNA damage. [12-15] This work has shown the first time that singlet oxygen can be generated from a Pt dihydroxido complex. The control experiments with samples saturated with argon or N_2 showed that the elimination of singlet oxygen is not affected by the dissolved oxygen gas in the solvent. Therefore, this work provides the first evidence of the release of singlet oxygen from a Pt^{IV} diazidodihydroxido complex upon irradiation with UVA/blue light in the absence of any exogenous source of oxygen gas. It is important to investigate the mechanism of oxygen generation and to figure out the source of oxygen.

Dioxygen transition metal complexes containing one or more O-O coordination motifs,[83] are potential models of key intermediates in catalytic reactions involving molecular oxygen, hydrogen peroxide, or alkyl hydroperoxide as the oxygen source. [84] Various types of Pt dioxygen complexes have been reported,[83, 85-87] two of which evolve oxygen gas upon irradiation of light: one is a platinum η^2-peroxo complex[88] and the other is a trapezoid-peroxo complex.[89] (**Figure 4.31**) The photoreleased oxygen molecules may adopt two different electronic states, namely, the ground triplet state ($^3\Sigma_g^-$) and the lowest excited singlet state ($^1\Delta_g$). Since the platinum complexes in this work are mononuclear, it is reasonable to assume that a η^2-peroxo ligand is a possible intermediate in the photorelease of oxygen gas.

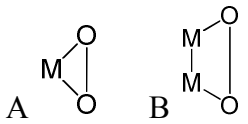

Figure 4.31 O-O binding motifs: A, η^2-peroxo; B, trapezoid-peroxo structures.[89]

The redox reaction between Pt^{II} and Pt^{IV} has been extensively studied. On the one hand, Abbott and coworkers reported the mechanism of oxidation of Pt^{II} to Pt^{IV} by hydrogen peroxide.[90] The oxidation reaction initiate with the addition of H_2O_2 to an axial position of the Pt^{II} square, followed by a one-step two-electron transfer. After that, the other axial site of the Pt^{IV} is coordinated by solvent, such as H_2O and MeOH. On the other hand, there are also a number of reports on the reduction of Pt^{IV} to Pt^{II}. It is widely accepted that a concerted two-electron transfer from other molecule, such as ascorbate or guanine, to the Pt^{IV} centre is involved.[53, 91] Similarly, the photoreduction of Pt^{IV} diazidodihydroxido complex and the release of oxygen gas may also be a two-electron transfer process. The evidence for the mechanisms is still being searched for.

4.4.4 Photoreaction with DNA/RNA bases and oligonucleotide

Complexes **5** (*trans,trans,trans*-$[Pt(N_3)_2(OH)_2(MA)(Py)]$) and **8** (*trans,trans,trans*-$[Pt(N_3)_2(OH)_2(MA)(Tz)]$) can bind to 5'-GMP rapidly and efficiently upon irradiation with light. In comparison, the binding of cisplatin to 5′-GMP at 310 K takes 7-8 hours to reach 50%.[92] The higher photochemistry kinetics of Pt^{IV} diazidodihydroxido complexes leads to various advantages. First, duration of the therapeutic treatment can be short so that the discomfort and side effects of the light dose to the patient can be minimized. Second, in the cisplatin-resistant cancer cells, cytoplasmic detoxification by cellular thiols is a very important mechanism of the

resistance to cisplatin. [93, 94] Rapid binding to DNA could reduce the side reactions via reduced chance to react with cellular thiols.

When comparing the binding rate of complexes **5** and **8** upon irradiation with blue light, it was observed that complex **8** react with 5'-GMP faster than complex **5**. The results from ^{1}H, ^{195}Pt NMR spectroscopy and HPLC-MS all supported this kinetic difference (see **Section 4.3.3**). The higher binding rate to guanine of complex **8** than complex **5** provides a possible explanation to the higher photocytotoxicity of complex **8** towards HaCaT and A2780 cell lines upon irradiation with blue light (See **Section 3.3.4**).

Interestingly, upon irradiation with blue light, complexes **5** and **8** preferentially form monofunctional [Pt(N_3)(MA)(Py/Tz)(GMP)] adducts when reacting with 5'-GMP, but when reacting with ss-DNA oligonucleotide, higher levels of possible bifunctional DNA intrastrand crosslinks [Pt(MA)(Py/Tz)(ss-DNA)] were produced (see **Section 4.3.5**). Moreover, the yield of bifunctional adducts increased over time. After the Pt complex bind to one nucleobase, forming [Pt(N_3)(MA)(Py/Tz)(ss-DNA)], it tends to lose the azido group and bind to another nucleobase, forming [Pt(MA)(Py/Tz)(ss-DNA)]. This is probably because the bidentate adducts formed from Pt and DNA are more stable than the monodentate adducts.

The novel binding mode of the Pt^{IV} diazidodihydroxido complexes to DNA may provide different features from cisplatin. On the one hand, cisplatin forms predominantly bifunctional intrastrand crosslinks (CLs) with DNA, namely d(GpG) 1,2 intrastrand (60 – 65% of all adducts) and d(ApG) 1, 2 intrastrand (20 – 25%) crosslinks,[93] which are believed to be the major cause of cell death. On the other hand, for *trans* Pt^{II} anticancer complexes, monofunctional adducts and a small

amount of bifunctional interstrand crosslinks are usually formed,[95, 96] which may lower the level of DNA repair synthesis and inhibit the transcription, so the cross-resistance to cisplatin may thus be overcome. Also, a monofunctional Pt^{II} anticancer complex has been rationally designed, which potently suppresses the growth of cancer cells by inhibiting RNA polymerase II and nucleotide excision repair.[97, 98] For the platinum complexes in this work, not only are monofunctional DNA adducts preferably formed, but also bifunctional adducts were possibly formed. As a result, complexes **5** and **8** can form both bifunctional and monofunctional lesions on DNA, which is a potential advantage of these novel photoactivatable anticancer complexes.

4.5 Conclusions

In this Chapter, the photochemistry of two Pt diazidodihydroxido complexes **5** (*trans,trans,trans*-$[Pt(N_3)_2(OH)_2(MA)(Py)]$) and **8** (*trans,trans,trans*-$[Pt(N_3)_2(OH)_2(MA)(Tz)]$) was investigated using various analytical methods. Photodecomposition pathways involving the azido ligands and the hydroxido ligands were elucidated. The release of free azide anion N_3^-, azidyl radical $N_3\bullet$, nitrogen gas N_2 and nitrene intermediate {Pt-N} were observed. Importantly, it was discovered that singlet oxygen ($^1O_2$) can be generated from the photoreaction. The photoinduced efficient binding to 5'-GMP and DNA oligonucleotide was also analysed. It was discovered for the first time that Pt-nitrene intermediates were produced and that the oxidation of 5'-GMP can occur in the photodecomposition of the Pt diazidodihydroxido complexes. It was also of importance to discover that singlet oxygen is generated from this photoreaction which is likely to cause oxidative damage to guanine. All these features contribute to the high photocytoxicity of this class of compounds. Also, the feature of releasing singlet oxygen in the absence of

exogenous source of oxygen overcomes the oxygen dependence of photodynamic therapy (PDT) and hence the Pt diazidodihydroxido complexes can find extraordinary application in photochemotherapy.

4.6 References

1. A. Gottlieb, *J. Am. Inst. Conserv.*, 1995, **34**, 11 - 32.
2. P. J. Bednarski, F. S. Mackay and P. J. Sadler, *Anti-Cancer Agent Med. Chem.*, 2007, **7**, 75-93.
3. A. Vogler, A. Kern and J. Hüttermann, *Angew. Chem. Int. Ed.*, 1978, **17**, 524-525.
4. O. Horváth and K. L. Stevenson, *Charge Transfer Photochemistry of Coordination Compounds*, VCH, Weinheim, Germany, 1993.
5. F. S. Mackay, J. A. Woods, H. Moseley, J. Ferguson, A. Dawson, S. Parsons and P. J. Sadler, *Chem. Eur. J.*, 2006, **12**, 3155-3161.
6. F. S. Mackay, J. A. Woods, P. Heringova, J. Kasparkova, A. M. Pizarro, S. A. Moggach, S. Parsons, V. Brabec and P. J. Sadler, *Proc. Natl. Acad. Sci. USA*, 2007, **104**, 20743-20748.
7. H. I. A. Phillips, L. Ronconi and P. J. Sadler, *Chem. Eur. J.*, 2009, **15**, 1588-1596.
8. L. Ronconi and P. J. Sadler, *Dalton Trans.*, 2011, **40**, 262-268.
9. L. Ronconi and P. J. Sadler, *Chem. Commun.*, 2008, 235-237.
10. N. J. Farrer, J. A. Woods, L. Salassa, Y. Zhao, K. S. Robinson, G. Clarkson, F. S. Mackay and P. J. Sadler, *Angew. Chem. Int. Ed.*, 2010, **49**, 8905-8908.
11. A. F. Westendorf, A. Bodtke and P. J. Bednarski, *Dalton Trans.*, 2011, **40**, 5342-5351.

12. B. Halliwell and J. Gutteridge, *Free Radicals in Biology and Medicine*, Oxford University Press, Oxford, UK, 2007.
13. S. Kanvah, J. Joseph, G. B. Schuster, R. N. Barnett, C. L. Cleveland and U. Landman, *Acc. Chem. Res.*, 2010, **43**, 280-287.
14. G. Pratviel and B. Meunier, *Chem. Eur. J.*, 2006, **12**, 6018-6030.
15. P. R. Ogilby, *Chem. Soc. Rev.*, 2010, **39**, 3181-3209.
16. D. E. J. G. J. Dolmans, D. Fukumura and R. K. Jain, *Nat. Rev. Cancer*, 2003, **3**, 380-387.
17. M. C. DeRosa and R. J. Crutchley, *Coord. Chem. Rev.*, 2002, **233-234**, 351-371.
18. C. Schweitzer and R. Schmidt, *Chem. Rev.*, 2003, **103**, 1685-1758.
19. P. I. Djurovich, D. Murphy, M. E. Thompson, B. Hernandez, R. Gao, P. L. Hunt and M. Selke, *Dalton Trans.*, 2007, 3763-3770.
20. V. Anbalagan, *J. Coord. Chem.*, 2003, **56**, 161-172.
21. W. A. Kibbe, *Nucleic Acids Res.*, 2007, **35**, W43-W46.
22. H. K. Hall, *J. Am. Chem. Soc.*, 1957, **79**, 5441-5444.
23. I. M. Ismail, S. J. S. Kerrison and P. J. Sadler, *Polyhedron*, 1982, **1**, 57-59.
24. N. J. Farrer, P. Gierth and P. J. Sadler, *Chem. Eur. J.*, 2011, **17**, 12059-12066.
25. J. Kent, *J. Chem. Phys.*, 1966, **44**, 3530.
26. The Engineering ToolBox, Solubility of Gases in Water, http://www.engineeringtoolbox.com/gases-solubility-water-d_1148.html, Accessed 15th Jan, 2012.
27. S. Wee, J. M. White, W. D. McFadyen and R. A. J. Hair, *Aust. J. Chem.*, 2003, **56**, 1201-1207.
28. J. Šima, *Coord. Chem. Rev.*, 2006, **250**, 2325-2334.
29. V. R. P. Verneker and M. Blais, *J. Phys. Chem.*, 1968, **72**, 774-778.

30. S. J. David and R. D. Coombe, *J. Phys. Chem.*, 1986, **90**, 3260-3263.
31. D. Rehorek, P. Thomas and H. Hennig, *Inorg. Chim. Acta*, 1979, **32**, L1-L2.
32. F. P. Sargent and E. M. Gardy, *Can. J. Chem.*, 1976, **54**, 275-279.
33. W. Kremers and A. Singh, *Can. J. Chem.*, 1980, **58**, 1592-1595.
34. B. Kalyanaraman, E. G. Janzen and R. P. Mason, *J. Biol. Chem.*, 1985, **260**, 4003-4006.
35. S. Luanpitpong, U. Nimmannit, P. Chanvorachote, S. Leonard, V. Pongrakhananon, L. Wang and Y. Rojanasakul, *Apoptosis*, 2011, **16**, 769-782.
36. Molecular Probes. Product information for SOSG. , http://probes.invitrogen.com/media/pis/mp36002.pdf?id=mp36002, Accessed 20 Jan, 2012.
37. A. Gollmer, J. Arnbjerg, F. H. Blaikie, B. W. Pedersen, T. Breitenbach, K. Daasbjerg, M. Glasius and P. R. Ogilby, *Photochem. Photobiol.*, 2011, **87**, 671-679.
38. C. Flors, M. J. Fryer, J. Waring, B. Reeder, U. Bechtold, N. R. Baker, P. M. Mullineaux, S. Nonell and M. T. Wilson, *J. Exp. Bot.*, 2006, **57**, 1725-1734.
39. X. Ragas, A. Jimenez-Banzo, D. Sanchez-Garcia, X. Batllori and S. Nonell, *Chem. Commun.*, 2009, 2920-2922.
40. K. I. Salokhiddinov, I. M. Byteva and G. P. Gurinovich, *J. Appl. Spectrosc.*, 1981, **34**, 561-564.
41. J. R. Hurst, J. D. McDonald and G. B. Schuster, *J. Am. Chem. Soc.*, 1982, **104**, 2065-2067.
42. O. Legrini, E. Oliveros and A. M. Braun, *Chem. Rev.*, 1993, **93**, 671-698.
43. K. Azrague, E. Bonnefille, V. Pradines, V. Pimienta, E. Oliveros, M.-T. Maurette and F. Benoit-Marquie, *Photochem. Photobio. Sci.*, 2005, **4**, 406-408.

44. Sigma-Aldrich Product Information of Quantofix® Peroxide 25 Test Sticks. , http://www.sigmaaldrich.com/catalog/ProductDetail.do?lang=en&N4=37214|FLUKA&N5=SEARCH_CONCAT_PNO|BRAND_KEY&F=SPEC, Accessed 28th Jan, 2012.
45. J. Reedijk, *Eur. J. Inorg. Chem.*, 2009, 1303-1312.
46. J. Reedijk, *Chem. Rev.*, 1999, **99**, 2499-2510.
47. B. M. Still, P. G. A. Kumar, J. R. Aldrich-Wright and W. S. Price, *Chem. Soc. Rev.*, 2007, **36**, 665-686.
48. P. S. Pregosin, *Coord. Chem. Rev.*, 1982, **44**, 247-291.
49. R. J. Robbins, L. L. N. Yang, G. B. Anderson and D. E. Falvey, *J. Am. Chem. Soc.*, 1995, **117**, 6544-6552.
50. P. V. Sudhakar and K. Lammertsma, *J. Am. Chem. Soc.*, 1991, **113**, 5219-5223.
51. D. Wild and A. Dirr, *Mutagenesis*, 1989, **4**, 446-452.
52. V. Voskresenska, R. M. Wilson, M. Panov, A. N. Tarnovsky, J. A. Krause, S. Vyas, A. H. Winter and C. M. Hadad, *J. Am. Chem. Soc.*, 2009, **131**, 11535-11547.
53. S. Choi, R. B. Cooley, A. S. Hakemian, Y. C. Larrabee, R. C. Bunt, S. D. Maupas, J. G. Muller and C. J. Burrows, *J. Am. Chem. Soc.*, 2004, **126**, 591-598.
54. S. Choi, R. B. Cooley, A. Voutchkova, C. H. Leung, L. Vastag and D. E. Knowles, *J. Am. Chem. Soc.*, 2005, **127**, 1773-1781.
55. R. A. J. O'Hair, in *Reactive Intermediates - MS Investigations in Solution*, ed. L. S. Santos, Wiley-VCH Verlag GmbH & Co. KGaA, Weinheim, 2010, ch. 6, pp. 199-227.

56. H. D. Gafney, J. L. Reed and F. Basolo, *J. Am. Chem. Soc.*, 1973, **95**, 7998-8005.

57. J. Vinje, J. A. Parkinson, P. J. Sadler, T. Brown and E. Sletten, *Chem. Eur. J.*, 2003, **9**, 1620-1630.

58. J. Pracharova, L. Zerzankova, J. Stepankova, O. Novakova, N. J. Farrer, P. J. Sadler, V. Brabec and J. Kasparkova, *Chem. Res. Toxicol.*, 2012.

59. M. D. Hall, H. R. Mellor, R. Callaghan and T. W. Hambley, *J. Med. Chem.*, 2007, **50**, 3403-3411.

60. M. D. Hall and T. W. Hambley, *Coord. Chem. Rev.*, 2002, **232**, 49-67.

61. N. A. Kratochwil and P. J. Bednarski, *Arch. Pharm.*, 1999, **332**, 279-285.

62. M. Coluccia and G. Natile, *Anti-Cancer Agent Med. Chem.*, 2007, **7**, 111-123.

63. J. K.-C. Lau and D. V. Deubel, *Chem. Eur. J.*, 2005, **11**, 2849-2855.

64. H. L. Li, Y. Zhao, H. I. A. Phillips, Y. L. Qi, T. Y. Lin, P. J. Sadler and P. B. O'Connor, *Anal. Chem.*, 2011, **83**, 5369-5376.

65. W. Beck and K. Schorpp, *Angew. Chem. Int. Ed.*, 1970, **9**, 735-735.

66. C. Bartocci and F. Scandola, *J. Chem. Soc., Chem. Commun.*, 1970.

67. G. N. Richards, *J. Appl. Polym. Sci.*, 1961, **5**, 539-544.

68. E. Finkelstein, G. M. Rosen and E. J. Rauckman, *Arch. Biochem. Biophys.*, 1980, **200**, 1-16.

69. S. M. Peiris and T. P. Russell, *J. Phys. Chem. A*, 2003, **107**, 944-947.

70. Z. B. Alfassi and R. H. Schuler, *J. Phys. Chem.*, 1985, **89**, 3359-3363.

71. K. B. Hewett and D. W. Setser, *J. Phys. Chem. A*, 1998, **102**, 6274-6281.

72. J. Butler, E. J. Land, A. J. Swallow and W. Prutz, *Radiat. Phys. Chem.*, 1984, **23**, 265-270.

73. H. Kunkely and A. Vogler, *Inorg. Chem. Commun.*, 2003, **6**, 553-554.

74. R. P. Smith, C. A. Louis, R. Kruszyna and H. Kruszyna, *Fundam. Appl. Toxicol.*, 1991, **17**, 120-127.

75. A. S. Faqi, D. Richards, J. W. Hauswirth and R. Schroeder, *Regul. Toxicol. Pharm.*, 2008, **52**, 158-162.

76. T. Ishikawa, B. L. Zhu and H. Maeda, *Toxicol. Ind. Health*, 2006, **22**, 337-341.

77. Y. W. Liu, Y. Liu, C. X. Wang, S. S. Qu and F. J. Deng, *Thermochim. Acta*, 2000, **351**, 51-54.

78. J. Harvey, S. C. Hardy and M. L. J. Ashford, *Br. J. Pharmacol.*, 1999, **126**, 51-60.

79. E. C. Miller and J. A. Miller, *Cancer*, 1981, **47**, 2327-2345.

80. M. Famulok and G. Boche, *Angew. Chem. Int. Ed.*, 1989, **28**, 468-469.

81. W. G. Humphreys, F. F. Kadlubar and F. P. Guengerich, *Proc. Natl. Acad. Sci. USA*, 1992, **89**, 8278-8282.

82. Z. Guo, J. Xue, Z. Ke, D. L. Phillips and C. Zhao, *J. Phys. Chem. B*, 2009, **113**, 6528-6532.

83. D. M. Wagnerová and K. Lang, *Coord. Chem. Rev.*, 2011, **255**, 2904-2911.

84. P. Fantucci, S. Lolli and M. Pizzotti, *Inorg. Chem.*, 1994, **33**, 2779-2789.

85. G. A. Ozin and W. E. Klotzbuecher, *J. Am. Chem. Soc.*, 1975, **97**, 3965-3974.

86. H. Kurosawa, T. Achiha, H. Kajimaru and I. Ikeda, *Inorg. Chim. Acta*, 1991, **190**, 271-277.

87. Y. Gong and M. Zhou, *Chemphyschem*, 2010, **11**, 1888-1894.

88. A. Vogler and H. Kunkely, *J. Am. Chem. Soc.*, 1981, **103**, 6222-6223.

89. J. Bould, T. s. Baše, M. G. S. Londesborough, L. A. Oro, R. n. Macías, J. D. Kennedy, P. Kubát, M. Fuciman, T. s. Polívka and K. Lang, *Inorg. Chem.*, 2011, **50**, 7511-7523.

90. S. O. Dunham, R. D. Larsen and E. H. Abbott, *Inorg. Chem.*, 1993, **32**, 2049-2055.

91. K. Lemma, J. Berglund, N. Farrell and L. I. Elding, *J. Biol. Inorg. Chem.*, 2000, **5**, 300-306.

92. A. Zenker, M. Galanski, T. L. Bereuter, B. K. Keppler and W. Lindner, *J. Chromatog. B*, 2000, **745**, 211-219.

93. L. Kelland, *Nat. Rev. Cancer*, 2007, **7**, 573-584.

94. L. R. Kelland, G. Abel, M. J. Mckeage, M. Jones, P. M. Goddard, M. Valenti, B. A. Murrer and K. R. Harrap, *Cancer Res.*, 1993, **53**, 2581-2586.

95. T. Suchankova, M. Vojtiskova, J. Reedijk, V. Brabec and J. Kasparkova, *J. Biol. Inorg. Chem.*, 2009, **14**, 75-87.

96. V. Brabec and M. Leng, *Proc. Natl. Acad. Sci. USA*, 1993, **90**, 5345-5349.

97. D. Wang, G. Zhu, X. Huang and S. J. Lippard, *Proc. Natl. Acad. Sci. USA*, 2010, **107**, 9584-9589.

98. G. Zhu, M. Myint, W. H. Ang, L. Song and S. J. Lippard, *Cancer Res.*, 2012, **72**, 790-800.

Chapter 5

Tuning the Wavelength of Photoactivation of Platinum Complexes

5.1 Introduction

Since it was discovered that cisplatin inhibits cell division in the 1960s, platinum-based drugs have been extensively studied against various tumours.[1-3] However, severe toxic and dose-limiting side-effects, including nausea, vomiting and nephrotoxicity accompany the treatment, which limit its application.[4] The use of prodrugs to tune the physicochemical, biopharmaceutical or pharmacokinetic properties of pharmacologically active agents is a promising approach to lower side-effects.[5, 6] Prodrugs are reversible derivatives of drug molecules that undergo an enzymatic and/or chemical transformation *in vivo* to release the active parent drug, which can then exert the desired pharmacological effect at the targeted site.[7]

Photoactivatable Pt^{IV} diazidodihydroxido anticancer complexes are a group of prodrugs that are inert and non-toxic in a biological environment in the dark. Upon irradiation with light these complexes can be selectively activated to become potently cytotoxic against a number of cancer cell lines.[8-12] However, these complexes would ideally be activated with long wavelength light in the so-called therapeutic window (400 − 800 nm[13, 14]) to allow treatment of larger tumours, as tissue-penetration of light is wavelength-dependent (see **Chapter 1**).

One aim of this work is to develop new Pt^{IV} complexes with broader clinical utility (activation wavelengths within the therapeutic window) by appropriate selection of the ligands of the complexes. In **Chapter 3**, it was demonstrated that replacing the NH_3 ligand by an aliphatic amine in *trans,trans,trans*-$[Pt(N_3)_2(OH)_2(NH_3)(Py)]$(**22**) can produce enhanced photocytotoxicity to cisplatin-resistant cancer cells and provide activation by blue light, as found for *trans,trans,trans*-$[Pt(N_3)_2(OH)_2(MA)(Py)]$ (**5**) and *trans,trans,trans*-$[Pt(N_3)_2(OH)_2(MA)(Py)]$ (**8**).

However, these complexes cannot be activated by light with $\lambda > 500$ nm. So the aim of this Chapter is to develop photoactive anticancer complexes with a longer activation wavelength.

In mononuclear metal complexes, ligand field (LF), LMCT, MLCT and LLCT are the most important transitions in the electronic spectra (see **Chapter 1**). It is important to lower the energy of these transitions to obtain new complexes with longer activation wavelengths. In the new Pt^{IV} complexes developed in this Chapter, azido groups and dihydroxido groups are retained to keep the photochemical properties. Hence, modifications are made on the other groups, such as the aromatic imine and aliphatic amine ligands.

Computational research by Huichung Tai, in this group, suggested that electron-withdrawing substituents on the pyridine ligand tend to lower the energies of the unoccupied orbitals of Pt^{IV} diazidodihydroxido complexes, resulting in lowered energy of absorption.[15] Inspired by this result, 4-nitropyridine was used to synthesize new Pt^{IV} complexes, with the aim of performing the achieving at longer wavelength.

Also, for charge-transfer transitions, electron-rich aromatic chromophores can shift the charge transfer band to longer wavelength. So 2,2'-bipyridine (Bpy) and terpyridine (Tpy) are used as in electron donors to synthesize new Pt^{IV} complexes.

Platinum(II) terpyridine complexes have recently attracted great interest in bioinorganic chemistry due to their activity in the interaction with nucleic acids and proteins.[16] The structure-function relationship can be easily tuned by altering the substitution group in the 4' position and the ligand occupying the fourth coordination site of Pt^{II}. There are two intrinsic properties of Pt terpyridine complex cations: (1) ease of displacement of the fourth coordination site ligand by nucleophiles and (2)

the propensity for stacking of the Tpy ligand via its π systems.[17] So Pt terpyridine complexes are promising for design of prodrugs with higher photocytotoxicity as well as longer activation wavelength.

5.2 Experimental

5.2.1 Materials, methods and instrument

4-Nitropyridine 1-oxide, 2,2′-bipyridine, 2,2':6',2"-terpyridine, 1, 5-cyclooctadiene, 4'-(4-Methylphenyl)-2,2':6',2"-terpyridine, NaN_3, H_2O_2 (30%) and Pt standard for ICP analysis are from Sigma-Aldrich, All other materials were used as obtained from commercial sources unless otherwise stated.

NMR spectra were recorded on Bruker DPX-400 (^{1}H, 400.03 MHz) or Bruker AVIII-600 (^{1}H, 600.13 MHz; ^{13}C, 150.9MHz; ^{195}Pt, 129.4 MHz) spectrometers. Specific parameters, along with other general parameters for acquisition are found in **Chapter 2**.

The X-ray crystallographic data collection and analysis were carried out by Dr Guy Clarkson in University of Warwick. Instrumentation, acquisition parameters and data processing can be found in **Chapter 2**.

Elemental analysis was performed by the Warwick Analytical Service.

Positive/negative ion electrospray mass spectrometry (ESI-MS) was performed on a Bruker Esquire 2000 mass spectrometer coupled with an Agilent 1100 HPLC (without column) as an automatic sample delivery system. Samples were prepared in 80% acetonitrile/20% water. HPLC coupled mass spectrometry (LC-MS) was performed on a Bruker HCT-Ultra mass spectrometer coupled with an Agilent 1200 HPLC system with an Agilent ZORBAX Eclipse Plus reverse phase C18 column

(4.6 × 250 mm, 5 μm). Flow rate, 1.0 ml/min; detecting wavelength, 254 nm; mobile phase A, H_2O with 0.1% formic acid (FA); mobile phase B, MeOH with 0.1% FA. A linear gradient from 5% to 55% B over 15 min was applied.

A semi-preparative HPLC method was used to purify the crude products that could not be purified by other methods. A HPLC analysis method was used to verify the purity of some of the compounds. Specific columns, mobile phase used and HPLC conditions are stated in the results section.

Electronic absorption spectra (UV-Vis) were recorded on a Varian Cary 300 UV-Vis spectrophotometer in a 1-cm path-length quartz cuvette. All spectra were referenced to neat solvent and data were processed with OriginLab Origin 7.0. Extinction coefficients (ε) were determined over a concentration range (A_{max} ~ 0.4 – 1.6) with at least 4 data points, using Pt concentrations determined by ICP-MS.

ICP-OES and ICP-MS were used to determine Pt concentration for the solubility and extinction coefficients of Pt^{IV} complexes. Five different concentrations diluted from one sample solution were measured. A series of Pt standards covering the range 1 – 25 ppm (for OES) or 0.25 – 500 ppb (for MS) were made as reference. Standard 1.001 ± 0.002 g/l Pt solution in 3% HNO_3 obtained from Sigma-Aldrich was used.

Photodecomposition of Pt complexes was carried out at 298 K by using a LZC-ICH2 photoreactor (Luzchem Research Inc.) equipped with a temperature controller and 8 UVA lamps (Hitachi, λ_{max} = 365 nm, 3.5 mW/cm^2) with no other sources of light filtration. ACULED® VHL™ LEDs (λ_{max} = 450 nm, 50 mW/cm^2) and High-Power 38 LED bulb/GU10 Green LEDs (λ_{max} = 517 nm, 25 mW/cm^2) were also used for irradiation of the samples. Their output spectra are listed in **Appendix 2**.

Action Spectrum

A modified Shimadzu RF-551 Fluorescence HPLC Monitor was used as the light source to give monochromatic irradiation with PWHH (peak width at half height) of *ca.* 15 nm. Filters were used to eliminate the second and higher order diffraction of shorter wavelengths in the specified longer wavelength monochromatic light from the grating.[18] Solutions of photoactivatable Pt^{IV} complex in a 1-cm path-length UV-Vis quartz cuvette (0.6 ml) were irradiated with the monochromatic light. The instrument setup is shown in **Figure 5.1**.

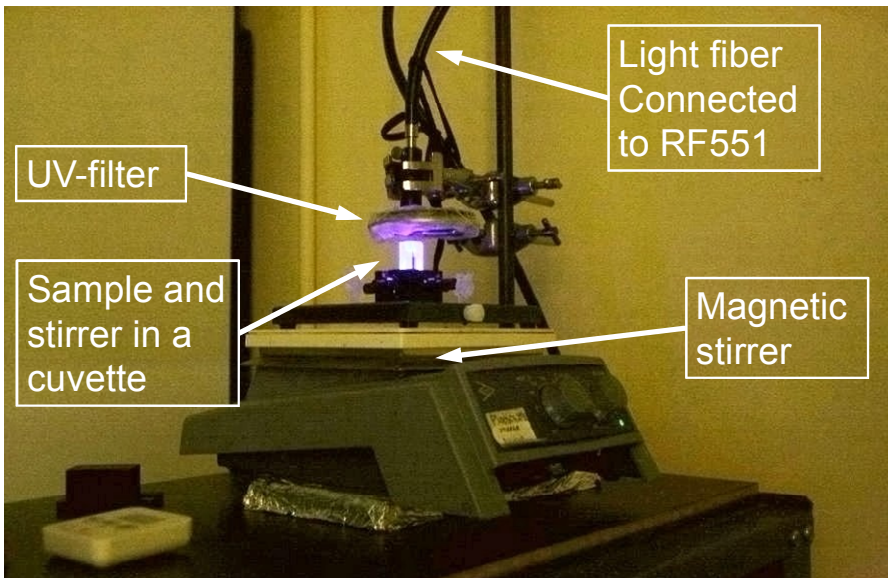

Figure 5.1 Instrument setup for the action spectrum.

The progress of the photoreaction, time-course data and the spectral output of the light source were monitored and recorded with a Varian Cary 300 UV-Vis spectrophotometer and data were processed with OriginLab Origin 7.0. UV-Vis spectra were recorded every minute during irradiation and the rate of loss of absorption at λ_{max} (average of 10 data points at 287 ± 1 nm) was monitored. In each case, the photolysis of the complex was taken to completion (1 – 18 h depending on λ_{irr}), but only data relating to < 10% photodecomposition were considered when

analysing the initial rate of photolysis of the complex. The rate data were the average of two independent runs at each λ_{irr}. The number of incident photons (einstein/s) was measured and calculated using a potassium ferrioxalate actinometer.[19, 20] The absorbance at λ_{max} (A_{287}) was plotted versus time (t); the average photolysis rate (dc/dt) is given by **Equation 5.1**, and pseudo quantum yield (Φ) was calculated from **Equation 5.2**.

$$\frac{dc}{dt} = \frac{dA_{287}}{dt}\frac{1}{l\varepsilon_{287}} \quad (\mathbf{5.1})$$

$$\Phi = \frac{\text{No. of reactions}}{\text{No. of incident photons}} \quad (\mathbf{5.2})$$

A blank control involving spectral acquisition for 12 h but no irradiation, showed that light from the UV-Vis spectrophotometer lamp had a negligible effect on the sample.

Cell Culture and Cytotoxicity for Pt complexes.

The photoactivated dose-dependent inhibition of cell viability for light-sensitive Pt^{IV} complexes was determined by Dr Julie A. Woods (University of Dundee). Details can be found in **Chapter 2**.

5.2.2 Synthesis and Characterisation

5.2.2.1 *Cis*-$[PtI_2(NH_3)_2]$ (25)

Cis-$[PtI_2(NH_3)_2]$ (**25**) and *cis*-$[PtCl_2(NH_3)_2]$ (cisplatin, **26**) were synthesized according to the reported method.[21] $K_2[PtCl_4]$ (2.075 g, 5.0 mmol) was dissolved in H_2O (30 mL) and KI (8.300 g, 50 mmol) added. After stirring for 1 h, NH_4Cl (0.535 g, 10 mmol) was added and the pH adjusted to 10 using 2 M KOH. The pH was

monitored and readjusted to 10 until it no longer decreased. The mixture was stirred for a further 2 – 4 h after which the yellow precipitate was collected by filtration, washed with minimal cold water, ethanol and diethyl ether and dried under vacuum.

Yield: 2.31 g (95.7 %)

ESI-MS (*m/z*): $[M - I + MeCN]^+$ found 396.8; calc. 396.9.

Elemental Analysis: $PtH_6N_2Cl_2$, found (%): H, 0.94, N, 5.62; calc.: H, 1.24, N, 5.80.

5.2.2.2 *Cis*-$[PtCl_2(NH_3)_2]$ (cisplatin, 26)

Cis-$[PtI_2(NH_3)_2]$ (2.31 g, 4.78 mmol) was suspended in H_2O (30 mL) and $AgNO_3$ (1.625 g, 9.56 mmol) added. The mixture was stirred at 328 K overnight. AgI precipitate was filtered off using celite followed by an inorganic membrane filter (Sartorius Minisart, 0.2 μm). NaCl (2.80 g, 47.8 mmol) was added and the mixture was stirred for a further 30 min, after which the yellow precipitate was collected by filtration, washed with minimal cold water, ethanol and diethyl ether and dried under vacuum. The product can be recrystallized in a minimal amount of 0.1 M HCl.

Yield: 1.331 g (92.7 %)

^{1}H NMR (d_6-DMSO): δ = 3.97 (broad, N$\underline{H}_3$, 6H).

Elemental analysis: $PtH_6N_2Cl_2$, found (%): H, 1.94, N, 9.23. Calc.: H, 2.02, N, 9.33.

5.2.2.3 4-Nitropyridine (27)

4-Nitropyridine (4-NO_2-Py) was synthesized according to a published method.[22] To 1 g. of 4-nitropyridine 1-oxide suspended in 15 ml of ice-cold chloroform, 1.9 ml of phosphorus trichloride was added slowly and the mixture was heated one hour at 343 – 353 K. *Caution, phosphorus trichloride is very toxic and corrosive, and should be treated with special care. Adding water to excess phosphorus trichloride should be carried out in well ventilated fume hood.* After cooling and the addition of water, the

reaction mixture was made alkaline by addition of sodium hydroxide and was extracted with chloroform. The chloroform solution was dried over sodium sulfate, evaporated to dryness, and the residue was recrystallized from petroleum ether. The NMR chemical shifts are consistent with those reported.[22]

Yield: 0.54g (61%).

^{1}H NMR (400 MHz, MeOD): δ = 8.93 (d, $\underline{H_{2,6}}$, 2H), 8.15 (d, $\underline{H_{3,5}}$, 2H), ^{13}C NMR (150.9 MHz, MeOD): δ = 155.5 ($\underline{C_4}$), 153.1 ($\underline{C_{2,6}}$), 117.8 ($\underline{C_{3,5}}$).

Elemental Analysis: $C_2H_{10}Cl_2N_2Pt$, Calc. C 48.39%, H 3.25%, N 22.57%, Found: C 48.31%, H 3.14%, N 22.46%.

5.2.2.4 *Trans*-[$PtCl_4(NH_3)$(4-nitropyridine)] (28)

Cisplatin (200 mg, 0.67 mmol) was suspended in 6 ml H_2O, and then 4-nitropyridine (4-NO_2-Py, 248 mg, 2.0 mmol) was added. The reaction was heated to 348 K with stirring and kept at this temperature for 90 min. *N.B. This intermediate is light sensitive!* The solution was allowed to cool to room temperature and HCl (12 M, 0.5 ml) was added and then the solution was heated at 373 K for *ca*. 48 h. The flask was cooled on ice and the yellow product was collected by filtration, washed successively with minimal cold H_2O, ethanol, and diethyl ether and then dried under vacuum. Crystals suitable for X-ray analysis were obtained from a minimal amount of 0.1 M HCl at 277 K.

Yield: 250 mg (75.6%).

^{1}H NMR (400 MHz, acetone-d_6): δ = 9.52 (d, $\underline{H_{2,6}}$, ^{3}J (^{195}Pt, ^{1}H) = 25 Hz, 2H), 8.54 (d, $\underline{H_{3,5}}$, 2H), 6.16 (t, N$\underline{H_3}$, ^{1}J (^{14}N, ^{1}H) = 54 Hz, ^{2}J (^{195}Pt, ^{1}H) = 54 Hz, 3H). ^{13}C NMR (150.9 MHz, MeOD): δ = 157.2 ($\underline{C_4}$), 156.6 ($\underline{C_{2,6}}$), 120.2 ($\underline{C_{3,5}}$, ^{3}J (^{195}Pt, ^{13}C) = 27 Hz). ^{195}Pt NMR (129.4 MHz, MeOD): δ = −354.3.

ESI-MS (*m/z*): $[M + Na]^+$ Calc., 499.9, Found, 500.0.

Elemental Analysis: $C_5H_8Cl_5N_3O_2Pt$ (M + HCl), found (%), C, 11.29; H, 1.44; N, 8.55; calc., C, 11.67; H, 1.57; N, 8.17.

5.2.2.5 *Trans*-[$PtCl_2(NH_3)$(4-nitropyridine)] (29)

Trans-[$PtCl_2(NH_3)$(4-NO_2-Py)] was synthesized according to the reported method for similar compounds.[23, 24] A suspension of *trans*-[$PtCl_4(NH_3)$(4-NO_2-Py)]•H_2O (50 mg) in water (2 ml) was treated with hydrazine hydrate (N_2H_4•H_2O) (6 µl, 2 mol equiv). *Caution, hydrazine is toxic, explosive and dangerous for the environment, and should be treated with care.* The reaction mixture was stirred and heated to reflux for 14 h. The solvent was evaporated under reduced pressure and the yellow residue obtained was washed with water and dried under vacuum.

Yield: 26 mg (63%)

^{1}H NMR (400 MHz, acetone-d_6): δ = 9.30 (d, $\underline{H_{2,6}}$, ^{3}J (^{195}Pt, ^{1}H) = 32 Hz, 2H), 8.23 (d, $\underline{H_{3,5}}$, 2H), 3.95 (broad, N$\underline{H_3}$, 3H). ^{13}C NMR (150.9 MHz, acetone-d_6): δ = 156.6 ($\underline{C_{2,6}}$), 154.7 ($\underline{C_4}$), 119.5 ($\underline{C_{3,5}}$). ^{195}Pt NMR (129.4 MHz, acetone-d_6): δ = −2023.2.

ESI-MS (*m/z*): $[M - Cl + CH_3CN]^+$ Calc., 413.0, Found, 413.0.

Elemental Analysis: $C_5H_4N_2O_2$, Calc., C, 14.75%; H, 1.73%; N, 10.32%; Found, C, 14.74%; H, 1.54%; N, 10.23%.

5.2.2.6 *Trans*-[$Pt(N_3)_2(NH_3)$(4-nitropyridine)] (30)

Caution! *No problems were encountered during this work, however heavy metal azides are known to be shock sensitive detonators, therefore it is essential that any platinum azide compound is handled with care. From this point on all syntheses were carried out under controlled (dim) lighting conditions.*

Trans-[$Pt(N_3)_2(NH_3)(4\text{-}NO_2\text{-}Py)$] was synthesized according to the reported method for similar compounds.[9, 11] *Trans*-[$PtCl_2(NH_3)(4\text{-}NO_2\text{-}Py)$] (20 mg) was suspended in H_2O 10 ml, and $AgNO_3$ (16 mg) was added and stirred at 323 K for 16 h. AgCl precipitate was filtered off using celite followed by an inorganic membrane filter (0.2 μm). NaN_3 (13 mg, 4 mol equiv) was added and the solution stirred at room temperature for 6h before leaving the flask in fridge overnight. The yellow precipitate was collected by filtration, washed with minimal cold H_2O and then dried under vacuum. Crystals qualified for X-ray analysis was obtained from methanol at 277 K.

Yield: 14 mg (68%).

^1H NMR (400 MHz, acetone-d_6): δ = 9.20 (d, $\underline{H_{2,6}}$, ^3J (^{195}Pt, ^1H) = 36 Hz, 2H), 8.34 (d, $\underline{H_{3,5}}$, 2H), 4.25 (broad, N$\underline{H_3}$). ^{13}C NMR (150.9 MHz, Acetone-d_6): δ = 155.6 ($\underline{C_{2,6}}$), 155.0 ($\underline{C_4}$), 120.2 ($\underline{C_{3,5}}$). ^{195}Pt NMR (129.4 MHz, acetone-d_6): δ = −2134.9.

ESI-MS (*m/z*): $[M + Na]^+$ Calc., 443.0, Found, 443.1.

Elemental Analysis: $C_5H_7N_9O_2Pt$, Calc., C, 14.29%; H, 1.68%; N, 30.00%; Found, C, 14.35%; H, 1.34%; N, 28.56%. The structure of this intermediate was verified by x-ray crystallography, and the product was only used in the synthesis. Azido complexes often give rise to larger deviation than normal in the nitrogen analysis.

5.2.2.7 *Trans, trans, trans*-[$Pt(N_3)_2(OH)_2(NH_3)$(4-nitropyridine)] (31)

Trans-[$Pt(N_3)_2(NH_3)(4\text{-}NO_2\text{-}Py)$] (30 mg) was placed in H_2O (12 ml) and H_2O_2 (0.66 ml, 30%) added and stirred at 313 K for 2 − 3 h, to give a clear yellow solution after filtration. Water (50 ml) was added to the solution which was then lyophilized to remove all the solvent.

Yield: 18 mg (55%).

^{1}H NMR (600 MHz, 90% H_2O/10% D_2O, pH=3.8): δ = 9.12 (d, $H_{2,6}$, ^{3}J (^{195}Pt, ^{1}H) = 24 Hz, 2H), 8.56 (d, $H_{3,5}$, 2H), 6.18 (t, NH_3, ^{1}J (^{14}N, ^{1}H) = 53 Hz, ^{2}J (^{195}Pt, ^{1}H) = 52 Hz, 3H). ^{13}C NMR (150.9 MHz, D_2O): δ = 156.5 (C_4), 152.6 ($C_{2,6}$), 120.9 ($C_{3,5}$). ^{195}Pt NMR (129.4 MHz, D_2O): δ = 857.7.

LC-ESI-MS (*m/z*): $[2M + H]^+$ Calc., 909.1, Found, 909.1; $[2M - OH]^+$ Calc., 891.1, Found, 891.1

Elemental Analysis: $C_5H_9N_9O_4Pt$, Calc. C 13.22%, H 2.00%, N 27.75%, Found: C 13.06%, H 1.94%, N 27.36%.

ε_{287}=18200 L mol^{-1} cm^{-1} (H_2O)

5.2.2.8 *Cis, trans*-[Pt(N$_3$)$_2$(OH)$_2$(Bpy)] (32)

Cis, trans-[$Pt(N_3)_2(OH)_2$(Bpy)] (Bpy = 2,2′-bipyridine) was synthesized according to a reported method.[25] [$Pt(N_3)_2$(Bpy)] [26] (10 mg) was placed in H_2O_2 (10 mL, 30 %), stirred at 323 K for 1 h, and the volume of solvent was reduced on a rotary evaporator to 1~2 ml, forming a bright yellow solution (usually takes 1~2 hours). Water (50 ml) was added and the solution lyophilized to remove all the solvent. Yellow needle crystals suitable for X-ray analysis was obtained from diffusion of ether to a minimal EtOH solution of the product at 277 K. The NMR chemical shifts are consistent with the reference. [25] The maximum solubility of complex **32** in H_2O at 293 K is > 21.7 mg/ml (46.2 mM), measured by ICP-OES.

Yield: 4.8 mg (84.6%).

^{1}H NMR (D_2O): δ = 9.16 (d, $\underline{H_{6,6'}}$, ^{3}J (^{195}Pt, ^{1}H) = 24 Hz, 2H), 8.65 (d, $\underline{H_{3,3'}}$, 2H), 8.48 (t, $\underline{H_{4,4'}}$, 2H), 8.04 (t, $\underline{H_{5,5'}}$, 2H).

ESI-MS: [M + Na^+] (*m/z*) found, 492.0, calc. 492.1.

Elemental analysis: $C_{10}H_{10}N_8O_2Pt$, Calc. C 25.59%, H 2.15%, N 23.88%, Found: C 25.38%, H 2.01%, N 23.61%.

5.2.2.9 [PtCl(Tpy)]Cl · $2H_2O$ (33)

Caution. Tpy (2,2':6',2''-terpyridine) and its complexes can be absorbed through the skin. Since these compounds are toxic, gloves should always be worn.

[PtCl(Tpy)]Cl · $2H_2O$ was synthesized according to a reported method.[27] $K_2[PtCl_4]$ (415 mg, 1 mmol) was dissolved in H_2O (20 mL), Tpy (2,2':6',2''-terpyridine) (280 mg, 1.2 mmol) was added and the stirred suspension was heated at reflux for 3.5 days until a clear red solution was received. *(N.B. Prolonged heating of the clear solution may result in product disproportionation, as metallic platinum was deposited onto the sides of the flask.)* The solution was filtered to remove any unwanted solid residue, and the filtrate was evaporated on a steam bath to a volume of 4 ~ 5 ml, at which point NaCl (120 mg, 2 mmol) was added to precipitate more product. The red-orange product precipitated upon cooling and was collected by filtration and washed with 0.1 *N* HCl and acetone.

Yield: 326 mg (0.63 mmol, 63%).

^{1}H NMR (400 MHz, D_2O) δ = 8.28 ~ 8.18 (5H), 8.04 (d, 4H), 7.55 (t, 2H). For discussion of NMR chemical shift see **Section 5.4.2**.

ESI-MS (*m/z*): $[M - 2H_2O - Cl]^+$: Calc., 463.0; Found, 463.0.

Elemental Analysis: $C_{15}H_{15}Cl_2N_3O_2Pt$, Calc., C, 33.66%; H, 2.82%; N, 7.85%; Found, C, 33.52%; H, 2.70%; N, 7.74%.

5.2.2.10 $[Pt(N_3)(Tpy)]PF_6$ (34)

$[Pt(N_3)(Tpy)]PF_6$ was synthesized according to the reported method.[28, 29] To an aqueous solution of [PtCl(Tpy)]Cl · $2H_2O$ (52 mg, 0.1 mmol) was added NaN_3 (13 mg, 0.2 mmol). A transparent deep red solution was precipitated. Upon addition of

NH_4PF_6 (32 mg, 2 mmol), an orange solid was obtained, which was collected by filtration, washed with H_2O and dried under vacuum.

Yield: 53 mg (92.3 %).

^{1}H NMR (400 MHz, acetone-d_6): δ = 8.82 ~ 8.61 (9H), 8.14 (d, 2H).

ESI-MS: $[M - PF_6]^+$: (*m/z*) found, 470.0; calc., 470.1.

5.2.2.11 [Pt(N$_3$)(Tpy)]N$_3$ (35)

$[Pt(N_3)(Tpy)]N_3$ was synthesized according to the reported method.[29] To an aqueous solution of $[PtCl(Tpy)]Cl \cdot 2H_2O$ (52 mg, 0.1 mmol) was added NaN_3 (130 mg, 2 mmol, 20 mol equiv). A red solid was produced. The mixture was stirred for a further 30 min after which the precipitate was collected by filtration, washed with minimal cold H_2O and dried under vacuum. The ^{1}H NMR was assigned with the assistance of 2D [^{1}H-^{1}H] CODY NMR spectroscopy.

Yield: 30 mg (60.5 %).

^{1}H NMR (600 MHz, D_2O): δ = 8.24 ~ 8.21 (t, $\underline{H_{4', 4, 4''}}$, 3H), 8.00 ~ 7.97 (t, $\underline{H_{3', 5', 3, 3''}}$, 4H), 7.72 (d, $\underline{H_{6, 6''}}$, 2H), 7.59 (t, $\underline{H_{5, 5''}}$, 2H). ^{13}C NMR (150.9 MHz, D_2O): δ =, 157.7 ($\underline{C_{2, 2''}}$); 153.9 ($\underline{C_{2', 6'}}$), 149.6 ($\underline{C_{6, 6''}}$), 143.7 ($\underline{C_{4, 4''}}$), 143.0 ($\underline{C_{4'}}$), 130.0 ($\underline{C_{5, 5''}}$), 126.2 ($\underline{C_{3, 3''}}$), 124.6 ($\underline{C_{3', 5'}}$). ^{195}Pt NMR (129.4 MHz, D_2O): δ = −2620.

ESI-MS (*m/z*): $[M - N_3]^+$: Calc., 470.1; Found, 470.0.

5.2.2.12 *Trans*-[Pt(N$_3$)(OH)$_2$(Tpy)] Cl (36)

$[Pt(N_3)(Tpy)]PF_6$ (31 mg, 0.05 mmol) was placed in H_2O_2 (25 ml, 30% aqueous solution) and stirred at 323 K for 1 h, and then the volume of solvent was reduced on a rotary evaporator to *ca.* 5 ml, forming a bright yellow solution (*ca.* 1 – 2 hours). (*The temperature was maintained below 323 K to avoid decomposition.)* Water (50 ml) was added and the solution was lyophilized to remove all the solvent. The

residue was purified by semi-preparative HPLC (see **Section 5.3.2.2**). The fraction was collected, HCl was added to adjust pH to *ca.* 0, and the solution was then lyophilized to remove TFA and all solvents. The ^{1}H NMR was assigned with the assistance of 2D [^{1}H-^{1}H] COSY NMR spectroscopy.

Yield: 10 mg (24%).

^{1}H NMR (400 MHz, D_2O): δ = 9.02 (d, $\underline{H_{6,\,6''}}$, ^{3}J (^{195}Pt, ^{1}H) = 24 Hz, 2H), 8.80 ~ 8.71 (m, $\underline{H_{3',\,5',\,4',\,3,\,3''}}$, 5H), 8.61 (t, $\underline{H_{4,\,4''}}$, 2H), 8.16 (t, $\underline{H_{5,\,5''}}$, 2H). ^{13}C NMR (150.9 MHz, D_2O): δ = 157.4 ($\underline{C_{2,\,2''}}$); 152.9 ($\underline{C_{2',\,6'}}$), 151.3 ($\underline{C_{6,\,6''}}$), 146.4 ($\underline{C_{4'}}$), 145.7 ($\underline{C_{4,\,4''}}$), 131.2 ($\underline{C_{5,\,5''}}$), 128.6 ($\underline{C_{3,\,3''}}$), 127.4 ($\underline{C_{3',\,5'}}$). ^{195}Pt NMR (129.4 MHz, D_2O): δ = 454.1.

ESI-MS (*m/z*): $[M - Cl]^{+}$: Calc., 504.0; Found, 504.1.

Elemental analysis: $C_{15}H_{13}ClN_6O_2Pt$, Calc. C 33.37%, H 2.43%, N 15.57%, Found: C 33.46%, H 2.54%, N 15.36%.

5.2.2.13 [$PtCl_2$(COD)] (37)

[$PtCl_2$(COD)] was synthesized according to the reported method.[30] To a 10 ml aqueous solution of $K_2[PtCl_4]$ (415 mg, 1 mmol), 10 ml acetic acid and 0.41 ml of 1, 5-cyclooctadiene (COD) were added. The mixture was stirred rapidly and heated to 363 K. Over 30 min, the deep red solution slowly became pale yellow and fine crystals were deposited. The volume was reduced to 5 ml on a rotary evaporator and the solution filtered to collect the light yellow needles. The product was washed successively with H_2O, ethanol and diethyl ether and then dried at 373 K for 60 min. *N.B., COD is volatile and pungent, so manipulations of COD should always be done in a fume hood.* The spectroscopy data for the product were consistent with those reported. [30]

Yield: 328 mg (81%).

^{1}H NMR (400 MHz, $CDCl_3$): δ = 5.62 (C$\underline{H}$, 4H), 2.71, 2.27 (C$\underline{H_2}$, 8H).

5.2.2.14 [PtCl(TTpy)]Cl (38)

This compound was synthesized using a slightly modified method from the literature.[30-32] 37.4 mg Pt[Cl_2(COD)] was suspended in 5 ml MeOH, and 32.3 mg TTpy was added. The mixture was heated at 333 K overnight, until the white powder in solution disappeared and only orange precipitate remained. The orange precipitate was collected by filtration, washed successively with H_2O, ethanol and diethyl ether and then dried under vacuum. The spectroscopic data are consistent with those reported.[30-32]

Yield: 45 mg (76.4%).

^{1}H NMR (400 MHz, DMSO-d_6): δ = 9.00 (s, $\underline{H_{3', 5'}}$, 2H), 8.95 (d, $\underline{H_{6, 6''}}$, 2H), 8.88 (d, $\underline{H_{3, 3''}}$, 2H), 8.55 (t, $\underline{H_{4, 4''}}$, 2H), 8.15 (d, tolyl-$\underline{H_{2, 6}}$, 2H) 7.97 (t, $\underline{H_{5, 5''}}$, 2H), 7.50 (d, tolyl-$\underline{H_{3, 5}}$, 2H), 2.44 (s, tolyl-C$\underline{H}_3$, 3H).

ESI-MS (*m/z*): $[M - Cl]^+$: Calc., 553.1; Found, 553.0.

5.2.2.15 [Pt(N_3)(TTpy)]N_3 (39)

Trans-[PtCl(TTpy)]Cl (30 mg, 0.05 mmol) was suspended in 5 ml DMF, and NaN_3 (65 mg, 1 mmol, 20 mole equivalent) was added. The mixture was stirred at room temperature, and then the orange precipitate was collected by filtration and was washed successively with H_2O, ethanol and diethyl ether. The product was then dried under vacuum.

^{1}H NMR (400 MHz, DMSO-d_6): δ = 8.70 (s, $\underline{H_{3', 5'}}$, 2H), 8.67 (d, $\underline{H_{3, 3''}}$, 2H), 8.37 (t, $\underline{H_{4, 4''}}$, 2H), 8.21 (d, $\underline{H_{6, 6''}}$, 2H), 7.94 (d, tolyl-$\underline{H_{2, 6}}$, 2H) 7.84 (t, $\underline{H_{5, 5''}}$, 2H), 7.37 (d, tolyl-$\underline{H_{3, 5}}$, 2H), 2.43 (s, tolyl-C$\underline{H}_3$, 3H). ^{13}C NMR (150.9 MHz, DMSO-d_6): δ = 157.7 ($\underline{C_{2, 2''}}$); 153.5 ($\underline{C_{2', 6'}}$), 152.3 ($\underline{C_{4'}}$), 149.1 ($\underline{C_{6, 6''}}$), 142.6 ($\underline{C_{4, 4''}}$), 142.2 (tolyl-$\underline{C_4}$),

131.1 (tolyl-$\underline{C_1}$), 130.0 (tolyl-$\underline{C_{3,5}}$), 129.2 ($\underline{C_{5,5''}}$), 127.7 (tolyl-$\underline{C_{2,6}}$), 126.1 ($\underline{C_{3,3''}}$), 120.3 ($\underline{C_{3',5'}}$), 21.1(tolyl-$\underline{C}H_3$). ^{195}Pt NMR (129.4 MHz, DMSO-d_6): δ = −2631.2.

ESI-MS (*m/z*): $[M - N_3]^+$: Calc., 560.1; Found, 560.0.

Elemental Analysis: $C_{22}H_{19}N_9OPt$ (M + H_2O), Found, C, 42.31%; H, 3.04%; N, 19.93%; Calc., C, 42.58%; H, 3.09%; N, 20.32%.

5.2.2.16 *Trans*-[Pt(N_3)$(OH)_2$(TTpy)]Cl (40)

[Pt(N_3)(TTpy)]N_3 (5 mg) was placed in H_2O_2 (5 ml, 30%) and stirred at 313 K for 14 h, before forming a clear yellow solution. Water (50 ml) was added to the solution which was then lyophilized to remove all the solvent. The residue was purified by semi-preparative HPLC. The fraction was collected, HCl was added to adjust the pH to 0, and the solution was then lyophilized to remove TFA and all solvents.

Yield: 2 mg (38%).

ESI-MS (*m/z*): $[M - Cl]^+$: Calc., 594.1; Found, 594.1.

^{1}H NMR (600 MHz, D_2O): δ = 9.03 (d, $\underline{H_{6,6''}}$, 2H), 8.99 (s, $\underline{H_{3',5'}}$, 2H), 8.78 (d, $\underline{H_{3,3''}}$, 2H), 8.63 (t, $\underline{H_{4,4''}}$, 2H), 8.16 (t, $\underline{H_{5,5''}}$, 2H), 7.98 (d, tolyl-$\underline{H_{2,6}}$, 2H), 7.57 (d, tolyl-$\underline{H_{3,5}}$, 2H), 2.50 (s, tolyl-C$\underline{H}_3$, 3H). ^{13}C NMR (150.9 MHz, D_2O): δ = 158.6 ($\underline{C_{2,2''}}$); 157.6 ($\underline{C_{2',6'}}$), 152.5 ($\underline{C_{4'}}$), 151.3 ($\underline{C_{6,6''}}$), 145,7 ($\underline{C_{4,4''}}$), 144.3 (tolyl-$\underline{C_4}$), 132.3 (tolyl-$\underline{C_1}$), 131.1 (tolyl-$\underline{C_{3,5}}$), 130.7 ($\underline{C_{5,5''}}$), 128.9 (tolyl-$\underline{C_{2,6}}$), 128.4 ($\underline{C_{3,3''}}$), 124.6 ($\underline{C_{3',5'}}$), 21.2(tolyl-$\underline{C}H_3$).

Elemental analysis: $C_{22}H_{20}ClN_6O_2Pt$, Calc. C 41.88%, H 3.19%, N 13.32%, Found: C 41.98%, H 3.54%, N 13.36%.

5.3 Results

5.3.1 Pt 4-nitropyridine complexes

5.3.1.1 X-ray crystallography

The solid state structures of *trans*-[$PtCl_4(NH_3)$(4-NO_2-Py)]·H_2O **(28 · H_2O)** and *trans*-[$Pt(N_3)_2(NH_3)$(4-NO_2-Py)] (**30**) were determined by single crystal X-ray crystallography, **Figure 5.2**. X-ray data are listed in **Table 5.1**. The geometry of **28 · H_2O** is octahedral and the Pt-Cl and Pt-N bond lengths do not differ significantly from those of published tetrachlorido Pt^{IV} complexes.[23, 33] The asymmetric unit contains a Pt complex and a molecule of water. In the crystal, two symmetry-related complexes are bridged by two waters, hydrogen bonded to the coordinated ammonia. This tetrameric unit lies on an inversion centre as illustrated in **Figure 5.3**.

In the structure of **30**, there are three crystallographically independent complexes in the asymmetric unit. One complex lies on a general position (Pt1, as shown in Figure S2b) and two on special positions (Pt2 and Pt3) on a two-fold axis. The Pt atom in this structure adopts a square-planar geometry, and the Pt–N bond lengths and angles are similar to those of published Pt^{II} diazido compounds.[34] The nitrogens in N_3 groups are essentially linear, with the N–N–N angle between 173° and 175°, which again agrees very well with the angles in previous published structures. One of the coordinated 4-nitropyridines (N301 – O309 in Pt3 complex) was disordered about the two fold axis. Initially attempts were made to restrain the ring on the axis but this led to an unstable refinement. The pyridine was refined using 1-2 and 1-4 distance restraints to keep it as an idealised six-membered ring. The nitro group was also refined with distance restraints and the whole pyridine ligand refined as disordered

about the two fold axis at 50% occupancy (**Figure 5.4**). The thermal parameters of the disordered pyridine were also restrained with SIMU restraints. The hydrogens on the coordinated ammonias (N116, N210 and N313) could not be located so were placed at calculated positions and refined with a riding model. Interestingly, in two of the complexes **30** (Pt1 and Pt2), the nitro groups are not within the pyridine plane but are twisted out of the plane with dihedral angle of 18° and 23° for N107 and N205, respectively. However, in the structure of **28 · H_2O**, this torsion is only 2°, which indicates that the nitro groups are essentially in the plane of pyridine. Previous reports showed that in the structure of free 4-nitropyridine ligand, the nitro group is coplanar with the pyridine ring plane.[35, 36] However, in the corresponding metal complexes, the angle of twist varies.[36, 37] It is reasonable to attribute the reason for the twist of nitro group to a crystal packing effect.

Table 5.1 Crystal structure data for the Pt complexes *trans*-[$PtCl_4(NH_3)$(4-NO_2-Py)] · H_2O (**28 ··H_2O**) and *trans*-[$Pt(N_3)_2(NH_3)$(4-NO_2-Py)] (**30**)

	28 ··H_2O	**30**
Empirical formula	$C_5H_9Cl_4N_3O_3Pt$	$C_{10}H_{14}N_{18}O_4Pt_2$
Formula weight	496.04	840.57
Crystal description	Block	Block
Crystal colour	Yellow	Yellow
Crystal system	Triclinic	Monoclinic
Space group	*P*-1	*C*2/*c*
a (Å)	6.8498(2)	13.5983(2)
b (Å)	9.4307(4)	27.6494(8)
c (Å)	11.0158(5)	11.3576(4)
α (°)	107.784(4)	90
β (°)	95.782(3)	94.651(2)
γ (°)	106.259(3)	90
Volume ($Å^3$)	636.85(4)	4256.2(2)

Z	2	8
Measurement temp.(K)	100(2)	100(2)
lambda	0.71073 A	0.71073 A
D_{calcd} (Mg/m^3)	2.587	2.624
F (000)	460	3104
μ_{calcd} (mm^{-1})	11.849	13.196
θ Range (°)	<29.38	<29.95
Reflections collected	11284	20852
Independent reflections	3160	5485
Goodness-of-fit F^2	1.058	1.071
Conventional *R1*	0.0166	0.0231
wR_2	0.0386	0.0509

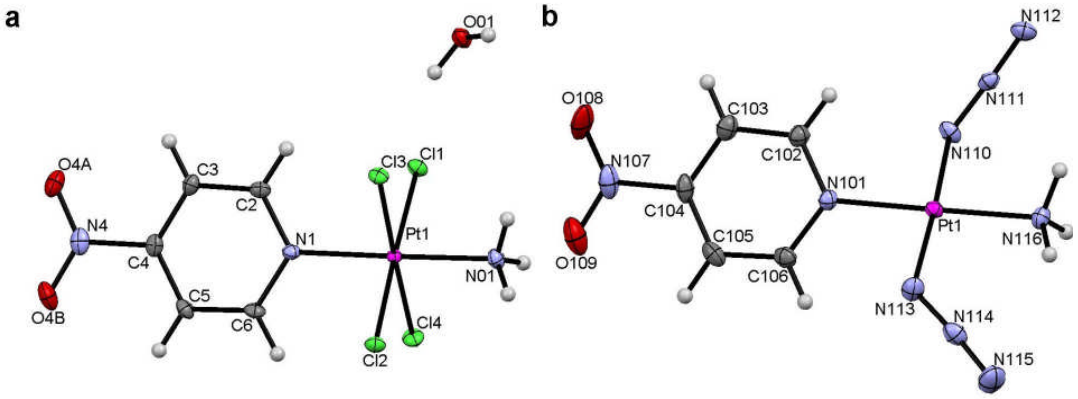

Figure 5.2 X-ray crystal structure of complexes (**a**) *trans*-[$PtCl_4(NH_3)(4\text{-}NO_2\text{-}Py)$]·$H_2O$ (**28 · H_2O**) and (**b**) *trans*-[$Pt(N_3)_2(NH_3)(4\text{-}NO_2\text{-}Py)$] (**30,** Pt1 complex) with ORTEP ellipsoids set at 50% probability (100 K).

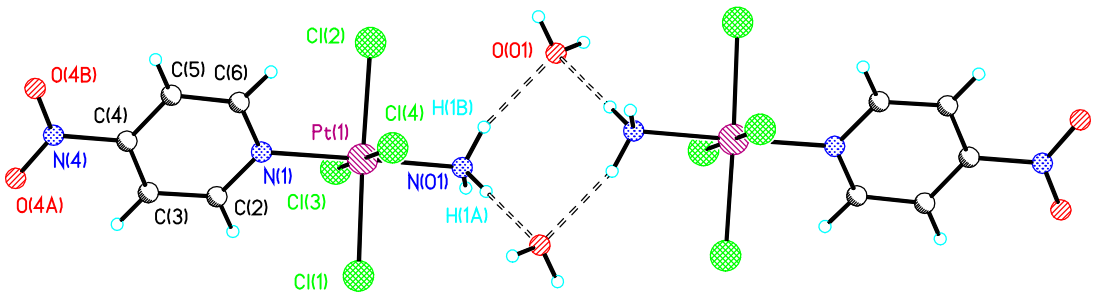

Figure 5.3 A water-bridged tetrameric unit that lies on an inversion centre in the solid state structure of **28 · H_2O**. The H-bonds are indicated by dash lines.

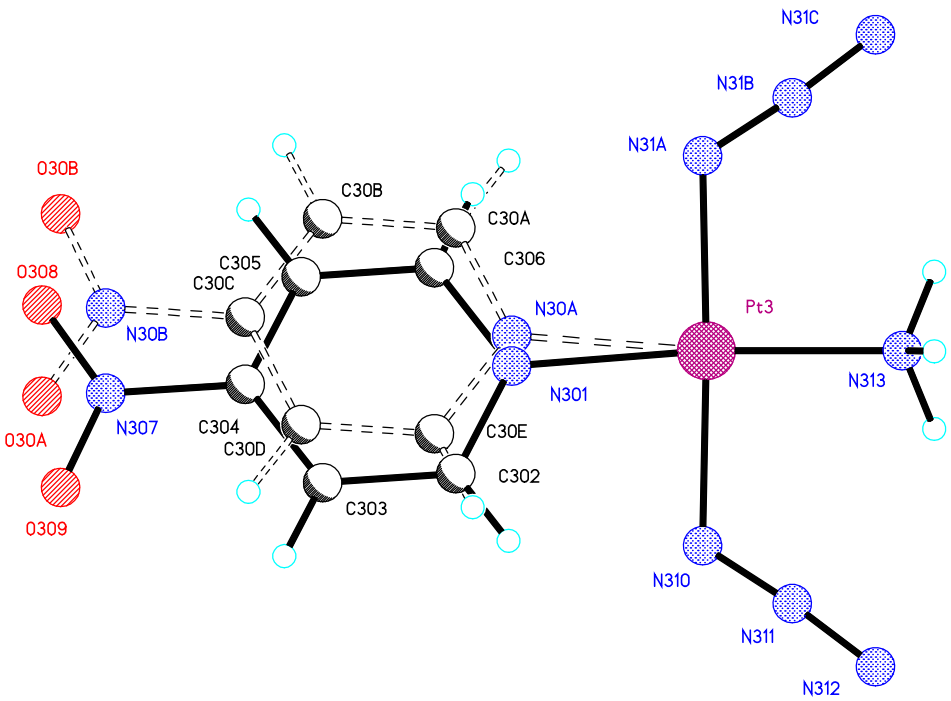

Figure 5.4 The disorder of the 4-nitopyridine ligand in one of the molecules (Pt3 complex) in the solid state structure of *trans*-[Pt(N_3)$_2$(NH_3)(4-NO_2-Py)] **30** showing the two orientations of the 4-nitropyridine ligand about the 2-fold axis. There is a 50:50 occupancy of the two orientations, one drawn with solid lines and one with dashed lines.

5.3.1.2 ^{195}Pt NMR characterization

The ^{195}Pt NMR spectra for complexes **28** – **31** were assigned in accordance with published data.[11, 23, 24, 38, 39] (**Figure 5.5**). The ^{195}Pt chemical shifts of complexes **28**, **29**, **30** and **31** are −354.3 ppm, −2023.2 ppm, −2135.9 ppm and 857.7 ppm, respectively, which are consistent with corresponding *trans*-{$Pt^{IV}Cl_4N_2$}, *trans*-{$Pt^{II}Cl_2N_2$}, {$Pt^{II}N_4$}, *trans*-{$Pt^{IV}N_4O_2$} species.

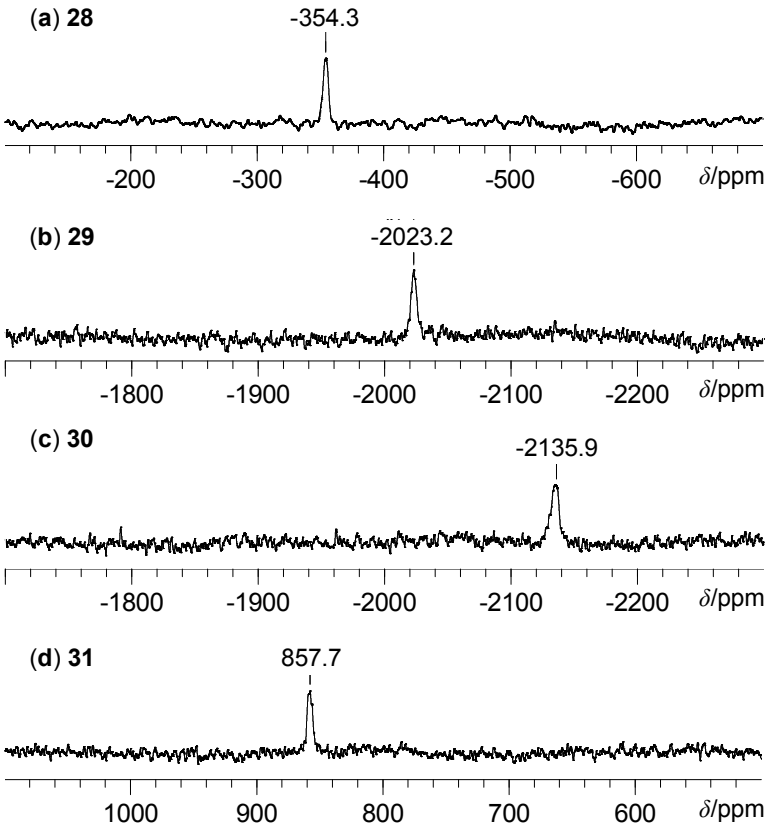

Figure 5.5 ^{195}Pt NMR (129.4 MHz, 298 K) spectra of complexes (**a**) *trans*-[$PtCl_4(NH_3)(4\text{-}NO_2\text{-}Py)$] (**28**); (**b**) *trans*-[$PtCl_2(NH_3)(4\text{-}NO_2\text{-}Py)$] (**29**); (**c**) *trans*-[$Pt(N_3)_2(NH_3)(4\text{-}NO_2\text{-}Py)$] (**30**); (**d**) *trans, trans, trans*-[$Pt(N_3)_2(OH)_2(NH_3)(4\text{-}NO_2\text{-}Py)$] (**31**).

5.3.1.3 Photodecomposition study

In the UV-Vis spectrum of complex **31** *trans,trans,trans*-[$Pt(N_3)_2(OH)_2(NH_3)(4\text{-}NO_2\text{-}Py)$] in aqueous solution (**Figure 5.6a**), there is an absorbance maximum at 287 nm (ε_{287}=18200 L mol^{-1} cm^{-1} in H_2O), which is assigned to a ligand (azide)-to-metal (Pt^{IV}) charge-transfer (LMCT) transition. The absorption intensity at > 400 nm is very small and no absorption was observed above 540 nm. When the sample was irradiated at 365 nm, the major absorption band decreased in intensity, indicating the cleavage of the Pt^{IV}-azide bonds (**Figure 5.6a**). For the purpose of investigating the relationship between the wavelength of irradiation and photodecomposition of **31** in

aqueous solution, an "action spectrum" was determined.[12, 40] The action spectrum recorded the rate of photodecomposition of the molecule upon the exposure to light of wavelength 365 to 540 nm. The pseudo quantum yield (Φ) (ratio of the number of photo reactions to the number of incident photons) was determined (**Figure 5.6b**, **Table 5.2** and **Table 5.3**). The pseudo quantum yield Φ for photolysis of complex **31** upon irradiation from 365 nm to 520 nm correlated closely with the extinction coefficient at that wavelength. At irradiation wavelengths > 540 nm (including 600 nm, 633 nm, 660 nm and 700 nm), the extent of photolysis was too small to detect under the experimental conditions used.

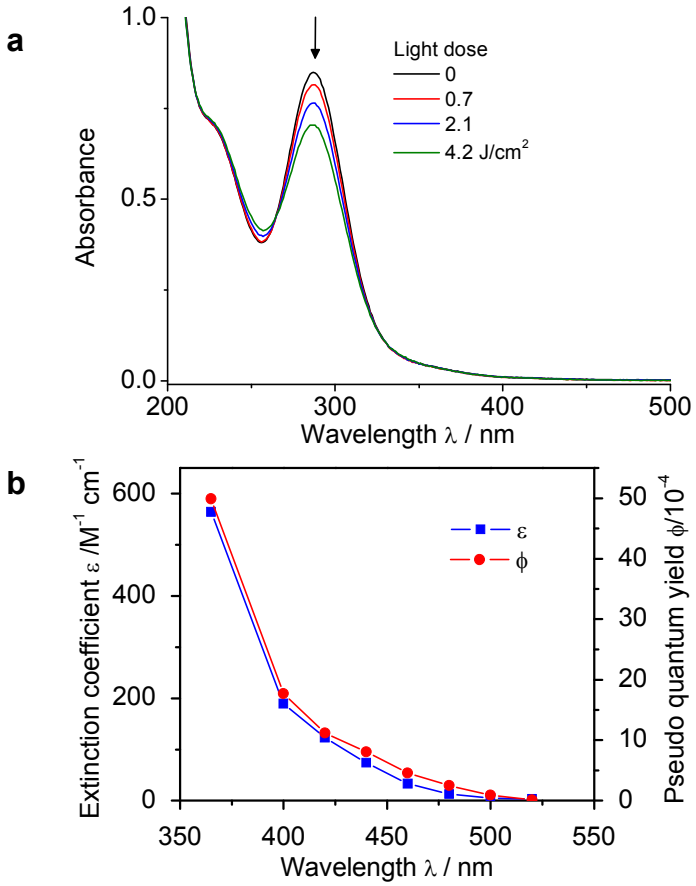

Figure 5.6 (**a**) UV-Vis spectra for **31** in H_2O upon irradiation at 365 nm. (**b**) Pseudo quantum yield Φ (red, circles) of action spectrum (wavelength-dependent photodecomposition) for **31**, in comparison with extinction coefficient ε (blue, squares). The data points are the average of two experiments.

Table 5.2 Pseudo quantum yields for photodecomposition of complex **31** at different wavelengths.

Wavelength λ (nm)	Reaction rate d*A*/d*t* ($\times 10^{-3}$)	Reaction rate d*c*/d*t* ($\times 10^{-9}$)	Incident photons ($\times 10^{-9}$ einstein/s)	Pseudo quantum yield Φ ($\times 10^{-3}$)
365	4.8	4.49	0.540	4.99
400	2.5	2.34	0.795	1.77
420	1.9	1.78	0.955	1.12
440	1.45	1.36	1.01	0.804
460	1.1	1.03	1.35	0.459
480	0.6	0.56	1.35	0.249
500	0.3	0.28	1.87	0.090
520	0.01	0.094	4.23	0.013

Table 5.3 Extinction coefficients of **31** at different wavelengths from a 3.12 mM aqueous solution (298 K). (The extinction coefficient is low at λ > 400 nm so higher concentrations allow a more accurate measurement).

Wavelength (nm)	Absorption	Extinction Coefficient ε (M^{-1} cm^{-1})
365	1.7601	564.1
400	0.5906	189.3
420	0.3833	122.8
440	0.2305	73.87
460	0.1031	33.05
480	0.03935	12.61
500	0.01628	5.219
520	0.00977	3.133

5.3.1.4 Action spectrum for *trans, trans, trans*-[Pt(N$_3$)$_2$(OH)$_2$(Py)$_2$] (24)

The wavelength-dependent photodecomposition action spectrum for *trans, trans, trans*-[Pt(N$_3$)$_2$(OH)$_2$(Py)$_2$] (**24**) was also measured using the same method as described above. Complex **24** has been reported to be a very potent photoactivatable anticancer compound.[12] The purpose of this experiment is to compare the difference between the UV-Vis absorption spectrum and the rate of photodecomposition at the corresponding wavelengths. The result shows that the difference is negligible.

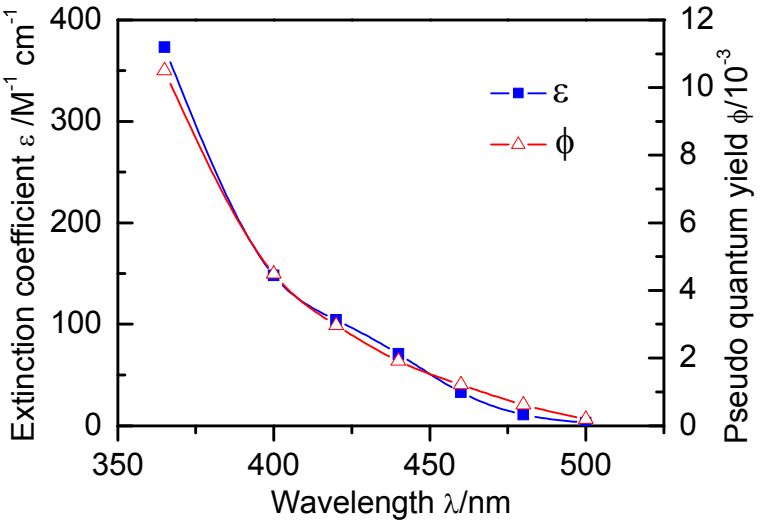

Figure 5.7 Pseudo quantum yield Φ (red, triangles) of action spectrum (wavelength-dependent photodecomposition) for **24**, in comparison with extinction coefficient ε (blue, squares). The data points are the average of two experiments.[12]

5.3.2 Pt 2,2'-bipyridine complexes

5.3.2.1 X-ray crystallography

The crystal structure of complex *cis, trans*-[Pt(N$_3$)$_2$(OH)$_2$(Bpy)] (**32**) was obtained as shown in **Figure 5.8**, and the data are listed in **Table 5.4**. The crystal system is orthorhombic and the space group is *Pbcn*. The asymmetric unit contained only half of the complex (half a Pt, half a Bpy, one OH and one azido). The Pt atom adopts

octahedral geometry and lies on a two-fold axis that relates the two azides and two hydroxides and runs through the phenyl-phenyl bond. There is a $\pi - \pi$ stacking interaction between two Bpy ligands related by an inversion centre, so mean planes through the interacting π systems are parallel (**Figure 5.9**). The $\pi - \pi$ stacking interaction adopts "face-to-face" geometry and the centroid-centroid distance between two pyridine planes is 3.70 Å, which suggests it a medium-strong interaction. There are several intra- and inter-molecular short contacts as shown in **Figure 5.10**. The inter-molecular H-bonds (2.18 Å) are of medium strength.

Table 5.4 Crystal structure data for complex *cis, trans*-$[Pt(N_3)_2(OH)_2(Bpy)]$ (**32**)

	32
Empirical formula	$C_{10}H_{10}N_8O_2Pt$
Formula weight	469.35
Crystal description	Block
Crystal colour	Yellow
Crystal system	Orthorhombic
Space group	*Pbcn*
a (Å)	13.4268(3)
b (Å)	9.5430(2)
c (Å)	9.9701(2)
α (°)	90
β (°)	90
γ (°)	90
Volume ($Å^3$)	1277.49(5)
Z	4
Measurement temp.(K)	100(2)
lambda	0.71073 A
D_{calcd} (Mg/m^3)	2.440
F (000)	880
μ_{calcd} (mm^{-1})	11.004
θ Range (°)	<32.59
Reflections collected	15261
Independent reflections	2239
Goodness-of-fit F^2	0.920
Conventional *R1*	0.0141
wR_2	0.0345

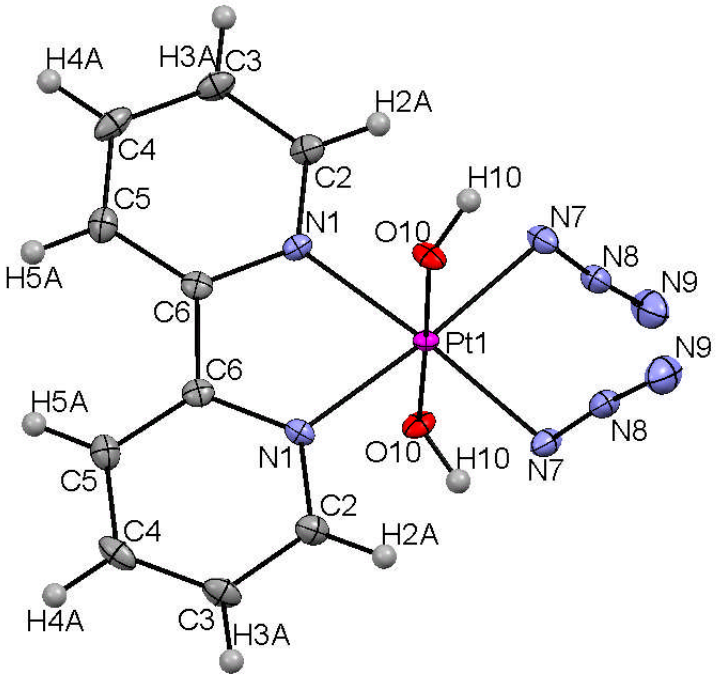

Figure 5.8 X-ray crystallographic structure of *cis, trans*-[$Pt(N_3)_2(OH)_2(Bpy)$] (**32**) with ellipsoids set at 50% probability. (100 K)

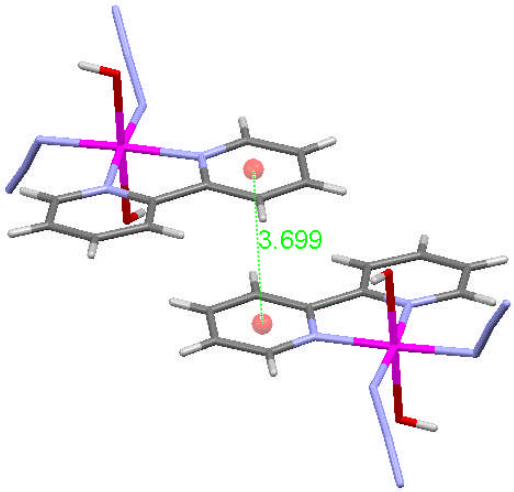

Figure 5.9 The "face-to-face" $\pi - \pi$ stacking interactions in structure of complex **32** between two parallel Bpy ligands related by an inversion centre (centroid-centroid distance, 3.699 Å).

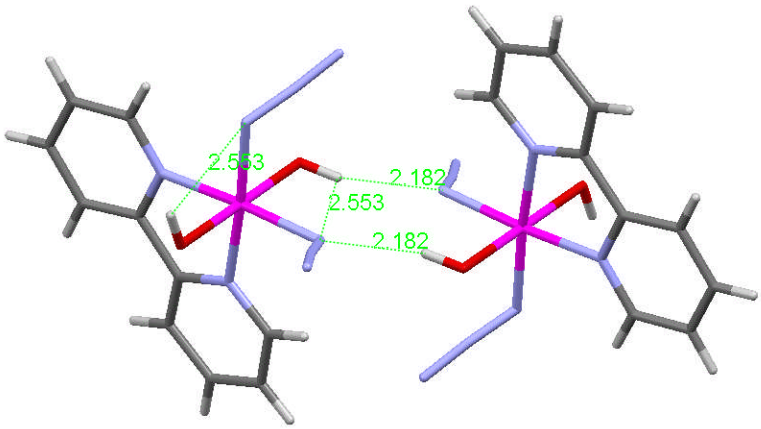

Figure 5.10 Intra- and inter-molecular H-bonds network formed by azido and hydroxido ligands in the structure of complex **32** which determines the orientation of the azido ligands.

5.3.2.2 HPLC purification test

Before the cytotoxicity test are carried out, it is important to ensure the purity of products > 95%. HPLC is a practical method to examine the purity of products. The HPLC purity of *cis, trans*-[$Pt(N_3)_2(OH)_2$(Bpy)] (**32**) was determined. All the other compounds in this work were also studied by similar methods. The HPLC chromatogram for complex **32** is shown in **Figure 5.11**. The detecting wavelength was set up at 254nm, so most of the organic and inorganic compounds could be detected. The percentage of each species was measured by the integration of each peak, (assume the ε_{254} for all species are similar) which was automatically calculated by the workstation. A blank sample was also run for comparison.

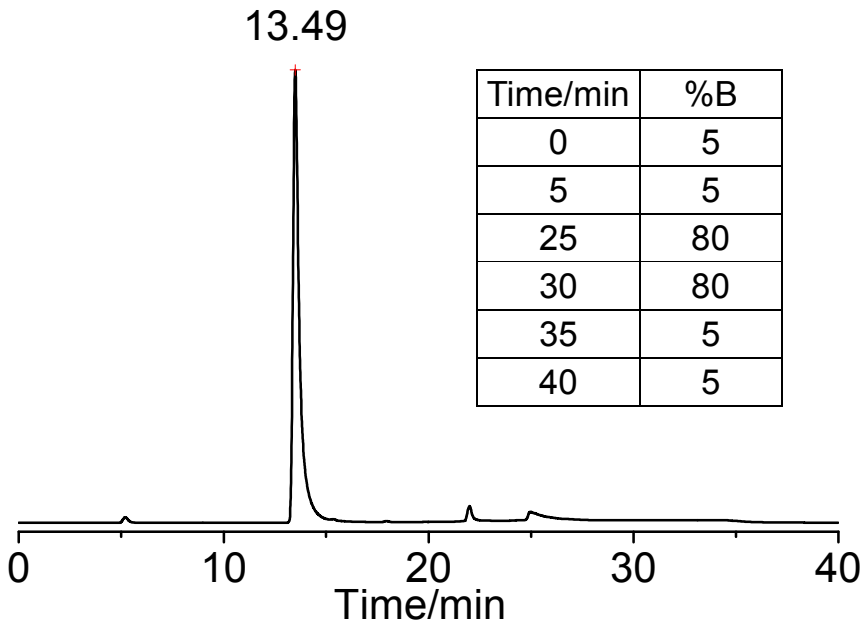

Figure 5.11 HPLC chromatogram for complex *cis, trans*-[Pt(N$_3$)$_2$(OH)$_2$(Bpy)] (**32**) based on peak areas. Purity is > 95%. HPLC conditions: HP1100 series. Column: Polymer Laboratories, PLRP-S, 250×4.6 mm, 100 Å, 5 μm. Flow rate, 1.00 ml/min. Wavelength: 254 nm. Mobile phases A, H_2O, 0.1% TFA; B, MeOH, 0.1% TFA. Insertion is the gradient of mobile phases used.

5.3.2.3 Photoactivation

UV-Vis spectroscopy is a quick and sensitive method to examine the photodecomposition of Pt^{IV} diazidodihydroxido complexes upon irradiation with various light sources. The aim of this chapter is discover Pt^{IV} complexes that can be activated with longer wavelengths. Therefore, the photoactivation of complex *cis, trans*-[Pt(N$_3$)$_2$(OH)$_2$(Bpy)] (**32**) was carried out upon irradiation with UVA (λ_{max} = 365 nm, 5.0 mW/cm^2), light of 450 nm (50 mW/cm^2) and 517 nm (25 mW/cm^2) in water at 298 K.

As shown in **Figure 5.12** (black curves), in the absence of light, the solution of complex **32** in water has three major absorption bands at 251, 303 and 315 nm. The

absorbance at wavelengths longer than 460 nm is close to zero. The intensity of major absorption bands decreased upon irradiation with UVA or at 450 nm, which is due to the photolysis of **32**. A lower dose of UVA irradiation induced the decomposition of complexes faster than a higher dose of 450 nm light, which is consistent with their extinction coefficients at these wavelengths. Interestingly, a small absorption band around 370 nm increased during the experiment, but it did not accelerate the rate of photodecomposition at this band. The photodecomposition of complex **32** upon irradiation at 517 nm was not observed, which is likely due to its extinction coefficient at this wavelength being close to zero.

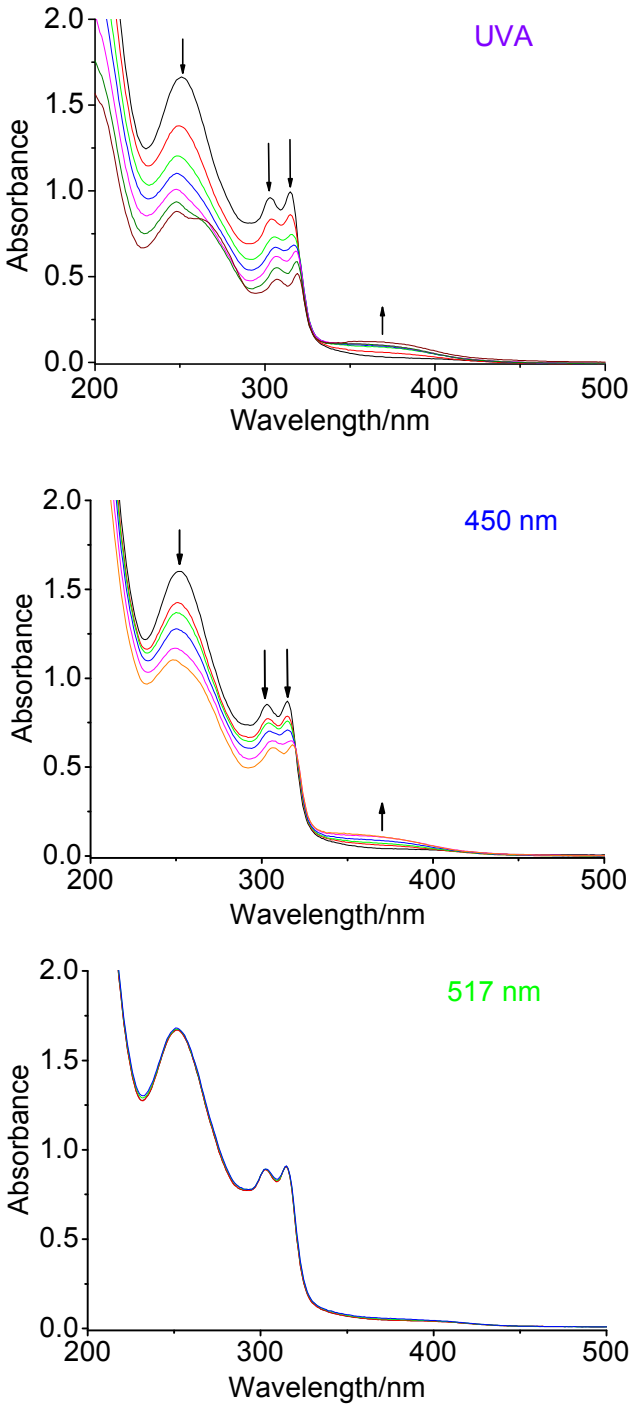

Figure 5.12 Photoactivation of complex *cis, trans*-[$Pt(N_3)_2(OH)_2(Bpy)$] (**32**) in H_2O upon irradiation with UVA (0, 1, 2, 3, 5, 15, 60 min), 450 nm (0, 10, 15, 30, 60, 120 min) and 517 nm (0, 5, 30, 60 min) (298 K).

5.3.3 Pt terpyridine complexes

5.3.3.1 HPLC purification

Difficulty was encountered in the synthesis of *trans*-$[Pt(N_3)(OH)_2(Tpy)]^+$ species. Pure product could not be easily obtained (see **section 5.4.1.3** for discussion), hence semi-preparative HPLC separation was used to purify this product.

First, LC-MS was carried out to analyse all the species in the product. The chromatogram and assignment of the species are summarized in **Figure 5.13** and **Table 5.5**. The peak at retention time 4.95 min is the desired product and was collected by semi-preparative HPLC. After the fraction was collected, HCl was added to adjust the pH to *ca.* 0 and the solution was then lyophilized twice to remove TFA (pK_a = 0.23) and all solvents. An ^{19}F NMR spectrum was recorded to examine if the residual TFA was all removed.

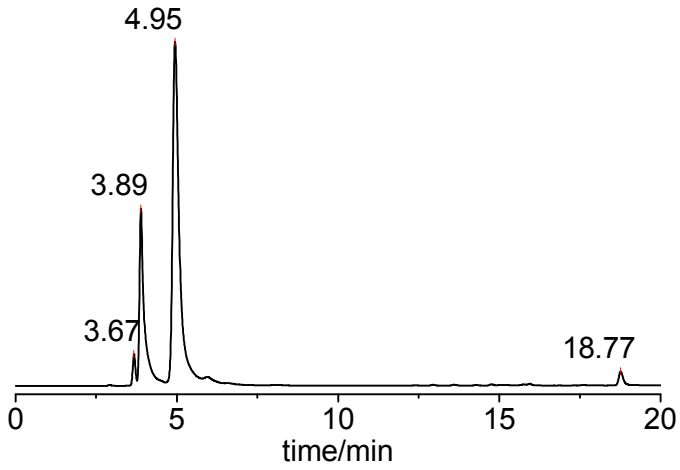

Figure 5.13 Typical HPLC chromatogram for **36** raw product. Semi-preparative HPLC was used to purify the product. The peak at retention time of 4.95 min was collected. HPLC conditions: HP1100 series. Column: Agilent ZORBAX Eclipse XDB-C18, 9.4 × 250 mm, 5 μm. Flow rate, 2 ml/min. Detection wavelength: 254 nm. Mobile phase A, H_2O with 0.1% TFA; B, MeOH with 0.1% TFA. The gradient used is the same as shown in **Figure 5.11**.

Table 5.5 LC-MS data for the unpurified product complex **36**.

r.t.	*m/z* (with Pt isotopes)	Assignment
3.67	479.0	$Pt[(OH)_3(Tpy)]^+$
3.89	445.0	$Pt[(OH)(Tpy)]^+$
	463.0	$Pt[Cl(Tpy)]^+$
	495.0	$Pt[(OH)_2(OOH)(Tpy)]^+$
4.95	504.0	$Pt[(N_3)(OH)_2(Tpy)]^+$
18.77	470.0	$Pt[(N_3)(Tpy)]^+$

After purification, HPLC analysis was carried to determine the purity of the final product. The chromatogram is shown in **Figure 5.14**. Compared to **Figure 5.13**, the major product of complex **36** was successfully isolated.

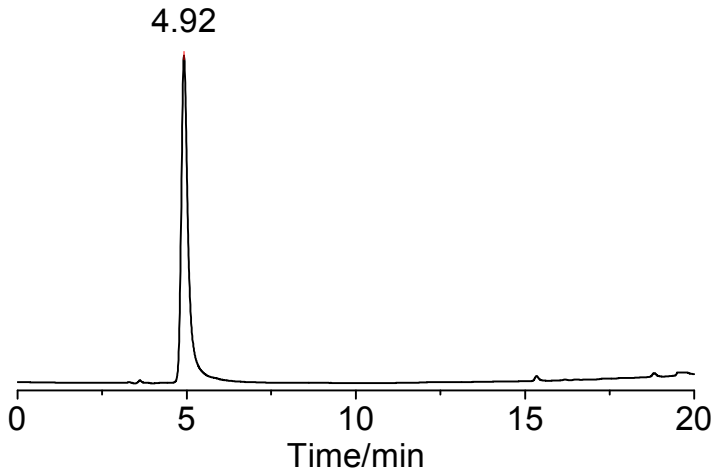

Figure 5.14 Product of complex **36** after HPLC purification. The purity was >95%. The same HPLC method was used as that in **Figure 5.13**.

5.3.3.2 Photolysis of Pt-Tpy complexes

Trans-$[Pt(N_3)(OH)_2(Tpy)]Cl$ (**36**) is photoactivatable. UV-Vis spectroscopy was used to follow the photodecomposition. **Figure 5.15a – c** show the UV-Vis spectra recorded for **36** in H_2O upon irradiation with UVA, light of 450 nm and 517 nm.

Before irradiation with light, the solution of complex **36** in water has three major absorption bands at 273, 339 and 355 nm (black curves in **Figure 5.15a** – **c**). The absorbance over 400 nm is small, but the low absorption extends up to *ca.* 530 nm. The intensity of major absorption bands decreased upon irradiation with the three light sources above, which is due to the photolysis of **36**. Further research is needed to explore the detail mechanism of the photoreaction. It was not a surprise to observe that a lower dose of UVA irradiation induced the decomposition of complexes faster than a much higher dose of 450 nm or 517 nm; hence this is consistent with their different extinction coefficients at these wavelengths.

The three major absorption bands of complex **36** at 273, 339 and 355 nm vanished upon irradiation with UVA, and four new peaks emerged at 249, 279, 328 and 341 nm. Interestingly, the shape of the UV-Vis spectrum after 30 min irradiation with UVA (**Figure 5.15a**, violet curve) looks exactly like the UV-Vis spectrum of complex [Pt(Tpy)Cl]Cl (**33**) (**Figure 5.15d**). Complex **33** is stable upon irradiation with UVA. Therefore, it is suggested that the photodecomposition of complex **36** generates a Pt^{II} species of the $[Pt(Tpy)Cl]^{+}$ type.

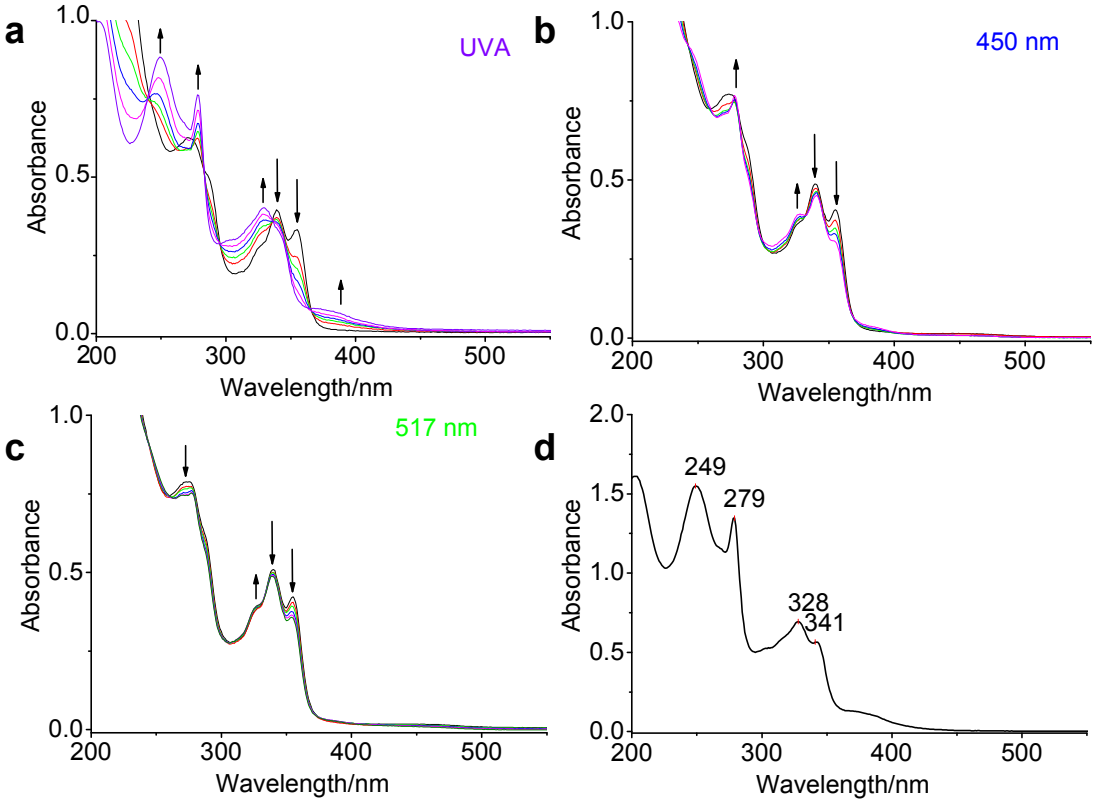

Figure 5.15 UV-Vis spectra recorded for *trans*-[Pt(N$_3$)(OH)$_2$(Tpy)]Cl (**36**) in H$_2$O upon irradiation with (**a**) UVA (4.55 mW/cm^2, irradiation time 0, 0.5, 1, 2, 5, 30 min), (**b**) at 450 nm (50 mW/cm^2, irradiation time 0, 5, 15, 30, 60 min) and (**c**) 517 nm (50 mW/cm^2, irradiation time 0, 5, 15, 30, 60, 120 min) at 298 K. (**d**) UV-Vis spectrum of [PtCl(Tpy)]Cl (**33**) in H$_2$O.

5.3.4 Photocytotoxicity

The photoactivated dose-dependent inhibition of cell viability (IC$_{50}$ values towards several human cell lines) for *cis, trans*-[Pt(N$_3$)$_2$(OH)$_2$(Bpy)] (**32**) and *trans*-[Pt(N$_3$)(OH)$_2$(Tpy)]Cl (**36**) are summarised in **Table 5.6**. The corresponding data for cisplatin, *trans, trans, trans*-[Pt(N$_3$)$_2$(OH)$_2$(MA)(Py)] (**5**) and *trans, trans, trans*-[Pt(N$_3$)$_2$(OH)$_2$(MA)(Tz)] (**8**) are also listed for comparison. Upon irradiation with UVA, complex **32** is photocytotoxic towards human keratinocytes (HaCaT), cisplatin-sensitive ovarian carcinoma cells (A2780) and an A2780 cisplatin resistant

subline (A2780cis). Upon the irradiation with blue light, it is photocytotoxic towards A2780, A2780cis and OE19 (oesophageal adenocarcinoma) cell lines. Also, it is nontoxic in the absence of light. The photocytotoxic effect of this compound is more potent than cisplatin under the experimental conditions used, but is not as potent as complexes **5** and **8**.

Complex **36** is photocytotoxic towards HaCaT, A2780, A2780cis and OE19 cell lines. However, it is also cytotoxic to these cells even in the absent of light. Hence further investigation of **36** was not carried out.

Table 5.6. Photocytotoxicity (IC_{50} value[a]/μM) *cis, trans*-$[Pt(N_3)_2(OH)_2(Bpy)]$ (**32**) and *trans*-$[Pt(N_3)(OH)_2(Tpy)]Cl$ (**36**), in comparison with cisplatin, complexes **5** and **8**.

Cell lines	HaCaT		A2780			A2780cis			OE19		
Light sources	UVA	Sham[e]	UVA	TL03[b]	sham	UVA	TL03	sham	UVA	TL03	sham
32	17.0	>213.1	9.2	14.8	>213.1	12.8	29.2	>213.1	NT[d]	26.5	NT
36	38.6	88.3	35.9	NT	66.7	39.9	NT	128.9	NT[c]	NT	NT
5	3.5	>232.9[c]	3.2	34.3	>232.9	5.3	14.1	>232.9	5.3	13.9	>232.9
8	2.6	>236.3	2.3	2.2	>236.3	4.4	14.0	>236.3	4.4	19.3	>236.3
Cisplatin (**26**)	144.0	173.3	151.3	NT	152.0	261.0	NT	229.0	261.0	NT	229.0

[a] IC_{50} is the concentration of complex that inhibited cell growth by 50%. The lower value indicates higher toxicity to cells. Each value is the mean of two or three independent experiments.

[b] TL03 is a blue light lamp (λ_{max} = 420 nm).

[c] > indicates IC_{50} greater than the concentration range used.

[d] Not tested.

[e] Sham: dark control.

5.4 Discussion

5.4.1 Synthesis

5.4.1.1 *Trans,trans,trans*-[$Pt(N_3)_2(OH)_2(NH_3)$(4-Nitropyridine)] (31).

Complex **31** *trans,trans,trans*-[$Pt(N_3)_2(OH)_2(NH_3)(4\text{-}NO_2\text{-}Py)$] was synthesized following the steps described in **Figure 5.16**. Initially, the attempt to synthesize *trans*-[$PtCl_2(NH_3)(4\text{-}NO_2\text{-}Py)$] (**29**) according to the method developed by Kauffman and Cowan[9, 41-45] produced the corresponding tetrachlorido Pt^{IV} species: *trans*-[$PtCl_4(NH_3)(4\text{-}NO_2\text{-}Py)$] (**28**). Although the facile oxidization of Pt^{II} to Pt^{IV} in aqueous HCl has been observed previously,[23, 24, 46] the mechanism of the oxidization is still not clear. Even when the reaction was carried out under argon, **28** was still the only product, which appears to rule out O_2 as the oxidizing agent. The electron withdrawing group (NO_2) in the pyridine ring can stabilize the Pt^{IV} product. **29** was reduced from **28** by hydrazine,[23, 24] and obtained with satisfactory purity and yield. The geometry of the product was assumed to be *trans* based on similar reactions reported in the literature[24] which give *trans*-products. Also, in this study, the crystal structure of *trans*-[$Pt(N_3)_2(NH_3)(4\text{-}NO_2\text{-}Py)$] (**30**) (discussed below) provided support for the geometry of *trans,trans,trans*-[$Pt(N_3)_2(OH)_2(NH_3)(4\text{-}NO_2\text{-}Py)$] (**31**) indirectly. Complex **30** was obtained by adding silver nitrate to remove the Cl^- from **29** followed by adding excess NaN_3. Then hydrogen peroxide (10%) was used to oxidize Pt^{II} to Pt^{IV}, forming **31**.

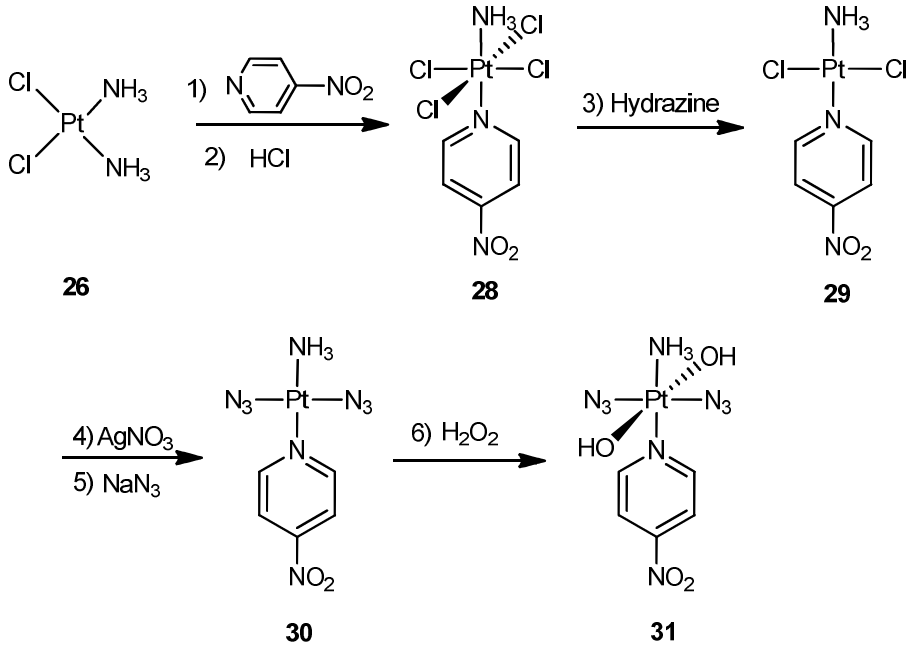

Figure 5.16 Synthetic route for *trans,trans,trans*-[$Pt(N_3)_2(OH)_2(NH_3)(4\text{-}NO_2\text{-}Py)$] (**31**).

5.4.1.2 The synthesis of *cis, trans*-[Pt $(N_3)_2(OH)_2(Bpy)$] (32)

Cis, trans-[$Pt(N_3)_2(OH)_2(Bpy)$] (**32**) was synthesized following the method developed by Fiona S. Mackay, a former member of the Sadler group.[25] In the step to synthesize [$Pt(N_3)_2(Bpy)$], after a reaction lasting for 2 days, an orange precipitate deposited in the DMF solution. When water was added to the mixture, the colour turned dark green very quickly. The orange and the dark green compound were both isolated and analysed. There was no difference between the NMR spectra (in DMSO-d_6) of those two compounds. It is postulated that they are the same complex, but different solvent effects make them show different colours. Adding water to the mixture precipitated more product from DMF, so the yield was improved by *ca.* 20% – 30%.

In the step to synthesize *cis, trans*-[$Pt(N_3)_2(OH)_2(Bpy)$] (**32**), reaction in 30% H_2O_2 for a longer time did not give a clear yellow solution. Some starting material

remained very difficult to oxidize. The oxidation was complete after the reaction mixture was kept on the rotary evaporator for 1 – 2 hours, during which time the reaction mixture was heated to 323 K and the H_2O_2 was concentrated.

5.4.1.3 The synthesis of *trans*-[Pt(N$_3$)(OH)$_2$(Tpy)]Cl (36)

The route for the synthesis of Pt-terpyridine complexes is shown in **Figure 5.17**. The idea of this work was to design and synthesize *trans*-[$Pt^{IV}(N_3)(OH)_2(Tpy)$] type of complexes and to investigate their cytotoxicity in the presence/absence of irradiation with visible light.

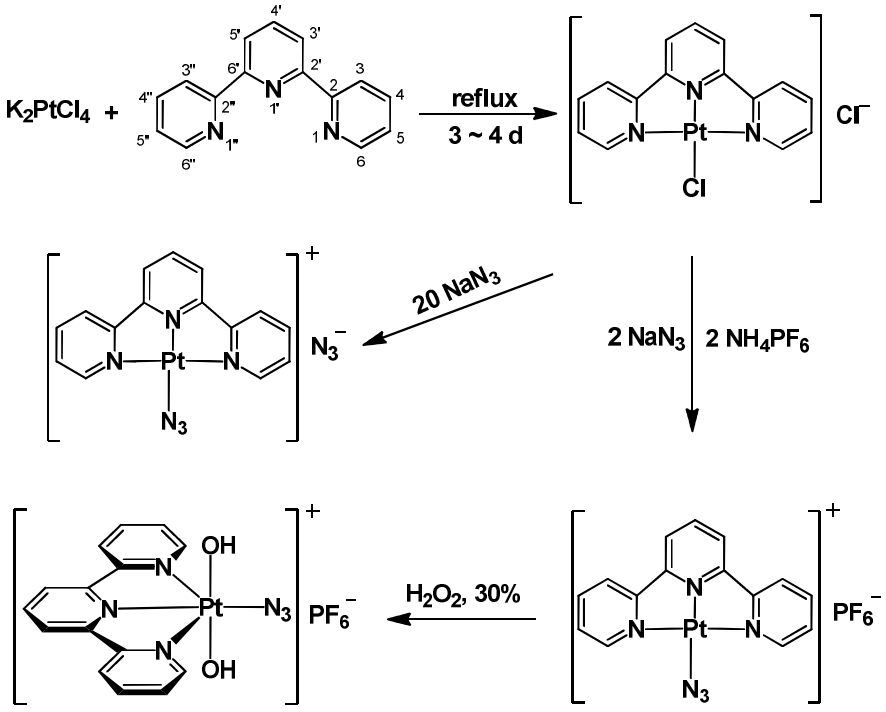

Figure 5.17 Synthetic route for the complex *trans*-$[Pt(N_3)(OH)_2(Tpy)]^+$.

The synthesis of [PtCl(Tpy)]Cl (**33**) has been reported and a recent review is available.[17] Upon heating a mixture of $K_2[PtCl_4]$ and Tpy, an insoluble red Magnus-type double salt $[Pt(Tpy)Cl]_2[PtCl_4]$ was formed along with an orange solution of [Pt(Tpy)Cl]Cl. The yield of the desired product can be increased to 65% by prolonged heating (1 ~ 4 days), but additional heating may result in decomposition to

Pt(0).[27] Several other methods can give better yields. Annibale and coworkers[31, 47] reported the rapid (15 min) and nearly quantitative formation of $[Pt(Tpy)Cl]^+$ from the reaction of $[Pt(COD)Cl_2]$ (COD=1,5-cyclooctadiene) with Tpy in water. The complex $[Pt(COD)Cl_2]$ can be prepared from $K_2[PtCl_4]$ and COD in 95% yield.[30] Another efficient preparation method is by heating *cis/trans*-$[PtCl_2(SMe_2)_2]$ with Tpy in warm $MeOH/H_2O$ for 30 ~ 40 min.[31, 48] ^{1}H-NMR chemical shifts of $[Pt(Tpy)X]^+$ type of complexes are dependent on solvent, ionic strength, concentration and temperature (See **Section 5.4.2** for discussion).

$[Pt(N_3)(Tpy)]^+$ can be easily obtained by adding 2 mol equiv NaN_3 to an aqueous solution of $[PtCl(Tpy)]^+$. N_3^- can directly substitute the Cl^- on Pt^{II}. Either excess NaN_3 or 2 mol equiv of NH_4PF_6 can precipitate the $[Pt(N_3)(Tpy)]^+$ cation, resulting in $[Pt(N_3)(Tpy)]N_3$ and $[Pt(N_3)(Tpy)]PF_6$ respectively. Many anions, such as CN^-, SCN^-, NO_2^-, N_3^-, $S_2O_3^{2-}$, $^-OSO_2CF_3$ and various thiols, NH_3, pyridines, ketones and acetylides can substitute the Cl^- in $[PtCl(Tpy)]^+$, forming the respective $[PtX(Tpy)]^+$ complexes.[17]

Repeat attempts to oxidise $[Pt(N_3)(Tpy)]PF_6$ with H_2O_2 always gave a mixture of products. Altering the reaction time from 0.5 h to 2 h and concentration of H_2O_2 from 1% to 30% did not improve much the yield of the main product. Recrystallization was not successful for this compound either. Therefore, semi-preparative HPLC purification was used the isolate the desired product (see **Section 5.3.3.1**).

5.4.1.4 The synthesis of *trans*-$[Pt(N_3)(OH)_2(TTpy)]Cl$ (40)

Since the direct synthesis of $[PtCl(Tpy)]Cl \cdot 2H_2O$ in this work gave poor yields (30% ~ 60%), an improved method was used to make Pt-TTpy (4'-(4-Methylphenyl)-

2,2':6',2''-terpyridine) complexes. Pt[Cl_2(COD)] is an intermediate in the synthesis of *cis*-platinum complexes.[27, 48] In this work, a satisfactory yield was obtained with Pt[Cl_2(COD)] as the intermediate for Pt-TTpy complexes.

Complex [PtCl(TTpy)]Cl (**38**) is only sparingly soluble in H_2O, so the substitution of Pt coordinated Cl^- with N_3^- was not applicable in water. This reaction proceeded well in DMF, producing [Pt(N_3)(TTpy)]N_3 (**39**).

The oxidation of **39** did not work well at 327 K. The product seemed to be unstable at this temperature. So rotary evaporation at 327 K should not be used to remove the solvent for this reaction. After a series of optimization experiments, reacting with 30% H_2O_2 at 313 K overnight was found to be the best way to obtain an acceptable yield of product of *trans*-[Pt(N_3)($OH)_2$(TTpy)]$^+$, and the solvent was removed by lyophilisation. The product was then purified by semi-preparative HPLC separation, giving *trans*-[Pt(N_3)($OH)_2$(TTpy)]Cl (**40**) as the final product.

5.4.2 Stacking of Pt-Tpy complex by NMR studies

The ^{1}H NMR chemical shift of terpyridineplatinum complexes varies depending on the experimental conditions (e.g. solvent, pH, concentration, and ionic strength, temperature). This is due to the stacking of [PtX(Tpy)]$^+$ cations, which is more favoured in concentrated than dilute aqueous solutions.[17, 49] [17, 49]The effect of stacking on the ^{1}H NMR resonances was investigated for complexes [PtCl(Tpy)]Cl · $2H_2O$ (**33**) and [Pt(N_3)(Tpy)](N_3) (**34**), as shown in **Figure 5.18** and **Figure 5.19**. It is evident that the chemical shift varies with ionic strength. In non-aqueous solvents, stacking can be minimized. This result is not new, so further investigation was not processed.

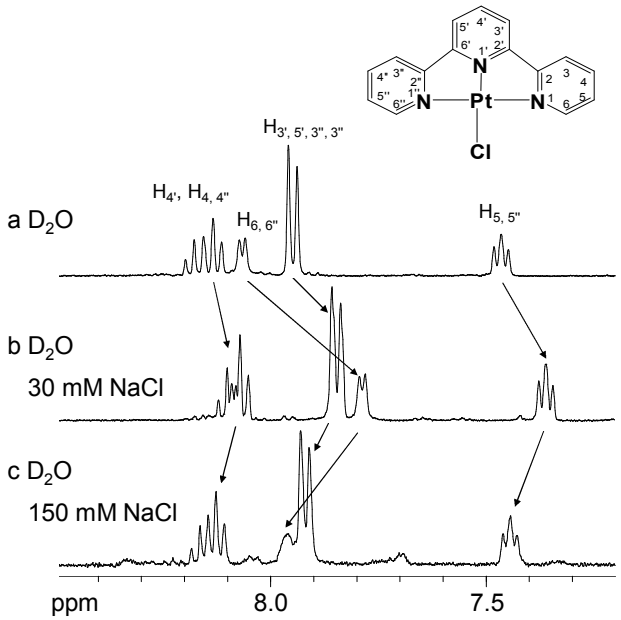

Figure 5.18 ^{1}H-NMR of [Pt(Cl)(tpy)]Cl (**33**) (10 mM) in (**a**) D_2O, (**b**) 30 mM NaCl in D_2O, (**c**) 150 mM NaCl in D_2O.

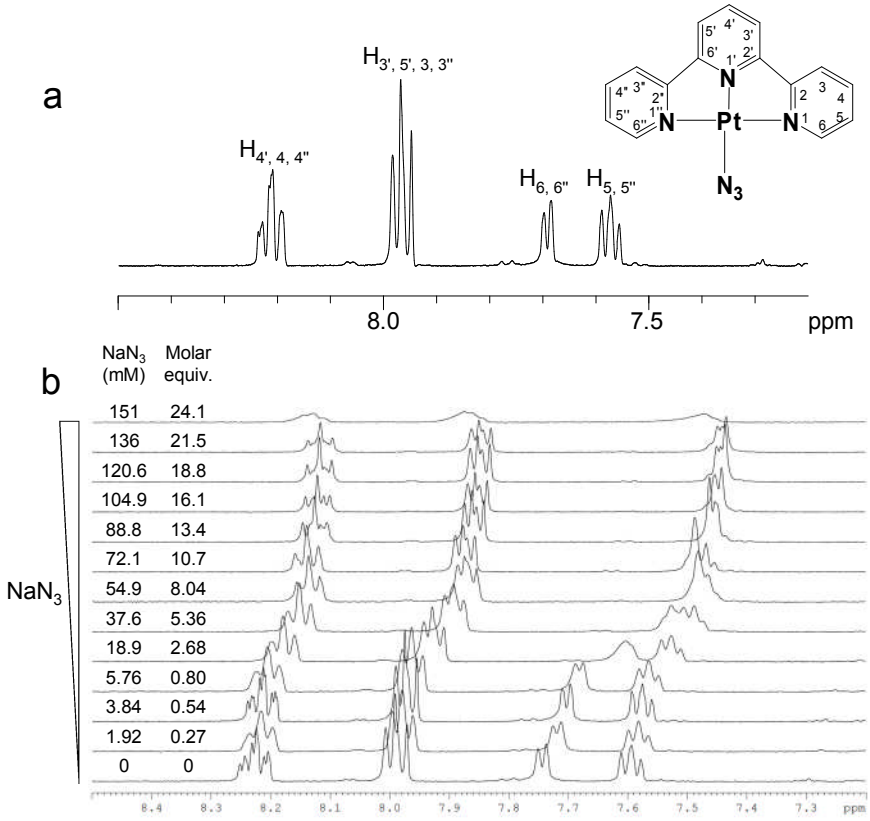

Figure 5.19 ^{1}H-NMR analysis for [Pt(Tpy)(N_3)](N_3) (**34**). (**a**) [Pt(Tpy)(N_3)](N_3) (7.16 mM) in D_2O. (**b**) [Pt(Tpy)(N_3)]N_3 + NaN_3 (0 – 151 mM) in D_2O. The concentration of NaN_3 over 151 mM lead to the precipitation of **34**.

5.4.3 Photoactivation wavelength and photocytotoxicity

The aim of this Chapter was to design new Pt^{IV} complexes with longer activation wavelengths, ideally within the therapeutic window. A series of pyridine-type ligands, e.g., 4-nitropyridine, 2,2'-bipyridine, and terpyridines, were introduced into new Pt^{IV} complexes. The action spectrum was measured for complex *trans, trans, trans*-[$Pt(N_3)_2(OH)_2(NH_3)(4\text{-}NO_2\text{-}Py)$] (**31**). The result suggested that this compound can be activated by light of wavelength as long as 520 nm. The action spectrum complex **31** and *trans, trans, trans*-[$Pt(N_3)_2(OH)_2(Py)_2$] (**24**) indicated that there is a correlation between the intensity of UV-Vis absorption and the rate of photodecomposition. Therefore, action spectra were not measured for other compounds. If the extinction coefficient of a Pt^{IV} diazidodihydroxido complex at a certain wavelength is zero, it cannot be activated at this wavelength. The extinction coefficients of *cis, trans*-[$Pt(N_3)_2(OH)_2(Bpy)$] (**32**) and t*rans*-[$Pt(N_3)(OH)_2(Tpy)$]Cl (**36**) indicate that they cannot be activated by light over 460 and 530 nm, respectively. These results were consistent with their photolysis irradiated with UVA or light of 450 nm and 517 nm.

Complex **32** is non-toxic in the dark but toxic to cancer cells upon irradiation with light. However, the photocytotoxicity of this compound is not as high as complexes **5** and **8** (**Chapter 3**). Complex **36** can be activated with green light, but it is toxic even in the dark. These disadvantages limit their application as anticancer prodrugs.

5.5 Conclusion

In this Chapter, a series of new photoactivatable Pt^{IV} anticancer complexes were developed and their photoactivation property and toxicity to cancer cells were examined. Two compounds were found to be photoactivated by green light.

However, their photocytotoxicity to cancer cells is not useful. Therefore, further effort is still needed to develop new photoactivatable Pt^{IV} complexes with good anticancer activity which can be activated by light of 500 – 600 nm or even longer wavelength.

5.6 Reference

1. B. Rosenberg, in *Cisplatin:Chemistry and Biochemistry of a Leading Anticancer Drug*, ed. B. Lippert, Verlag Helvetica Chimica Acta, Zurich, 1999, pp. 1-27.
2. E. Wong and C. M. Giandomenico, *Chem. Rev.*, 1999, **99**, 2451-2466.
3. L. Kelland, *Nat. Rev. Cancer*, 2007, **7**, 573-584.
4. T. Boulikas, *Expert Opin Inv Drug*, 2009, **18**, 1197-1218.
5. F. Kratz, I. A. Muller, C. Ryppa and A. Warnecke, *Chemmedchem*, 2008, **3**, 20-53.
6. J. Rautio, H. Kumpulainen, T. Heimbach, R. Oliyai, D. Oh, T. Jarvinen and J. Savolainen, *Nat. Rev. Drug Discov.*, 2008, **7**, 255-270.
7. V. J. Stella, *J. Pharm. Sci.*, 2010, **99**, 4755-4765.
8. F. S. Mackay, J. A. Woods, H. Moseley, J. Ferguson, A. Dawson, S. Parsons and P. J. Sadler, *Chem. Eur. J.*, 2006, **12**, 3155-3161.
9. F. S. Mackay, J. A. Woods, P. Heringova, J. Kasparkova, A. M. Pizarro, S. A. Moggach, S. Parsons, V. Brabec and P. J. Sadler, *Proc. Natl. Acad. Sci. USA*, 2007, **104**, 20743-20748.
10. N. J. Farrer and P. J. Sadler, *Aust. J. Chem.*, 2008, **61**, 669-674.
11. N. J. Farrer, J. A. Woods, V. P. Munk, F. S. Mackay and P. J. Sadler, *Chem. Res. Toxicol.*, 2010, **23**, 413-421.

12. N. J. Farrer, J. A. Woods, L. Salassa, Y. Zhao, K. S. Robinson, G. Clarkson, F. S. Mackay and P. J. Sadler, *Angew. Chem. Int. Ed.*, 2010, **49**, 8905-8908.
13. L. Brancaleon and H. Moseley, *Laser Med. Sci.*, 2002, **17**, 173-186.
14. M. R. Detty, S. L. Gibson and S. J. Wagner, *J. Med. Chem.*, 2004, **47**, 3897-3915.
15. H. Tai, PhD thesis, University of Warwick, 2012.
16. S. D. Cummings, *Coord. Chem. Rev.*, 2009, **253**, 1495-1516.
17. S. D. Cummings, *Coord. Chem. Rev.*, 2009, **253**, 449-478.
18. Mackenzi.La and Frainbel.W, *Br. J. Dermatol.*, 1973, **89**, 251-264.
19. H. J. Kuhn, S. E. Braslavsky and R. Schmidt, *Pure Appl. Chem.*, 2004, **76**, 2105-2146.
20. S. L. Murov, G. L. Hug and I. Carmichael, *Handbook of Photochemistry*, M. Dekker, New York, 1993.
21. R. A. Alderden, M. D. Hall and T. W. Hambley, *J. Chem. Educ.*, 2006, **83**, 728-734.
22. E. Ochiai, *J. Org. Chem.*, 1953, **18**, 534-551.
23. M. J. Macazaga, J. Rodriguez, A. G. Quiroga, S. Peregina, A. Carnero, C. Navarro-Ranninger and R. M. Medina, *Eur. J. Inorg. Chem.*, 2008, 4762-4769.
24. S. Shamsuddin, M. S. Ali, S. Huang and A. R. Khokhar, *J. Coord. Chem.*, 2002, **55**, 659-665.
25. F. S. Mackay, PhD Thesis, University of Edinburgh, 2007.
26. F. S. Mackay, N. J. Farrer, L. Salassa, H. C. Tai, R. J. Deeth, S. A. Moggach, P. A. Wood, S. Parsons and P. J. Sadler, *Dalton Trans.*, 2009, 2315-2325.
27. M. Howe-Grant and S. J. Lippard, *Inorg. Synth.*, 1980, **20**, 101-103.

28. H.-K. Yip, L.-K. Cheng, K.-K. Cheung and C.-M. Che, *J. Chem. Soc., Dalton Trans.*, 1993.

29. S. Wee, M. J. Grannas, W. D. McFadyen and R. A. J. O'Hair, *Aust. J. Chem.*, 2001, **54**, 245-251.

30. J. X. McDermott, J. F. White and G. M. Whitesides, *J. Am. Chem. Soc.*, 1976, **98**, 6521-6528.

31. G. Annibale, B. Pitteri, M. H. Wilson and D. McMillin, *Inorg. Synth.*, 2004, **34**, 76-78.

32. H. Bertrand, D. Monchaud, A. De Cian, R. Guillot, J.-L. Mergny and M.-P. Teulade-Fichou, *Org. Biomol. Chem.*, 2007, **5**, 2555-2559.

33. A. Martinez, J. Lorenzo, M. J. Prieto, R. de Llorens, M. Font-Bardia, X. Solans, F. X. Aviles and V. Moreno, *Chembiochem*, 2005, **6**, 2068-2077.

34. F. S. Mackay, S. A. Moggach, A. Collins, S. Parsons and P. J. Sadler, *Inorg. Chim. Acta*, 2009, **362**, 811-819.

35. T. Rybalova, V. Sedova, Y. Gatilov and O. Shkurko, *Chem. Heterocycl. Compd.*, 1998, **34**, 1161-1165.

36. J. Kuduk-Jaworska, A. Puszko, M. Kubiak and M. Pelczynska, *J. Inorg. Biochem.*, 2004, **98**, 1447-1456.

37. C. A. Marrese and C. J. Carrano, *Inorg. Chem.*, 1984, **23**, 3961-3968.

38. B. M. Still, P. G. A. Kumar, J. R. Aldrich-Wright and W. S. Price, *Chem. Soc. Rev.*, 2007, **36**, 665-686.

39. P. S. Pregosin, *Coord. Chem. Rev.*, 1982, **44**, 247-291.

40. D. Loganathan and H. Morrison, *Photochem. Photobiol.*, 2006, **82**, 237-247.

41. G. B. Kauffman and D. O. Cowan, *Inorg. Synth.*, 1963, **7**, 239-245.

42. L. Cubo, A. G. Quiroga, J. Y. Zhang, D. S. Thomas, A. Carnero, C. Navarro-Ranninger and S. J. Berners-Price, *Dalton Trans.*, 2009, 3457-3466.

43. M. Van Beusichem and N. Farrell, *Inorg. Chem.*, 1992, **31**, 634-639.

44. U. Bierbach, M. Sabat and N. Farrell, *Inorg. Chem.*, 2000, **39**, 3734-3734.

45. A. G. Quiroga, J. M. Perez, C. Alonso, C. Navarro-Ranninger and N. Farrell, *J. Med. Chem.*, 2006, **49**, 224-231.

46. A. M. Pizarro, V. P. Munk, C. Navarro-Ranninger and P. J. Sadler, *Angew. Chem. Int. Ed.*, 2003, **42**, 5339-5342.

47. G. Annibale, M. Brandolisio and B. Pitteri, *Polyhedron*, 1995, **14**, 451-453.

48. M. G. Hill, M. J. Irwin, C. J. Levy, L. M. Rendina and R. J. Puddephatt, *Inorg. Synth.*, 1998, **32**, 153-158.

49. K. W. Jennette, J. T. Gill, J. A. Sadownick and S. J. Lippard, *J. Am. Chem. Soc.*, 1976, **98**, 6159-6168.

Chapter 6

Two-photon Excitation

6.1 Introduction

Two-photon absorption was originally predicted in 1931 by Maria Göppert-Mayer in her doctoral dissertation. [1] It was theoretically demonstrated that two photons being almost simultaneously (*ca.* 10^{-16} s) absorbed by an atom or molecule produces a transition equivalent to the absorption of the single photon of twice the energy (**Figure 6.1**).[2] In other word, two-photon absorption (TPA) of longer wavelength light can initiate the same photophysical or photochemical processes as one-photon absorption (OPA) of shorter wavelength ($\lambda_{effective} \geq 1/2\ \lambda_{incident}$). For example, lower-energy photons (e.g. 700 nm) can promote transitions of higher-energy (e.g. 350 nm).[2, 3] Therefore, two-photon activation provides an alternative mechanism for photoactivation.

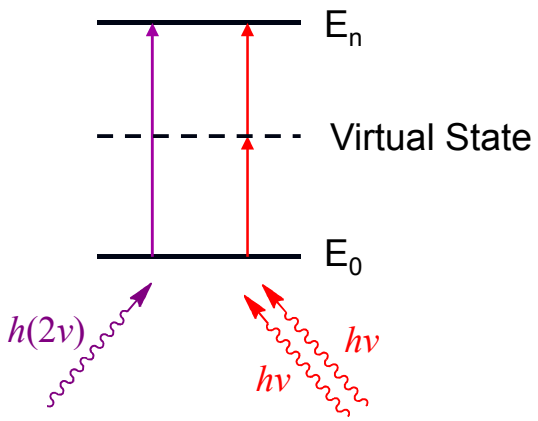

Figure 6.1 Energy level diagram showing that the absorption of two photons from the red region (700 nm) can excite an atom of molecule to the same state as one photon from the violet region (350 nm).

Conventional one-photon absorption is dependent linearly on the light intensity. By contrast, TPA has a quadratic dependence on the light intensity, as it depends on two photons interacting with a molecule almost simultaneously. TPA probabilities are

extremely small, so it was not until 30 years after Göppert-Mayer's paper was published that the first experimental evidence was obtained using a ruby laser. [4] After the 1990s, the application of sub-picosecond lasers (e.g., the Ti:sapphire laser), which generate a very high instantaneous photon density, greatly facilitated the investigation of TPA.[2] TPA probabilities are extremely small, so it is necessary to focus the light beam to increase the local intensity at the focus point. Away from the focus point, TPA probabilities drop down rapidly.

Two-photon absorption cross section (δ) is an important property of a molecule undergoing TPA.[2, 5] It is not absolutely related to molecule dimensions, rather the strength of the optical transitions and selection rules are important. TPA cross-sections can be simply imagined as a relative capture area, or as the extinction coefficient of one-photon absorption. TPA cross sections for most compounds are very small numbers in SI units, so they are usually reported in Göppert-Mayer units (1 GM $\equiv 10^{-50}$ cm^4 s photons^{-1} molecule^{-1}).[2] A large number of organic molecules and complexes with large TPA cross sections have been designed and synthesized. [3, 5-7] Anderson and coworkers[2] have summarized the general features for chromophores with large TPA cross-section:

- Long, π-conjugated chains with enforced coplanarity;
- Donor and acceptor groups at the centre and ends of the molecule;
- A strong OPA transition close to the TPA wavelength;
- Narrow one- and two-photon absorption bands.

The theory of TPA can also be applied to the absorption of three or more photons.[8] Research on multi-photon excitation is a rapidly expanding area due to the recent availability of commercial pulsed femtosecond lasers. Wide applications has been

developed, such as three-dimensional data-storage,[9, 10] fluorescence microscopy,[11, 12] microfabrication,[13] optical power limiting,[14] up-converted lasing[15] and photodynamic therapy (PDT).[7, 16-18] Recently, the first demonstration of *in vivo* photodynamic therapy using a TPA photosensitizer was reported.[19]

In general, the depth of penetration of light is inversely proportional to the wavelength within the spectrum of visible and near infrared (see **Chapter 1**).[17, 20, 21] It is obvious that TPA has the advantage of accessing longer wavelength for photoactivation.[22, 23] The LMCT bands (N_3 to Pt^{IV}) of the photoactivatable Pt^{IV} azido complexes used in this work are centred in the UV region (300 nm). The wavelength of activation restricts their clinic application to tumours in suface tissue. If the TPA is applied to the photoactivatable platinum(IV) anticancer complexes, this disadvantage can be overcome.

In this Chapter, according to the rules for chromophores with large TPA cross sections, a ligand with a large π-conjugation system and strong electron donor, 4-[2-(4-methoxyphenyl)ethynyl]pyridine (MOPEP), was rationally designed and used in a new two-photon-activatable platinum complex. As a starting point, *cis*-$[PtCl_2(MOPEP)_2]$ was synthesized and characterized. The OPA and TPA properties of this compound were examined as well.

6.2 Experimental

6.2.1 Materials, methods and instrument

All materials were used as obtained from commercial sources unless otherwise stated. DMF-d_7 was obtained from Cambridge Isotope Laboratories, Inc. 4-Bromopyridine

hydrochloride, 1-ethynyl-4-methoxy benzene, bis(triphenylphosphine)palladium(II) chloride, and tetrabutylammonium fluoride trihydrate were from Sigma-Aldrich.

NMR spectra were recorded on Bruker DPX-400 (^{1}H, 400.03 MHz), Bruker DPX-300 (^{1}H, 300.0 MHz; ^{13}C, 75.5 MHz;) or Bruker AVIII-600 (^{1}H, 600.13 MHz; ^{13}C, 150.9MHz; ^{195}Pt, 129.4 MHz) spectrometers. Specific parameters, along with other general parameters for acquisition are found in **Chapter 2**.

Elemental analysis was performed by the Warwick Analytical Service.

Electronic absorption spectra (UV-Vis) were recorded on a Varian Cary 300 UV-Vis spectrophotometer in a 1-cm path-length quartz cuvette. All spectra were referenced to neat solvent and data were processed with OriginLab Origin 7.0.

Positive/negative ion electrospray mass spectrometry (ESI-MS) was performed on a Bruker Esquire 2000 mass spectrometer coupled with an Agilent 1100 HPLC (without column) as an automatic sample delivery system. Samples were prepared in 80% acetonitrile/20% water.

One-photon absorption decomposition of Pt complexes were carried out at 298 K by using a LZC-ICH2 photoreactor (Luzchem Research Inc.) equipped with a temperature controller and 8 UVA lamps (Hitachi, λ_{max} = 365 nm) or 16 Visible light lamps (Sylvania cool white, λ ~ 400 – 700 nm, λ_{max} = 580 nm) with no other sources of light filtration.

HPLC conditions: HP1100 series. Column: Agilent ZORBAX Eclipse XDB-C18 column, 5 μm, 4.6 × 250 mm. Flow rate, 1.0 ml/min. Detection wavelength: 315 nm. Mobile phase A, H_2O, 0.1% FA; B, MeOH, 0.1% FA. A linear gradient from 5% to 80% B over 15 min and maintained at 80% B for 5 min was applied.

Melting points and thermo decomposition were determined on a Sanyo Gallenkamp Melting Point Meter.

The two-photon experiments were carried out with the assistance of Dr Gareth M. Roberts and Mr S. E. Greenough, Mr Will H. Powell and Prof Vasillios G. Stavros from the University of Warwick. The experimental setup is found in **Figure 6.2**. Femtosecond (fs) laser pulses were derived from a commercial Ti:Sapphire oscillator and regenerative amplifier system (Spectra-Physics, Tsunami and Spitfire XP, respectively).[24] And an optical parametric amplifier (OPA) (Light Conversion, TOPAS model 4/800/f) which generates tuneable pump pulses (325 – 400 nm, ~5 μJ/pulse or 600 – 700 nm, ~20 μJ/pulse). The size of the output beam is 6 mm. A 75 cm lens was used to focus the beam and the diameter of the focus was 0.11 mm (for 700 nm as an example). Diameter of the focus is: $D_f = 4\lambda f / \pi D_b$, where λ is wavelength; f is focal distance; D_b is diameter of the beam. The power density of each pulse at focus is 2.2×10^{12} W/cm^2. The intensity of the pulse is: $I = E / tA$, where E is the energy of each pulse; t is the duration of the pulse; A is the area of the beam.

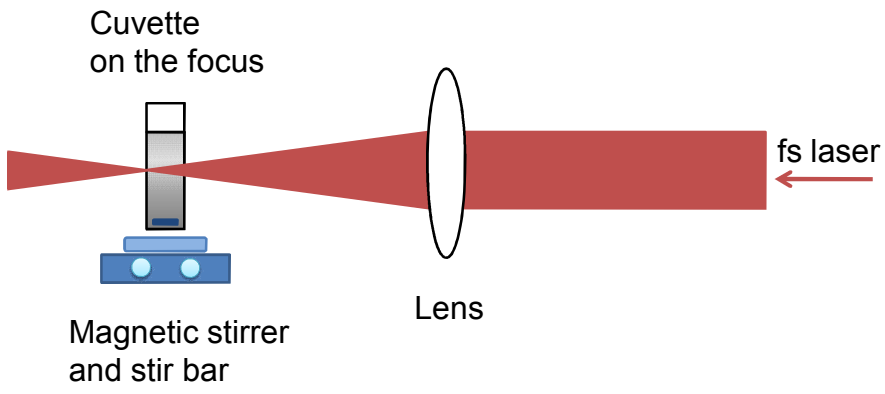

Figure 6.2 Instrument setup for TPA experiments.

6.2.2 Synthesis and characterisation

6.2.2.1 4-[2-(4-methoxyphenyl)ethynyl]pyridine (MOPEP, 41)

4-[2-(4-Methoxyphenyl)ethynyl]pyridine (**MOPEP**) was synthesized according to a published method.[25] 4-Bromopyridine hydrochloride (0.194 g, 1 mmol), 1-ethynyl-4-methoxy benzene (0.158 g, 1.2 mmol), $PdCl_2(PPh_3)_2$ (21 mg, 0.03 mmol), and tetrabutylammonium fluoride trihydrate (0.784 g, 3 mmol) were stirred at 353 K for 1 h under N_2 until complete consumption of starting material as monitored by TLC. After the mixture was washed with water, extracted with diethyl ether, and evaporated, the light yellow residue was purified by recrystallization in petroleum ether. The spectroscopic data are consistent with those reported.[25]

Yield: 0.16 g (84.6%).

^{1}H NMR (300 MHz, $CDCl_3$) δ = 8.58 (d, 2H), 7.50 (d, 2H), 7.36 (d, 2H), 6.91 (d, 2H), 3.84 (s, 3H); ^{13}C NMR (75.5 MHz, $CDCl_3$) δ = 160.3, 149.6, 133.4, 131.8, 125.3, 114.1, 94.2, 85.6, 55.3.

ESI-MS: (*m/z*) [M + H^+], calc., 210.1; found, 210.1.

Elemental analysis: $C_{14}H_{11}NO$, Cal. C 80.36%, H 5.30%, N 6.69%; Found: C 79.94%, H 5.31%, N 6.36%

6.2.2.2 *Cis*-[$PtCl_2$(MOPEP)$_2$] (42)

$K_2[PtCl_4]$ (415 mg, 1.0 mmol) was dissolved in H_2O (1 ml) and MOPEP (437 mg, 2.1 mmol) in THF 2 ml was added. The mixture was stirred at room temperature overnight. A yellow-orange solid precipitated and was collected by filtration and washed with ice cold water, ethanol, and diethyl ether, then dried under vacuum. This product was crystalized in DMF at ambient temperature over several months, but the quality was not good enough for X-ray crystallography.

Yield: 401 mg (58 %).

^{1}H NMR (300 MHz, $CDCl_3$) δ = 8.68 (d, 2H), 7.58 (d, 2H), 7.31 (d, 2H), 6.90 (d, 2H), 3.84 (s, 3H). ^{195}Pt NMR (DMF-d_7, 129.4 MHz) δ = −1980.

ESI-MS: (*m/z*) [M+Na^+], calc., 707.1; found, 707.1.

Elemental analysis: $C_{28}H_{22}Cl_2N_2O_2Pt$, Cal. C 49.13%, H 3.24%, N 4.09%; Found: C 48.85%, H 3.31%, N 3.89%

6.3 Results

6.3.1 Synthesis and characterization

Complex *cis*-[$PtCl_2$(MOPEP)$_2$] (**42**) was synthesized according to a reported method for *cis*-Pt^{II} dichlorido complexes with pyridine type ligands (**Figure 6.3**).[26] When a slight excess of the pyridine type ligand was added to an aqueous solution of K_2PtCl_4 (Pt : ligand ratio 1 : 2.1) with stirring, the complex *cis*-[$Pt(Py)_2Cl_2$] precipitated.

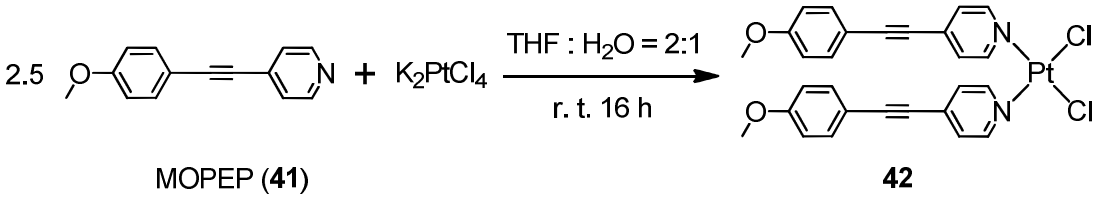

Figure 6.3 Synthetic reaction for complex *cis*-[$PtCl_2$(MOPEP)$_2$] (**42**).

There are two classic methods to determine the *trans* or *cis* geometry of Pt^{II} dichlorido complexes, Kurnakov test[27] and far infrared spectroscopy.[28] Because of the poor solubility of complex **42**, a mixed solvent (H_2O-acetone) was used in the Kurnakov test,[27] but the result was equivocal. Herein, a ^{195}Pt NMR method was subsequently used to verify the *cis* geometry of complex **42**. ^{195}Pt NMR chemical shifts of Pt^{II} diamine/imine dichlorido complexes are closely related to the nature of the amine/imine ligands and geometry of complexes. On the one hand, the lower pK_a

of the protonated pyridine type ligands, the smaller the electron donation effect in the L–M σ bond. The electron density on the Pt nucleus is thus reduced, resulting in a deshielding of the ^{195}Pt NMR resonance.[29] If the reported $\delta(^{195}\text{Pt})$ values of the *cis*-$[\text{Pt(Ypy)}_2\text{Cl}_2]$ (Ypy = substituted pyridine ligands) complexes are plotted against the pK_a of the protonated ligands, there seems to be a trend that the higher pK_a often leads to a resonance in higher field (lower chemical shift) (**Figure 6.4**).[30-32] On the other hand, the $\delta(^{195}\text{Pt})$ of the *cis* isomer is generally 50 ppm lower than the *trans* isomer. The pK_a of the MOPEP ligand is 4.80[33] and the $\delta(^{195}\text{Pt})$ was determined to be −1980 ppm in this work. Therefore, according to the trend in **Figure 6.4**, it is reasonable to assign this complex as having *cis* geometry.

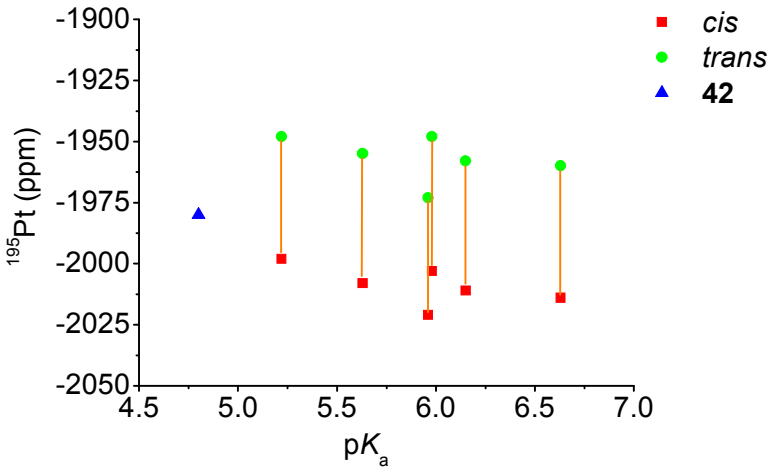

Figure 6.4 Plot of the $\delta(^{195}\text{Pt})$ of some reported $[\text{Pt(Ypy)}_2\text{Cl}_2]$ (Ypy = substituted pyridine ligands) complexes against the pK_a of the protonated ligands.[29] Green circles, *trans* isomers; red squares, *cis* isomers; blue triangles, complex **42**. Isomers with a specific Ypy ligand are connected with orange lines.

6.3.2 Absorption spectrum and stability

The absorption spectra of *cis*-$[\text{PtCl}_2\text{(MOPEP)}_2]$ (**42**) and MOPEP (**41**) in acetonitrile (MeCN) are shown in **Figure 6.5**. Compound **41** has two major absorption bands at

λ = 297 and 310 nm. These bands are assigned as n → π* and π → π* transitions. Compound **42** has a major absorption band at λ = 344 nm, which corresponds to the intra-ligand charge transfer band. The coordination to Pt lowers the electron density of pyridine moiety in the ligand, which hence facilitates the charge transfer. Therefore, the absorption wavelength of the band for **42** was red-shifted compared to free ligand **41**. In MeCN, it has no absorbance over 500 nm and it is hence stable in the dark or upon irradiation with light λ > 500 nm, as judged by UV-Vis spectroscopy. This compound was also stable in MeCN when heated to 343 – 353 K. (MeCN b.p., 355 K) The melting point of crystalline complex **42** was measured, but only decomposition was observed over 473 K.

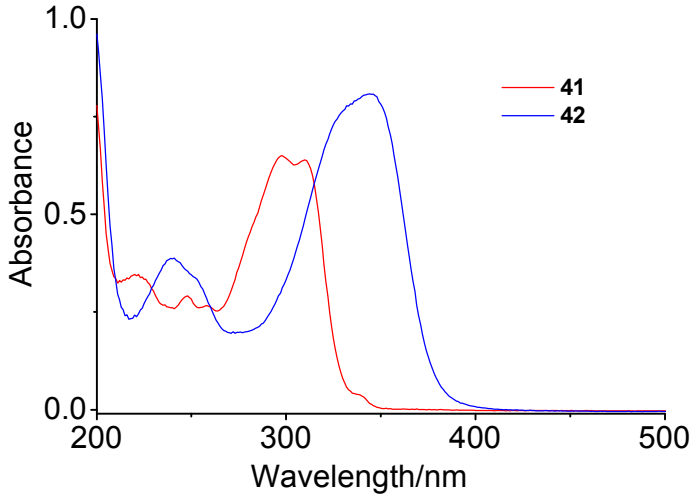

Figure 6.5 UV-Vis pectra of MOPEP (**41**) and *cis*-[$PtCl_2$(MOPEP)$_2$] (**42**) in MeCN at 298 K. For compound **41** ε_{297nm} = 32445 M^{-1} cm^{-1}, **42** ε_{344nm} = 40420 M^{-1} cm^{-1}.

6.3.3 OPA decomposition

Complex *cis*-[$PtCl_2$(MOPEP)$_2$] (**42**) is light sensitive. UV-Vis spectroscopy was used to follow the photodecomposition in MeCN. Upon irradiation with UVA or a broad-band white light, the intensity of the major absorption band (λ = 344 nm) in the UV-Vis spectrum decreased, as shown in **Figure 6.6** and **Figure 6.7**. After

irradiation with UVA for 5 min (**Figure 6.6**, green curve) or white light for 30 min (**Figure 6.7**, magenta curve), the absorbance at λ = 344 nm disappeared, indicating the complete consumption of starting material. Also, two strong absorption bands at *ca.* 300 nm emerged in the UV-Vis spectra which are exactly the same shape as that of the ligand MOPEP (**Figure 6.5**). Therefore, it is suggested that the photodecomposition of complex **42** generates the free ligand MOPEP. The mechanism of the photodecomposition may also involve solvent substitution, in which MeCN replaces one or two of the MOPEP ligands in complex **42**. When irradiation with UVA was stopped after 1 or 10 min, no recovery of complex **42** was observed after 12 hours in the dark, as followed by UV-Vis spectrophotometry.

The rate of photodecomposition upon irradiation with UVA is much faster than that with white light, despite the lower power of UVA. This is reasonable as only the light below 500 nm (especially below 400 nm) is effective.

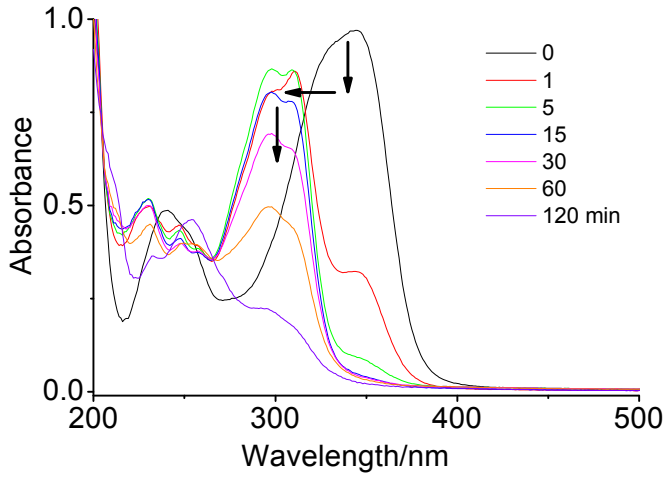

Figure 6.6 Photoactivation of *cis*-[$PtCl_2(MOPEP)_2$] (**42**) upon irradiation with UVA (λ_{max} = 365 nm, 3.5 mW/cm^2, irradiation time 0, 1, 5, 15, 30, 60, 120 min) in MeCN at 298 K.

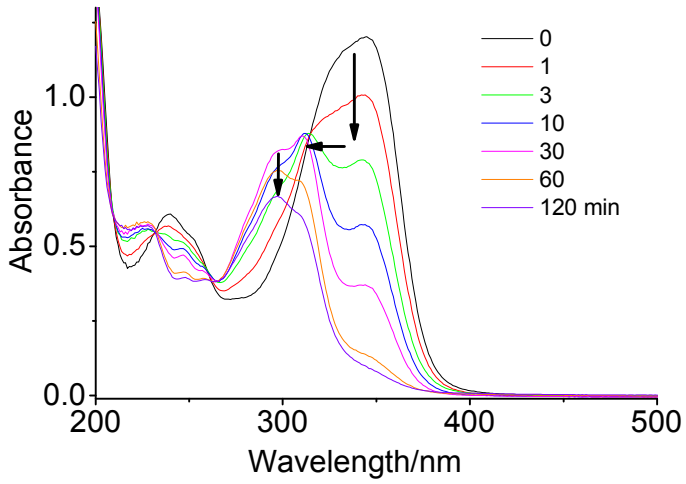

Figure 6.7 Photoactivation of *cis*-[$PtCl_2(MOPEP)_2$] (**42**) with white light (λ ~ 400 – 700 nm, 12 mW/cm^2, irradiation time 0, 1, 3, 10, 30, 60, 120 min) in MeCN at 298 K.

Upon longer period of irradiation in both experiments (over 5 min by UVA and 30 min by white light), the major absorption bands that corresponding to the ligand decreased, which suggests decomposition of the ligand. The decomposition of the ligand MOPEP upon irradiation with UVA was confirmed by a control experiment (**Figure 6.8**). A sample of MOPEP in MeCN was irradiated with UVA for 30 min and the major absorption band decreased in a similar manor as that in **Figure 6.6** after 5 min.

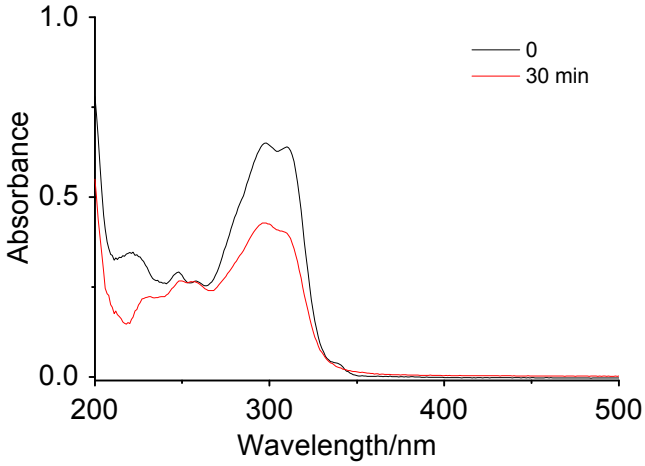

Figure 6.8 Photodecomposition of MOPEP (**41**) with UVA (λ_{max} = 365 nm, 3.5 mW/cm^2, irradiation time 0, 30 min) in MeCN. (20 mM, 298 K)

The photodecomposition of complex *cis*-[$PtCl_2(MOPEP)_2$] (**42**) in MeCN was examined by ^{1}H NMR (**Figure 6.9**). Complex **42** was dissolved in MeCN-d_3 for 20 μM. Before irradiation with light, the resonances of Pt coordinated ligand was observed, e.g., δ ($\underline{H_a}$) = 8.63, δ ($\underline{H_c}$) = 7.55. After irradiation with UVA for only 5 min, the signals of coordinated ligand were completely lost, and a set of resonances corresponding to the free ligand were observed, e.g., δ ($\underline{H_{a'}}$) = 8.57, δ ($\underline{H_{c'}}$) = 7.53. The shifts of the other signals were very tiny, and the spectrum in **Figure 6.9B** is consistent with the NMR spectrum of a genuine sample of the ligand.

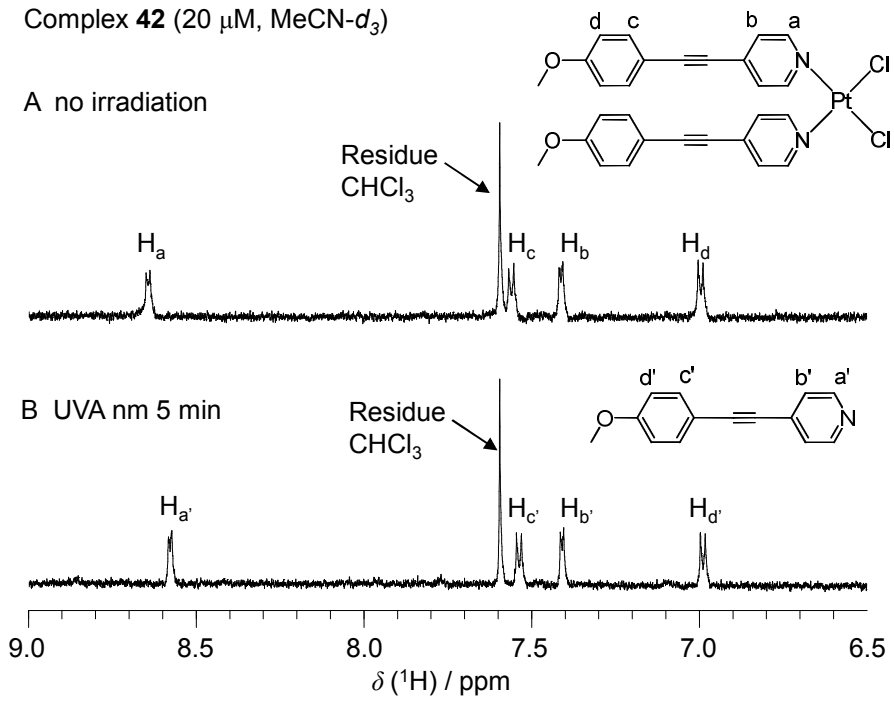

Figure 6.9 ^{1}H NMR spectra of *cis*-[$PtCl_2(MOPEP)_2$] (**42**) (20 μM, MeCN-d_3) before (**A**) and after (**B**) irradiation with UVA for 5 min.

The photodecomposition of complex *cis*-[$PtCl_2(MOPEP)_2$] (**42**) in MeCN was also examined by HPLC and LC-ESI-MS analysis. **Figure 6.10A** and **B** shows the HPLC chromatograms of the photolysis of **42** and control samples of intact ligand MOPEP **41** and **42**. The detection wavelength was 315 nm. The retention time (RT) for **41** is

22.3 min and for **42** 24.3 min. These peaks were further confirmed by LC-ESI-MS analysis. When a solution of **42** in MeCN was irradiated with UVA for 1 min (**Figure 6.10**C) a peak for ligand **42** was observed. Also, there was another small peak with RT 23.3 min, which can be reasonably assigned as *cis*-[$PtCl_2$(MOPEP)(MeCN)]. When the irradiation with UVA was extended to 10 min and 60 min, only the peak corresponding to the ligand **41** was found and this peak diminished in intensity at longer times. These results confirm the conclusion from the UV-Vis study that complex **42** can rapidly lose the ligand **41** upon irradiation with UVA for only one minute, and ligand **41** decompose upon prolonged irradiation with UVA.

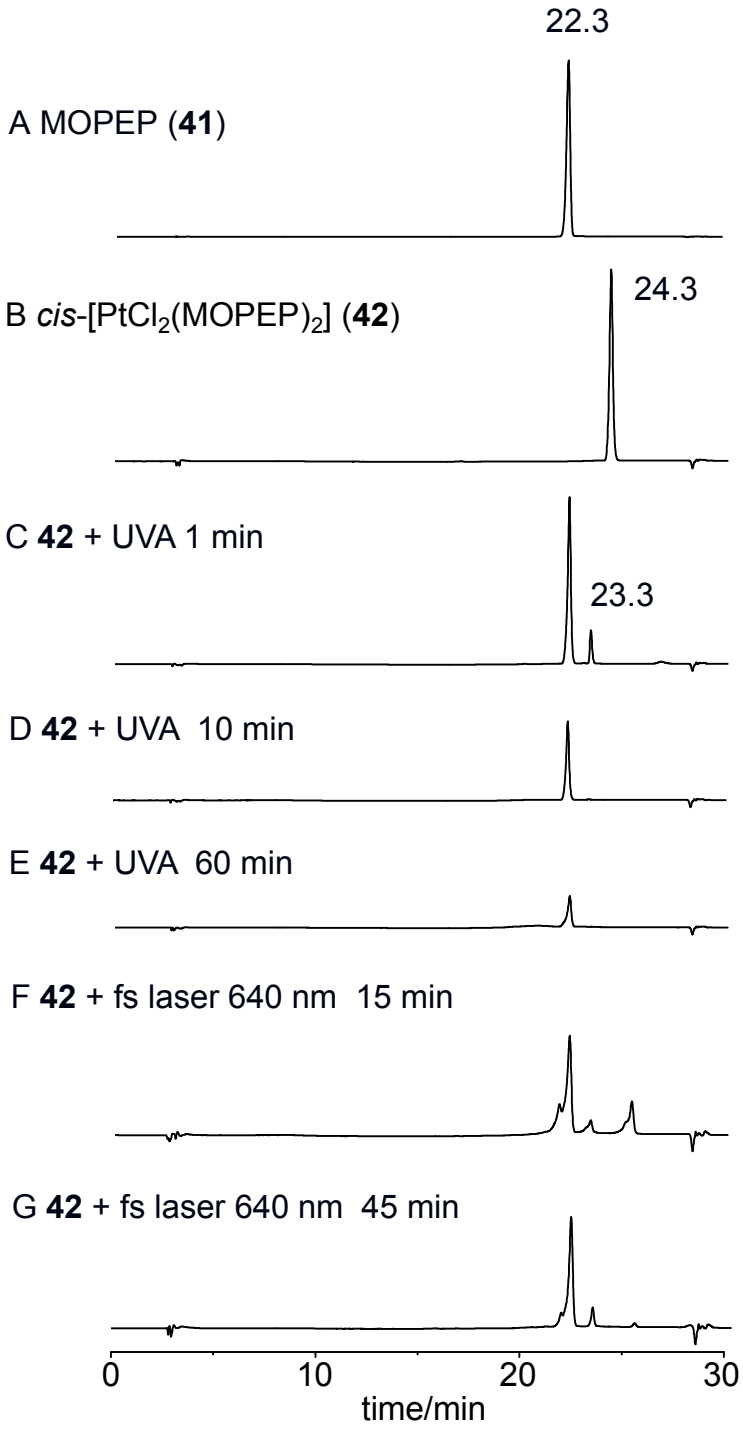

Figure 6.10 HPLC analysis of (**A**) MOPEP (**41**) (RT = 22.3 min); (**B**) *cis*-$[PtCl_2(MOPEP)_2]$ (**42**) (RT = 24.3 min) and the photolysis of **42** in MeCN upon irradiation with UVA (3.5 mW/cm^2) for (**C**) 1 min, (**D**) 10 min, (**E**) 60 min; and upon irradiation with a focused 640 nm fs laser light (**F**) 15 min, (**G**) 45 min. Detection wavelength: 315 nm.

6.3.4 TPA decomposition

When the solution of complex *cis*-[$PtCl_2(MOPEP)_2$] (**42**) was irradiated with a focused femto-second (fs) laser at the wavelength 600, 650 and 700 nm, a decrease in the intensity of the major absorption band (λ = 344 nm) was again observed. The reaction mixture was analysed by ESI-MS and the signal of the ligand MOPEP (*m/z* = 210.1 for $[M + H]^+$) was observed. HPLC was carried out to analyse the photoproduct of two-photon activation (2PA). **Figure 6.10F** and **G** are the chromatograms of complex **42** in MeCN upon irradiation with fs laser at 640 nm for 15 and 45 min. Compared to the other chromatograms in **Figure 6.10**, it is obvious that free MOPEP ligand and a small amount of *cis*-[$PtCl_2$(MOPEP)(MeCN)] were produced during the 2PA and the starting material was all consumed after 45 min. It is safe to conclude that the photoreaction initiated by two-photon excitation was the same as it was by UVA.

The time-dependent decrease of absorbance at 344 nm is summarized in **Figure 6.11**. Although the powers of the three wavelengths were slightly different, it was still reasonable to conclude that TPA activation at 650 nm was faster than that at 700 or 600 nm.

Several control experiments were carried out (**Figure 6.12**). Irradiation with unfocused fs laser pulses at 700 nm could hardly activate the photodecomposition of complex **42**. But irradiation with unfocused fs laser at 325, 350 and 400 nm easily activated OPA photodecomposition. The activation efficiencies are consistent with their OPA absorption at the corresponding wavelengths. These control experiments confirmed that when the power density of red light is very high, the photodecomposition of complex **42** could be initiated.

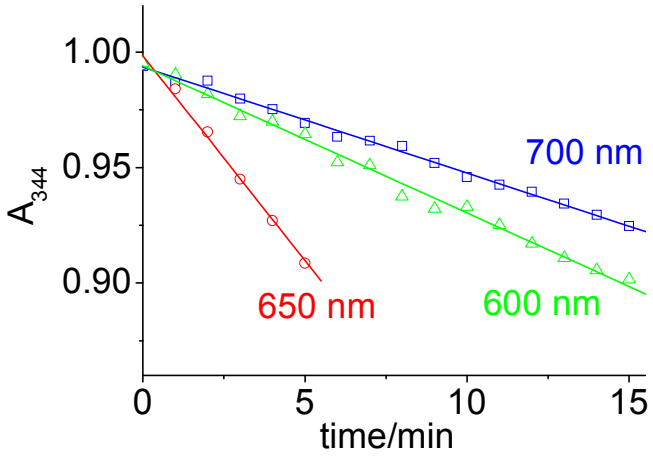

Figure 6.11 Time-dependent decrease of absorbance at 344 nm for complex **42** by two-photon absorption. Power of the laser at these wavelengths: 600 nm, 16 μJ/pulse; 650 nm, 21 μJ/pulse; 700 nm, 21 μJ/pulse.

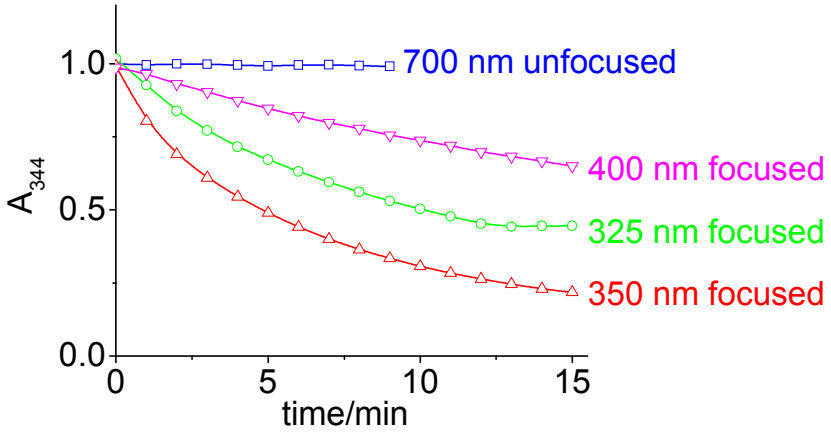

Figure 6.12 Control experiments for time-dependent decrease of absorbance at 344 nm for complex **42**. Irradiation with fs laser pulses at 700 nm (unfocused beam) and 325, 350, 400 nm (focused beam).

6.4 Discussion

Platinum(IV) diazidodihydroxido complexes have been reported to be photosensitive and related studies has been carried out in this work. Also, Pt^{IV} dichloridodihydroxido or tetrachlorido complexes are also reported to be sensitive to light.[34, 35] However, the photo-induced disassociation/substitution can occur with the

Cl, OH or N_3 ligands. Evidence from literature reports[36] and this work suggests that Pt-pyridine bonds are very stable on Pt upon irradiation with UVA. However, there are a few reports of the photodissociation of pyridine from Pt^{II} upon irradiation at 254 nm[37] and pyridine derivatives from Pt^{II} upon irradiation with UVA[38] or broad band UV light.[39] A time-dependent DFT calculation suggested that for complex $[(en)Pt(PyH)_2]^{2+}$, the absorption band at 305 nm can be ascribed to a HOMO-LUMO transition. The LUMO is dominated by antibonding $d_{x^2-y^2}$ orbital, so the excitation of this charge-transfer transition should weaken the Pt^{II}-Py coordination bond.[38] As the output of the UVA lamp is between 320 – 400 nm, the photolabilization of Pt^{II}-Py bond was not observed in this work. However, in this chapter, the derived pyridine ligand MOPEP is a chromophore with a larger π-conjugation system (**Figure 6.13**) and is also a strong electron donor. Therefore, lower energy is needed to excite the MOPEP-Pt^{II} charge-transfer transition, and hence light of longer wavelengths could weaken the Pt^{II}-MOPEP bond.

The photo-decomposition of complex **42** is likely to take place in two steps: the two MOPEP ligands can bereleased one by one rapidly upon irradiation with UVA (**Figure 6.13**).

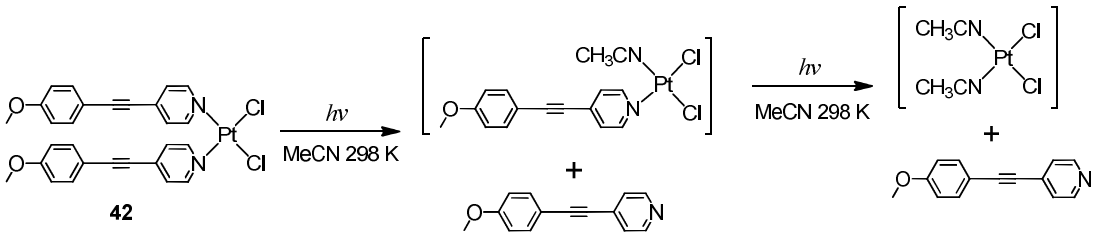

Figure 6.13 Proposed photoreaction of complex *cis*-$[PtCl_2(MOPEP)_2]$ (**42**).

To the best knowledge of the author, this work is the first report of the two-photon excitation induced disassociation of a pyridine type ligand, 4-[2-(4-methoxyphenyl)ethynyl] pyridine (MOPEP), from the corresponding Pt^{II} complex

cis-[$PtCl_2(MOPEP)_2$] (**42**). The TPA decomposition initiated by irradiation of fs laser light at 650 nm is faster than that at 700 and 600 nm. This result implies that there could be a TPA maximum between 700 and 600 nm, although a full two-photon absorption spectrum of complex **42** has not yet been determined. The absorption maximum for OPA is at 344 nm (**Figure 6.5**). Usually, the TPA maximum is more or less consistent with the corresponding OPA peak at $\lambda_{ex} \approx 2\lambda_{OPA}$.[3, 6, 40] For complex **42**, the wavelength-dependent photodecomposition efficiency of two-photon excitation almost coincides their one-photon absorbance at half of the corresponding wavelength.

6.5 Conclusion

To conclude, a new two-photon-activatable platinum(II) complexes has been designed, synthesized and characterized. Its one-photon and two-photon absorption properties and photochemistry were examined. It was discovered that this complex is sensitive to one photon excitation below 500 nm and the pyridine-type ligand MOPEP undergo a quickly solvent MeCN substitution from Pt upon irradiation. The same photoreaction can be triggered upon irradiation with fs-pulsed laser between 600 – 700 nm. This interesting property can be applied to design new photoactivatable anticancer complexes.

6.6 Reference

1. M. Göppert-Mayer, *Ann. Phys.*, 1931, **401**, 273-294.
2. M. Pawlicki, H. A. Collins, R. G. Denning and H. L. Anderson, *Angew. Chem. Int. Ed.*, 2009, **48**, 3244-3266.

3. J. E. Rogers, J. E. Slagle, D. M. Krein, A. R. Burke, B. C. Hall, A. Fratini, D. G. McLean, P. A. Fleitz, T. M. Cooper, M. Drobizhev, N. S. Makarov, A. Rebane, K. Y. Kim, R. Farley and K. S. Schanze, *Inorg. Chem.*, 2007, **46**, 6483-6494.
4. W. Kaiser and C. G. B. Garrett, *Phys. Rev. Lett.*, 1961, **7**, 229.
5. M. Albota, D. Beljonne, J. L. Bredas, J. E. Ehrlich, J. Y. Fu, A. A. Heikal, S. E. Hess, T. Kogej, M. D. Levin, S. R. Marder, D. McCord-Maughon, J. W. Perry, H. Rockel, M. Rumi, C. Subramaniam, W. W. Webb, X. L. Wu and C. Xu, *Science*, 1998, **281**, 1653-1656.
6. A. Picot, F. Malvolti, B. Le Guennic, P. L. Baldeck, J. A. G. Williams, C. Andraud and O. Maury, *Inorg. Chem.*, 2007, **46**, 2659-2665.
7. M. Khurana, H. A. Collins, A. Karotki, H. L. Anderson, D. T. Cramb and B. C. Wilson, *Photochem. Photobiol.*, 2007, **83**, 1441-1448.
8. G. S. He, L.-S. Tan, Q. Zheng and P. N. Prasad, *Chem. Rev.*, 2008, **108**, 1245-1330.
9. D. A. Parthenopoulos and P. M. Rentzepis, *Science*, 1989, **245**, 843-845.
10. D. A. Parthenopoulos and P. M. Rentzepis, *J. Appl. Phys.*, 1990, **68**, 5814-5818.
11. W. Denk, J. Strickler and W. Webb, *Science*, 1990, **248**, 73-76.
12. W. Denk, *Proc. Natl. Acad. Sci. USA*, 1994, **91**, 6629-6633.
13. C. N. LaFratta, J. T. Fourkas, T. Baldacchini and R. A. Farrer, *Angew. Chem. Int. Ed.*, 2007, **46**, 6238-6258.
14. C. W. Spangler, *J. Mater. Chem.*, 1999, **9**, 2013-2020.
15. T.-C. Lin, S.-J. Chung, K.-S. Kim, X. Wang, G. He, J. Swiatkiewicz, H. Pudavar and P. Prasad, ed. K.-S. Lee, Springer Berlin / Heidelberg, 2003, vol. 161, pp. 157-193.

16. W. G. Fisher, W. P. Partridge, C. Dees and E. A. Wachter, *Photochem. Photobiol.*, 1997, **66**, 141-155.
17. K. Ogawa and Y. Kobuke, *Anti-Cancer Agent Med. Chem.*, 2008, **8**, 269-279.
18. L. Beverina, M. Crippa, M. Landenna, R. Ruffo, P. Salice, F. Silvestri, S. Versari, A. Villa, L. Ciaffoni, E. Collini, C. Ferrante, S. Bradamante, C. M. Mari, R. Bozio and G. A. Pagani, *J. Am. Chem. Soc.*, 2008, **130**, 1894-1902.
19. H. A. Collins, M. Khurana, E. H. Moriyama, A. Mariampillai, E. Dahlstedt, M. Balaz, M. K. Kuimova, M. Drobizhev, V. X. D. Yang, D. Phillips, A. Rebane, B. C. Wilson and H. L. Anderson, *Nat. Photonics*, 2008, **2**, 420-424.
20. L. Carroll and T. R. Humphreys, *Clin. Dermatol.*, 2006, **24**, 2-7.
21. R. L. Goyan and D. T. Cramb, *Photochem. Photobiol.*, 2000, **72**, 821-827.
22. L. Brancaleon and H. Moseley, *Laser Med. Sci.*, 2002, **17**, 173-186.
23. M. R. Detty, S. L. Gibson and S. J. Wagner, *J. Med. Chem.*, 2004, **47**, 3897-3915.
24. G. M. Roberts, A. S. Chatterley, J. D. Young and V. G. Stavros, *J. Phys. Chem. Lett.*, 2012, **3**, 348-352.
25. Y. Liang, Y. X. Xie and J. H. Li, *J. Org. Chem.*, 2006, **71**, 379-381.
26. S. Haghighi, C. A. McAuliffe, W. E. Hill, H. H. Kohl and M. E. Friedman, *Inorg. Chim. Acta*, 1980, **43**, 113-119.
27. P.-C. Kong and F. D. Rochon, *Can. J. Chem.*, 1979, **57**, 526-529.
28. R. J. H. Clark and C. S. Williams, *Inorg. Chem.*, 1965, **4**, 350-357.
29. C. Tessier and F. D. Rochon, *Inorg. Chim. Acta*, 1999, **295**, 25-38.
30. F. D. Rochon and V. Buculei, *Inorg. Chim. Acta*, 2004, **357**, 2218-2230.
31. F. D. Rochon and H. Titouna, *Inorg. Chim. Acta*, 2010, **363**, 1679-1693.

32. B. M. Still, P. G. A. Kumar, J. R. Aldrich-Wright and W. S. Price, *Chem. Soc. Rev.*, 2007, **36**, 665-686.

33. A. R. Katritzky, D. J. Short and A. J. Boulton, *J. Chem. Soc.*, 1960, 1516-1518.

34. L. Cubo, A. M. Pizarro, A. G. Quiroga, L. Salassa, C. Navarro-Ranninger and P. J. Sadler, *J. Inorg. Biochem.*, 2010, **104**, 909-918.

35. C. Loup, A. Tesouro Vallina, Y. Coppel, U. Létinois, Y. Nakabayashi, B. Meunier, B. Lippert and G. Pratviel, *Chem. Eur. J.*, 2010, **16**, 11420-11431.

36. N. J. Farrer, J. A. Woods, L. Salassa, Y. Zhao, K. S. Robinson, G. Clarkson, F. S. Mackay and P. J. Sadler, *Angew. Chem. Int. Ed.*, 2010, **49**, 8905-8908.

37. C. Bartocci, F. Scandola and V. Carassiti, *J. Phys. Chem.*, 1974, **78**, 2349-2354.

38. K.-i. Yamashita, M. Kawano and M. Fujita, *J. Am. Chem. Soc.*, 2007, **129**, 1850-1851.

39. S. J. Pike and P. J. Lusby, *Chem. Commun.*, 2010, **46**, 8338-8340.

40. C.-K. Koo, K.-L. Wong, C. W.-Y. Man, Y.-W. Lam, L. K.-Y. So, H.-L. Tam, S.-W. Tsao, K.-W. Cheah, K.-C. Lau, Y.-Y. Yang, J.-C. Chen and M. H.-W. Lam, *Inorg. Chem.*, 2009, **48**, 872-878.

Chapter 7

Conclusions and Future Work

7.1 Conclusions

This thesis is concerned with the development of a series of novel photoactivatable Pt^{IV} diazidodihydroxido complexes so as to achive higher photocytotoxicity, lower cross-resistance and longer wavelength of activation. The photodecomposition pathways of selected complexes were studied in detail. MS spectrometry, HPLC, multinuclear NMR, UV-Vis, EPR and fluorescence spectroscopy were used extensively to probe the photoreactions of Pt complexes as well as with some biomolecules and identify their photoproducts.

A series of Pt^{IV} diazidodihydroxido complexes with *trans* azido, *trans* hydroxido groups and mixed *trans* aliphatic/aromatic amines, were designed, synthesized and characterized and their activities as photoactivatable anticancer prodrugs were determined. It was discovered that *trans, trans, trans*-[$Pt(N_3)_2(OH)_2$(MA)(Py)] (**5**) and *trans, trans, trans*-[$Pt(N_3)_2(OH)_2$(MA)(Tz)] (**8**) are potently cytotoxic towards human ovarian carcinoma cells (A2780), A2780cis (cisplatin resistant subline of A2780), OE19 (oesophageal adenocarcinoma) and HaCaT (human keratinocytes) upon irradiation with UVA**.** Remarkably, they also showed potent cytotoxic effects towards A2780cis, the cisplatin-resistant ovarian cancer A2780 cell subline. Also, the photocytotoxicity towards the A2780, A2780cis, OE19 and HaCaT cell lines were similar upon irradiation with blue light (λ_{max} = 420 nm) compared to that upon irradiation with UVA. Last but not least, these complexes are highly inert in the absence of light and almost no dark toxicity was observed. These results suggest that they are promising candidates for use in the cancer photochemotherapy.

In order to explore the photocytotoxic effect of Pt-diazidodihydroxido complexes from the chemistry point of view, the photochemistry of the mixed amines

methylamine (MA)/pyridine (Py) complex *trans, trans, trans*-$[Pt(N_3)_2(OH)_2(MA)(Py)]$ (**5**) was investigated in detail. Various analytical methods, such as ^{1}H NMR, ^{14}N NMR, UV-Vis, EPR and fluorescence spectroscopy were used to track the hydroxido groups, azido groups and the other ligands. The photodecomposition pathways involving the azido ligands and the hydroxido ligands were elucidated. Evidence for the release of free azide anions N_3^-, azidyl radicals N_3•, nitrogen gas N_2 and formation of nitrene intermediates {Pt-N} were observed. It was of importance to discover that singlet oxygen ($^{1}O_2$) is generated from photoreactions in the absence of an exogenous source of oxygen, whereas hydrogen peroxide (H_2O_2) and hydroxyl radical intermediates did not seem to be formed. These photoreactions may contribute to the photocytotoxicity of the complexes.

The photoinduced efficieny of binding of *trans, trans, trans*-$[Pt(N_3)_2(OH)_2(MA)(Py)]$ (**5**) and the thiazole (Tz) complex *trans, trans, trans*-$[Pt(N_3)_2(OH)_2(MA)(Tz)]$ (**8**) to 5'-GMP and a DNA oligonucleotide was also analysed. Mono-functional and bi-functional Pt adduct were captured by LC-MS and high-resolution MS. It was discovered for the first time that the oxidation of 5'-GMP can occur during the photoreaction of complex **5** upon irradiation with light (especially UVA). Singlet oxygen and nitrene intermediates generated from this photoreaction are likely to be the cause of the oxidative damage to guanine. These features contribute to the high photocytoxicity of this class of compounds. Also, the formation of singlet oxygen does not need an exogenous source of O_2 and hence the Pt-diazidodihydroxido complexes have a potentially novel mechanism of photochemotherapeutic activity.

For the purpose of activating complexes with longer wavelength, two series of new photoactivatable Pt^{IV} anticancer complexes were synthesized and their

photoactivation and toxicity to cancer cells were investigated. 4-Nnitropyridine, 2,2'-bipyridine, and terpyridines were used as ligands in novel Pt (di)azido complexes for one-photon excitation. Two complexes *trans, trans, trans*-$[Pt(N_3)_2(OH)_2(NH_3)(4\text{-}NO_2\text{-}Py)]$ (**31**) and *trans*-$[Pt(N_3)(OH)_2(Tpy)]Cl$ (**36**) were found to be photoactivated by green light. However, the photocytotoxicity of the complexes measured so far towards cancer cells are not satisfied. Complex *cis, trans*-$[Pt(N_3)_2(OH)_2(Bpy)]$ (**32**) is non-toxic in the absence of irradiation but the photocytotoxicity is at 10 μM scale, not as good as complexes **5** and **8**. Complex *trans*-$[Pt(N_3)(OH)_2(Tpy)]Cl$ (**36**) is also toxic in the dark and the difference between dark toxicity and photo toxicity is not satisfied. Further effort is still needed to develop new photoactivatable Pt^{IV} complexes with good anticancer activities and can be activated by light of wavelength 500 – 600 nm or even longer.

A new two-photon-activatable Pt^{II} complex, *cis*-$[PtCl_2(MOPEP)_2]$(**42**), has also been designed, synthesized and characterized. Its one-photon and two-photon absorption properties and photochemistry were determined with continuous wave light sources and fs-pulses laser light, respectively. It was observed that this complex is sensitive to one-photon excitation below 500 nm and the pyridine type ligand MOPEP underwent rapid solvent (acetonitrile) substitution upon irradiation. The same photoreaction was also triggered by irradiation with fs-pulses laser light between wavelength 600 – 700 nm. This interesting property could be applied to the design of novel photoactivatable anticancer complexes.

7.2 Future work

First, the reason for the unprecedented potent photocytotoxicity and the circumvention of cisplatin cross-resistance of Pt^{IV} diazidodihydroxido complexes

trans, trans, trans-[$Pt(N_3)_2(OH)_2(MA)(Py)$] (**5**) and *trans, trans, trans*-[$Pt(N_3)_2(OH)_2(MA)(Tz)$] (**8**) from the biological point of view is still not clear. The different aliphatic amine and heterocyclic imine groups also change the hydrophilicity/lipophilicity of the complexes and the shape of the molecules which could influence their cellular uptake and accumulation.[1, 2] The mono-functional and bi-functional DNA adducts found in cell-free media may also present as lesions in the cancer cells. This may lead to DNA distortions including bending, kinking and unwinding,[3] and inhibit the enzyme-driven transcription[4] and repair. Also, singlet oxygen[5-8] and the nitrene intermediate may also cause oxidative damage to the DNA.[9-13] Further experiments need to be carried out to investigate this process.

Second, the mechanism of singlet oxygen generation in the photochemical reaction of Pt^{IV} diazidodihydroxido complexes needs to be investigated and the source of oxygen determined. The release of singlet oxygen could be confirmed in two other ways, EPR spectroscopy using 2,2,6,6-tetramethyl-4-piperidone (TEMP)[14] as a $^1O_2$ trap or the direct detection of the phosphorescence of $^1O_2$ at 1270 nm (monomol emission) and 630/710 nm (dimol emission) using an extremely sensitive detector.[15, 16] A good strategy to follow the source of oxygen is to perform the reaction in $H_2{}^{18}O$ (water-^{18}O). The released oxygen gas could be captured and analyse directly in GC-MS[17] or using an oxygen trap,[18] such as $Ir(PEt_3)_3Cl$, and then analysing by ESI-MS spectrometry. From the isotope composition of the released oxygen, it could be possible to determine the source of oxygen: the Pt complex and/or the solvent H_2O. Another method to track the pathway of OH groups in the photoreaction of Pt complexes is time-resolved infra-red (TR-IR) studies. TR-IR could shed further light on the breaking of Pt-O bond and generation of short-lived intermediates at

picosecond timescale. However, solvent should be carefully selected as H_2O has a broadband absorption for OH stretching in IR.

Third, the photocytotoxicities of a few Pt^{IV} diazidodihydroxyl complexes, such as *trans, trans, trans*-[$Pt(N_3)_2(OH)_2(NH_3)$(4-nitropyridine)] (**31**) and *trans*-[$Pt(N_3)(OH)_2$(TTpy)]Cl (**40**), still need to be determined. The photoreactions of Pt^{IV} mono-azido complexes, such as *trans*-[$Pt(N_3)(OH)_2$(Tpy)]Cl (**36**), are of great interest. It was generally believed that two azido groups should release as $\bullet N_3$ radicals together[19] and avoid formation of an unstable Pt^{III} product. However, in this work, it was discovered that one azido group disassociated from Pt without affecting the other and the Pt^{IV} was still reduced to Pt^{II}, so the second electron must be from the other groups, such as the OH ligand.[20-22]

Fourth, a two-photon absorption spectrum of complex *cis*-[$PtCl_2$(MOPEP)$_2$] (**42**) will be recorded. The dissociation of pyridine ligands from Pt has been applied in the development of interesting molecule devices, such as catenations.[23] The photolabilization of the Pt^{II}-Py bond can also be used in designing photoactivatable anticancer drugs. A receptor-specific pyridine derivative could be designed so as to make new Pt complexes that could be selectively accumulated in the tumour cells or tissues. Thereafter, the complexes could be activated by two-photon excitation with Near-IR laser light. These complexes could also be made water-soluble without compromising the two-photon activity.[24]

Fifth, various types of novel Pt^{IV} anticancer prodrugs could be developed with a broad range of features. The Pt complex could be coupled with cancer cell targeting peptides, such as RGD,[25] NGR,[26] LHRH[27] and IFLLWQR[28] peptides or encapsulated in polymeric carriers, such as ethylene glycol nanoparticles[29, 30] to increase the

accumulation of drug and reduce the side effects. Ligands with larger π-conjugation systems, such as dipyridoquinoxaline and dipyridophenazine could be used in making new Pt^{IV} diazido complexes. These ligands are not only good chromophores for red or near IR light absorption, but also are efficient photosensitizers.[31-34] Taking advantage of these features, absorption of light in the therapeutic window as well as potent PDT could be obtained.

7.3 References

1. L. Kelland, *Nat. Rev. Cancer*, 2007, **7**, 573-584.
2. Z. Liu, A. Habtemariam, A. M. Pizarro, S. A. Fletcher, A. Kisova, O. Vrana, L. Salassa, P. C. A. Bruijnincx, G. J. Clarkson, V. Brabec and P. J. Sadler, *J. Med. Chem.*, 2011, **54**, 3011-3026.
3. T. Suchankova, M. Vojtiskova, J. Reedijk, V. Brabec and J. Kasparkova, *J. Biol. Inorg. Chem.*, 2009, **14**, 75-87.
4. D. Wang, G. Zhu, X. Huang and S. J. Lippard, *Proc. Natl. Acad. Sci. USA*, 2010, **107**, 9584-9589.
5. P. R. Ogilby, *Chem. Soc. Rev.*, 2010, **39**, 3181-3209.
6. B. Halliwell and J. Gutteridge, *Free Radicals in Biology and Medicine*, Oxford University Press, Oxford, UK, 2007.
7. S. Kanvah, J. Joseph, G. B. Schuster, R. N. Barnett, C. L. Cleveland and U. Landman, *Acc. Chem. Res.*, 2010, **43**, 280-287.
8. G. Pratviel and B. Meunier, *Chem. Eur. J.*, 2006, **12**, 6018-6030.
9. V. Voskresenska, R. M. Wilson, M. Panov, A. N. Tarnovsky, J. A. Krause, S. Vyas, A. H. Winter and C. M. Hadad, *J. Am. Chem. Soc.*, 2009, **131**, 11535-11547.

10. E. C. Miller and J. A. Miller, *Cancer*, 1981, **47**, 2327-2345.
11. M. Famulok and G. Boche, *Angew. Chem. Int. Ed.*, 1989, **28**, 468-469.
12. W. G. Humphreys, F. F. Kadlubar and F. P. Guengerich, *Proc. Natl. Acad. Sci. USA*, 1992, **89**, 8278-8282.
13. Z. Guo, J. Xue, Z. Ke, D. L. Phillips and C. Zhao, *J. Phys. Chem. B*, 2009, **113**, 6528-6532.
14. S. Xu, X. Zhang, S. Chen, M. Zhang and T. Shen, *Photochem. Photobio. Sci.*, 2003, **2**, 871-876.
15. P. Bilski, M. E. Daub and C. F. Chignell, *Methods Enzymol.*, 2002, **352**, 41-52.
16. M. Niedre, M. S. Patterson and B. C. Wilson, *Photochem. Photobiol.*, 2002, **75**, 382-391.
17. W. M. Singh, D. Pegram, H. Duan, D. Kalita, P. Simone, G. L. Emmert and X. Zhao, *Angew. Chem.*, 2012, **124**, 1685-1688.
18. S. W. Kohl, L. Weiner, L. Schwartsburd, L. Konstantinovski, L. J. W. Shimon, Y. Ben-David, M. A. Iron and D. Milstein, *Science*, 2009, **324**, 74-77.
19. A. Vogler, A. Kern and J. Hüttermann, *Angew. Chem. Int. Ed.*, 1978, **17**, 524-525.
20. W. Beck and K. Schorpp, *Angew. Chem. Int. Ed.*, 1970, **9**, 735-735.
21. S. J. David and R. D. Coombe, *J. Phys. Chem.*, 1986, **90**, 3260-3263.
22. S. M. Peiris and T. P. Russell, *J. Phys. Chem. A*, 2003, **107**, 944-947.
23. K.-i. Yamashita, M. Kawano and M. Fujita, *J. Am. Chem. Soc.*, 2007, **129**, 1850-1851.
24. M. K. Kuimova, H. A. Collins, M. Balaz, E. Dahlstedt, J. A. Levitt, N. Sergent, K. Suhling, M. Drobizhev, N. S. Makarov, A. Rebane, H. L. Anderson and D. Phillips, *Org. Biomol. Chem.*, 2009, **7**, 889-896.

25. S. Mukhopadhyay, C. M. Barnés, A. Haskel, S. M. Short, K. R. Barnes and S. J. Lippard, *Bioconjugate Chem.*, 2008, **19**, 39-49.

26. M. W. Ndinguri, R. Solipuram, R. P. Gambrell, S. Aggarwal and R. P. Hammer, *Bioconjugate Chem.*, 2009, **20**, 1869-1878.

27. S. S. Dharap, Y. Wang, P. Chandna, J. J. Khandare, B. Qiu, S. Gunaseelan, P. J. Sinko, S. Stein, A. Farmanfarmaian and T. Minko, *Proc. Natl. Acad. Sci. USA*, 2005, **102**, 12962-12967.

28. S. Hatakeyama, K. Sugihara, T. K. Shibata, J. Nakayama, T. O. Akama, N. Tamura, S.-M. Wong, A. A. Bobkov, Y. Takano, C. Ohyama, M. Fukuda and M. N. Fukuda, *Proc. Natl. Acad. Sci. USA*, 2011, **108**, 19587-19592.

29. S. Dhar, N. Kolishetti, S. J. Lippard and O. C. Farokhzad, *Proc. Natl. Acad. Sci. USA*, 2011.

30. S. Dhar, F. X. Gu, R. Langer, O. C. Farokhzad and S. J. Lippard, *Proc. Natl. Acad. Sci. USA*, 2008, **105**, 17356-17361.

31. S. Roy, S. Saha, R. Majumdar, R. R. Dighe and A. R. Chakravarty, *Polyhedron*, 2010, **29**, 2787-2794.

32. B. Maity, M. Roy, B. Banik, R. Majumdar, R. R. Dighe and A. R. Chakravarty, *Organomet.*, 2010, **29**, 3632-3641.

33. S. Saha, R. Majumdar, M. Roy, R. R. Dighe and A. R. Chakravarty, *Inorg. Chem.*, 2009, **48**, 2652-2663.

34. P. K. Sasmal, S. Saha, R. Majumdar, S. De, R. R. Dighe and A. R. Chakravarty, *Dalton Trans.*, 2010, **39**, 2147-2158.

Appendices

Appendix 1 Table of compounds referred.

Compound Name	Structure
Cis-[$PtI_2(MA)_2$] (**1**)	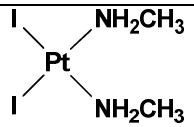
Cis-[$PtCl_2(MA)_2$] (**2**)	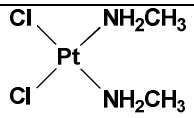
Trans-[$Pt(Cl)_2(MA)(py)$] (**3**)	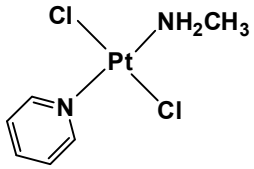
Trans-[$Pt(N_3)_2(MA)(py)$] (**4**)	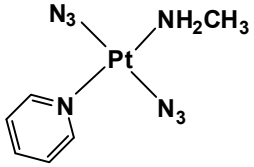
Trans, trans, trans- [$Pt(N_3)_2(OH)_2(MA)(py)$] (**5**)	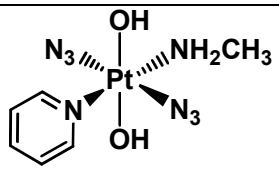
Trans, trans, trans- [$Pt(^{15}N_3)_2(OH)_2(MA)(py)$] (**5***)	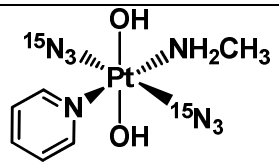
Trans-[$Pt(MA)(Py)(5'\text{-}GMP)_2 - 2H$] (**5a**)	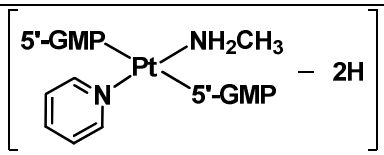
(*SP*-4-4)-[$Pt(N_3)(MA)(Py)(5'\text{-}GMP) - H$] (**5b**)	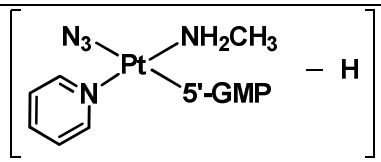

Trans-[Pt(MA)(Py)(H_2O)$_2$](BF_4)$_2$ (**5g**)	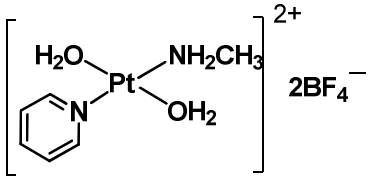
Trans-[Pt(Cl)$_2$(MA)(tz)] (**6**)	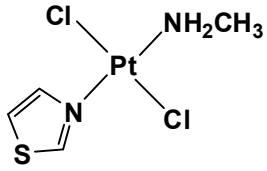
Trans-[Pt(N_3)$_2$(MA)(tz)] (**7**)	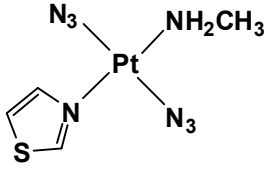
Trans, trans, trans-[Pt(N_3)$_2$(OH)$_2$(MA)(tz)] (**8**)	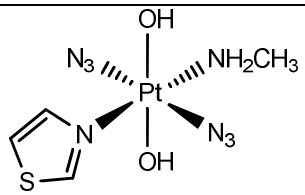
Trans-[Pt(MA)(Tz)(5'-GMP)$_2$ − 2H] (**8a**)	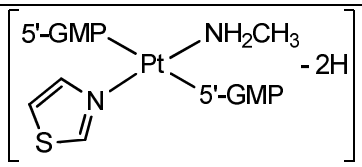
(*SP*-4-4)-[Pt(N_3)(MA)(Tz)(5'-GMP) − H] (**8b**)	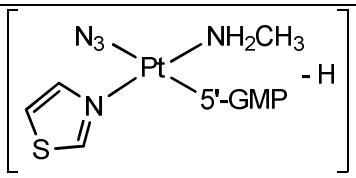
Cis-[PtI_2(DMA)$_2$] (**9**)	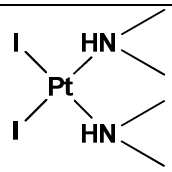
Cis-[PtCl_2(DMA)$_2$] (**10**)	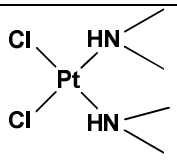
Trans-[Pt(Cl)$_2$(DMA)(tz)] (**11**)	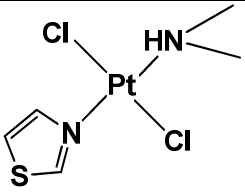

Trans-[Pt(N$_3$)$_2$(DMA)(tz)] (**12**)	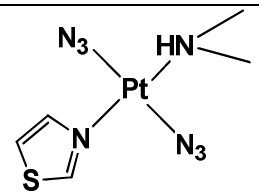
Trans, trans, trans- [Pt(N$_3$)$_2$(OH)$_2$(DMA)(tz)] (**13**)	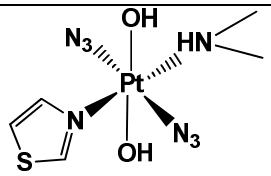
Trans-[Pt(Cl)$_2$(DMA)(py)] (**14**)	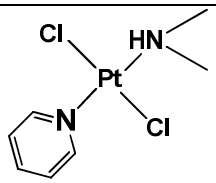
Trans-[Pt(N$_3$)$_2$(DMA)(py)] (**15**)	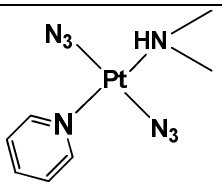
Trans, trans, trans- [Pt(N$_3$)$_2$(OH)$_2$(DMA)(py)] (**16**)	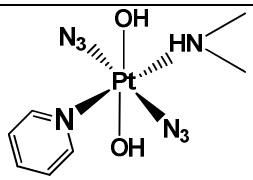
Cis-[PtCl$_2$(IPA)$_2$] **(17**)	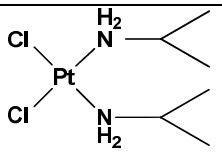
Trans-[Pt(Cl)$_2$(IPA)(tz)] (**18**)	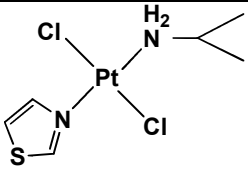
Trans-[Pt(Cl)$_2$(IPA)(py)] (**19**)	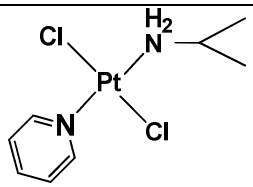
Trans-[Pt(N$_3$)$_2$(IPA)(py)] (**20**)	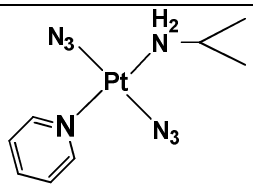

Trans, trans, trans-$[Pt(N_3)_2(OH)_2(IPA)(py)]$ (**21**)	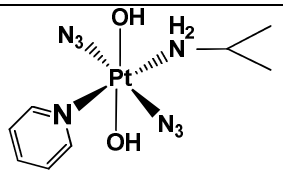
Trans, trans, trans-$[Pt(N_3)_2(OH)_2(NH_3)(Py)]$ (**22**)	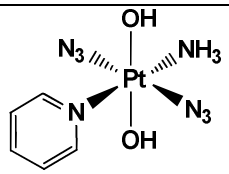
Trans, trans, trans-$[Pt(N_3)_2(OH)_2(NH_3)(Tz)]$ (**23**)	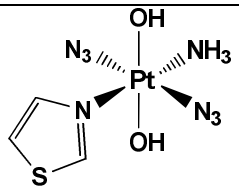
Trans, trans, trans-$[Pt(N_3)_2(OH)_2(Py)_2]$ (**24**)	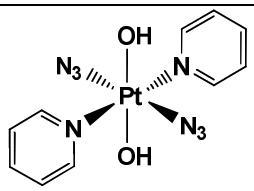
Cis-$[PtI_2(NH_3)_2]$ (**25**)	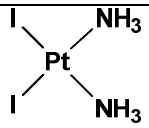
Cis-$[PtCl_2(NH_3)_2]$ (**26**)	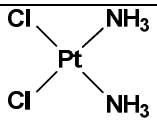
4-Nitropyridine (4-NO_2-Py, **27**)	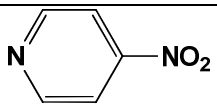
Trans-$[Pt(Cl)_4(NH_3)(4\text{-py-}NO_2)]$ (**28**)	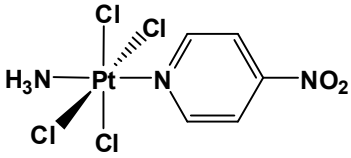
Trans-$[Pt(Cl)_2(NH_3)(4\text{-py-}NO_2)]$ (**29**)	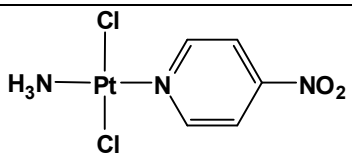
Trans-$[Pt(N_3)_2(NH_3)(4\text{-py-}NO_2)]$ (**30**)	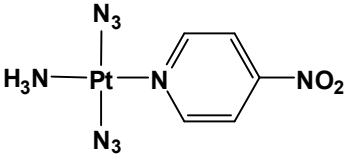

Trans, trans, trans-$[Pt(N_3)_2(OH)_2(NH_3)(4\text{-py-}NO_2)]$ (**31**)	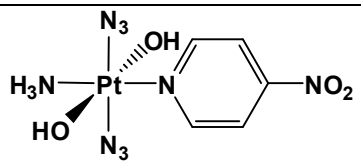
Cis, trans-$[Pt(N_3)_2(OH)_2(bpy)]$ (**32**)	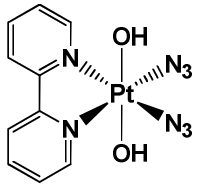
$[Pt(Cl)(Tpy)]Cl \cdot 2H_2O$ (**33**)	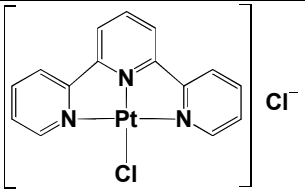
$[Pt(N_3)(Tpy)]PF_6$ (**34**)	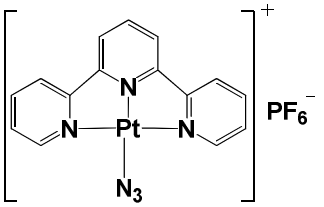
$[Pt(N_3)(Tpy)]N_3$ (**35**)	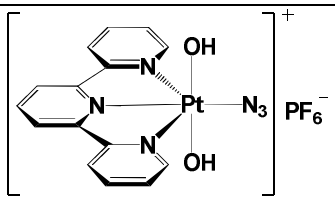
Trans-$[Pt(N_3)(OH)_2(Tpy)]Cl$ (**36**)	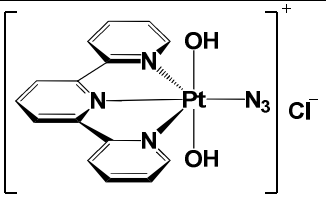
$[PtCl_2(COD)]$ (**37**)	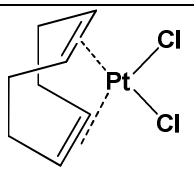
$[PtCl(TTpy)]Cl$ (**38**)	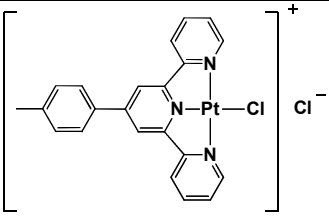

$[Pt(N_3)(TTpy)]N_3$ (**39**)	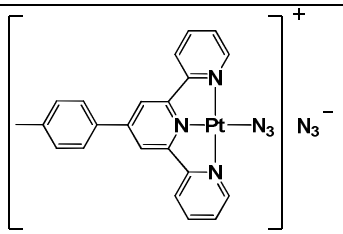
Trans-$[Pt(N_3)(OH)_2(TTpy)]Cl$ (**40**)	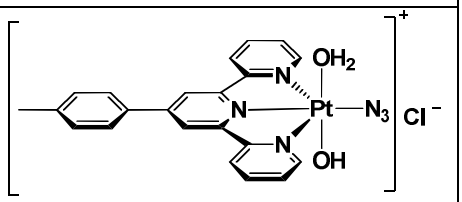
4-[2-(4-methoxyphenyl)ethynyl]pyridine (MOPEP, **41**)	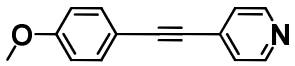
Cis-$[PtCl_2(MOPEP)_2]$ (**42**)	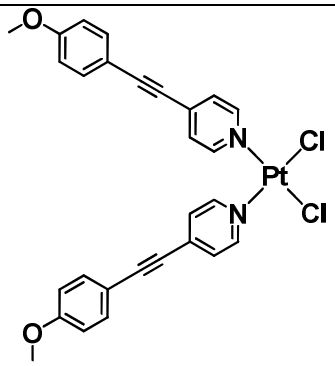

Appendix 2 Output spectra of light sources.

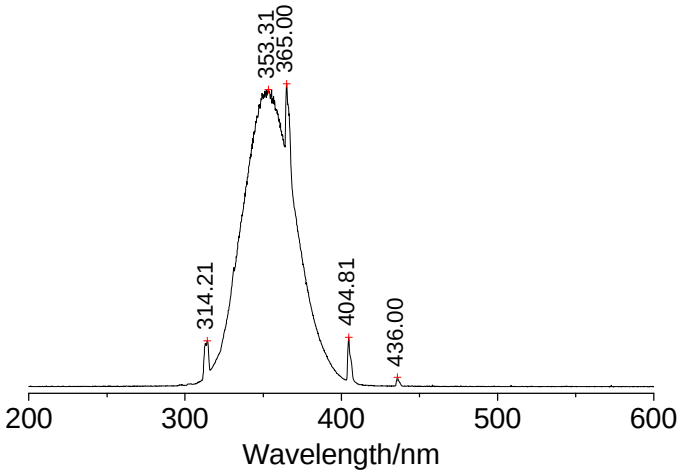

Figure A.1 Output spectrum of Hitachi UVA lamps.

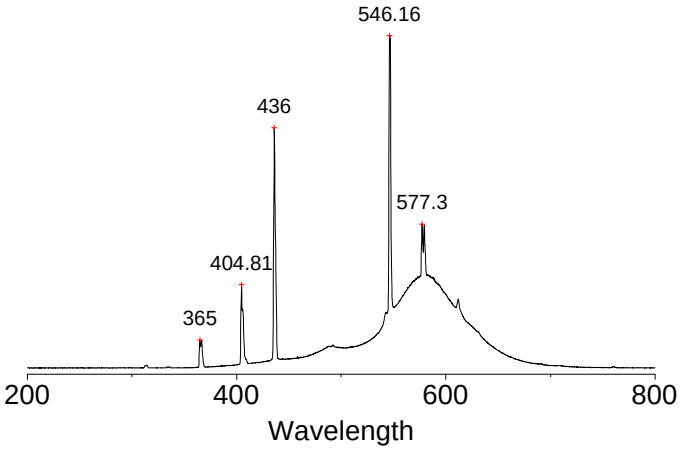

Figure A.2 Output spectrum of Hitachi visible lamp.

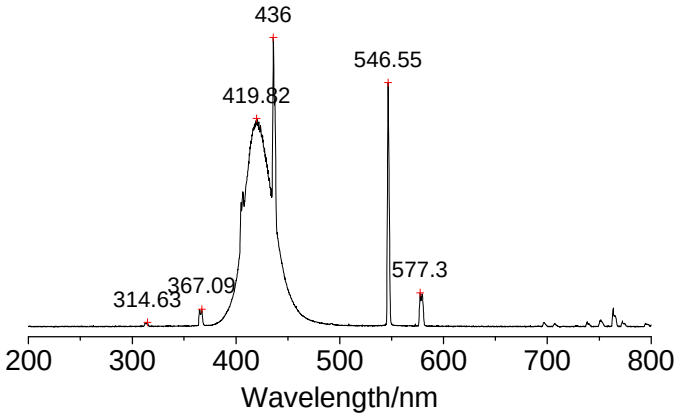

Figure A.3 Output spectrum of Luzchem LZC-420 lamps.

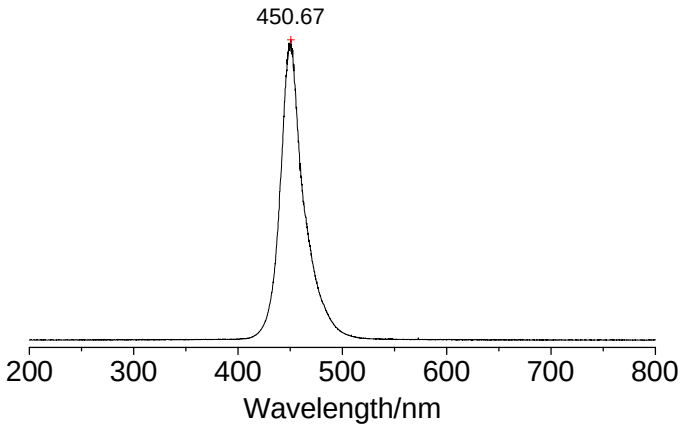

Figure A.4 Output spectrum of ACULED® VHL™ 450 nm LEDs.

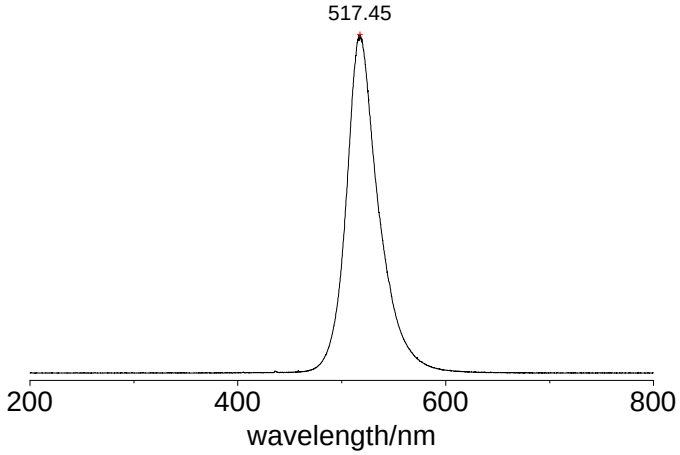

Figure A.5 Output spectrum of High-Power 38 LED bulb/GU10 Green LEDs.